



HAL
open science

New analytical approaches for copper diagnosis, prognosis and follow up of Wilson disease

M. Carmen Garcia Poyo

► **To cite this version:**

M. Carmen Garcia Poyo. New analytical approaches for copper diagnosis, prognosis and follow up of Wilson disease. Analytical chemistry. Université de Pau et des Pays de l'Adour, 2021. English. NNT : 2021PAUU3041 . tel-03615599

HAL Id: tel-03615599

<https://theses.hal.science/tel-03615599>

Submitted on 21 Mar 2022

HAL is a multi-disciplinary open access archive for the deposit and dissemination of scientific research documents, whether they are published or not. The documents may come from teaching and research institutions in France or abroad, or from public or private research centers.

L'archive ouverte pluridisciplinaire **HAL**, est destinée au dépôt et à la diffusion de documents scientifiques de niveau recherche, publiés ou non, émanant des établissements d'enseignement et de recherche français ou étrangers, des laboratoires publics ou privés.

THÈSE PRÉPARÉE ET PRÉSENTÉE EN COTUTELLE
INTERNATIONALE A :
UNIVERSITÉ DE PAU ET DES PAYS DE L'ADOUR (UPPA)
ET
UNIVERSIDAD DE ZARAGOZA (UNIZAR)

Présentée et soutenue le (date)
par **M^aCarmen García Poyo**

pour obtenir le grade de **DOCTOR**
Spécialité: **Chimie analytique**

New analytical approaches for copper diagnosis, prognosis and follow up of Wilson disease

MEMBRES DU JURY

RAPPORTEURS

Frank Vanhaecke
Franck Poitrasson
Thomas Walczyk

Université de Ghent
Université Paul Sabatier
Université de Singapour

EXAMINATEURS

Beatriz Fernandez Garcia
Bénédicte Lelievre

Université de Oviedo
Centre Hospitalier Universitaire d'Angers

DIRECTEURS

• Christophe Pécheyran
• Martín Resano

Université de Pau et des pays de l'Adour
Université de Zaragoza



Universidad
Zaragoza

Tesis Doctoral

New analytical approaches for copper diagnosis, prognosis and follow up of Wilson disease

Autor

M^aCarmen Garcia Poyo

Director/es

Christophe Pécheyran
Martín Resano Ezcaray

Facultad de Ciencias / Departamento de Química Analítica
2021

Acknowledgements

**Interreg
POCTEFA**



Fondo Europeo de Desarrollo Regional (FEDER)

The project has been 65% cofinanced by the European Regional Development Fund (ERDF) through the Interreg V-A Spain-France-Andorra programme (POCTEFA 2014-2020). POCTEFA aims to reinforce the economic and social integration of the French–Spanish–Andorran border. Its support is focused on developing economic, social and environmental cross-border activities through joint strategies favouring sustainable territorial development.

Also it was cofinanced by project PGC2018-093753-B-I00 (MCIU/AEI//FEDER,UE) and the Aragon Government (Construyendo Europa desde Aragón, Grupo E43_20R).



IPREM
Institut des sciences analytiques
et de physico-chimie
pour l'environnement et les matériaux



**UNIVERSITÉ
DE PAU ET DES
PAYS DE L'ADOUR**



**Universidad
Zaragoza**



Acknowledgements

During almost four years of my PhD, I have received support from many people, without whom this work would not have been possible.

First of all, I would like to thank my both supervisors, Christophe Pécheyran and Martin Resano, for giving me the chance to be part of their research group, teaching me, supporting me and transmitting me all their knowledge. I hope I have proven to be worthy. Of course, it was not all about work, so I would also like to thank for the chatters, laughs and good times both inside and outside the lab. Martin, thank you for teaching me the "art of the beer". Thanks to all of these moments, I have been able to endure my doctorate.

I would also like to thank the components of my 2 research groups for their help and above all for the good times we have had. From PAMAL, I would like to thank Fanny, Gaëlle, Asmodeé and above all Nagore, who helped me a lot since my arrival in Pau, and today is a very good friend. From MARTE, I would like to thank my friends Raul, Antonio, Andre, Esperanza, and specially Flavio and Maite for their advice, corrections and patience.

I would like to thank everyone who has made this work possible, helping me directly or indirectly with the analysis, sample collection, etc.

I want to thank also all the people who have been supporting me and with whom I have lived unforgettable moments over the years. Both friends I have met during the doctorate and my lifelong friends, who are always with me. Of course, I want to thank my family, specially my parents and my two great loves, my brother and my boyfriend. Vicente thanks for making me feel that you are by my side even though we are far away. I would like to pay a special tribute to my grandmother, who unfortunately cannot be here with me today because, without her and her advice, I would not be where I am right now.

Finally, I would like to remark I did not mention anyone in particular before because probably someone would be missed. Luckily, this list is very long, and all the people who I am referring to knows who s/he is, so please include yourself here. Everyone who knows me realizes that I am not the one who is just talk, I prove to them. And I hope I have done it.

Table of contents

Abstract (English)	I
Resumen (Español)	VI
Résumé (Français)	XII
List of figures.....	XVIII
List of tables.....	XXVI
List of acronyms.....	XXIX

Chapter 1 : Introduction

1. Biomonitoring.....	1
2. New alternative of sampling and/or analysis.....	2
2.1 Biosensors.....	3
2.2 Dried matrix Spot (DMS).....	5
2.2.1 Dried blood spot (DBS).....	6
2.2.2 Dried Plasma Spots (DPSs).....	10
2.2.3 Dried urine Spots (DUSs).....	11
2.2.4 Dried oral fluids (DOFs) or dried saliva spots (DSSs).....	11
3. Introduction systems.....	12
3.1 Liquid sample introduction systems.....	12
3.1.1 Flow Injection analysis.....	12
3.1.2 Micro-nebulizer.....	14
3.2 Solid sample introduction systems.....	18
3.2.1 Electrothermal atomization (ETA) or electrothermal vaporization system (ETV).....	18
3.2.2 Laser.....	20
4. Why focusing on elemental determination?.....	26
5. Techniques for the elemental determination.....	28
5.1 Bulk elemental analysis.....	28
5.1.1 Atomic absorption spectrometry (AAS).....	29

5.1.2 Inductively coupled plasma techniques.....	32
5.1.2.1 Inductively couple plasma optical emission spectrometer (ICP-OES).....	33
5.1.2.2 Inductively couple plasma mass spectrometer (ICP-MS).....	34
5.2 Speciation analysis.....	37
5.3 Isotopic analysis.....	39
5.3.1 Thermal ionization mass spectrometry (TIMS).....	39
5.3.2 Multi-collector inductively couple plasma-mass spectroscopy (MC-ICP- MS).....	41
6. Copper in clinical analysis.....	43
6.1 Copper metabolism.....	43
6.2 Disorders of Cu metabolism.....	45
6.3 Diseases related to ATP-Transporter.....	46
6.4 Wilson's disease treatment.....	48
6.5 Ways to diagnose Wilson's disease.....	49
7. References.....	50

Chapter 2: Objectives.....61

Chapter 3: Determination of Cu in blood via direct analysis of dried blood spots using high-resolution continuum source graphite furnace atomic absorption spectrometry.....62

1. Introduction.....	63
2. Experimental.....	66
2.1 Instrumentation.....	66
2.2 Reagents and materials.....	67
2.3 Samples and sample preparation.....	70
2.4 Measurement protocol.....	71
3. Results and discussion.....	74
3.1 Method optimization.....	74
3.1.1 Wavelength selection.....	74
3.1.2 Modifier selection.....	74

3.1.3 Optimization of the temperature program.....	76
3.2 Figures of merit.....	81
3.3 Determination of Cu in whole blood reference material using DBSs. Evaluation of the accuracy of the method.....	84
3.4 Cu determination in real blood samples. Venipuncture vs DBSs.....	86
4. Conclusions.....	87
5. References.....	88
6. Supplementary information.....	91

Chapter 4: Time-absorbance profile ratio background correction: introducing TAP to correct for spectral overlap in high-resolution continuum source graphite furnace atomic absorption spectrometry.....92

1. Introduction.....	93
2. Experimental.....	96
2.1 Instrumentation.....	96
2.2 Reagents, standards, and samples.....	97
2.3 Procedures for the development of the correction model and for analyses of the samples.....	97
3. Results and discussion.....	99
3.1 Time-absorbance profile.....	99
3.2 Ratio normalization in TAP.....	102
3.3 Application of TAP correction.....	104
3.4 TAP correction for direct analysis of reference materials.....	109
4. Conclusions.....	114
5. References.....	116
6. Supplementary information.....	119

Chapter 5. Laser ablation of microdroplets for copper isotopic analysis via MC-ICP-MS. Analysis of serum microsamples for the diagnosis and follow-up treatment of Wilson's disease.....120

1. Introduction.....	120
----------------------	-----

2. Experimental.....	123
2.1 Instrumentation	123
2.2 Standards and reagents.....	124
2.3 Samples and sample preparation.....	125
2.4 Measurement protocol.....	128
2.4.1 Determination of total Cu.....	128
2.4.2 Determination of Cu isotope ratios.....	130
3. Results and discussion.....	132
3.1 Sample preparation.....	132
3.1.1 Cu isolation.....	132
3.1.2 Preconcentration and volume of sample needed for analysis.....	134
3.2 Results for Cu concentration in the serum samples	135
3.3 Analysis with fs-LA-MC-ICP-MS.....	135
3.3.1 Optimization of sample preparation for LA analysis.....	136
3.3.2 Optimization of LA-MC-ICP-MS instrumental parameters.....	138
3.3.3 Calculating the isotope ratio.....	140
3.4 Validation of Cu isotopic monitoring via fs-LA-MC-ICPMS	142
3.5 Analysis of real samples.....	143
4. Conclusion.....	146
5. References.....	147
6. Supplementary information.....	151

Chapter 6. Evaluation of electrothermal vaporization for sample introduction aiming at Cu isotopic analysis via multicollector-inductively coupled plasma mass spectrometry.....158

1. Introduction.....	158
2. Experimental.....	161
2.1 Instrumentation.....	161
2.2 Standards and reagents.....	161
2.3 Samples and sample preparation.....	162
2.4 Measurement protocol.....	162

3. Results.....	165
3.1 Optimization of the temperature program.....	165
3.2 Data treatment.....	167
3.3 Precision and accuracy of the method.....	172
4. Conclusions.....	175
5. References.....	175

Chapter 7: Comparison of different biomarkers for diagnosis and follow up of Wilson’s disease.....178

1. Introduction.....	179
2. Experimental.....	181
2.1 Instrumentation.....	181
2.2 Materials and reagents.....	182
2.3 Samples and sample preparation.....	183
2.4 Measurement protocol.....	185
2.4.1 Determination of both exchangeable Cu and total Cu.....	185
2.4.2 Determination of Cu isotope ratios.....	186
3. Results and discussion.....	189
3.1 Evaluation of the method for Cu Exch determination.....	189
3.2 Analysis of the samples for total copper, exchangeable copper and REC.....	192
3.3 Isotopic analysis.....	198
4. Conclusion.....	203
5. References.....	204
6. Supplementary information.....	207

Chapter 8: Conclusion (English).....250

Conclusión (Español).....254

Conclusion (Français).....259

Abstract

Biomonitoring of different elements/molecules is important to control the health state. By analysing biomarkers, it is possible to detect abnormal levels in the organism, and to predict the consequences to take appropriate actions, in the event that the biomarker levels deviate significantly from the reference values. Moreover, biomonitoring is critical for the follow-up of patients, particularly when they are under therapy, to ensure a suitable interaction with the medical drugs.

Usually, biomonitoring is carried out using blood samples collected by venipuncture. This way to collect sample is invasive and requires the collection of at least some milliliters of blood. Moreover, patients must travel to the hospital or the medical analysis laboratory, because these kinds of samples must be collected by skilled people and under controlled conditions. As a result, conventional sampling for routine analysis is a tedious task, especially for newborns (due to the very limited sample availability) and for patients who live in remote areas, or for patients with limited mobility that due to their personal/logistical requirements, may find this approach inconvenient.

In an attempt to solve these problems, new trends have emerged with the patient in mind. It could be said that there is a tendency towards personalized medicine. The intention is that sampling should be as minimally invasive as possible to prevent the patients from suffering significant pain and/or stress. Moreover, another goal consists in minimizing or completely avoiding the patients' trips to the lab to carry out the routine analyses.

In this way, new sampling devices that only need few μL of sample (microsampling) and that, moreover can be used by the patient and, if it is possible, provide results quickly, even in real time, are continuously, under investigation. In practice, this is covered by two major research fields: biosensors, and dried matrix spots (DMSs), where the sample is deposited onto a filter paper, dried at room temperature and, once dried, it can be sent by regular post to the hospital or clinical laboratory for analysis.

In parallel with the development of new micro-sampling devices, alternative microsample introduction systems have been developed, allowing for lower detection limits and for the use of the smallest possible sample volume, which in turn reduce the use of chemical reagents, the waste generated, etc. Some of the micro-sampling introduction systems developed are

flow injection analysis (FIA), micro-nebulizers, laser ablation (LA) and electrothermal vaporization/atomization systems (ETV/ETA).

These kind of micro-sampling introduction systems can be used for elemental analysis coupled to different techniques such as atomic absorption spectrometry (AAS), inductively coupled plasma optical emission spectrometry (ICP-OES), and inductively coupled plasma mass spectrometry (ICP-MS), among others. Also for isotopic analysis they can be coupled to mass spectrometric techniques such as thermal ionization mass spectrometry (TIMS) and multi-collector inductively couple plasma-mass spectroscopy (MC-ICP-MS).

Cu is an essential metal involved in many metabolic reactions. Moreover, it is linked to Wilson's disease (WD). WD is caused by the mutation of the ATP7B gen. This mutation causes the synthesis of a dysfunctional ATP7B protein, which assists the transfer of Cu ions to the main plasma Cu protein (ceruloplasmin). Moreover, it is involved in the process of Cu excretion into the bile. When this function is altered, free Cu levels start building up in the liver and in other organs of the body, such as the brain, the eyes (Kayser–Fleischer rings), the kidneys, etc. This disease can be fatal if it is untreated. Although the treatment is relatively simple and effective, the problem is to be able to diagnose the disease early enough, before any symptoms appear.

In this context, different methods have been developed in the framework of this thesis for both Cu elemental determination and for Cu isotopic analysis, focusing on microsampling.

In particular, two methods have been developed and evaluated for Cu elemental analysis, one for direct solid analysis and the other for liquid sample analysis. In addition, three methods have been developed and evaluated for Cu isotopic analysis.

For direct solid analysis, the performance of state-of-the-art high-resolution continuum source graphite furnace atomic absorption spectrometry (HR CS GFAAS) instrumentation and four novel devices to produce dried blood spots (DBSs) of perfectly defined volumes (Mitra, HemaXis DB10, Capitainer qDBS and HemaPEN) have been evaluated with the aim of developing a simple, direct method for the determination of Cu in blood samples.

Cu determination was carried out via simple external calibration with aqueous standards using Pt as modifier. To evaluate the methods, the four different devices were tested to prepared DBSs with three whole blood (WB) reference materials (RMs), L-1, L-2 and L-3. In every case, the results obtained were in good agreement with the values provided by the

RMs. However, the precision was found to depend on the blanks levels. Better blanks were obtained for HemaXis DB10 and HemaPEN than for Capitainer qDBS and for Mitra. Thus, HemaXis DB10 and HemaPEN should be preferred when abnormally low Cu levels ($500 \mu\text{g L}^{-1}$ or lower), associated with some diseases, need to be determined. The results demonstrate that accurate values with RSD values below 10% can be achieved for these devices even for such Cu levels, while for Capitainer qDBS and, to a higher extent, for Mitra, the blank variations will ultimately increase the uncertainty. Finally, four real blood samples collected by both venipuncture and DBS preparation were analyzed for copper concentration. The results obtained showed a very good agreement between DBS and venipuncture. This indicates that the proposed approach could be readily applied, so that patients with disorders requiring Cu control can prepare their own samples and submit them *via* postal mail to the lab for HR CS GFAAS direct and fast analysis.

In the same way, an attempt was made to carry out the elemental determination of Cu in dried plasma spots (DPSs). However, there was an unknown interference hampering such determination that could not be resolved and corrected by least square background correction.

To overcome this problem, a new correction method that does not require the user to know the interfering species has been developed. It has been called time-absorbance profile (TAP) correction. It is based on the fact that the time-absorbance profile of a species, measured under the same instrumental HR CS AAS conditions using a graphite furnace (GF) as the atomizer, should be the same at every wavelength measured. Therefore, using a TAP normalized spectrum of the interfering species should be sufficient to subtract it from the normalized absorbance of the atomic line, leaving only the analytical signal of the analyte for quantification. This novel approach enabled Cu determination in DPSs created after deposition of whole blood Seronorm RMs.

A new micro-analysis method for Cu concentration in liquid sample *via* single quad ICP-MS was also developed. The method consisted in the direct injection of $1 \mu\text{L}$ of pretreated serum samples into an ICP-MS. The injection was carried out manually, introducing the μL with a micropipette into the peristaltic tube and working with a flow rate of $100 \mu\text{L min}^{-1}$. To improve the precision, Ni was used as internal standard (IS). The methods offered a LOD of $3 \mu\text{g L}^{-1}$.

Prior to the isotopic analysis *via* MC-ICP-MS, it is necessary to carry out a sample preparation to isolate the element of interest from the matrix to avoid possible interferences. For that

purpose, two different resins were tested, AG-MP1 and Triskem resin. Triskem resin provided better results for both Cu recovery and Na removal in only one separation than the AG-MP1 resin in two consecutive separations.

Three different methods for Cu isotopic microanalysis were also developed and evaluated. The first one was based on the coupling a femtosecond laser (fs-LA) to a multicollector-inductively coupled plasma mass spectrometry (MC-ICP-MS). The analysis was carried out using only 1 μL of pre-treated sample deposited onto a Si wafer. Two consecutive depositions of 0.5 μL of sample onto a mini-well of 1.8 mm diameter previously created by laser ablation of Si wafer were carried out. Cu isotopic analysis of NIST 3114 at 1 mg L^{-1} Cu concentration with the self-bracketing method provided average $\delta^{65}\text{Cu}$ values of $-0.01 \pm 0.19\text{‰}$ (2SD). The ratios were calculated using the point-by-point (PBP) method, after time lag detector correction (TDC).

The second method deployed a commercially available electrothermal vaporization (ETV) device coupled to a MC-ICP-MS. Analyses were performed using 5 μL of pre-treated sample using Pt as modifier. Cu isotopic analysis of NIST 3114 at 1 mg L^{-1} of Cu, using self-bracketing, provided average $\delta^{65}\text{Cu}$ values of $0.00 \pm 0.17\text{‰}$ (2SD, $n=10$). In this case, the ratios were also calculated using the PBP method after TDC. Moreover, a criterion to reject potential outliers was proposed and applied.

The third method was similar way to the method for Cu elemental determination *via* ICP-MS. Here 3 μL of pre-treated sample were injected instead of 1 μL , and the sample was introduced by self-aspiration into the MC-ICP-MS (no peristaltic pump was used) to improve stability. Moreover, to improve the sensitivity a desolvator system (Aridus 3) was used. The analysis of NIST 3114 at 1 mg L^{-1} of Cu was carried out resulting in a $\delta^{65}\text{Cu}$ values of $0.11 \pm 0.19\text{‰}$ (2SD, $n=10$), using self-bracketing and Ni as IS. The ratios were calculated using the linear regression slope method (LRS).

The information obtained by Cu determination and Cu isotopic analysis can be useful when investigating Wilson's disease. It can provide a better understanding of the metabolism of Cu in general and, especially, for WD patients. It may also result in an easier way diagnose and follow up of WD patients. Thus, samples of WD patients under different treatments (chelators and/or Zn salts), healthy people (controls), patients with liver diseases different from WD, and newborns (NB) have been analyzed.

Elemental analyses were carried out in both bulk serum (total Cu) and exchangeable Cu fractions (Cu Exch). Cu Exch is the fraction of Cu that is not bound to ceruloplasmin, which means that this Cu fraction is bound to albumin and to a lesser extent, to transcuprein (alpha-2-macroglobulin) (α -2M)), and to other amino acids. It is easily complexed with high-Cu-affinity chelating agents such as EDTA. Moreover, relative exchangeable Cu (REC) was calculated.

The results obtained for Cu concentration in bulk serums samples generally show lower values for WD than for the rest of the group tested. However, overlaps have been observed, especially with NB, while the results obtained in the Cu Exch fraction did not show significant differences between the groups tested. However, higher values seem to be linked to acute liver disease.

Relative exchangeable copper (REC) was calculated dividing the Cu Exch by the total Cu expressed in %. In this case, the results showed that all the WD patients showed a REC higher than 17%, while the rest had lower REC values.

On the other hand, Cu isotopic analysis in both fractions (bulk serum and Cu Exch fraction) was carried out.

The results of $\delta^{65}\text{Cu}$ obtained in whole serum and in the Cu Exch fractions followed the same trend. $\delta^{65}\text{Cu}$ values were lower for WD patients under chelating treatment and for patients with hepatic problems than for WD under Zn treatments, controls, and NBs.

The $\delta^{65}\text{Cu}$ values obtained for samples originating from WD patients obtained at the moment of the diagnosis were similar to the values found for the WD patient under Zn treatment. It should be noted that that these patients were asymptomatic. Hence, the decreased $\delta^{65}\text{Cu}$ seems to be linked to Cu release from the liver.

Based on these results, it appears that REC is the only parameter that can be readily used for WD diagnosis. The rest of parameters ($\delta^{65}\text{Cu}$, Cu concentration) seems to be useful to follow up the evolution of the treatment, to detect possible cases of non-compliance with the treatments or to be used as a marker of liver damage.

Resumen

La biomonitorización de diferentes elementos/moléculas es importante para controlar el estado de salud. Mediante el análisis de los biomarcadores, es posible detectar niveles anormales en el organismo, y predecir las consecuencias para tomar las medidas adecuadas, en el caso de que los niveles de los biomarcadores se desvíen significativamente de los valores de referencia. Además, la biomonitorización es fundamental para el seguimiento de los pacientes, sobre todo cuando están bajo un tratamiento, para asegurar una correcta interacción con los fármacos.

Por lo general, la biomonitorización se lleva a cabo mediante muestras de sangre recogidas por venopunción. Esta forma de recoger la muestra es invasiva y requiere la recogida de al menos algunos mililitros de sangre. Además, requiere que los pacientes se tengan que desplazar al hospital o al laboratorio de análisis clínico, ya que este tipo de muestras deben ser recogidas por personas cualificadas y en condiciones controladas. Como consecuencia, la toma de muestras convencional para los análisis de rutina es una tarea tediosa, especialmente para los recién nacidos (debido a que la disponibilidad de muestras es muy limitada) y para los pacientes que viven en zonas remotas, o con movilidad limitada que, debido a sus requisitos personales/logísticos, pueden encontrar inconvenientes para poder desplazarse.

Para intentar resolver estos problemas, han surgido nuevas tendencias pensando en el paciente. Podría decirse que existe una tendencia hacia la medicina personalizada. La intención es que la toma de muestras sea lo menos invasiva posible para evitar que los pacientes sufran un dolor y/o estrés importante. Además, otro objetivo consiste en minimizar o evitar por completo los desplazamientos de los pacientes al laboratorio para realizar los análisis rutinarios.

En este sentido, se están investigando continuamente nuevos dispositivos de muestreo que sólo necesitan unos pocos μL de muestra (micromuestreo) y que, además, pueden ser utilizados por el paciente y, si es posible, que proporcionen resultados rápidamente, incluso en tiempo real. En la práctica, esto se cubre con dos grandes campos de investigación: los biosensores y las manchas de matriz seca (DMS), en los cuales la muestra se deposita en un papel de filtro, se seca a

temperatura ambiente y, una vez seca, puede enviarse por correo ordinario al hospital o al laboratorio clínico para su análisis.

Paralelamente al desarrollo de nuevos dispositivos de micromuestreo, se han desarrollado sistemas alternativos de introducción de micromuestras que permiten reducir los límites de detección y utilizar el menor volumen de muestra posible, lo que a su vez reduce el uso de reactivos químicos, residuos generados, etc. Algunos de los sistemas de introducción de micromuestras desarrollados son el análisis por inyección de flujo (FIA), los micronebulizadores, la ablación por láser (LA) y los sistemas de vaporización/atomización electrotérmica (ETV/ETA).

Este tipo de sistemas de introducción de micromuestras pueden utilizarse para el análisis elemental acoplado a diferentes técnicas como la espectrometría de absorción atómica (AAS), la espectrometría de emisión óptica por plasma acoplado inductivamente (ICP-OES) y la espectrometría de masas por plasma acoplado inductivamente (ICP-MS), entre otras. También para el análisis isotópico pueden acoplarse a técnicas de espectrometría de masas como la espectrometría de masas por ionización térmica (TIMS) y la espectroscopia de masas por plasma de acoplamiento inductivo con multicolector (MC-ICP-MS).

El Cu es un metal esencial que interviene en muchas reacciones metabólicas. Además, está relacionado con la enfermedad de Wilson (WD). La enfermedad de Wilson está causada por la mutación del gen ATP7B. Esta mutación provoca la síntesis de una proteína ATP7B disfuncional, que ayuda a la transferencia de iones de Cu a la principal proteína plasmática de Cu (ceruloplasmina). Además, participa en el proceso de excreción de Cu en la bilis. Cuando esta función se altera, los niveles de Cu libre comienzan a acumularse en el hígado y en otros órganos del cuerpo, como el cerebro, los ojos (anillos de Kayser-Fleischer), los riñones, etc. Esta enfermedad puede ser mortal si no se trata. Aunque el tratamiento es relativamente sencillo y eficaz, el problema es poder diagnosticar la enfermedad a tiempo, antes de que aparezcan los síntomas.

En este contexto, se han desarrollado diferentes métodos en el marco de esta tesis tanto para la determinación elemental del Cu como para el análisis isotópico del mismo, centrándose en el micromuestreo.

En particular, se han desarrollado y evaluado dos métodos para el análisis elemental del Cu, uno para el análisis directo de sólidos y otro para el análisis de muestras líquidas. Además, se han desarrollado y evaluado tres métodos para el análisis isotópico del Cu.

Para el análisis directo de sólidos, se ha evaluado el rendimiento del instrumento de espectrometría de absorción atómica de horno de grafito de fuente continua de alta resolución (HR CS GFAAS) y cuatro dispositivos novedosos para producir manchas de sangre seca de volúmenes perfectamente definidos (Mitra, HemaXis DB10, Capitainer qDBS y HemaPEN) con el objetivo de desarrollar un método sencillo y directo para la determinación del Cu en muestras de sangre.

La determinación del Cu se llevó a cabo mediante una simple calibración externa con estándares acuosos utilizando Pt como modificador. Para evaluar los métodos, se probaron los cuatro dispositivos diferentes con manchas de sangre seca (DBS) preparadas con tres materiales de referencia (RM) de sangre entera (WB), L-1, L-2 y L-3. En todos los casos, los resultados obtenidos coincidieron con los valores proporcionados por los RM. Sin embargo, se observó que la precisión dependía de los niveles de los blancos. Se obtuvieron mejores blancos para HemaXis DB10 y HemaPEN que para Capitainer qDBS y para Mitra. Por lo tanto, HemaXis DB10 y HemaPEN son especialmente útiles cuando se necesiten determinar niveles de Cu anormalmente bajos ($500 \mu\text{g L}^{-1}$ o menos), asociados a algunas enfermedades. Los resultados demuestran que se pueden conseguir valores precisos con valores de RSD inferiores al 10% para estos dispositivos incluso para tales niveles de Cu, mientras que para Capitainer qDBS y, en mayor medida, para Mitra, las variaciones en blanco acabarán aumentando la incertidumbre. Por último, se analizaron cuatro muestras de sangre real recogidas tanto por venopunción como por preparación de DBS para determinar la concentración de cobre. Los resultados obtenidos mostraron muy buena concordancia entre los DBS y la venopunción. Esto indica que el enfoque propuesto podría aplicarse fácilmente, de modo que los pacientes con trastornos que requieren el control del Cu pueden preparar sus propias muestras en casa y enviarlas por correo postal al laboratorio para el análisis directo y rápido *via* HR CS GFAAS.

Del mismo modo, se intentó llevar a cabo la determinación elemental del Cu en manchas de plasma seco (DPS). Sin embargo, existía una interferencia desconocida

que dificultaba dicha determinación y que no pudo ser resuelta ni corregida mediante la corrección de fondo por mínimos cuadrados (LSBC).

Para superar este problema, se ha desarrollado un nuevo método de corrección que no requiere que el usuario conozca las especies interferentes. Se ha denominado corrección del perfil de absorbancia en el tiempo (TAP). Se basa en el hecho de que el perfil de absorbancia en el tiempo de una especie, medido en las mismas condiciones instrumentales HR CS AAS utilizando un horno de grafito (GF) como atomizador, debería ser el mismo en cada longitud de onda medida. Por lo tanto, el uso de un espectro normalizado, TAP, de la especie interferente debería ser suficiente para restarla de la absorbancia normalizada de la línea atómica, dejando sólo la señal analítica del analito para la cuantificación. Este novedoso enfoque permitió la determinación del Cu en los DPSs creados tras la deposición de los RMs Seronorm de sangre entera.

También se desarrolló un nuevo método de microanálisis para la concentración de Cu en muestras líquidas mediante un cuadrupolo ICP-MS. El método consistió en la inyección directa de 1 μL de muestras de suero pretratadas en un ICP-MS. La inyección se realizó manualmente, introduciendo el μL con una micropipeta en el tubo peristáltico, trabajando a un flujo de 100 $\mu\text{L min}^{-1}$. Para mejorar la precisión, se utilizó Ni como estándar interno (IS). El método ofreció un LOD de 3 $\mu\text{g L}^{-1}$.

Antes del análisis isotópico mediante MC-ICP-MS, es necesario realizar una preparación de la muestra para aislar el elemento de interés de la matriz y evitar posibles interferencias. Para ello, se probaron dos resinas diferentes, la AG-MP1 y la resina Triskem. La resina Triskem proporcionó mejores resultados tanto en la recuperación del Cu como en la eliminación del Na en una sola separación que la resina AG-MP1 en dos separaciones consecutivas.

También se desarrollaron y evaluaron tres métodos diferentes para el análisis isotópico del Cu. El primero se basó en el acoplamiento de un láser femtosegundo (fs-LA) a un MC-ICP-MS. El análisis se llevó a cabo utilizando sólo 1 μl de muestra pretratada depositada en una lámina de Si. Se realizaron dos deposiciones consecutivas de 0,5 μL de muestra sobre un minipocillo de 1,8 mm de diámetro creado previamente por ablación láser de la lámina de Si. El análisis isotópico de Cu del NIST 3114 a una concentración de 1 mg L^{-1} de Cu con el método de auto-bracketing

proporcionó valores medios de $\delta^{65}\text{Cu}$ de $-0,01 \pm 0,19\%$ (2SD). Las relaciones isotópicas se calcularon utilizando el método punto por punto (PBP), tras la corrección aplicada para corregir el desfase temporal del detector (TDC).

El segundo método empleó un dispositivo de vaporización electrotérmica (ETV), disponible en el mercado, acoplado a un MC-ICP-MS. Los análisis se realizaron con 5 μl de muestra pretratada utilizando Pt como modificador. El análisis isotópico del Cu de la muestra NIST 3114 a 1 mg L^{-1} de Cu, utilizando el “*self-bracketing*”, proporcionó valores medios de $\delta^{65}\text{Cu}$ de $0,00 \pm 0,17\%$ (2SD, $n=10$). En este caso, los ratios se calcularon también con el método PBP después de TDC. Además, se propuso y se aplicó un criterio para rechazar posibles valores atípicos.

El tercer método fue similar al de la determinación elemental del Cu mediante ICP-MS. Aquí se inyectaron 3 μL de muestra pretratada en lugar de 1 μL , y la muestra se introdujo por autoaspiración (no se utilizó una bomba peristáltica) para mejorar la estabilidad. Además, para mejorar la sensibilidad se utilizó un sistema de desolvatación (Aridus 3). Se llevó a cabo el análisis del NIST 3114 a 1 mg L^{-1} de Cu, dando como resultado unos valores de $\delta^{65}\text{Cu}$ de $0,11 \pm 0,19\%$ (2SD, $n=10$), utilizando la autoaspiración y el Ni como IS. Las proporciones se calcularon mediante el método de la pendiente de la regresión lineal (LRS).

La información obtenida mediante la determinación del Cu y el análisis isotópico del Cu puede ser útil al investigar la enfermedad de Wilson (WD). Puede proporcionar una mejor comprensión del metabolismo del Cu en general y, especialmente, para los pacientes con WD. También puede facilitar el diagnóstico y el seguimiento de los pacientes con WD. En este trabajo, se han analizado muestras de pacientes con WD bajo diferentes tratamientos (quelantes y/o sales de Zn), de personas sanas (controles), de pacientes con enfermedades hepáticas diferentes a WD y de recién nacidos (NB).

Los análisis elementales se llevaron a cabo tanto en el suero total (Cu total) como en las fracciones de Cu intercambiable (Cu Exch). El Cu Exch es la fracción de Cu que no está unida a la ceruloplasmina, lo que significa que esta fracción de Cu está unida a la albúmina y, en menor medida, a la transcurreína (alfa-2-macroglobulina) (α -2M), y a otros aminoácidos. Se acompleja fácilmente con agentes quelantes de alta afinidad por el Cu, como el EDTA. También, se calculó el Cu intercambiable relativo (REC).

Los resultados obtenidos para la concentración de Cu en las muestras de sueros total muestran, en general, valores más bajos para WD que para el resto de grupos analizados. Sin embargo, se han observado solapamientos, especialmente con los recién nacidos, mientras que los resultados obtenidos en la fracción de Cu Exch no mostraron diferencias significativas entre los grupos analizados. Sin embargo, los valores más altos parecen estar relacionados con una enfermedad hepática aguda.

El cobre intercambiable relativo (REC) se calculó dividiendo el Cu Exch por el Cu total expresado en %. En este caso, los resultados mostraron que todos los pacientes con WD presentaban un REC superior al 17%, mientras que el resto tenía valores de REC inferiores.

Por otro lado, se llevó a cabo el análisis isotópico del Cu en ambas fracciones (suero total y fracción de Cu Exch).

Los resultados de $\delta^{65}\text{Cu}$ obtenidos en el suero total y en las fracciones de Cu Exch siguieron la misma tendencia. Los valores de $\delta^{65}\text{Cu}$ fueron más bajos para los pacientes con WD siguiendo un tratamiento con quelante y para los pacientes con problemas hepáticos que para los pacientes con WD siguiendo tratamientos con Zn, los controles y los recién nacidos.

Los valores de $\delta^{65}\text{Cu}$ obtenidos para las muestras procedentes de pacientes con WD obtenidas en el momento del diagnóstico fueron similares a los valores encontrados para el paciente con WD bajo tratamiento con Zn. Cabe destacar que estos pacientes eran asintomáticos. Por lo tanto, la disminución de $\delta^{65}\text{Cu}$ parece estar relacionada con la liberación de Cu desde el hígado.

En base a estos resultados, parece que el REC es el único parámetro que puede utilizarse fácilmente para el diagnóstico de la WD. El resto de parámetros ($\delta^{65}\text{Cu}$, concentración de Cu) parece ser útil para seguir la evolución del tratamiento, para detectar posibles casos de incumplimiento de los tratamientos o para ser utilizado como marcador de daño hepático.

Résumé

La biosurveillance de différents éléments/molécules est importante pour contrôler l'état de santé d'un individu. En analysant les biomarqueurs, il est possible de détecter des niveaux anormaux dans l'organisme, et de prévoir les conséquences pour prendre les mesures appropriées, dans le cas où les niveaux de biomarqueurs s'écartent significativement des valeurs de référence. Par ailleurs, la biosurveillance est essentielle pour le suivi des patients, notamment lorsqu'ils sont sous traitement, afin de garantir une interaction adéquate avec les médicaments.

Habituellement, la biosurveillance est effectuée à l'aide d'échantillons de sang prélevés par ponction veineuse. Cette méthode de collecte d'échantillons est invasive et nécessite le prélèvement d'au moins quelques millilitres de sang. De plus, les patients doivent se rendre à l'hôpital ou au laboratoire d'analyses médicales, car ce type d'échantillons doit être prélevé par des personnes qualifiées et dans des conditions contrôlées. Par conséquent, le prélèvement conventionnel pour les analyses de routine est une tâche fastidieuse, en particulier pour les nouveau-nés (en raison de la disponibilité très limitée des échantillons) et pour les patients qui vivent dans des régions éloignées, ou pour les patients à mobilité réduite qui, en raison de leurs exigences personnelles/logistiques, peuvent trouver cette approche peu pratique.

Pour tenter de résoudre ces problèmes, de nouvelles tendances ont vu le jour en tenant compte du confort du patient et s'orientant vers une médecine personnalisée. L'intention est que le prélèvement soit aussi peu invasif que possible afin d'éviter aux patients de souffrir de douleurs et/ou de stress importants. En outre, un autre objectif consiste à minimiser ou à éviter complètement les déplacements des patients au laboratoire pour effectuer les analyses de routine.

Ainsi, de nouveaux dispositifs d'échantillonnage qui ne nécessitent que quelques μL d'échantillon (micro-échantillonnage) et qui, en outre, peuvent être utilisés par le patient et, si possible, fournir des résultats rapidement, voire en temps réel, sont continuellement à l'étude. Dans la pratique, deux grands domaines de recherche sont concernés : les biocapteurs et les taches de matrice séchées (DMS), où l'échantillon est déposé sur un papier filtre, séché à température ambiante et, une fois séché, il

peut être envoyé par courrier ordinaire à l'hôpital ou au laboratoire d'analyse médicale pour analyse.

Parallèlement au développement de nouveaux dispositifs de micro-échantillonnage, d'autres systèmes d'introduction de micro-échantillons ont été mis au point, permettant d'abaisser les limites de détection et d'utiliser le plus petit volume d'échantillon possible, ce qui réduit l'utilisation de réactifs chimiques, les déchets générés, etc. Certains des systèmes d'introduction de micro-échantillons développés sont l'analyse par injection de flux (FIA), les micro-nébuliseurs, l'ablation laser (LA) et les systèmes de vaporisation/atomisation électrothermiques (ETV/ETA).

Ces systèmes d'introduction de micro-échantillons peuvent être utilisés pour l'analyse élémentaire couplée à différentes techniques telles que la spectrométrie d'absorption atomique (SAA), la spectrométrie d'émission optique à plasma à couplage inductif (ICP-OES) et la spectrométrie de masse à plasma à couplage inductif (ICP-MS), entre autres. Pour l'analyse isotopique, ils peuvent également être couplés à des techniques de spectrométrie de masse telles que la spectrométrie de masse par ionisation thermique (TIMS) et la spectroscopie de masse à plasma inductif multi-collecteurs (MC-ICP-MS).

Le cuivre est un métal essentiel qui intervient dans de nombreuses réactions métaboliques. Il est en particulier lié à la maladie de Wilson (WD) causée par la mutation du gène ATP7B. Cette mutation entraîne la synthèse d'une protéine ATP7B dysfonctionnelle. La protéine ATP7B facilite en temps normal le transfert des ions Cu vers la principale protéine plasmatique Cu (céruloplasmine). De plus, elle est impliquée dans le processus d'excrétion du Cu dans la bile. Lorsque cette fonction est altérée, les niveaux de Cu libre commencent à s'accumuler dans le foie et dans d'autres organes du corps, tels que le cerveau, les yeux (anneaux de Kayser-Fleischer), les reins, etc. Cette maladie peut être mortelle si elle n'est pas traitée. Bien que le traitement soit relativement simple et efficace, le problème est de pouvoir diagnostiquer la maladie suffisamment tôt, avant l'apparition des symptômes.

Dans ce contexte, différentes méthodes ont été développées dans le cadre de cette thèse pour la détermination élémentaire du Cu et pour l'analyse isotopique du Cu, en mettant l'accent sur le micro-échantillonnage.

En particulier, deux méthodes ont été développées et évaluées pour l'analyse élémentaire du Cu, une pour l'analyse directe des solides et l'autre pour l'analyse des échantillons liquides. De plus, trois méthodes ont été développées et évaluées pour l'analyse isotopique du Cu.

Pour l'analyse directe des solides, les performances de l'instrumentation de pointe de spectrométrie d'absorption atomique à source continue à haute résolution (HR CS GFAAS) et de quatre nouveaux dispositifs permettant de produire des taches de sang séché de volumes parfaitement définis (Mitra, HemaXis DB10, Capitainer qDBS et HemaPEN) ont été évaluées dans le but de développer une méthode simple et directe pour la détermination du Cu dans les échantillons de sang.

La détermination du Cu a été réalisée par un simple étalonnage externe avec des étalons aqueux utilisant le Pt comme modificateur. Pour évaluer les méthodes, les quatre différents dispositifs ont été testés sur des taches de sang séché (DBS) préparées avec trois matériaux de référence (RM) de sang total (WB), L-1, L-2 et L-3. Dans tous les cas, les résultats obtenus étaient en bon accord avec les valeurs fournies par les RM. Cependant, nous avons constaté que la précision dépendait des niveaux de cuivre dans les blancs. De meilleurs blancs ont été obtenus pour HemaXis DB10 et HemaPEN que pour Capitainer qDBS et Mitra. Ainsi, l'HemaXis DB10 et l'HemaPEN devraient être préférés lorsque des niveaux de Cu anormalement bas ($500 \mu\text{g L}^{-1}$ ou moins), associés à certaines maladies, doivent être déterminés. Les résultats démontrent que des valeurs précises avec des valeurs RSD inférieures à 10% peuvent être obtenues pour ces appareils même pour de tels niveaux de Cu, alors que pour le Capitainer qDBS et, dans une plus large mesure, pour le Mitra, les variations du blanc augmenteront finalement l'incertitude. Enfin, quatre échantillons de sang réels collectés à la fois par ponction veineuse et par préparation DBS ont été analysés pour la concentration en cuivre. Les résultats obtenus ont montré une très bonne concordance entre le DBS et la ponction veineuse. Cela indique que l'approche proposée pourrait être facilement appliquée, de sorte que les patients souffrant de troubles nécessitant un contrôle du Cu peuvent préparer leurs propres échantillons et les envoyer par courrier postal au laboratoire pour une analyse directe et rapide par HR CS GFAAS.

De la même manière, une tentative a été faite pour effectuer la détermination élémentaire du Cu dans les taches de plasma séché (DPS). Cependant, une

interférence inconnue gênait cette détermination et ne pouvait être résolue et corrigée par la correction du fond par les moindres carrés.

Pour surmonter ce problème, une nouvelle méthode de correction ne nécessitant pas que l'utilisateur connaisse l'espèce interférente a été développée. Elle a été appelée correction du profil temps-absorbance (TAP). Elle est basée sur le fait que le profil temps-absorbance d'une espèce interférente, mesuré dans les mêmes conditions instrumentales HR CS AAS utilisant un four en graphite (GF) comme atomiseur, devrait être le même à chaque longueur d'onde mesurée. Par conséquent, l'utilisation d'un spectre normalisé, TAP, de l'espèce interférente devrait suffire à la soustraire de l'absorbance normalisée de la raie atomique, ne laissant que le signal analytique de l'analyte pour la quantification. Cette nouvelle approche a permis la détermination du Cu dans les DPSs créés après le dépôt de RMs Seronorm de sang total.

Une nouvelle méthode de micro-analyse pour la concentration de Cu dans un échantillon liquide via un ICP-MS à quadruple voie a également été développée. La méthode consistait en l'injection directe de 1 μL d'échantillons de sérum prétraités dans un ICP-MS. L'injection a été réalisée manuellement, en introduisant un microlitre d'échantillon avec une micropipette dans le tube péristaltique et en travaillant avec un débit de 100 $\mu\text{L min}^{-1}$. Pour améliorer la précision, Ni a été utilisé comme étalon interne (IS). Les méthodes ont offert une limite de détection de 3 $\mu\text{g L}^{-1}$.

Avant l'analyse isotopique par MC-ICP-MS, il est nécessaire d'effectuer une préparation de l'échantillon pour isoler l'élément d'intérêt de la matrice afin d'éviter d'éventuelles interférences. A cette fin, deux résines différentes ont été testées, AG-MP1 et la résine Triskem. La résine Triskem a donné de meilleurs résultats pour la récupération du Cu et l'élimination du Na en une seule séparation que la résine AG-MP1 en deux séparations consécutives.

Trois méthodes différentes de microanalyse isotopique du Cu ont également été développées et évaluées. La première était basée sur le couplage d'un laser femtoseconde (fs-LA) avec une spectrométrie de masse à plasma inductif multicollection (MC-ICP-MS). L'analyse a été réalisée en utilisant seulement 1 μL d'échantillon prétraité déposé sur un wafer de silicium. Deux dépôts consécutifs de 0,5 μL d'échantillon sur un mini-puits de 1,8 mm de diamètre préalablement créé par ablation laser d'un wafer de silicium ont été effectués. L'analyse isotopique du Cu du

NIST 3114 à une concentration de 1 mg L^{-1} de Cu avec la méthode de l'auto-bracketing a fourni des valeurs moyennes de $\delta^{65}\text{Cu}$ de $-0,01 \pm 0,19\text{‰}$ (2SD). Les rapports ont été calculés par la méthode point par point (PBP), après correction décalage temporel des détecteurs (TDC).

La deuxième méthode met en œuvre un dispositif de vaporisation électrothermique (ETV) disponible dans le commerce, couplé à un MC-ICP-MS. Les analyses ont été réalisées en utilisant $5 \mu\text{L}$ d'échantillon prétraité avec du Pt comme modificateur. L'analyse isotopique du Cu du NIST 3114 à 1 mg L^{-1} de Cu, en utilisant l'auto-bracketing, a fourni des valeurs moyennes de $\delta^{65}\text{Cu}$ de $0,00 \pm 0,17\text{‰}$ (2SD, $n=10$). Dans ce cas, les ratios ont également été calculés par la méthode PBP après le TDC. De plus, un critère de rejet des valeurs aberrantes potentielles a été proposé et appliqué.

La troisième méthode était similaire à la méthode de détermination élémentaire du Cu par ICP-MS. Ici, $3 \mu\text{L}$ d'échantillon prétraité ont été injectés au lieu de $1 \mu\text{L}$, et l'échantillon a été introduit dans le MC-ICP-MS par auto-aspiration (aucune pompe péristaltique n'a été utilisée) pour améliorer la stabilité. De plus, pour améliorer la sensibilité, un système de désolvateur (Aridus 3) a été utilisé. L'analyse du NIST 3114 à 1 mg L^{-1} de Cu a été effectuée, ce qui a donné des valeurs de $\delta^{65}\text{Cu}$ de $0,11 \pm 0,19\text{‰}$ (2SD, $n=10$), en utilisant l'auto-aspiration et le Ni comme IS. Les ratios ont été calculés par la méthode de la pente de régression linéaire (LRS).

Les informations obtenues par la détermination du Cu et l'analyse isotopique du Cu peuvent être utiles lors de l'étude de la maladie de Wilson. Elles peuvent permettre de mieux comprendre le métabolisme du Cu en général et, en particulier, celui des patients atteints de la maladie de Wilson. Elles peuvent également faciliter le diagnostic et le suivi des patients atteints de la maladie de Wilson. Ainsi, des échantillons de patients atteints de la maladie de Wilson sous différents traitements (chélateurs et/ou sels de zinc), de personnes saines (témoins), de patients atteints de maladies hépatiques différentes de la maladie de Wilson et de nouveau-nés ont été analysés.

Les analyses élémentaires ont été effectuées à la fois dans le sérum brut (Cu total) et dans les fractions de Cu échangeable (Cu Exch). Cu Exch est la fraction de Cu qui n'est pas liée à la céruloplasmine, ce qui signifie que cette fraction de Cu est liée à

l'albumine et, dans une moindre mesure, à la transcupréine (alpha-2-macroglobuline) (α -2M)), et à d'autres acides aminés. Il est facilement complexé par des agents chélateurs à haute affinité pour le Cu, comme l'EDTA. En outre, le Cu échangeable relatif (REC) a été calculé.

Les résultats obtenus pour la concentration globale de Cu dans les échantillons de sérums montrent généralement des valeurs plus faibles pour les malades atteints de la maladie de Wilson (WD) que pour le reste du groupe testé. Cependant, des chevauchements ont été observés, notamment avec les nouveau-nés (NBs), tandis que les résultats obtenus dans la fraction Cu Exch n'ont pas montré de différences significatives entre les groupes testés. Cependant, des valeurs plus élevées semblent être liées à une maladie hépatique aiguë.

Le cuivre échangeable relatif (REC) a été calculé en divisant le Cu Exch par le Cu total exprimé en %. Dans ce cas, les résultats ont montré que tous les patients WD présentaient un REC supérieur à 17%, tandis que les autres avaient des valeurs REC inférieures.

D'autre part, une analyse isotopique du Cu dans les deux fractions (sérum total et fraction Cu Exch) a été réalisée.

Les résultats de $\delta^{65}\text{Cu}$ obtenus dans le sérum total et dans les fractions Cu Exch ont suivi la même tendance. Les valeurs de $\delta^{65}\text{Cu}$ étaient plus faibles pour les patients WD sous traitement chélateur et pour les patients ayant des problèmes hépatiques que pour les WD sous traitements Zn, les contrôles et les nouveau-nés.

Les valeurs de $\delta^{65}\text{Cu}$ obtenues pour les échantillons provenant de patients atteints de WD obtenus au moment du diagnostic étaient similaires aux valeurs trouvées pour le patient WD sous traitement au Zn. Il faut noter que ces patients étaient asymptomatiques. Par conséquent, la diminution du $\delta^{65}\text{Cu}$ observé semble être liée à la libération de Cu par le foie.

Sur la base de ces résultats, il apparaît que le REC est le seul paramètre qui peut être facilement utilisé pour le diagnostic du WD. Les autres paramètres ($\delta^{65}\text{Cu}$, concentration de Cu) semblent être utiles pour suivre l'évolution du traitement, pour détecter d'éventuels cas d'un mauvais suivi de la prescription médicale de la part du patient ou pour être utilisés comme marqueur de l'atteinte hépatique.

List of Figures

Chapter 1.

Figure 1. Categories of biosensors.

Figure 2. A) Mitra device; B) Capitainer dDBS device; C) HemaPEN device, D) HemaXis DB10 device and E) Touch-activated phlebotomy.

Figure 3. Schematic illustration of the procedure of the plasma extraction card.

Figure 4. Schemes of basic flow injection systems: A) normal flow injection analysis system (FIA), B) reversed flow injection analysis system (rFIA), C) multicommutated flow analysis with multichannel pump system (MCFA), D) multi-pumping flow analysis system, E) multisyringe flow injection analysis system (MSFIA), F) sequential injection analysis system (SIA) and G) batch injection analysis system (BIA).

Figure 5. Different pneumatic nebulizers. A) Conventional concentric nebulizer, B) concentric nebulizer with recessed capillary, C) parallel-path nebulizer, D) cross-flow nebulizer, E) V-groove nebulizer and F) flow-focusing/blurring nebulizer.

Figure 6: Comparison of standard concentric tip with micro-flow HEN nebulizer tip.

Figure 7: Schematic illustration of Aridus desolvating nebulizer system from CETAC Technologies.

Figure 8. Electrothermal vaporization device (ETV) from Spectral Systems, Fürstfeldbruck, Germany.

Figure 9. Diagram of a laser cavity.

Figure 10. Schematic of a laser ablation system, using ICP-OES and/or ICP-MS detection.

Figure 11. Laser-matter interactions in both a) nanosecond laser and b) femtosecond pulse lasers. Images show the ablation of polished brass c) with a nanosecond laser and d) with a femtosecond laser. Note that Fig 11a and 11b is an artwork that might

be confusing, as it does not take into account any time scale: for instance laser pulse duration is in the nanosecond range while particles are ejected few microseconds after the pulse. In the same vein, cracks might appear few milliseconds and even few seconds after the pulse.

Figure 12. Effect of the thermal conductivity of gas on the size of the plasma created on the sample surface and the growth of particles.

Figure 13. Dose-response diagram for an essential element.

Figure 14. Diagram of the main components that constitute an atomic absorption spectrometer.

Figure 15 Scheme of the components that make up the HR CS AAS spectrometer.

Figure 16. Scheme of the processes carried out by the sample inside/near the plasma.

Figure 17. Optical diagram of a sequential ICP optical emission spectrometer. All moving parts are under computer control, and their modes of motion are indicated by the three-dimensional arrows. Moving parts include the grating, a mirror for transducer selection, a refractor plate for optimizing signal throughput, and a viewing mirror to optimize the plasma viewing position. The spectrometer contains a mercury lamp for automatic wavelength calibration.

Figure 18. Scheme of a quadrupole mass filter.

Figure 19. Scheme of a thermal ionization mass spectrometer.

Figure 20. Scheme of a multi-collector inductively coupled plasma mass spectrometer.

Figure 21. Diagram of Cu metabolism.

Chapter 3

Figure 1. Mitra device without blood (left) and after collection of approximately 10 μL of blood (right).

Figure 2. HemaXis DB10 device: (a) empty; (b) microfluidic chips filled with blood (approximately 10 μL each); (c) after the device is closed and blood is deposited onto the filter paper for DBS production.

Figure 3. Capitainer qDBS device: (a) empty; (b) after blood deposition onto the indicated area; (c) DBSs produced after deposition of blood (approximately 10 μL) onto the filter paper found in the back of the device.

Figure 4. HemaPEN device: (a) fully commercial HemaPEN; (b) empty QCPEN (inner part of commercial HemaPEN); (c) QCPEN with microcapillaries filled with blood (approximately 2.74 μL each); (d) after deposition of blood onto the filter paper for DBS production.

Figure 5. Deposition of DBSs onto the graphite platform before its introduction into the graphite furnace for subsequent HR CS GFAAS analysis. a) Mitra, b) HemaXis DB10, c) Capitainer qDBS and d) HemaPEN.

Figure 6. Devices after GFAAS temperature programme (See **Table 1**). a) Mitra using Pd; b) Mitra using Pt; c) HemaXis DB10 using Pt; d) Capitainer qDBS using Pt and e) HemaPEN using Pt.

Figure 7. Atomization and pyrolysis temperature optimization. The error bars represent the standard deviation ($n=5$).

Figure 8. Time-resolved absorbance profile of the three central pixels, without blank correction, obtained from the optimization of the atomization temperature setting the pyrolysis temperature at 1300 $^{\circ}\text{C}$ for: a) Mitra, b) HemaXis DB10 and c) Cu standard solution.

Figure 9. Time-resolved absorbance profile of the three central pixels, without blank correction, obtained using the temperature program shown in **Table 1** for DBSs produced *via* Capitainer qDBS ($\lambda=249.215$ nm) and for HemaPEN. ($\lambda=222.570$ nm).

Chapter 4.

Figure 1. Wavelength- and time-resolved spectra recorded in the vicinity of 217.000 nm (spectral window = 0.28 nm) for: (A) 0.1 ng Pb and 10 μg P; (B) 10 μg P; and (C)

Figure 1A corrected spectrum using LSBC. All the measurements were carried out using 5 μg Pd + 0.5 μg Mg as chemical modifiers. $T_{\text{pyrolysis}} = 800\text{ }^{\circ}\text{C}$, $T_{\text{atomization}} = 1600\text{ }^{\circ}\text{C}$.

Figure 2. PO molecule absorption spectra recorded in the vicinity of 217.000 nm (spectral window = 0.28 nm) for: (A) 10 μg P; (B) 1.0 μg P; and (C) **Figure 2A** corrected spectrum using **Figure 2B** as reference for LSBC. All the measurements were carried out using 5 μg Pd + 0.5 μg Mg as chemical modifiers. $T_{\text{pyrolysis}} = 800\text{ }^{\circ}\text{C}$, $T_{\text{atomization}} = 1600\text{ }^{\circ}\text{C}$.

Figure 3. Time-resolved spectra of the PO molecule from **Figure 1A** (vicinity of 217.000 nm, spectral window 0.28 nm) for 12 different detection pixels (labelled “p” plus pixel number).

Figure 4. Time-resolved spectrum of pixel 71 ($\lambda = 216.958\text{ nm}$) from **Figure 1A**, showing every absorbance value obtained from the CCD detector each $\sim 0.07\text{ s}$ (red squares).

Figure 5. Time-resolved spectra of the PO molecule shown in **Figure 3** (vicinity of 217.000 nm, spectral window 0.28 nm) for 12 different detection pixels normalized to each t_{max} (labelled “np” plus pixel number), and the average normalized absorbance (red-dashed line).

Figure 6. (A) Time-resolved spectrum for the pixel 101 from **Figure 1A** (vicinity of 217.000 nm, spectral window 0.28 nm) showing the overlap of the PO molecule and the Pb absorbance profiles; and (B) the normalized **Figure 6A** spectrum (np 101, black line), the TAP correction model (red-dashed line, see **Figure 5**), and the corrected normalized spectrum (blue line) obtained by subtracting the TAP model from np101.

Figure 7. Time- and wavelength-resolved spectrum from **Figure 1A** (vicinity of 217.000 nm, spectral window 0.28 nm) corrected using TAP correction model.

Figure 8. Time-resolved spectra of the sum of the three central pixels (100,101 and 102) of **Figure 1A** (vicinity of 217.000 nm, spectral window 0.28 nm) after correction with LSBC (black line) and TAP (red line).

Figure 9. Time- and wavelength-resolved spectra recorded in the vicinity of Cu analytical line 222.570 nm (spectral window 0.15 nm) for: (A) DPS blank (without blood); (B) DPS of whole blood L-1; (C) spectrum of **Figure 9B** corrected using LSBC with DPS blank (**Figure 9A**) as reference; and (D) spectrum of **Figure 9B** corrected using TAP correction. The temperature program is displayed in **Table 1**.

Figure 10. Time-resolved spectra of the Cu atomic line recorded at 222.570 nm (spectral window 0.15 nm) for DPS of whole blood L-1. The sum of the 3 central pixels is represented. The black line represents the raw spectrum, the red-dashed line is the TAP model, and the blue line shows the final, corrected spectra.

Figure S1. Time-resolved raw and corrected spectrum of 0.1 ng Pb at 217.000 nm (5 μg Pd+0.5 μg Mg) using TAP correction with P mass (as PO molecular interference) of (A) 10 μg , (B) 50 μg , and (C) 100 μg . The value is the mean integrated absorbance of three measurements, and the uncertainty is the standard deviation.

Chapter 5.

Figure 1. Example of two transient signals obtained with two consecutive injections of 1 μL of a solution containing 1 mg L^{-1} Cu and 50 $\mu\text{g L}^{-1}$ Ni at a flow rate of 100 $\mu\text{L min}^{-1}$. Conditions shown in **Table 2** for TRA analysis were used. The first peak corresponds to the 1 μL droplet introduction in the ICPMS. The second peak corresponds to the rinsing of the tubing after the 2% HNO_3 solution is reconnected to the peristaltic tube.

Figure 2. Optic microscope images of the Si wafers after ablation. A) Ablation with a space between spots of 10 μm (20 kHz, 200 mm s^{-1}) and B) ablation with a space between spots of 5 μm (20 kHz, 100 mm s^{-1}).

Figure 3. fs-LA-MC-ICP-MS image of 100 ng of Cu (double deposition of 0.5 μL of 100 mg L^{-1} onto pre ablated Si wafer heated at 80°C. A) Image of the uncorrected isotopic composition ($^{65}\text{Cu}/^{63}\text{Cu}$) B) Image of ^{63}Cu signal intensity and C) Image of ^{65}Cu signal intensity.

Figure 4. Example of transient signal obtained for ablation of 1 μL of a Cu standard solution of 4 mg L^{-1} (4 ng of Cu) deposited onto a silicon wafer and using the conditions described in section 3.3.2. A) before time drift correction and B) after time drift correction. The signal profile is represented by the blue points, while the red bars

represent the integration limits. Green points (A) and navy-blue points (B) represent the individual ratios calculated point by point (1 point every 0.5 s) before and after time drift correction, respectively.

Figure 5. Concentration vs. isotopic information plot for the serum samples of the 5 different groups considered in the investigation. Isotope ratios presented were obtained with the fs-LA-MC-ICP-MS method. Uncertainties on the delta values are expressed as 2SD on the average value obtained for the five different replicates (n = 5) carried out for every sample.

Figure S1: Schematic of the 1 μl injection process.

Figure S2. Cu calibration curves using the analytical protocol described in S1 A) without IS correction and B) with correction of Ni as IS.

Figure S3. A) Elution profile for selected elements using AG-MP1 resin (Bio-Rad). B) Elution profile for selected elements using Cu-specific resin (Triskem). The Clincheck whole blood reference material L-3 (as described in section 2.3) was measured.

Figure S4. A) Cu recovery in 3 different reference materials after 2 consecutive separations using AG-MP1 (orange bars) and only one separation step employing the Cu-specific resin (Triskem) (green bars). B) Na removal in 3 different reference materials after 2 consecutive separations using AG-MP1 (orange bars) and only one separation step employing the Cu-specific resin (Triskem) (green bars). Two replicates were carried out per sample.

Chapter 6.

Figure 1. Example of transient signals of both ^{65}Cu (red) and ^{63}Cu (blue) isotopes obtained using 5 μL of a Cu standard of 1 mg L^{-1} (5 ng of Cu) and 10 μL of a Pd standard of 1 g L^{-1} carried out with a temperature program with $T_{\text{pyrolysis}} = 350\text{ }^{\circ}\text{C}$ and A) $T_{\text{vaporization}} = 600\text{ }^{\circ}\text{C}$ and B) $T_{\text{vaporization}} = 700\text{ }^{\circ}\text{C}$.

Figure 2. Examples of transient signals with their respective representations of the individual ratios calculated for each point (1 point every 0.5s) for 5 μL of a solution of 0.5 mg L^{-1} of Cu prepared with the NIST SRM 3114 + 10 μL of 1 g L^{-1} of Pd. In all cases, the conditions used were the same ($T_{\text{pyrolysis}} = 350\text{ }^{\circ}\text{C}$ and $T_{\text{vaporization}} =$

600 °C). (A) Typical ratio profile; (B) ratio profile altered but with a slight drop; and (C) ratio profile altered with a more pronounced drop. The portion of the signal using for calculation is represented between the red bars.

Figure 3. Example of application of the exclusion criterion.

Figure 4. Example of transient signal obtained for the introduction with an ETV of 5 µL of a 4 mg L⁻¹ (20 ng of Cu) Cu standard solution A) before time drift correction and B) after time drift correction. The signal profile is represented by the blue points, while the red bars represent the data processing limits. Green points (A) and navy-blue points (B) represent the individual ratios calculated point by point (1 point every 0.5 s) before and after time drift correction, respectively.

Figure 5. Correlation analysis for the $\delta^{65}\text{Cu}$ (‰) values obtained for the same samples analyzed by the ETV-MC-ICP-MS and *via* fs-laser-MC-ICP-MS. Error bars represent external precision as 2SD (n=5). The black line represents a perfect agreement (slope=1), while the red line represents the actual regression.

Chapter 7.

Figure 1. Results of total Cu determination of serum samples of the four different groups considered in this study after Cu isolation step with Cu specific resin (Triskem). C refers to control samples, HD to hepatic disease patients, NB to newborns and WD to Wilson's disease patients.

Figure 2. Results of Cu Exch levels of serum samples of the four different groups considered in this work. C refers to control samples, HD to hepatic disease patients, NB to newborns and WD to Wilson's disease patients.

Figure 3. Results of REC of serum samples of the 4 different groups considered in the current work. C refers to control samples, HD to hepatic disease patients, NB to newborns and WD to Wilson's disease patients.

Figure 4. Boxplot obtained for Cu isotopic composition, expressed as $\delta^{65}\text{Cu}$ (‰) of both fractions of serum samples analyzed (Bulk serum, dark colors, and Cu Exch fraction, light colors) for the six different groups considered in this investigation. Where, C refers to control samples, HD to hepatic disease patients, NB to newborns and WD-C to Wilson's disease patients under chelator treatment, WD-Zn to Wilson's disease patients under zinc salts treatment and WD to Wilson's disease patients at the moment of diagnosis,

Figure 5. Boxplot obtained for $\Delta^{65}\text{Cu}$ (‰) for the six different groups considered in the current study. C refers to control samples, HD to hepatic disease patients, NB to newborns and WD-C to Wilson's disease patients under chelator treatment, WD-Zn to Wilson's disease patients under zinc salts treatment and WD to Wilson's disease patients at the moment of diagnosis,

Figure S1. Example of transient signal obtained with injections of 1 μL of a solution containing 1 mg L^{-1} Cu and 50 $\mu\text{g L}^{-1}$ Ni at a flow rate of 100 $\mu\text{L min}^{-1}$. Conditions shown in **Table 1** for TRA analysis were used. The first peak corresponds to the 1 μL droplet introduction in the ICPMS. The second peak corresponds to the rinsing of the tubing after the 2% HNO_3 solution is reconnected to the peristaltic tube.

Figure S2. Example of transient signal obtained when 3 μL of 1 mg L^{-1} sample is injected (3 ng of Cu). Cu ratios showed are uncorrected by Ni.

List of Tables

Chapter 1

Table 1. Classification of column chromatography methods.

Table 2. Routine tests for diagnosis of Wilson's disease.

Chapter 3

Table 1. Graphite furnace temperature program for Cu determination in DBS and liquid blood samples using HR CS GFAAS. Argon was used as purge gas.

Table 2. Figures of merit for the Cu determination using the current methods *via* HR CS GFAAS. For the method limits: 10 blank replicates were measured in each case, except for Mitra for which 15 measurements were carried out.

Table 3. Cu concentrations obtained for the analysis of the blank devices tested using the method described in section 2.4. Results are expressed as $\bar{x} \pm U$, where $U = (t s)/\sqrt{n}$; for a 95% confidence interval. The concentration was calculated considering the volume absorbed by each type of DBS device.

Table 4. Direct Cu determination in whole blood reference materials *via* HR CS GFAAS using different DBS devices. Results are expressed as $\bar{x} \pm U$, where $U = (t s)/\sqrt{n}$ for a 95% confidence interval. The concentration was calculated taking into account the volume absorbed by each type of DBS device.

Table 5. Results obtained for analysis of real blood samples both in liquid form and as DBS prepared with the different devices tested. Results are expressed as $\bar{x} \pm U$, where $U = (t s)/\sqrt{n}$ for a 95% confidence interval.

Table S1. Direct Cu determination in whole blood reference materials *via* HR CS GFAAS using different DBS filter papers. Results are expressed as $\bar{x} \pm U$, where $U = (t s)/\sqrt{n}$ for a 95% confidence interval. The concentration was calculated taking into account the volume absorbed by the DBS device (n=5).

Chapter 4.

Table 1. Temperature program for the different analyses carried out by means of HR CS GFAAS. The wavelength range (spectral window) of each analyte is in parenthesis after the wavelength.

Table 2. Integrated absorbance data obtained after three measurements of Pb at 217.00 nm (3 detection pixels, $CP \pm 1$) using 0.2 ng Pb (analyte), 5 μg Pd + 0.5 μg Mg (chemical modifiers) and 5 μg P (interference) by HR CS GFAAS.

Table 3. Determination of the Cu concentration at 222.570 nm in whole blood RMs as DPSs using ICP-MS (with Rh as internal standard) and HR CS GFAAS (either applying none or else two different correction models). Experimental uncertainties are expressed as 95% confidence intervals ($n=5$).

Chapter 5.

Table 1. Protocol for the Cu isolation with the anion exchange chromatography Cu specific resin (Triskem).

Table 2. ICP-MS Spectrometer setting and data acquisition parameters for the determination of total Cu in blood samples.

Table 3. Instrumental conditions for Cu isotopic analysis of serum using LA-MC-ICP-MS.

Table 4. Cu concentration obtained after Cu separation step in serum using Cu-specific resin (Triskem) and redissolution in 3 different volumes.

Table 5. Results obtained with the fs-LA-MC-ICP-MS method through the analysis of the NIST3114 at different concentrations using the PBP method for the isotopic calculation.

Table S1. Concentration of Cu, Na and Mg and percentage of Cu recovery and percentage of Na and Mg removal obtained after Cu separation step using Cu-specific resin (Triskem). Results are expressed as $\bar{x} \pm U$, where $U = (t_s) / \sqrt{n}$; for a 95% confidence interval ($n=5$).

Chapter 6.

Table 1. ETV temperature program and instrumental conditions for Cu isotopic analysis of serum using ETV-MC-ICP-MS.

Table 2. Results of the analysis of the NIST SRM 3114 at different concentrations.

Chapter 7.

Table 1. ICP-MS spectrometer settings and data acquisition parameters for the determination of total Cu and Cu Exch in serum samples.

Table 2. Protocol for Cu isolation with the anion exchange Cu specific resin (Triskem).

Table 3. Instrumental conditions for Cu isotopic analysis of serum using direct injection to MC-ICP-MS.

Table 4. Results obtained by the two laboratories for analysis of serum RM. Results are expressed as $\bar{x} \pm U$, where $U = (t.s)/\sqrt{n}$ for a 95% confidence interval.

Table 5. Results obtained with the μ -injection method through the analysis of the 3 μ L of NIST3114 after the two consecutive procedures at different concentrations using the LRS method for the isotopic calculation.

List of acronyms

α-2M - alpha-2-macroglobulin

AAS - Atomic absorption spectrometer

BIA - Batch injection analysis

C - Controls, healthy patients

CCDs - Charge coupled devices

COX - cytochrome C oxidase

CTR1 - Cu transporter 1

Cu Exch - Exchangeable copper

Cu UF - Ultrafiltrable Cu

CYBR1 - Cytochrome b reductase 1

DBS - Dried blood spot

DCN - Desmountable Capillary Nebulize

DIHEN - Direct injection high efficiency nebulizer

DIN - Direct injection nebulizers

DMS - Dried matrix spot

DMT1 - Divalent metal transporter 1

DOFs - Dried oral fluids

DPA - D-penicillamine

DPS - Dried Plasma Spot

DSS - Dried saliva spot

DUS - Dried urine Spots

ETA - Electrothermal atomization

ETAAS - Electrothermal atomic absorption spectrometer

ETV - Electrothermal vaporization

FAAS - Flame atomic absorption spectrometer

FIA - Flow injection analysis

FP - Filter paper

fs - femtosecond

GF - Graphite furnace

GFAAS - Graphite furnace absorption spectrometer

HBM - Human biomonitoring

hCG - Human chorionic gonadotrophin

HCLs - hollow cathode lamps

HD - Patients with hepatic disorders different from WD

HECFMN - High-Efficiency Cross-Flow Micronebulizer

HEN - High-Efficiency Nebulizer

HESIS - High-efficiency sample-introduction system

HR CS AAS - High resolution continuous source atomic absorption spectrometer

hTISIS - High temperature torch integrated sample introduction system

ICP - Inductively Coupled Plasma

ICP-MS - Inductively coupled plasma mass spectrometer

ICP-OES - Inductively coupled plasma optical emission spectrometer

ID – Isotopic dilution

IS - Internal standard

LA - Laser ablation

LE - Long-Evans rats

LEC - Long-Evans Cinnamon rats

LOD - Detection limit

LOQ - Quantification limit

LOV - Lab-on-valve

LRS - Linear Regression Slope

LSBC - Least-squares background correction

m/z -Mass-to-charge

MCFA - Multicommutated flow analysis

MCN - Microconcentric nebulizer

MD - Menkes disease

MM - MicroMist Nebulizer

MSFIA - Multisyringe flow injection analysis

NB - Newborns

OCN - Oscillating Capillary Nebulizer

OHS - Occipital horn syndrome

PBP - Point by point

PCDBS - Pre-cut dried blood spot

PFA - PFA Micronebulizer

REC - Relative exchangeable Cu

RF - Radio frequency

rFIA - Reverse flow injection analysis

RM - Reference materials

RSD - Relative standard desviation

SD - Standard desviation

SIA - Sequential injection analysis

SOD - Superoxide dismutase

SSB - Sample-standard bracketing

SSN - Sonic Spray Nebulizer

STEAP - 6-transmembrane epithelial antigen of the prostate family protein

TAP - Time-absorbance profile

TDC - Time Drift Correction or time lag detector correction

TETA - Trientine

TIMS - Thermal ionization mass spectrometry

TISIS - Torch integrated sample introduction system

TRA - Time resolved analysis

UV - Ultraviolet

VAMS - Volumetric absorptive microsampling

Vulkan DIN - Vulkan direct injection nebulizer

WB - Whole blood

WD – Wilson's disease

WHO - World Health Organization

Chapter 1: Introduction

1. Biomonitoring

Human biomonitoring (HBM) can be defined as the systematic, continuous or repetitive activity for the collection of biological samples for the determination of molecules or elements with biological interest, with the objective of controlling their levels, comparing them with the reference thresholds to evaluate if it is necessary to take any further action. The compounds measured are known as biomarkers or bioindicators. They are linked to the internal dose of the element/molecule in the human body and are used to control the stage of health of an organism. Measuring biomarkers is possible to detect abnormal levels in the organism due to external factors but also due to metabolic problems. Moreover, they can be used to predict the consequences produced by these elements/molecules.¹ Control measurements should be used to monitor and take appropriate actions in the event that the biomarker levels deviate significantly from the reference values, reducing the exposure to the “contaminant” as much as possible in the case of excess, or else increasing such exposure to this element/molecule when deficiency is the problem (*e.g. via* supplements). Moreover, they are used for the follow-up of the patients, particularly when they are under therapy to ensure a suitable interaction with the medical drugs.

To carry out biomonitoring, it is necessary to fulfil some requirements.²

- i) Biological materials used for the analysis should be easily accessible to permit carrying out routine analysis.
- ii) The biomarkers selected should be a reflection of the internal concentration and/or biological effects.
- iii) The analytical methods deployed should ensure the veracity of the results.
- iv) It is necessary to have suitable reference values and limits to properly interpret the results.

There are a lot of biological matrices that can be used for biomonitoring.^{1,3,4} In some cases, the samples can be obtained *via* non-invasive approaches, as it is the case when using urine, hair, nails, breast milk, saliva, etc. In other cases, invasive procedures are needed to collect the samples. Such is the case for blood, biopsies, etc. In general, the biological matrices

most commonly used for biomonitoring are blood, urine and saliva. Blood is a good matrix for HBM because it is in contact with all organs and tissues where chemicals are deposited. The concentration of these chemicals is therefore in equilibrium between organs/tissues and blood. Urine matrix also is widely used because it is one of the main routes of excretion. It can be used as indicative of disorders due to excess or for accumulation. Moreover, a large volume of urine can be available in a non-invasive way. Another matrix that can be obtained non-invasively and it is widely used is saliva. Saliva can be used as there is a correlation between blood and saliva concentration for different analytes.⁵

In contrast to urine and saliva analyses, conventional blood analysis, as commented before, requires the use of invasive protocols to collect the sample, which is not convenient, especially for newborns and for patients in need of routine testing. To carry out conventional blood analysis at least some milliliters (mL) of blood must be collected which can be a problem, particularly for newborns. Moreover, patients must travel to the hospital or the medical analysis laboratory, because these kinds of samples must be collected by skilled people and under controlled conditions. They need to be analyzed immediately, or else be preserved in specific conditions (-80°C). In addition, during sample manipulation and its posterior analysis, all remains and residues produced are biohazardous and should be disposed of according to strict procedures. Moreover, storing samples for biobanking can be a problem due to the space they take up.

2. New alternative of sampling and/or analysis.

In an attempt to solve these problems, new trends have emerged with the patient in mind. It could be said that there is a tendency towards personalized medicine. The intention is that sampling should be as minimally invasive as possible to prevent the patients from suffering as much pain as possible. Moreover, another goal consists in minimizing or completely avoiding the patients' trips to the lab to carry out the routine analyses.

Now more than ever, due to the COVID-19 pandemic, the interest in this type of sampling and/or analysis is on the rise.⁶ We have been locked up at home without being able to go out or go to the hospital, unless strictly necessary, because they were saturated and there was a risk of contagion.

For example, patients with COVID could monitor themselves (if they had the necessary devices) their temperature, blood pressure and oxygen levels, so that they could go to the hospital if they detect any alert symptoms. Also, antibody tests for COVID detection have been developed. Such tests can be purchased in pharmacies and run by the patient at home.⁷⁻⁹

In this way, new sampling devices that can be used by the patient and if it possible provide results quickly, even in real time, are continuously, under investigation. In practice, this is covered by two major research fields: biosensors and dry matrix spots (DMSs).

2.1 Biosensors

Biosensors are devices that transform chemical information into a signal that can be detected or/and measured, and that is directly related to the concentration of the analyte. Chemical information ranges from the concentration of a specific analyte to total composition.^{10,11} The term “biosensor” was proposed by Cammann in 1977.¹² Biosensors must be highly selective (specific) to produce positive results only when interacting with the target analyte, and stable and robust not to be unaffected by parameters such as pH and temperature. Moreover, they have to be sensitive to detect the analyte(s) at very low levels (ng mL^{-1}). They must be easily reproducible, as it is necessary to fabricate multiple identical biosensors that show the same response to the analyte.^{13,14}

Clark and Lyons were the pioneers to propose a biosensor for glucose monitoring in the early 1960s.¹⁵ Since this moment, biosensors have been under investigation and development evolving considerably. Nowadays, there are many types of sensors, but all of them consists of two different parts: the bioelement and the transducer. The bioelement is responsible for the recognition of a specific analyte, and the transducer produces a signal that can be detected. Biosensors can be classified by the type of biological mechanism they use for detecting the analyte (biological recognition) or by the type of transducer they use. (See **Figure 1**)

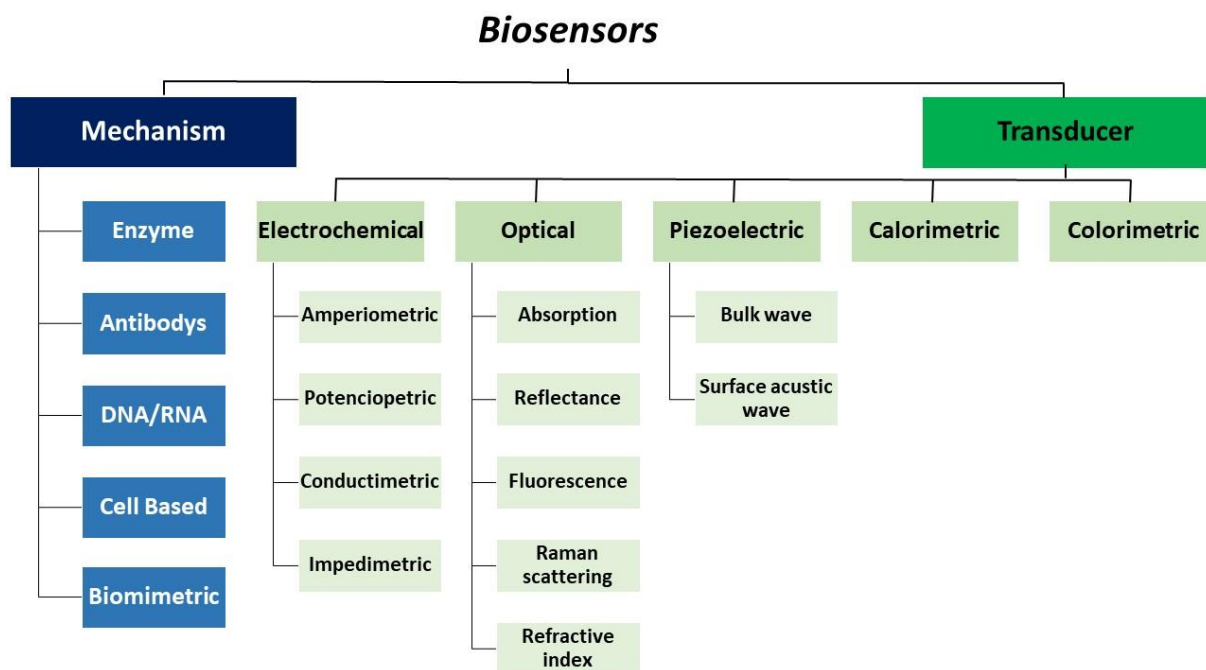


Figure 1. Categories of biosensors.

The biological recognition is a crucial step for the biosensor to be selective and sensitive, reacting only with the target element and preventing interferences from other matrix substances. There are 5 major mechanisms for biological recognition used by the biosensors.¹⁶ Enzyme based biosensors, immunosensors (antibodies based biosensors), nucleic acid biosensors, cell based sensors and biomimetic sensors. The last one is a synthetic/artificial sensor that shows the same functions than a natural biosensor.

Biosensors also can be classified by the transduction method that they deploy. From this point of view, there are 5 major groups. i) Electrochemical biosensors are those that measure the current produced by the oxidation-reduction reactions. This current is proportional to the analyte and can be monitored. Depending on the electrochemical change detected during the reaction these in turn can be classified as amperometric, potentiometric, conductometric and impedimetric. ii) Optical biosensors can measure absorption, reflectance, fluorescence, Raman scattering, and refractive index of the light caused by the interactions of the specific biomolecule. iii) Piezoelectric based biosensors are manufactured with piezoelectric materials, such as quartz, that vibrate at a natural frequency. The change in the frequency caused by the analyte of interest will produce changes in the current. This change is correlated with the analyte concentration. Within this group, there are 2 different types: bulk waves and surface acoustic waves. These sensors have received less attention in the

literature compared with the others. iv) Calorimetric biosensors carry out the analysis by taking into account the heat absorbed or produced by a reaction involving the analyte of interest. Selective enzymes are used and, when they are put in contact with the analyte, the reaction produces or absorbs heat which is linked to the concentration of the element. v) Colorimetric biosensors allow the detection of certain substances by means of a simple colour change that can be easily visible.

Biosensors have different applications in different fields such as food industry, environmental field (pollution monitoring), medical field, etc.

In clinical analysis, the development of biosensors and their applicability is growing exponentially. Nowadays, there are many commercial biosensors in this field. Some are used for the follow-up of a disease and others for diagnosis.

From the point of the view of monitoring diseases, one of the most common and well-known applications of biosensors is the measurement of glucose for monitoring diabetes. The evolution on these types of sensors is spectacular. The first generation were sensors that were non-portable; the second generation were portable and of single-use; and the third generation are implantable for continuous *in vivo* monitoring of blood glucose.^{17,18} Other biosensors are commonly used for biomonitoring blood pressure,^{19,20} and blood oxygen saturation.²¹

From the point of the view of diagnosis, there are tests available for human chorionic gonadotrophin (hCG), commonly known as pregnancy tests. Also there are biosensors for cardiovascular disease, cancer, influenza, HIV, etc.^{14,22}

This field is in continuous development, and tends both to try to detect/measure new substances and to the miniaturization and portability of such devices, for example incorporating them into devices such as phones, watches, etc.^{23,24}

2.2 Dried matrix Spot (DMS)

On the other hand, in cases where the sample must be analyzed in a specialized laboratory, the tendency is to move towards easier and less invasive forms of sampling that allow for less traumatic routine analyses and, if possible, for avoiding the continuous displacement of the patient to the hospital. Nowadays, as commented before, conventional sampling needs

qualified persons to collect the samples and for that the patient has to move to the hospital to be tested. In addition, these tests require bulk quantity of sample, and sample specific preservation is mandatory. These inconveniences result in conventional sampling for routine analysis being a tedious task, especially for newborns (NBs) (due to the very limited sample availability) and for patients who live in remote areas, or patients with reduced mobility that due to their personal/logistical requirements may have problems traveling to the hospital.

The term dried matrix spot (DMS) involves the deposition of a biological fluid onto a filter paper or another material. DMS can be prepared with different biological fluids such as blood, urine, saliva, etc., which will be discussed in more detail below. They were developed to solve some disadvantages of the conventional sampling approaches.

2.2.1 Dried blood spot (DBS)

In the early 1960s, R. Guthrie and A. Susi published a work about determination of phenylalanine for the screening of phenylketonuria using capillary blood from the heel of newborns.²⁵ This paper laid the conceptual basis for using dried blood spots (DBSs) in newborn screening programs facilitating the diagnosis of multiples congenital and hereditary disorders at an early age.

However, this is not the first paper related to DBS. In 1913, Bang carried out glucose determination using blood deposited onto filter paper.²⁶ In any case, it was not until the publication of R. Guthrie and A. Susi that DBSs really began to be used for neonatal screening programs.

Nowadays, they are used in NB screening programs for many diseases such as phenylketonuria, congenital hypothyroidism, galactosemia, cystic fibrosis, etc.²⁷ In addition to be used for NBs, DBSs are also used for testing many diseases in adults,²⁸ for therapeutic drug monitoring, for toxicology, etc.²⁸⁻³² Their applications continue growing up due to the many advantages^{33,34} that this type of sampling shows. DBS provides a way to collect the sample in an easy, quick and inexpensive way. Only a few microliters (μL) of sample are required instead of some mL. Moreover, the sample is collected directly from the finger or from the heels, after puncturing with a lancet. This way of collecting the sample is much less invasive and easy than venipuncture. Because of this, DBS collection can be carried out by the patients themselves at home. Once the DBS are prepared, they can be stored and transported without the stringent conditions required for liquid samples. For DBSs, it is only

necessary to dry the sample at room temperature. Once dried, the devices should be stored in plastic bags to avoid the ambient humidity and, moreover, very high temperatures should also be avoided.^{35,36} Periods of storage at room temperature vary depending on the analyte of interest and the conditions.^{34,37} Several studies have demonstrated that filter paper has an stabilizing effect on the sample because in dried samples there are not enzymatic reactions and microorganisms are inactivated.^{34,38,39} Moreover, it has been demonstrated that the used of dried samples on blotting filter papers produce damages in the capsid of viruses such as HIV, HCV, etc. reducing the possibility of contagion.²⁸ This enables DBSs to be send by ordinary post to the hospital avoiding the displacement of patients.

In addition to improving the quality of life of patients, the use of DBS also shows practical and economic implications. It leads to increased participation in epidemiological or prevention programs as patients can donate samples without having to travel to the hospital.⁴⁰ Moreover, due to the size and low storage requirements, the use of DBS facilitates the creation of biobanks.⁴¹

In general, in the hospitals for NB screening, DBS are produced by the direct deposition of blood (50 – 100 μ L) onto the filter paper (FP). Generally, FPs are made of pure cotton. Currently, there are only two brands of FPs that meet the requirements to class II medical devices set by the Clinical and Laboratory Standard Institute: Whatman 903 and Perkin Elmer 226. The results obtained using DBS are acceptable, as pointed out Mei et al “The filter paper blood collection device has achieved the same level of precision and reproducibility that analytical scientists and clinicians have come to expect from standard methods of collecting blood, such as vacuum tubes and capillary pipettes. Like these devices, FP has associated with it some level of imprecision that can be characterized to standardize the device and to minimize the variation in measurements due to the filter paper matrix”.⁴²

Theoretically, these clinical FPs should absorb a constant amount of blood per area so that it is not necessary to know the exact volume of blood deposited to carry out the analysis. However, this is a difficult task because it has been demonstrated that the volume deposited per area and the distribution of the analytes are influenced by some physiochemical factors such as haematocrit levels (more information in Chapter 3).

DBS analysis are commonly carried out by punching out a portion of the DBS (circles of 3.2 mm of diameter is often the standard) from the whole DBS. Taking a portion of the DBS can

lead to erroneous results since, as mentioned above, the distribution of the sample volume and analytes are influenced by various parameters, including haematocrit levels.⁴³ This may not suppose a problem for qualitative analysis, but it represents a potential source of bias when quantitative analysis is aimed at.

To minimize the haematocrit effect, new DBS devices have been developed to have a better control of sample volume. Moreover, the volume used for these devices is typically lower, and there is a tendency consisting in analysing the entire spot.

In this way, one of the first new devices developed were the pre-cut dried blood spot (PCBBS).⁴⁴ These devices improve the control of the sample volume creating blood spot delimited and smaller, which would also facilitate the complete analysis of DBS. PCBBS device showed lower variation and higher accuracy than normal DBS. Even so, although to a lesser extent, there was still an effect produced by the haematocrit level that had to be solved.

In the last years, this situation has started to change with the development of new specimens to produce DBSs with a reproducible and known volume, regardless of the haematocrit level.⁴⁵ New devices are designed to work with lower volumes (<30 μL). The most common commercial devices are:

- i) The Mitra device commonly named volumetric absorptive microsampling (VAMS), which is based on the absorption of a fixed volume of sample (10, 20 or 30 μL) onto a porous hydrophilic tip by wicking,⁴⁶ as shown in **Figure 2A**.
- ii) Capitainer is a device that makes use of microfluidics to produce volume defined DBSs on conventional DBS filter paper,⁴⁷ as explained elsewhere by Lenk *et al.*⁴⁸ It is shown in **Figure 2B**.
- iii) HemaPen is a device based on the volumetric application of blood onto pre-cut FP discs to produce 4 DBSs at the same time.⁴⁹ It consists of 4 capillaries that are filled when in contact with the sample, and then, by pressure, come into contact with the pre-cut filter papers giving rise to the DBSs. It is shown in **Figure 2C**.

iv) Hemaxis device is based on taking a known volume of sample with a capillary. Subsequently, the DBS is produced putting into contact the capillary with the FP by closing the card⁵⁰ (**Figure 2D**). More details of all these devices are provided in Chapter 3.



Figure 2. A) Mitra device; B) Capitainer dDBS device; C) HemaPEN device, D)HemaXis DB10 device and E) Touch-activated phlebotomy. Reproduced from Delahaye et al.⁵¹

This kind of devices are continuously under development, appearing devices such as: the Touch-activated phlebotomy (TAP) devices.⁵¹ It collects the blood with a microneedles by vacuum pressure in a virtual painless manner.⁵² It has 30 microneedles that go out when the button is pushed introducing into the skin (**Figure 2E**). Then, the vacuum created when the microneedles go out produce the collection of 100 μ L. The storage place into the device contain lithium heparin anticoagulant. Once the sample is collected, the entire device can be sent to the laboratory. In this form of the device, the sampled is taken in a liquid form. However, the intention is that in the future it can produce DBSs as well.

DBSs are the most used DMSs. However, as mentioned before, there are others DMSs based on other types of biological fluids such as urine, plasma, saliva, etc. which interest is growing up.⁵³

2.2.2 Dried Plasma Spots (DPSs)

Plasma is an alternative to blood matrix and is widely used in clinical analysis. It does not contain blood cells and, therefore, haematocrit effects in these devices are negligible. The conventional way to obtain plasma is by centrifuging the blood. Recently, devices capable of separating plasma from blood and producing DPSs without the necessity of centrifugation have been developed.

One of the most popular is the Noviplex Plasma Prep Cards, and it was reported for the first time in 2013.⁵⁴ This device is a microsampling device that separates the plasma by passing the blood through membrane filters. The process to generate the DPSs are produced by depositing a droplet of blood onto the top layer of the device, until the indicator circle is colored. Under the first layer, there is a membrane capable of retaining the red blood cells (by size) while allowing the plasma to pass through. The FP is located under the membrane to collect the plasma (see **Figure 3**) After 3 minutes, the top layer has to be removed. The DBS is then left to dry for at least 15 min more.⁵⁴ The volume of blood deposited is around 25 μL while the DPS produced only have 2.5 μL of plasma.

DPS are growing interest for applications, particularly for therapeutic drug monitoring.⁵³

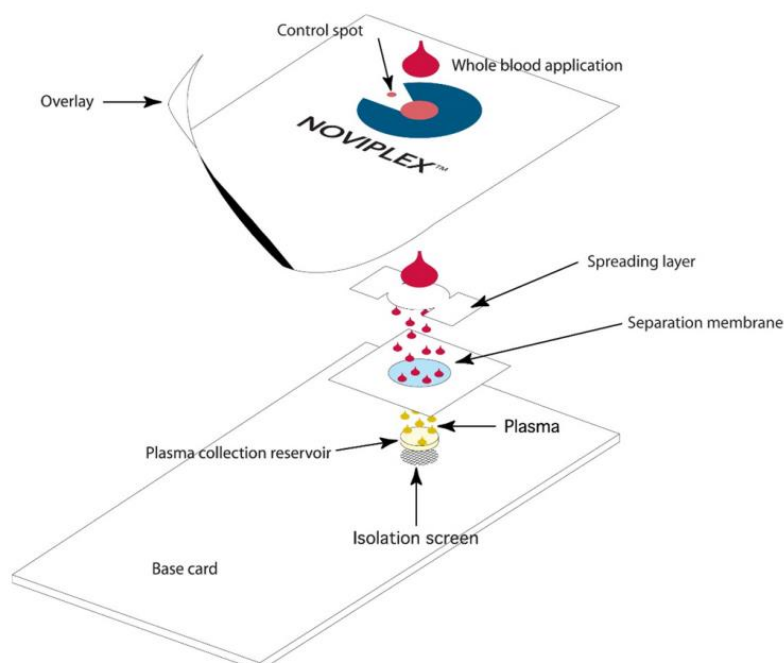


Figure 3. Schematic illustration of the procedure of the plasma extraction card. Reproduced from Kim *et al.*⁵⁴

2.2.3 Dried urine Spots (DUSs)

As commented before, urine is another of the most widely used biological matrices for clinical analysis, especially for the analysis of drugs and their metabolites, and to ascertain the renal function of the patients. The principal advantage of this matrix is that it can be collected without any invasive procedures, and it is abundant because is an excretion biological fluid. In addition, drugs and metabolites are normally present at higher levels in urine than in blood and, in some cases, they can be detected even time after they have been consumed.⁵⁵

The way to produce DUSs, is the same as for DBSs, depositing a drop of urine onto a clinical FP. Please remember that these clinical FPs theoretically absorb a fixed sample volume. However, when it is necessary to know exactly the volume of deposited urine, the abovementioned devices developed for DBSs can be used for DUSs as well. In some cases, a new calibration of the volume collected by the devices is needed due to the change of physicochemical properties between blood and urine. For example, Mitra's manufacturer provides 2 different volumes: one for absorbed blood and another for water, which is more similar to urine. In any case, some of the DBSs devices have been tested for urine providing satisfactory results.⁵⁶

2.2.4 Dried oral fluids (DOFs) or dried saliva spots (DSSs)

Saliva or oral fluid is an emerging sampling matrix that, like urine, enables the samples to be obtained easily and without invasive procedures. This type of sample has received special attention for therapeutic drugs monitoring, but also for drug detection in different situations, such as drug-impaired driving studies, to detect possible drug misuse in athletes at sport events, etc.^{53,55} Common saliva sampling approaches include passive drooling, oral rinsing and oral swab. DSSs also can be prepared in the same way as the other matrices discussed above, by spotting the oral fluid onto a FP and then letting it dry.

In view of the success of these types of microsampling devices, more and more arrays are being used for clinical analysis. In addition to those already mentioned above, there are studies and even special devices that have been developed for other matrices such as tears, etc.⁵⁷

3. Introduction systems

Parallel to the development of new microsampling devices, alternative microsample introduction systems have been developed allowing lower detection limits and the use the smallest possible sample volume which in turn reduce the use of chemical reagents and the waste generated, etc. In other words, the trend is towards what is known as green chemistry. In addition, there is also a tendency to automate the analytical processes to cope with the increasing number of analytical controls required in many areas as in the health field.

3.2 Liquid sample introduction systems

3.1.1 Flow Injection analysis

The flow injection analysis (FIA) was proposed by J. Ruzicka y E. H. Hansen in 1975.⁵⁸ This type of sample introduction system has to introduce a discrete, well-defined volume of sample, has to be reproducible and precise and the signal generated normally is a transient signal.⁵⁹ Nowadays, FIA present 3 principal characteristics:⁶⁰

- 1- A small and well-defined volume of sample is injected or inserted into the measurement system. Usually, sample volume injected is range of 20 – 200 μL , although smaller volume can be used, decreasing both reagent and sample volumes as waste products.
- 2- The analytical signal is obtained during the flow of the sample solution through the flow detector, resulting in lower detection (LOD) and quantification (LOQ) limits.
- 3- Most FIA configurations consist of several modules to perform different chemical processes such as digestion, separation, preconcentration, dilution, etc.⁶¹ That entails the reduction of sample preparation time by the operator and also the whole procedure precision is higher. In addition, they are automatable, so sample throughput increases.

These advantages have increased the scientific community's interest in FIA. Numerous instrumental modification have been developed for improve on-line sample processing and the flow-through detector to use FIA for many applications.⁶⁰

In a more general way, flow injection systems can be classified in 3 groups depending on the way to carry out the analysis.

1. Flow injection analysis (FIA): These systems inject the sample into the carrier solution in a normal system (see **Figure 4A**). In reverse systems (rFIA), the reagent solution is introduced into the carrier while the sample solution is continuously aspirated (see **Figure 4B**). Normal systems are used when the volume of sample is limited while reverse systems are used when the reagent solution is critical. Both systems can be equipped with additional modules for sample processing, depending on the necessities of each application. Decades of development have given rise to many different FIA systems constructions. Generally, for pumping solutions, peristaltic pump or syringes are used. One of the FIA systems that have received more attention are multicommutated flow analysis (MCFA) known as multi-pump system based on the combination of a single channel solenoid pumps and valve (see **Figure 4C**), or a multichannel pump with several solenoid valves (see **Figure 4D**). In addition, multisyringe flow injection analysis (MSFIA) has received special attention because it usually provides more stable signals. In these systems, the single-syringe pump is substituted by a multi-syringe pump (see **Figure 4E**).
2. Sequential injection analysis (SIA): These systems inject both the sample and the reagent solution into the carrier in a sequential way. The SIA idea is to replace the continuous flow by introducing small volumes of sample and reagent(s) into a single tube (see **Figure 4F**). The systems most used are those with a multiposition rotary injection valve and a syringe pump. Recently, a SIA systems called lab-on-valve (LOV) has been developed.^{62,63} This system improves the conventional multiposition valve systems by adding different channels that serve as microcolumns where a bed of solid sorbent and also a fiber optic-assisted photometric flow-through cell can be placed. These can use either peristaltic pumps or syringes for sample pumping.
3. Batch injection analysis (BIA): These systems deposit sample onto the detector using an automated pipette (see **Figure 4G**).

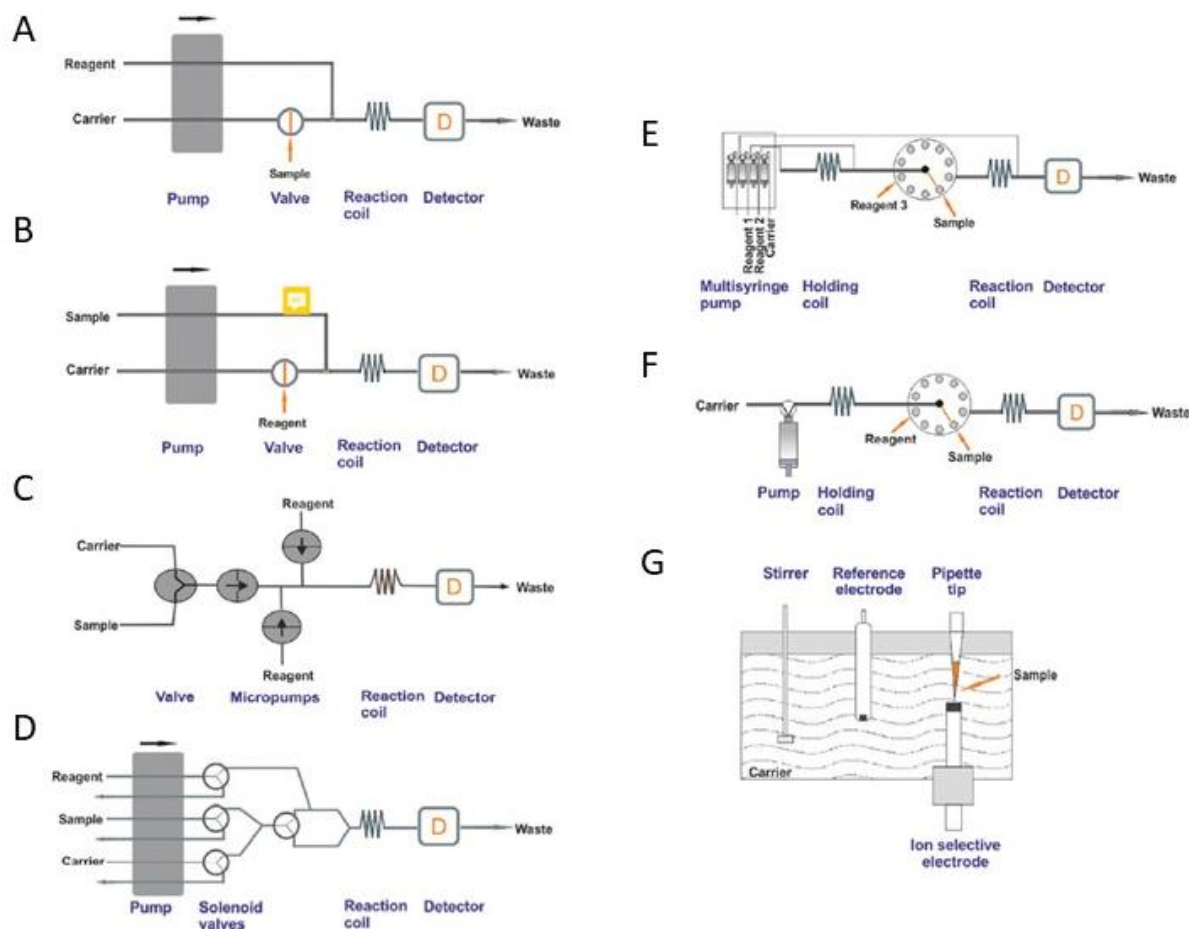


Figure 4. Schemes of basic flow injection systems: A) normal flow injection analysis system (FIA), B) reversed flow injection analysis system (rFIA), C) multicommutated flow analysis with multichannel pump system (MCFA), D) multi-pumping flow analysis system, E) multisyringe flow injection analysis system (MSFIA), F) sequential injection analysis system (SIA) and G) batch injection analysis system (BIA). Reproduced from Trojanowicz *et al.*⁶⁰

3.1.2 Micro-nebulizer

Conventionally, sample introduction into systems such as Inductively Coupled Plasma (ICP) is carried out in liquid mode. In this way, samples are homogeneous and the dilution process is easy. The systems most commonly used for this purpose are nebulizers. They dispersed the solution into a fine and gas-borne aerosol. Usually, they are coupled to a spray chamber to eliminate larger droplets from the aerosol by gravity or inertia, such as only the smallest ones arrive to the plasma (generally droplets smaller than 10 microns).⁶⁴ There are many types of nebulizers such as pneumatic, thermic, hydraulic, ultrasonic, electrostatic and rotary, which differ in the mechanism used for generating the aerosol and in their configuration.⁶⁵

The nebulizers more widely used for routine analysis in atomic spectroscopy are pneumatic nebulizers. These types of nebulizers generate the aerosol as a consequence of the interaction between a liquid and a gaseous stream at high speed.⁶⁶ Conventional systems work at flows ranging between 0.3 and 2.5 mL min⁻¹. Within this type of nebulizers, it is possible to find many different configurations, such as concentric, parallel-path, cross-flow, V-groove flow-focusing/blurring, to name a few. (see **Figure 5**).^{65,67}

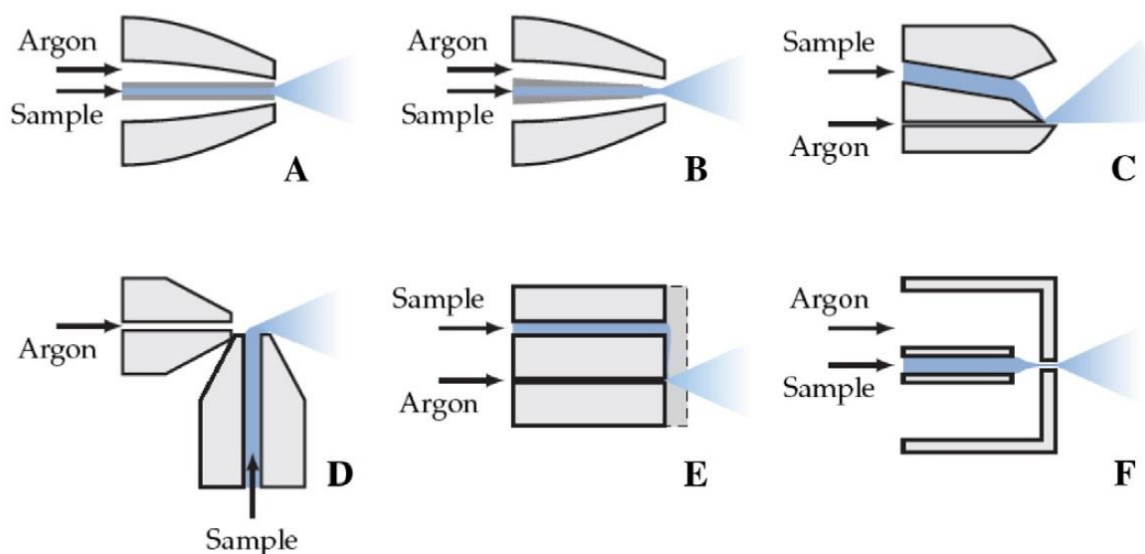


Figure 5. Different pneumatic nebulizers. A) Conventional concentric nebulizer, B) concentric nebulizer with recessed capillary, C) parallel-path nebulizer, D) cross-flow nebulizer, E) V-groove nebulizer and F) flow-focusing/blurring nebulizer. Reproduced from Bings et al.⁶⁶

It is not always possible to work at such a high flow, particularly when the volume of sample is scarce or valuable. To deal with this problem, micro nebulizers have been developed. They work at low, micro flows (1 -100 $\mu\text{L min}^{-1}$), generally coupling to spray chambers of reduced size.

The use of these low flow micronebulizers shows several advantages. The transport efficiency is improved, making it possible to achieve values close to 80% in the best cases. Hence, it is possible to analyze a very small volume of sample without excessive loss of sensitivity. In addition, it is possible to reduce the size of the spray chamber reducing the washout time⁶⁸ or even to work without spray chamber (direct injection systems). The speciation effects and the interferences generated in the spray chamber also can be reduced dramatically. Currently, the most common micronebulizers are also pneumatic nebulizers

which dimensions have been reduced, specially the exit section of the gas and the liquid (See **Figure 6**).⁶⁹ This reduction entails the obtainment of thinner aerosol as consequence of a better gas-liquid interaction, which enables better transport efficiencies, as mentioned before, leading to higher sensitivities and lower limits of detection.⁷⁰ As a disadvantage, it needs to be mentioned that they are more prone to clogging.

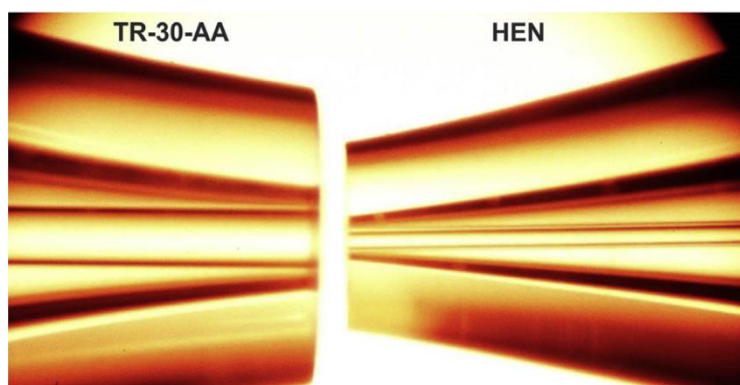


Figure 6: Comparison of standard concentric tip with micro-flow HEN nebulizer tip. Reproduced from Burgener et al.⁶⁵

There are many commercial nebulizers such as High-Efficiency Nebulizer (HEN), MicroMist Nebulizer (MM), PFA Micronebulizer (PFA), Microconcentric nebulizer (MCN), Desmountable Capillary Nebulizer (DCN), Oscillating Capillary Nebulizer (OCN), Sonic Spray Nebulizer (SSN), High-Efficiency Cross-Flow Micronebulizer (HECFMN), to name a few.⁶⁵⁻⁶⁷

Working at a very low flow, fluctuation in the signal caused by the peristaltic pump used for pumping the sample may appear. To avoid these fluctuations, it is recommended to work with self-aspiration or with syringe pumps, to achieve better control of the flow without perturbations. Automated systems that work with μL s by pumping the sample by syringes have been developed.

As mentioned above, the nebulizers are coupled to a spray chamber. This coupling is needed to have an interface between the nebulizer and the torch, to remove the largest droplets that can affect the plasma conditions. However, the use of the spray chamber can also have some disadvantages, such as memory effects, loss of sensitivity (typically 5% to 10% of the aerosol produced with a conventional pneumatic nebulizer are introduced into the ICP), waste generation, etc.

To avoid these disadvantages, nebulizers that introduce the sample directly into the torch had been developed. These are known as direct injection nebulizers (DIN) or total sample-consumption nebulizers. With these nebulizers is mandatory to work at very low liquid flow to avoid plasma extinction and the goal is to achieve transport efficiency close to 100%, improving the sensitivity when compared with those nebulizers coupled to the conventional spray chamber.⁶⁹ Moreover, they reduce the washout time close to zero, as well as the cross sample contamination.

Currently, there are not too many direct nebulizers commercially available. Among the direct injection nebulizers is possible to find the Direct injection nebulizer (DIN), Direct injection high efficiency nebulizer (DIHEN) and Vulkan direct injection nebulizer (Vulkan DIN).⁶⁷

As commented before, this design implies that sample droplets arrive to the plasma at full size, and their desolvation should take place inside the plasma. However, total desolvation and vaporization is not always possible in these cases, particularly if the droplets are large. Thus, matrix effect can occur, especially when working with organic solvent. This is probably due to changes in the plasma conditions affecting the results.

To solve or reduce this problem keeping the 100% transport efficiency or very close, some systems have been developed by optimizing the size and configuration of the chamber, the temperature used, etc. For example, the torch integrated sample introduction system or TISIS^{71,72} or the high temperature torch integrated sample introduction system (hTISIS)⁷³⁻⁷⁵.

Another way to improve transport efficiency, while increasing sensitivity at the same time that the interferences are reduced, is using desolvation systems. They are known as high-efficiency sample-introduction system (HESIS).⁷⁶ These are based on evaporation of the solvent in two consecutive steps. In the first step, the aerosol generated by the nebulizer is heated and, in the second one, the evaporated solvent is eliminated from the aerosol stream.

Nowadays systems such as the Aridus desolvating nebulizer from CETAC Technologies exist, which consists of a spray chamber connected to a fluoropolymer, both heated. The spray chamber is heated up to 110 °C to maintain the sample vaporized. Then, the sample enters the membrane desolvator module, heated at 140 °C. A flow of Ar (sweep gas) circulates against the tide to remove the solvent while the analyte passes through the middle of the tube to be transported to the ICP (see **Figure 7**). This system removes the

interferences produced by the solvent (oxides, hydrides, etc.) and increase sensitivity roughly by a factor 5 to 10.⁷⁷

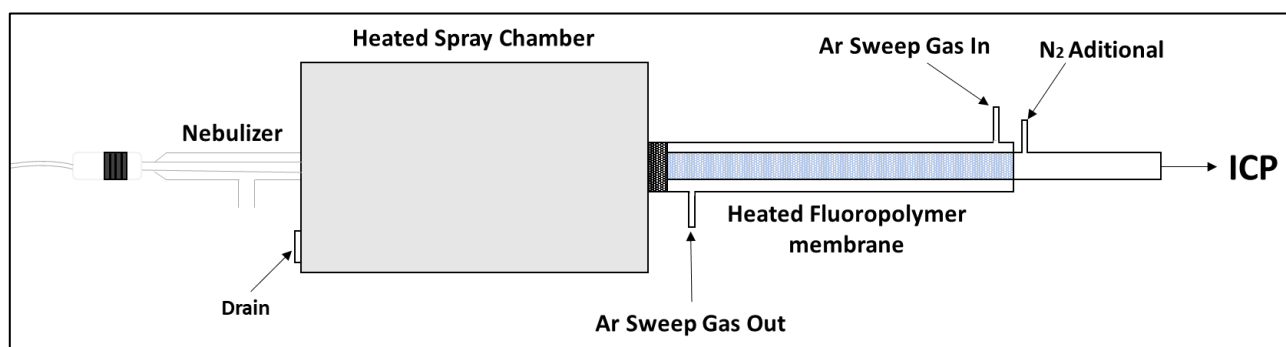


Figure 7: Schematic illustration of Aridus desolvating nebulizer system from CETAC Technologies.

3.2 Solid sample introduction systems

As mentioned above, generally sample introduction is performed in liquid mode. For that, when a solid needs to be analyzed, first it has to be dissolved, with the corresponding issues that such process entail, such as use of concentrated, hazardous potential analyte loss, sample dilution and risks of sample contamination. In addition, dissolution is time-consuming, because it can involve tedious multi-step sample pre-treatment protocols. The use of direct solid analysis can overcome these problems. Some of the most common sample introduction systems used for solid samples in atomic spectrometry are electrothermal atomization (ETA) or electrothermal vaporization (ETV) systems, and laser ablation (LA).

3.2.1 Electrothermal atomization (ETA) or electrothermal vaporization system (ETV)

ETA and ETV (**Figure 8**) share the same basic principle. They are based on the resistive heating of a graphite furnace (commercial systems) or a filament (home-made systems). In commercial systems, the solid sample is deposited onto a platform and is introduced into the graphite furnace. There, it is heated causing the sample release into the gas phase to be introduced into the system of detection. The detection system for ETA is an atomic absorption spectrometer (AAS) while for ETV is an inductively coupled plasma system, either optical emission spectrometer (ICP-OES) or mass spectrometer (ICP-MS).⁷⁸ In any case, heating is carried out following a temperature program, which normally involve four different subsequent steps:

- 1- Drying: It is the step devoted to evaporating the solvent. The temperature used is typically around the boiling point of the solvent.
- 2- Pyrolysis: It aims at separating the matrix from the analyte of interest by decomposing the matrix. The temperature used is often the highest possible without analyte lost.
- 3- Atomization / Vaporization: In this step is when the atomization / vaporization of the analyte of interest takes place. Generally, the temperature used is the lowest temperature that enables full atomization / vaporization of the analyte.
- 4- Cleaning: Its goal is to remove any residue that may remain after step 3, to avoid contamination between runs. For that, the highest temperature reached by the system (aprox. 2600-2700 °C) is often used.



Figure 8. Electrothermal vaporization device (ETV) from Spectral Systems, Fürstfeldbruck, Germany.

It is very common to add chemical modifiers to assist in the separation between the matrix and the analyte(s). Modifiers can act facilitating the matrix decomposition and/or stabilizing the analyte(s), permitting to vaporize/atomize it/them at higher temperatures enabling prior matrix removal without losses. But, it may also happen that the element of interest vaporizes/atomizes before the matrix. The modifiers used in this case are added to stabilize the matrix and/or to facilitate the vaporization/atomization of the analyte at lower temperatures.

ETA coupled to an atomic absorption spectrometer (AAS) was the first to appear as reported by L'vov.⁷⁹ However, the first application for solid samples with a commercial ETAAS was published in 1971.⁸⁰ Afterwards, the ETV was coupled to an ICP-OES in 1974^{81,82} and

subsequently in 1983 to an ICP-MS .This coupling was reported by Gray and Date.⁸³ More details are provided in Chapter 6.

3.2.2 Laser

The word LASER is the acronym of Light Amplification by the Stimulated Emission of Radiation, and was coined by Gordon Gould.⁸⁴ The stimulated emission caused by a photon on an excited atom results in the emission of a photon with the same energy, direction and in phase with the stimulating radiation, known as coherent light. This property is used for the light amplification and consequently the laser formation. For laser generation, the system is formed by three elements: 1) An active medium (a crystal, a gas or a liquid with dyes) that is the material that emits the radiation. For this purpose, it is necessary to achieve a population inversion, which means that there are more atoms in excited stage than in the fundamental stage. 2) A system pump, which is responsible for the population inversion. It is triggered by an external source supplied by light (optical pumping) or electrical current (electrical pumping). 3) A resonant cavity placed between two mirrors, one totally reflective and the other partially reflective. The system pump supplies energy that excites the atoms of the active medium. When the excited atoms receive a photon, they emit another photon with the same wavelength and with the same direction. The photons emitted strike other atoms, which in turn emit more photons with the same characteristics. As the active medium is between 2 mirrors (resonant cavity), the photons bounce back and forth, colliding with more atoms and causing more photons of the same characteristic. The result is a coherent light that comes out when the aperture is opened in one of the mirrors. **Figure 9** shows a schematic of the laser light production process.

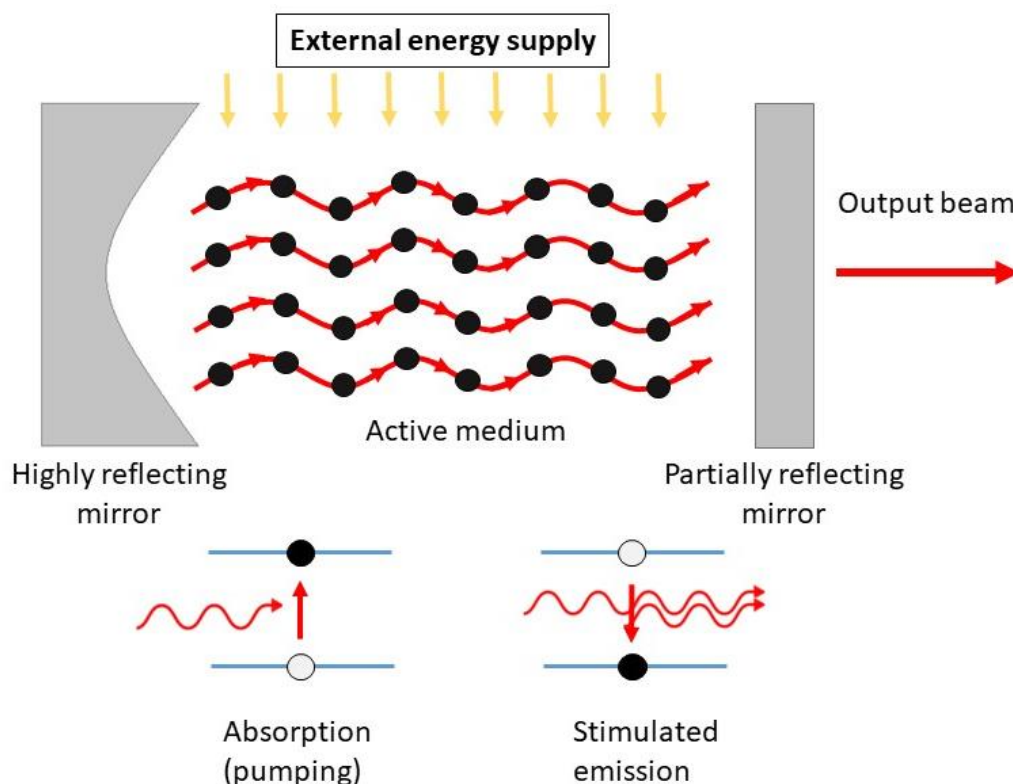


Figure 9. Diagram of a laser cavity.

The laser, as commented before, can be used as sample introduction system in atomic spectrometry. For that, a short-pulse with a high-power laser beam is focused onto a sample surface. The laser beam makes a small volume of particles to be instantly converted into their vapour phase. Then, the radiation emitted can be measured (LIBS) or alternatively the particles resulting from phase condensation or hydrodynamic sputtering can be transported to other systems, such as an inductively coupled plasma (ICP), for subsequent analysis.

The coupling of LA with inductively coupled plasma systems was reported in the early 80s. It was first coupled to an ICP-OES,⁸⁵ and then to an ICP-MS.⁸⁶ From then on, this technique has been widely explored and nowadays is one of the most versatile techniques in analytical chemistry, for both elemental and isotopic analysis of solid samples. In addition to the advantages to do solid analysis (direct analysis, not sample preparation, low risk of contamination, etc.), laser ablation is an almost non-destructive technique, requires a small amount of sample only, enables highly spatially-resolved information to be achieved, as well as to perform depth-resolved analysis. And it is very useful for trace analysis due to its low detection limits.

To perform laser ablation, the sample is placed into a hermetic ablation cell that is flushed with an inert gas Ar, He or a mixture^{87,88} to transport the ablated particles to the ICP. The laser beam is focused onto the sample surface through the transparent window of the ablation cell, thanks to an optical system. If the laser energy is high enough, the material of the sample surface is extracted in form of an aerosol and transported to the ICP through a tube leading from the ablation cell to the ICP torch. The process is summarized in **Figure 10**. The analysis can be carried out in dry plasma, introducing only the aerosol produced by the laser, or in wet plasma, where, in addition to the aerosol generated by the laser, a liquid solution is introduced simultaneously.

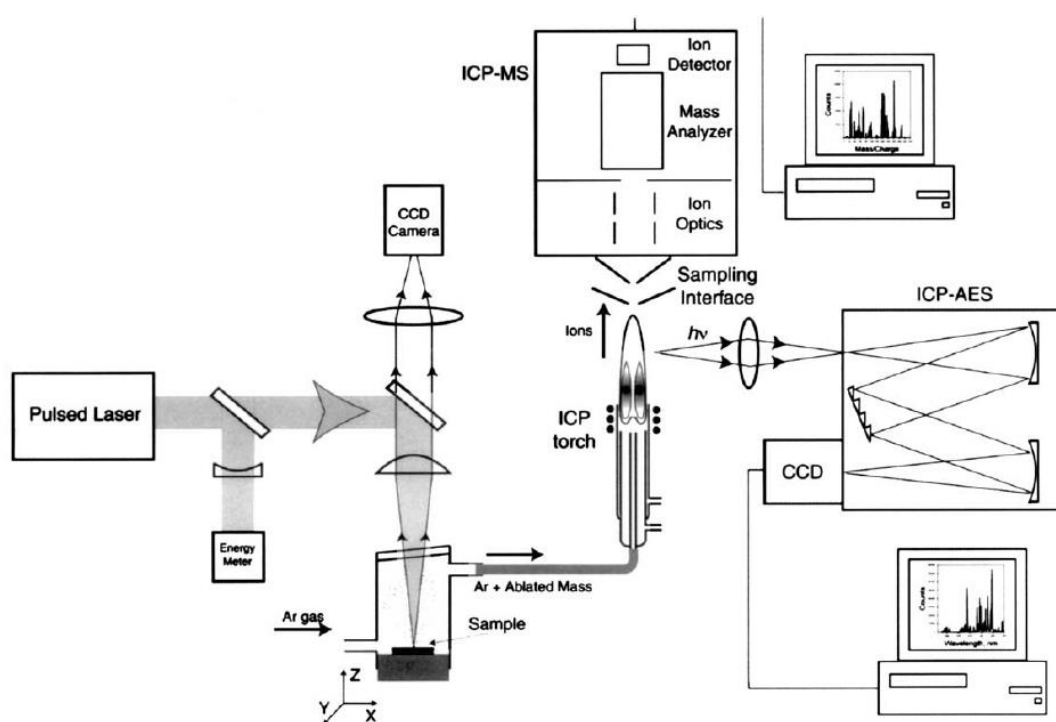


Figure 10. Schematic of a laser ablation system, using ICP-OES and/or ICP-MS detection. Reproduced from Russo *et al.*⁸⁹

There are two types of common lasers used in analytical chemistry: 1) solid-state lasers based on ion-doped crystals which are pumped by discharge lamps or laser diodes. The amplification medium is a crystal (Nd:YAG, Yb-KGW and Ti:sapphire) imposing the pulse duration capabilities (typically few nanoseconds for Nd-YAG, few femtoseconds for Yb-KGW and Ti-Sapphire) and fundamental wavelength (Nd-YAG @ 1064 nm, Yb-KGW @ 1030 nm, Ti-Sapphire @ 800nm), 2) excimer lasers where the active medium is a gas, such as ArF (delivering nanoseconds pulses @ 193 nm) or F₂ (delivering nanoseconds pulses @ 157 nm).

The laser technology for laser ablation analysis has been developed to improve the capabilities of laser ablation systems in terms of sampling efficiency, signal sensitivity, accuracy, precision, and recently micron scale imaging. Some physical parameters such as pulse duration^{90–92}, wavelength,^{93,94} transport gas,⁹⁵ optic and more recently ablation cell design have been identified as key parameters that are receiving increasing interest from instrument developers.

Elemental fractionation is one of the most important effect in LA ablation techniques. Elemental fractionation occurs when the detected elemental composition of the ablated mass does not correspond with the real sample composition. Two main process can explain the elemental fractionation. 1) Selective evaporation: It is a result of the interaction between the laser and the material. The vapor phase is enriched with elements with low sublimation enthalpy. Hence, the aerosol composition does not represent the real sample composition (non stoichiometric sampling). It is governed by the ablation conditions (temperature, the time duration of the interaction, the laser induced plasma, the surface of interaction, the carrier gas (He, Ar), etc.) and the physical properties of the sample. This thermal effect is evidenced by monitoring U ($\Delta H_v = 422.6$ kJ/mol) and Pb ($\Delta H_v = 179,4$ kJ/mol) signal during the ablation of a homogenous sample in a crater mode. Pb/U signal ratio is then increasing over the course of the ablation as a result of heat accumulation in the crater due to the laser induced plasma, Pb being evaporated preferentially than U. 2) Particle size: The biggest particles are less efficiently atomized in the ICP than the smaller. The most volatile elements contained in the particles diffuse faster than the most refractory. This generates mass bias if the particle is not completely atomized. This phenomenon is also indirectly governed by the ablation conditions⁹⁶ such as pulse duration. The particles atomization efficiency is generally verified by monitored by the U/Th ratio of a certified reference samples that should match with the stoichiometric composition of the sample. As a matter of fact, as these elements have similar ionization potential (6,2 V and 6,1 V respectively for U and Th) they should be atomized similarly in the ICP. In addition, these isotopes having similar masses (^{282}Th , ^{238}U), they should be transmitted evenly in the mass spectrometer. In some extent ICP condition (power, or carrier gas for instance) can be adjusted to improve the particles atomization efficiency, generally at the expense of signal sensitivity.

In order to estimate the elemental fractionation a fractionation index relative to a given element (generally Ca or Si) can be calculated. It depends on the laser wavelength, pulse duration, energy, beam size, etc., and also on the sample properties (thermal, optical).⁹⁷

Elemental fractionation can be reduced by using matrix matching to have similar fractionation in the sample and the standard or using less fractionating lasers (ultra-short pulses, deep UV, etc.).⁹⁸

When the pulse duration is reduced below the picoseconds, the sample damage caused by the collateral heating is reduced as well. Femtosecond laser supplies ultra-short pulses (in terms of duration), which do not provide enough time for dissipating the energy into the surrounding area of the material. In contrast, thermal effects is a typical issue of nanosecond lasers that results in melting leading to the ejection of some large, dense and spherical particles as a result of the hydrodynamic sputtering (**Figure 11**).⁹⁶ So, using shorter pulses, typically below 500 fs, the thermal effect is limited, which produces smaller particles, and a better depth resolution. Moreover, ICP-MS shows enhanced signal intensity and more stability when using femtosecond lasers, compared to nanosecond lasers, especially when considering metal samples.^{90,99}

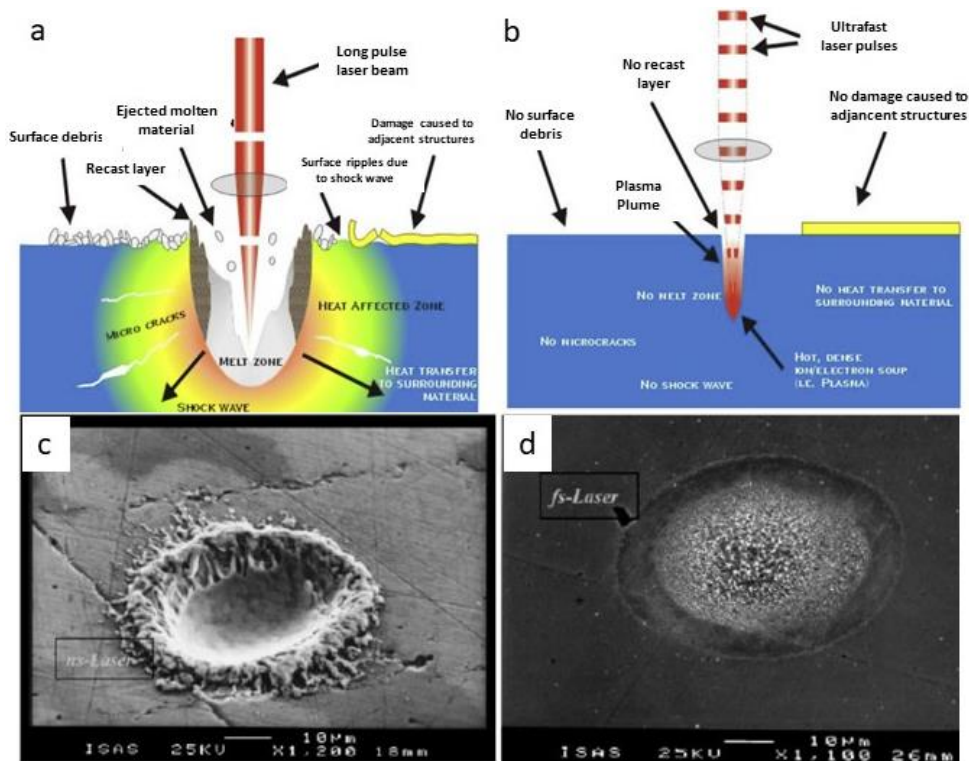


Figure 11. Laser-matter interactions in both a) nanosecond laser and b) femtosecond pulse lasers. Images show the ablation of polished brass c) with a nanosecond laser and d) with a femtosecond laser. Figure a and b from Fernández *et al.*⁹⁶ Figure c and d reproduced from Hergenröder *et al.*¹⁰⁰ Note that Fig 11a and 11b is an artwork that might be confusing, as it does not take into account any time scale: for instance, laser pulse duration is in the nanosecond range while particles are ejected few microseconds after the pulse. In the same vein, cracks might appear few milliseconds and even few seconds after the pulse.

The choice of carrier gas, in addition to influencing the ionization conditions of the ICP plasma, also influences the particle size and the transport efficiency. Helium shows a higher thermal conductivity than argon. The high conductivity of helium also allows cooling of the plasma created on the surface of the sample causing smaller particles, as shown in the **Figure 12**. For that, the use of He improve the analyte signal intensity and provides a faster washout.¹⁰¹

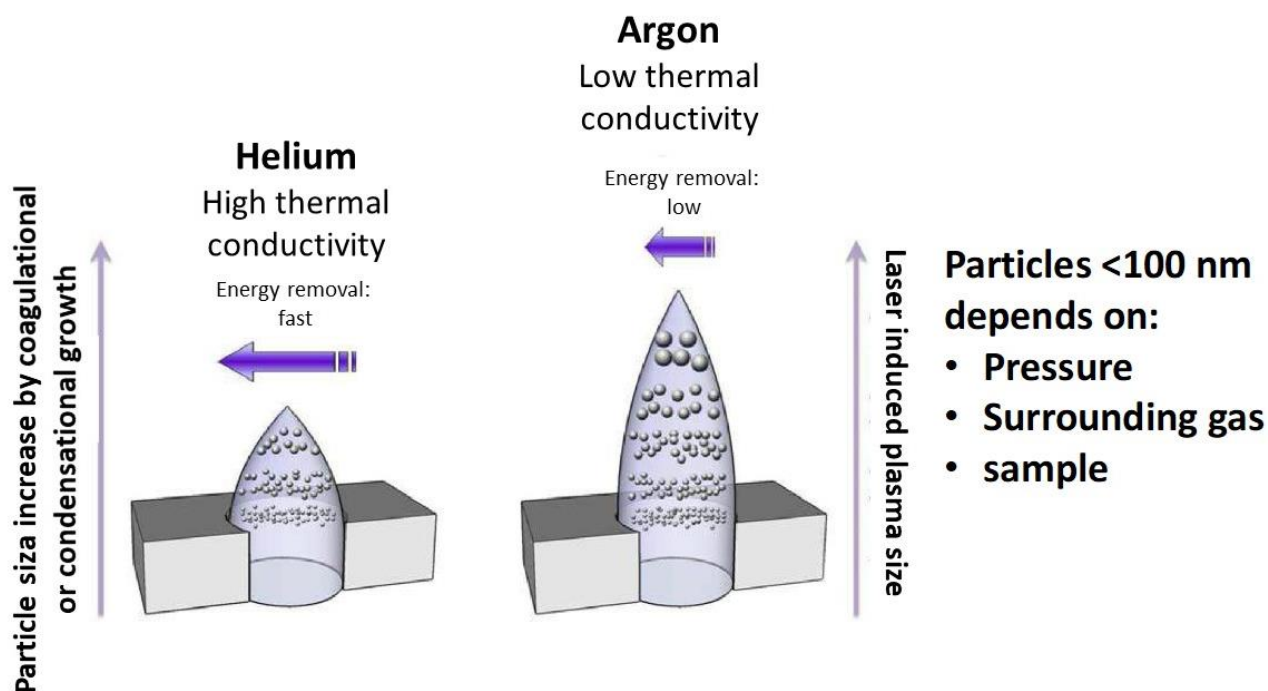


Figure 12. Effect of the thermal conductivity of gas on the size of the plasma created on the sample surface and the growth of particles. Adapted from Horn *et al.*¹⁰¹

The ablation is influenced by the wavelength, particularly for nanosecond lasers. The ablation mechanisms depend on the photon energy of the laser, among other factors. Shorter wavelengths present higher photon energy to break the bonds and also for the ionization processes, thus limiting traditional heating effects. Consequently, most of the materials in UV offer lower optical penetration depth and consequently provides more laser energy per unit volume for ablation and smaller particles sizes.^{93,97} Moreover, elemental fractionation drastically reduced when working with lower wavelengths, especially with nanosecond laser, although this also depends on the material ablated.^{88,102}

In the case of femtosecond laser, the wavelength affect in a less extent the quality of the analysis, especially for metallic matrices. However, for very transparent samples (crystals for instance), shorter wavelength (266 nm, 257 nm, 200 nm) were found to even improve elemental fractionation.

4. Why focusing on elemental determination?

The majority of the works on biomonitoring have focused on organic molecules.^{103–107} However, nowadays the interest for elemental analysis is growing because many elements

are linked to many biochemical reactions that occur in our body and a lot of information can be obtained from them.

In the human body, elements can be classified as: i) organic elements or bulk elements that are the elements that form most our body: C, H, N and O; ii) macro elements, which are essentials for the human body such as Na, K, Mg, Ca, Cl, P and S; iii) trace or ultra-trace elements, which are presents in levels of mg L^{-1} or $\mu\text{g L}^{-1}$

The World Health Organization (WHO) classifies trace elements in 3 groups: i) essential elements, ii) probably essential elements (beneficial) and iii) potential toxic elements.

The concept of essential element in biology has been defined in many ways. All of them agree that essential elements are those are totally necessary for vital functions, as their absence causes irreversible damage, or even death.^{108,109}

However, even if they are indispensable, an excess of these elements also produces adverse effects. Thus, they can become toxic. **Figure 13** shows an example of a dose-response diagram for essential elements based on the Bertrand diagram pointing to the Paracelsus principle “the dose makes the poison”. Therefore, both excess and deficiency can be crucial, hence the importance of controlling the levels of these elements.¹⁰⁹

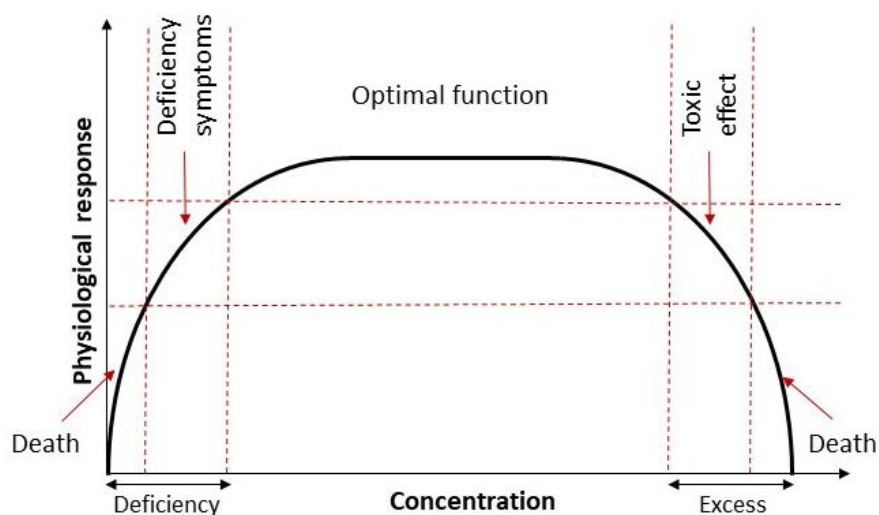


Figure 13. Dose-response diagram for an essential element.

Nowadays, there is controversy as which elements are essential or beneficial to the human body. Currently, the essential elements for the human body (besides the organic elements and the macro elements) are B, Co, Cu, F, Fe, I, Mn, Mo, Se and Zn. In addition, other

elements such as Br, Ni, Si, Sn, V are suspected to be essential, but this has not been proven yet. These are considered as beneficial elements. Cr also was included in the essential elements list. However, recently, it has been removed from it on the basis of results obtained with experimental animals.^{110,111} Currently, these elements are considered as beneficial elements;

Beneficial elements are considered those that only improve the organism's functions. Their deficiency disturbs some biological processes resulting in a reduction of biological functions from optimal to suboptimal, but it does not cause death.

Toxic elements are those that should not be present in the human body such as cadmium (Cd), chromium (Cr⁶⁺), lead (Pb), and mercury (Hg).¹¹² Their presence, even in low concentration, causes severe damage to the body; and excessive exposure can be fatal.

The analysis of such toxic metals are very common because the consequences of their presence are well known.¹¹²⁻¹¹⁵ However, elemental analysis for biomonitoring does not have to be solely focused on the toxic elements for the reason above-mentioned. Changes in the levels of essential elements also are useful to control the health status.

In routine clinical tests based on blood or urine the main elements monitored are calcium (Ca), iron (Fe), magnesium (Mg), potassium (K) and sodium (Na); but also minor elements such as copper (Cu), zinc (Zn), among others.

5. Techniques for the elemental determination

There are many techniques for elemental analysis that can be classified depending on the type of analysis that carry out: i) bulk analysis, ii) speciation analysis and iii) isotopic analysis.

5.1 Bulk elemental analysis

Usually bulk elemental analyses are carried out using techniques such as atomic absorption spectrometry (AAS), inductively coupled plasma optical emission spectrometry (ICP-OES), and inductively coupled plasma mass spectrometry (ICP-MS), among others.

5.1.1 Atomic absorption spectrometry (AAS)

Atomic absorption spectrometry (AAS) is an analytical technique based on the measurement of every element through the absorbed radiation by its atoms in the gas phase. Each atom absorbs at specific wavelengths. Thus, each element shows a specific line spectrum. The AAS principles were established for the first time by Kirchhoff and Bunsen in 1860, who experimentally observed that the atoms emitted light at the same wavelength as they absorbed it. ^{117,118}

The relation between the atom structure and its interaction with the radiation was established by Plank in 1900 through the equation (1):

$$\varepsilon = h\nu = \frac{hc}{\lambda} \quad \text{Eq (1)}$$

Where ε is the variation of energy between 2 states, ν is the frequency, both characteristics of each atomic species; h is the Planck's constant, c is the speed of the light, and λ is the wavelength.

However, in 1955 Alan Walsh, known as the "father" of the AAS, established the foundations of atomic absorption spectroscopy, by developing the first spectrometer, and establishing AAS as a useful analytical technique. ^{119,120}

The main components of an AAS spectrometer are: i) a radiation source that emit the spectrum of the analyte; ii) atomizer, which, as its name indicates, is where the atomization of the sample takes place; iii) monochromator for scattering the radiation and separate the wavelengths; and iv) detector, as shown schematically in **Figure 14**.

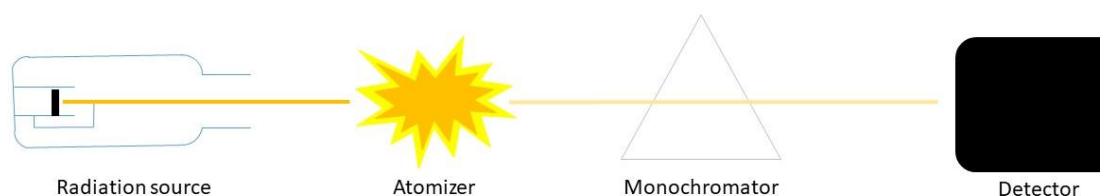


Figure 14. Diagram of the main components that constitute an atomic absorption spectrometer.

The radiation source emits radiation that reaches the detector, as does the radiation from the atomizer and the surroundings. The photons that are detected are called incident radiant power (Φ_i). Subsequently, the analyte is introduced and atomized, exposed to the radiation, which cause a reduction of the photons incident on the detector, as these are partially absorbed. This light signal is called transmitted radiant power (Φ_{tr}). The ratio between the transmitted power and the incident power is known as transmittance. It is proportional to the number of atoms that absorbed the radiation. The logarithm of the inverse of the transmittance is known as the absorbance, which shows a linear relationship with the concentration of the analyte, as expressed by the Lambert-Beer law (Equation 2).¹¹⁷

$$A = -\log \frac{\Phi_{tr}}{\Phi_i} = k c d \quad \text{Eq (2)}$$

Where k is the molar absorption coefficient, c is the molar concentration and d is the optical path length.

The most common radiation sources are the hollow cathode lamps (HCLs), which consists of a glass tube containing a cathode, an anode and a buffer gas (usually Ar or Ne). When a high voltage is applied between the anode and cathode, the gas present is ionized giving rise to a plasma. The ions are then accelerated towards the cathode and succeed in detaching atoms from the cathode. The gas, the plasma and the detached atoms will be in an excited state from which they will fall to a lower level after emitting photons with a characteristic wavelength that depends of the material the lamp is made of.^{117,121}

More recently, continuous source lamps have been used thanks to the improvement of higher resolution monochromators (double monochromators). These are composed of a prism and diffraction grating (echelle grating), which together make it possible to separate wavelengths with a resolution of at least 2 pm (width of an atomic line). This gave rise to the high resolution continuous source AAS (HR CS-AAS) technique.^{122,123} In this case, the configuration is more complex, as can be seen in the **Figure 15**. The lamp used in HR CS AAS is a high-pressure xenon short-arc lamp. More details will be provided in Section 3

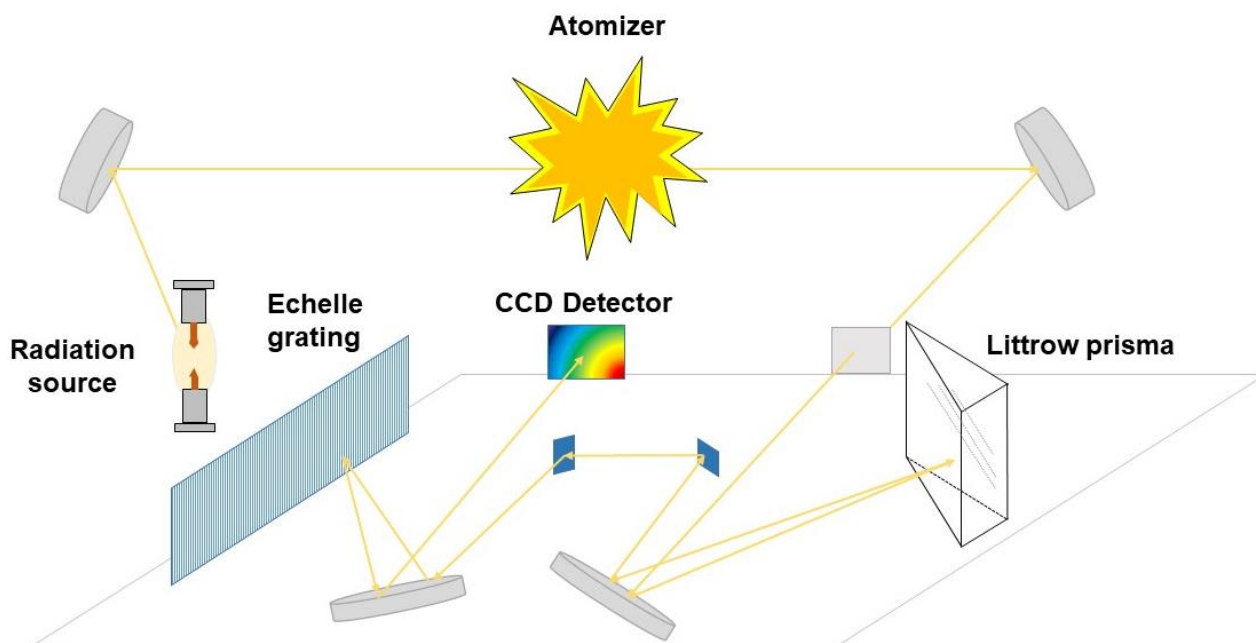


Figure 15 Scheme of the components that make up the HR CS AAS spectrometer.

The most commonly used atomizers are the flame and the graphite furnace. Instruments that work with a flame are known as Flame AAS (FAAS), which are limited to liquid sample analysis. Alternatively, instruments that work with graphite furnace are known as Electrothermal AAS (ETAAS), which is actually a more general concept comprising also other atomizers such as tungsten wires, or graphite furnace AAS (GFAAS), which is more specific. GFAAS enables working with both liquid and solid samples, as mentioned in Section 3.2.1.

The detectors used to measure photons are photomultipliers and charge coupled devices (CCDs). Photomultipliers are used in FAAS, ETAAS, etc.¹¹⁷ while CCDs are used in HR-CS-AAS.¹²²

AAS suffers from two large groups of interferences: spectral and non-spectral.

Non-spectral interferences are due to the matrix influence on the signal and can be minimized *via* sample preparation and/or adjusting careful optimization of the temperature program.

Spectral interferences occur when there is an overlap between the analytical signal and that from another species (atoms or molecules). One of the strategies used to circumvent this type of interference, for instance, is choosing another analytical line free from interferences, when it is possible. HR CS AAS provides the option to correct spectral interferences

mathematically using a least-squares algorithm, although there are a number of requisites for the successful application of such approach.¹²²

GFAAS presents a drastic improvement in terms of sensitivity compared to FAAS, roughly by 2 orders of magnitude. Limits of detections (LOD) obtained in FAAS are in the ng/g range while LOD obtained in GFAAS are in the pg g⁻¹ range. In addition, GFAAS allows working with micro samples since few micrograms only are necessary for one analysis. However, the sample throughput is widely reduced with GFAAS, since the different analytical steps (drying, pyrolysis, atomization and furnace cleaning) limit the analysis of a single elements in 3 - 4 minutes, compared to less than 10 s in AAS.

5.1.2 Inductively coupled plasma techniques

Inductively coupled plasma techniques are those that use a plasma to carry out the ionization of the atoms for their subsequent detection. To generate the plasma, a torch surrounded by a radio frequency (RF) coil through which an Ar flow circulates is needed. The RF coil supplies energy (typically 600-1500 W) that induces an oscillate electric and magnetic field inside the torch to stabilize the plasma. When a high voltage discharge (Tesla spark) is applied, Ar ions are formed and collision between them due to the oscillating field forming the coupled plasma. The plasma generated has a temperature around 7500 K with an electron density of 10¹⁵ cm⁻³.¹²⁴ To avoid torch melting, a high Ar flow (around 15 - 17 L min⁻¹) is applied to the outer tubes of the torch. The sample is introduced through the inner tube of the torch, using the sample introduction systems mentioned above (see Section 3). When the sample is introduced, it is vaporized, atomized, and finally ionized due to the high temperature and the collision with Ar*, Ar⁺ and electrons. (**Figure 16**). The efficiency of ionization depends on the ionization energy of the element. Ions with an ionization energy lower than 8 eV are ionized very efficiently (>90%), although elements with higher ionization energy can still be ionized if their ionization energy is lower than of Ar (E = 15.75 eV).^{124,125}

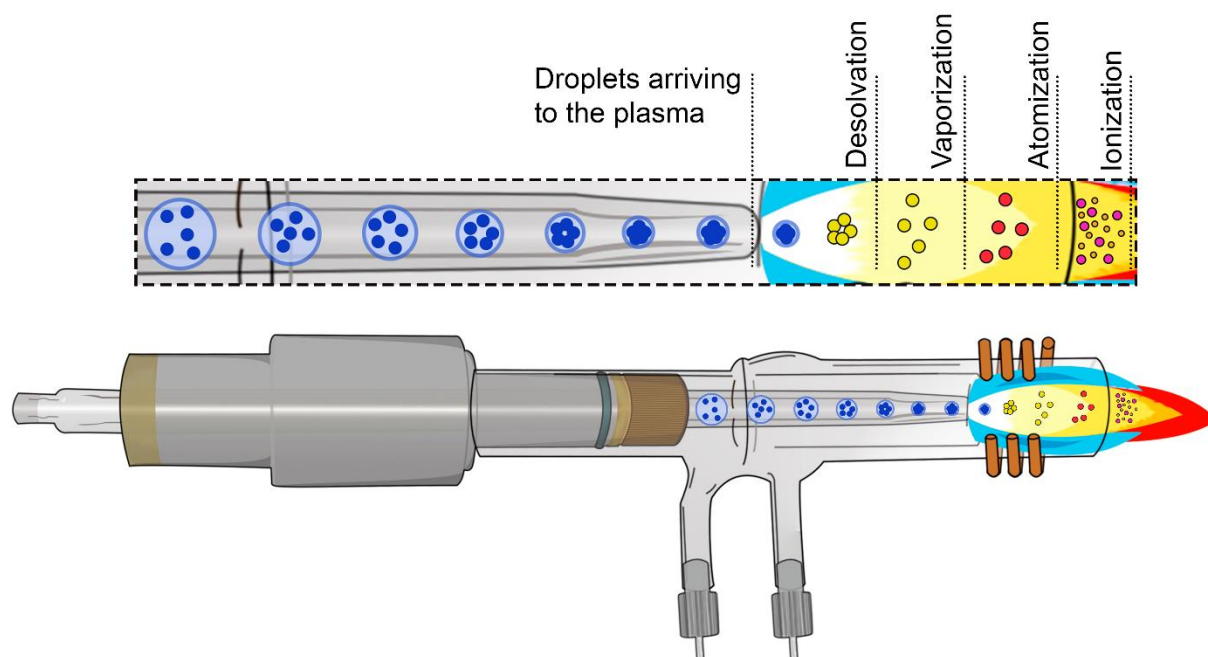


Figure 16. Scheme of the processes carried out by the sample inside/near the plasma.

Depending on the detection technique, we can find: Inductively couple plasma optical emission spectrometer (ICP-OES) and inductively couple plasma mass spectrometer (ICP-MS).

5.1.2.1 Inductively couple plasma optical emission spectrometer (ICP-OES)

ICP-OES is based on the measurement of the emission of photons from atoms and ions that have been excited in the plasma. It was developed by Greenfield *et al.* and Wendt *et al.* in the mid-1960s.^{126,127} However, the first commercial ICP-OES was not introduced until 1974.¹²⁸

In this technique, the sample arrives to the plasma in aerosol form. As mentioned above, the collisions produced inside the plasma provide additional energy that causes the electrons of the atoms to be promoted to excited states and, if the energy is high enough, one electron can be removed forming ions and, subsequently, promote the ions into excited stages. When the excited electrons return to the ground state of both atoms and ions, they emit photons. Each photon shows a characteristic energy that depend on the quantic levels of the atom. This energy is linked to the wavelength, which is specific for each atom. The number of photons is directly proportional to the element concentration.

The ICP-OES instrumentation is composed of: i) an introduction system, ii) a ionization source (ICP), iii) an optical systems, iv) a monochromator and v) a detector. The photons emitted by the atoms/ions when the sample goes through the plasma are directed with the help of lens and concave mirrors to the monochromator where the radiation is separated. Subsequently, specific wavelengths are selected, depending on the elements of interest, to be detected by a photodetector.¹²⁹ (See **Figure 17**) This technique is able to provide simultaneous determinations for up to 70 elements in about 2 minutes, although its sensitivity is often not enough for trace and ultratrace elemental analysis in the clinical field.

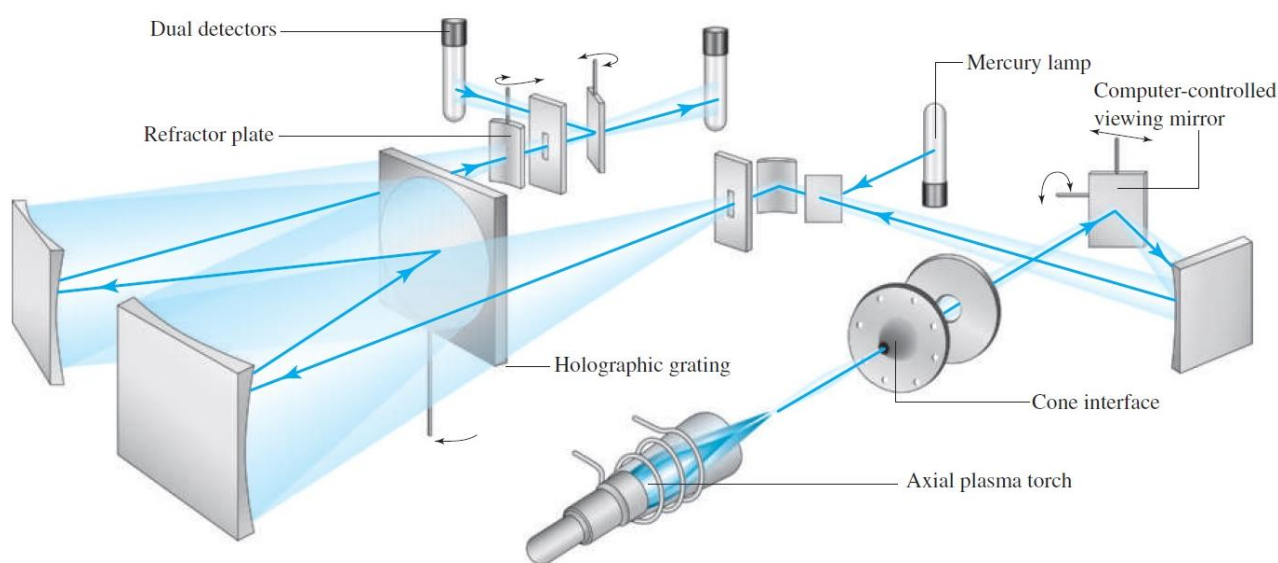


Figure 17. Optical diagram of a sequential ICP optical emission spectrometer. All moving parts are under computer control, and their modes of motion are indicated by the three-dimensional arrows. Moving parts include the grating, a mirror for transducer selection, a refractor plate for optimizing signal throughput, and a viewing mirror to optimize the plasma viewing position. The spectrometer contains a mercury lamp for automatic wavelength calibration. Notice the axial viewing geometry. Reproduced from Skoog *et al.*¹³⁰

5.1.2.2 Inductively couple plasma mass spectrometer (ICP-MS).

ICP-MS techniques are based on differentiating between nuclides by their mass-to-charge relation. Hence, neutral atoms cannot be analyzed by this technique. Negative ions could be analyzed in principle, but not with the commercially available instruments.

As mentioned before, when the sample travels through the plasma, ions are generated by the elimination of an electron due to the collisions and the high temperature. Subsequently,

ions are extracted by the vacuum interface and guided to the mass analyzer, where they are separated by mass-to-charge ratio (m/z), and then detected, as it will be explained hereinafter.

ICP-MS was introduced in 1980 by Houk *et al.*¹³¹ However, the first commercial ICP-MS appear in 1983. Since then, ICP-MS has been one of the most powerful analytical techniques for trace analysis. It is capable to carry out multi-elemental analysis, it shows a wide dynamic range (over 12 orders of magnitude), and it provides very low detection limits. Also, it is possible to determinate isotopic ratios using ICP-MS.¹³² Nowadays, it continues to be considered as one of the most powerful analytical techniques thanks to the continuous instrumental improvements. Every new generation of instruments are more reliable and robust, provide lower limits of detection (ng L^{-1} or pg L^{-1} , in the best cases), are capable to reduce or eliminate spectral interferences, show the possibility of working with lower volumes, of monitor micro/nano structures, etc.^{132–135}

The basic ICP-MS is formed by: i) an introduction system; ii) an ionization source (ICP); iii) an interface; iv) a mass spectrometer; and v) an ion detector. Both the introduction systems and the ionization source (ICP) were explained previously.

The interface is a region that allows to sample a portion of the ions present in the plasma (which is at atmospheric pressure (~ 1 bar)) and transport them to the low-pressure region ($10^{-8} - 10^{-12}$ bars) where the mass analyzer is located. It consists of two consecutive cones with a small orifice in the centre, the sampling and the skimmer, which typically are made of nickel or platinum. The sampler cone is located closer to the plasma and its orifice is “bigger” than the skimmer cone to obtain a smooth transition between the different pressures. The ion beam passes through the centre of the cones and is accelerated by the vacuum generated by the rotary pump. Subsequently, it is introduced into the lens system that focuses it into the entrance of the mass spectrometer. The lenses are negatively charged, and, therefore, positive ions are concentrated in the middle of the beam, while the rest of the neutral atoms or negative ions are eliminated from the ion beam by the vacuum. At this point, it is possible that “space charge effects” occur, which it will explained hereinafter (Section 5.1.2.1).

The mass filter region is where the ions are separated by m/z ratio from the ion beam. There are different analyzers, such as time-of-flight mass spectrometer^{71,72} or sector field mass spectrometer,^{73,74} but the one most widely used is the quadrupole mass analyzer. It consists

of four parallel metal rods, equidistant from the ion beam. (**Figure 18**). The opposing rods are electrically connected, and voltages are applied to both rod pairs. The ion beam enters the quadrupole and travels down the central axis where the ions start to oscillate due to the voltages applied. The ion oscillation is influenced by both mass and charge. The ions with extreme oscillations are ejected from the stable transition regions. Therefore, the voltages are optimized so that only ions of a certain m/z ratio enjoy a stable trajectory and reach the detector. As it is possible to rapidly adjust these potentials; the quadrupole can scan the full elemental ions mass spectrum in less than one second.

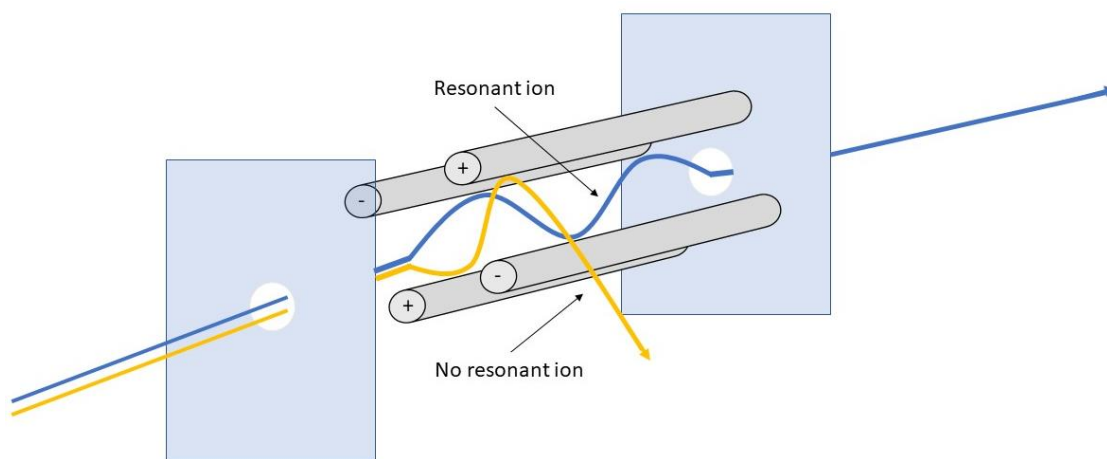


Figure 18. Scheme of a quadrupole mass filter.

The ion detector is responsible for detecting the ions coming out of the mass analyzer and transforming them into an electrical signal. The detector most commonly used nowadays is the discrete dynode type detector, which can operate in two modes, pulse counting or analogue. This permits extending the dynamic range.

Similar to AAS, ICP-MS technique suffer from potential spectral and non-spectral interferences.

Spectral interferences are produced when more than one ionic species shows the same m/z ratio. These interferences can be classified into two categories: isobaric and polyatomic interferences.¹³⁶

Isobaric interferences are caused by the overlap of the isotopes of different elements. This type of interference can be predicted because the different isotopes possessed by each element are well known. For example: $^{58}\text{Fe}^+$ and $^{58}\text{Ni}^+$

Polyatomic interferences are those produced by the formation of ionic molecules that show the same m/z as the element of interest. They usually come from the plasma (Ar) and atmospheric gas components that enter the plasma (C, O, H, N), from the acids or solvents, from matrix elements, etc.^{136,137,138}

To avoid or reduce polyatomic interferences, several approaches have been developed, such as sample separation protocols, cool plasma technology, desolvators, collision/reaction cells, among others.

The collision/reaction cell is situated between the interface and the mass spectrometer. Such cell is filled with a low pressure gas, which in the case of the collision cell is an inert gas to collide with the ions, while in the reaction cell it is a gas that reacts with the target ions. Collisions can break the molecular bond removing some polyatomic interferences or else slow them down, such that they cannot pass a certain kinetic barrier at the end of the cell. In the case of the reaction cell, the gas can react with the polyatomic interference producing other species that does not interfere, or else can react with the analyte giving rise to another species that can be measured at a free m/z . The most common gases used are He for the collision cells, and ammonia, methane or oxygen for the reaction cells.^{139–141} Also new technologies has been developed such as triple quadrupole systems capable of performing ICP-MS/MS,¹³³ or high-resolution mass analyzers,¹⁴² to name a few.¹⁴³

Non-spectral interferences come from sample matrix. The matrix can influence many process that occur during the analysis such as sample transport, ionization, ion extraction and transmission of the ion beam (space charge effect). This is due to coulombic interactions between ions in the extracted beam. This effect ejects the ions away from the central axis. The lighter isotopes undergo a greater displacement than the heavy ions, due to their smaller kinetic energy, and their transport efficiency is therefore lower, leading to mass bias.^{144–147} This effect can be reduced or eliminated by separating the element of interest from the rest of the matrix.

5.2 Speciation analysis

Speciation analyses are those that provide information of the abundance of species of an element and about their bioavailability. It is widely known that information about different species of an element is needed for fully understanding their reactivity and their toxicity. For

example, it is well known that free ionic Cu is toxic for humans. However, when it is complexed by natural ligands, its toxicity is reduced or eliminated.^{148,149}

Speciation analyses are commonly carried out using chromatography techniques coupled to a mass spectrometer. These techniques separate the compound of interest from the rest of the mixture to then be measured by a mass analyzer.

The coupling between the chromatography techniques with MS was achieved in the 1950s; however, it was not commercial until 1970, but they were not used in routine analysis until the mid 1990s.^{136,150}

In these separation techniques, the components of a sample are separated into two different phases, arranged in such a way that while one remains stationary within the system (stationary phase), the other moves along it (mobile phase). The key to separation in chromatography is that the rate at which each substance moves depends on its relative affinity for both phases (distribution equilibrium). That means that the separation process is based on the repeated interaction processes occurring during the displacement of the components of a mixture entrained by the mobile phase along the stationary phase (elution). Those compounds with fewer interactions with the stationary phase come out the column first.¹³⁶

The chromatographic methods can be classified according to the types of mobile and stationary phases and its interaction, as shown in **Table 1**.

Table 1. Classification of column chromatography methods. Reproduced from Skoog *et al.*¹³⁰

General Classification	Specific Method	Stationary Phase	Type of Equilibrium
1. Gas chromatography (GC)	a. Gas-liquid chromatography (GLC)	Liquid adsorbed or bonded to a solid surface	Partition between gas and liquid
	b. Gas-solid	Solid	Adsorption
2. Liquid chromatography (LC)	a. Liquid-liquid (partition)	Liquid adsorbed or bonded to a solid surface	Interaction with or partitioning between immiscible liquids*
	b. Liquid-solid or adsorption	Solid	Adsorption
	c. Ion exchange	Ion-exchange resin	Ion exchange
	d. Size exclusion	Liquid in interstices of a polymeric solid	Partition/sieving
	e. Affinity	Group-specific liquid bonded to a solid surface	Partition between surface liquid and mobile liquid
3. Supercritical fluid chromatography (SFC; mobile phase: supercritical fluid)		Organic species bonded to a solid surface	Partition between supercritical fluid and bonded surface

5.3 Isotopic analysis

Isotopic analyses are those that provide information about the different isotopes of an element. Isotopes are atoms that have the same number of protons but a different number of neutrons in the nuclei. Currently, investigation of the isotopic analysis in geosciences, archeometry, and, particularly, in biological samples is on the rise,^{151–155} because the variation in the isotopic signature of some elements can provide information about metabolism, healthy problems, etc.

Isotopic analysis is usually carried out using mass spectrometric techniques such as thermal ionization mass spectrometry (TIMS) and multi-collector inductively couple plasma-mass spectroscopy (MC-ICP-MS).

5.3.1 Thermal ionization mass spectrometry (TIMS)

TIMS is based on the drying, atomization and ionization of the analyte that is first deposited onto a filament surface, where it is heated. Generally, the filament is made of high purity rhenium, tantalum, tungsten and platinum.¹⁵⁶ TIMS devices consist of an ion source, a mass analyzer and detectors under vacuum, as shown in **Figure 19**.

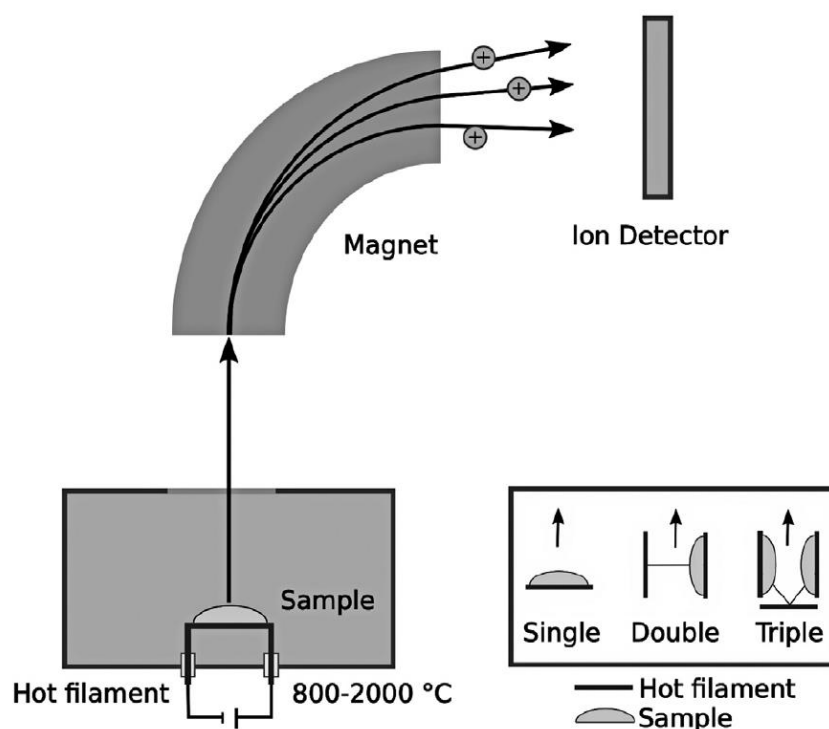


Figure 19. Scheme of a thermal ionization mass spectrometer. Reproduced from Walther *et al.*¹⁵⁷

As mentioned before, to generate ions, the sample is deposited onto the filament and then it is heated. This process takes place under vacuum. Single, double and triple filaments are used in TIMS as ion source. Only one filament is used when it is not necessary to separate the evaporation and ionization process; double or triple filaments are used when it is better to separate the evaporation process from the ionization process.¹⁵⁸

Positive ions can be expected for compounds that show a low first ionization potential (lower than 7 eV) by using a filament material with high conductivity. Negative ions can be obtained for compounds with high electron affinity (at least 2eV), using filaments with low conductivity.¹⁵⁸ The efficiency of ionization depends on the ionization energy of the element or the electron affinity.

When the ions are generated, they are accelerated toward the mass spectrometer using an extraction electrode together with a beam forming electrostatic lens. Once in the mass analyzer, they are separated by m/z ratios using an electromagnet (in a similar way that the MC-ICP-MS, as discussed in next section (5.3.2)). Subsequently, they are detected and collected in a multi-Faraday cup detector system.¹⁵⁹

5.3.2 Multi-collector inductively couple plasma-mass spectroscopy (MC-ICP-MS)

MC-ICP-MS is based on the same principles as ICP-MS. However, the detection is carried out simultaneously improving the isotopic ratio determination. It was introduced in the early 90s by Walder et Freedman.¹⁶⁰ MC-ICP-MS instrumentation is similar to that of the ICP-MS, with the difference that this instrument uses a double focusing sector field mass spectrometer with a multi-collector set-up with Faraday cups for ion detection. (See **Figure 20**)

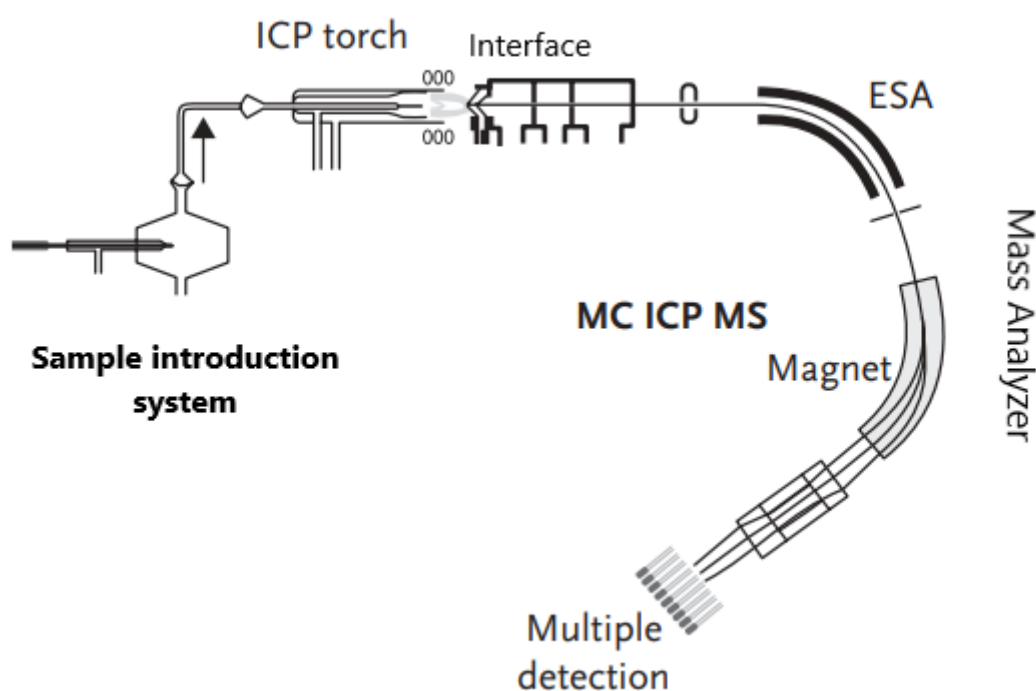


Figure 20. Scheme of a multi-collector inductively coupled plasma mass spectrometer. Reproduced from Donard *et al.*¹²⁴

The double focusing sector field mass spectrometer provides the best physical resolution among the commercial ICP-MS devices. The double focusing term is used because this device focuses the beam according to the ion energy and the direction. MC-ICP-MS uses a configuration called Nier-Johnson geometry, which uses a 90° electrostatic sector positioned after the ion source, followed by 90° magnetic sector. The electrostatic sector filters by kinetic energy while the magnetic sector separates the ions by their mass-to-charge ratio.

The exit slit situated between the mass spectrometer and the detector is wider than the entrance slit placed in front of the mass spectrometer to avoid significant ion losses. High resolution can be achieved with a narrow slit to allow only the selected ion to pass through.¹²⁴

The main feature of an MC-ICP-MS is that it is able to carry out truly simultaneous measurements unlike most types of ICP-MS devices, which operate sequentially (on a millisecond scale). This is possible because it possesses several detectors (usually between 10 and 15). The simultaneous detection implies that small fluctuations in the delivery of the ion beam should not affect the results, resulting in a better precision for isotopic ratio measurements. The most common detectors are Faraday cups and ion counters.¹²⁵

Isotopic analysis using MC-ICP-MS is very precise, but it suffers from spectral interferences and non-spectral interferences, as any kind of ICP-MS.

Spectral interferences can be removed and space charge effects limited with a previous sample preparation procedure to isolate the element of interest, and this approach is practically mandatory before isotopic analysis. However, mass bias persists after the isolation procedure and it must be corrected. Several strategies have been developed over the years for this^{124,155}, sample-standard bracketing (SSB) and external correction being the most common ones:

Sample-standard bracketing (SSB). The sample analysis is sandwiched between two measurements of a standard of known isotopic composition. The measured isotope ratio of the sample can be corrected relative to that of the standard.¹⁶² If both sample and standard are free from the matrix and show similar concentrations, it can be assumed that mass discrimination for both the standard and the sample are similar. Another use of the SSB is the calculation of the delta notation (δ) (see Chapter 5, 6 and 7).

External correction. To carry out this correction, it is necessary to add an element (of known isotopic composition) as internal standard (IS). The IS should have similar atomic number to the analyte (so that it is subject to the same space charge effects as the analyte) and not to be present in the sample. The measurement of the isotopic ratio of this IS is used to calculate the target isotopic ratio *via* a mathematical correction. The most used one is the exponential law proposed by Maréchal¹⁶³ (more details in Chapter 7).

6. Copper in clinical analysis

The importance of elemental biomonitoring as well as some of the techniques commonly used for their determination has been presented so far. This work has chosen to focus on copper because Cu is an essential transition metal for human and can be found in almost every cell of the humans body.^{109,164,165} Due to its redox properties, Cu exists in two forms in the human body: the oxidized form (Cu^{2+}) and the reduced form (Cu^+). Thanks to its ability to transfer and accept electrons, Cu plays a role in many metabolic processes, principally acting as a cofactor of numerous critical enzymes for oxidation-reduction reactions, such as Lysyl oxidase, Ceruloplasmin, Cytochrome c oxidase, Copper-zinc superoxide dismutase, Histaminase, Dopamine- β -hydroxylase, Tyrosinase, etc.¹⁶⁶ Consequently, it plays a role in vital activities like mitochondrial respiration, iron metabolism or neurotransmitter metabolism, just to name a few; it is crucial for the normal functioning of neurological, haematological, vascular, skeletal, and antioxidant systems. For example, cytochrome c oxidase plays an important role catalyzing the reduction of oxygen (O_2) to water (H_2O) to obtain energy for the organism in the mitochondria.¹⁶⁷ Lysyl oxidase intervenes in the biogenesis of connective tissues matrices by cross-linking reaction and insolubilization of collagen and elastin.¹⁶⁸ Ceruloplasmin is responsible to transport Cu from the liver to the bloodstream and to the rest of the body parts. Moreover, it oxidizes iron ($\text{Fe}^{2+} \rightarrow \text{Fe}^{3+}$) for the formation of Fe (III)-transferrin, which is necessary to provide iron for the haemoglobin.¹⁶⁹

However, despite Cu being an essential element, its accumulation is toxic because due to its redox capacity it can give rise to free radical species that damage key cellular compounds, such as DNA.¹⁷⁰ Therefore, a proper Cu metabolism regulation is necessary.

6.1 Copper metabolism

Cu is introduced in the human body *via* the diet, with an average Cu intake of about 2 - 5 mg per day.¹⁷¹ Cu absorption occurs in the duodenum, and also in the stomach and the proximal small intestine, but to a lower extent.¹⁷² Cu absorption depends on the Cu intake; being lower in a high Cu diet than in a low Cu diet.¹⁷³ That means that the intestinal barrier is the first regulator of Cu.¹⁷⁴ Once Cu is absorbed, to be introduced into the erythrocyte, it has to be reduced to its cuprous ion form (Cu^+). This process is carried out by the cytochrome b reductase 1 (CYBR1) and the 6-transmembrane epithelial antigen of the prostate family protein (STEAP) (**Figure 21A**) in the apical membrane. Cu in its reduced form is absorbed

mainly through Cu transporter 1 (CTR1) and, to a lesser extent, by divalent metal transporter 1 (DMT1).^{175,176} Once Cu enters the enterocyte, there are four possibilities; i) it can be used by the enterocyte; ii) it can be bound to the metallothionein, to be stored; iii) it can be transported to the rest of the organism; and iv) it can be eliminated by cellular desquamation to the gastrointestinal tract. To transport the Cu to the rest of the body, Cu must be secreted to the bloodstream. For that, Cu is bound to the metallochaperone (ATOX1), which is responsible for Cu transport to the ATP7A protein that is an energy-dependent copper pump. This protein, use the energy obtained from ATP hydrolysis to transport the Cu from the enterocytes into the bloodstream (**Figure 21B**). This process is controlled by the Cu concentration present into the enterocytes. Cu secretion to the blood is carried out when Cu concentration is high, to prevent intracellular accumulation and toxicity. Cu is secreted as Cu^{2+} into the bloodstream and is transported to the liver (principal organ for Cu homeostasis), *via* the hepatic portal vein, bound to albumin and, to a lesser extent, to transcuprein (alpha-2-macroglobulin, α -2M) and to amino acids such as histidine, glutamine, threonine and cysteine (**Figure 21C**).^{177,178} The bond between Cu bound to these low mass molecules is easily exchangeable. When Cu reaches the liver, it is introduced into the hepatocytes through the CTR1, in the same way in which it enters the enterocytes. In the liver, Cu is either bind to metallothionein for storage or bind to chaperones to be distributed in three pathways by copper chaperone for superoxide dismutase (SOD), cytochrome C oxidase (COX), and the copper chaperones ATOX1, depending on the function to be performed. When Cu is bound to the metallochaperone (ATOX1), is transported to the ATP7B protein. ATP7B is responsible for Cu incorporation into ceruloplasmin, which is secreted into the bloodstream. Cu bound to ceruloplasmin accounts for 75 – 95% of plasma Cu. However, when hepatocytes Cu levels rise, ATP7B changes to excrete the excess of Cu through the bile to regulate the Cu levels in the body (**Figure 21D**). Of the total Cu absorbed by the body, only about 0.9 mg per day¹⁷⁴ is needed while the rest is excreted, mostly through the bilis.¹⁷⁹

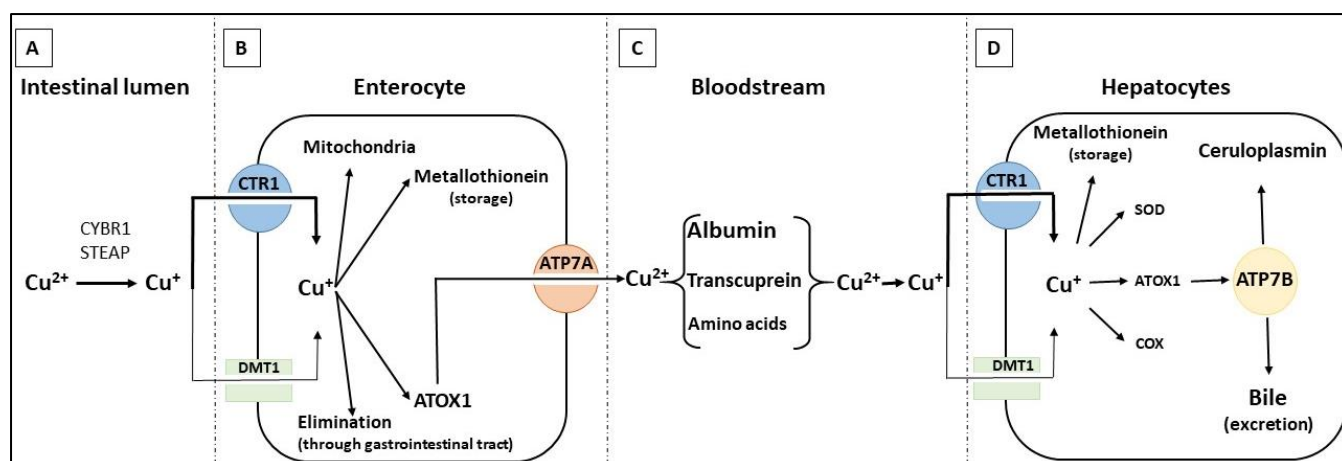


Figure 21. Diagram of Cu metabolism.

6.2 Disorders of Cu metabolism

The recommended amount of Cu is about 1.1 to 2 mg per day, but only 20 – 50% is absorbed.¹⁶⁶ Excess or deficit of Cu may be due to inadequate Cu levels intakes or some health problems.

Cu deficiency, or hypocupremia, can be due to multiple factors, either hereditary or acquired. Cu deficit can be caused by insufficient Cu intake through the diet, malabsorption of Cu due to disorders as chronic diarrhea, Crohn's disease, inflammatory bowel disease, in addition to some procedures such as bariatric surgery or provision of Zn therapy. Excess of Cu losses due to disorders caused by major burns¹⁸⁰ or renal replacement therapy¹⁸¹ also cause Cu deficiency. Thus, many factors affect Cu status such as: age, healthy bowel, level of dietary antagonists, etc. Moreover, some genetic diseases contribute to Cu deficiency, such as Menkes disease (MD),¹⁸² among others.

Cu deficiency can manifest itself in several ways: i) the hematologic way through anaemia, leukopenia, neutropenia, to name only the most common disorders;^{183,184} ii) the neurological pathway with the appearance of degeneration of spinal cord, optic neuropathy, etc;¹⁸⁵ iii) the cardiovascular way, such as severe life-threatening bradycardia, hypertension, high cholesterol levels in plasma, heart failure, etc;¹⁸⁶ iv) through skeletal changes, particularly in children, such as mimicking scurvy, severe osteoporosis, fractures of bones, among others; v) immunological manifestations, where the concentration of some immunological cells is disrupted;¹⁸⁷ and vi) through cutaneous manifestations, the most common of which are lax or easily extensible skin.

Excess of Cu, or hypercupremia, can occur in clinical situations such as Wilson´s disease (WD) (see Chapter 5 and 7), thyrotoxicosis, etc. In healthy women during pregnancy, Cu levels increase, although this variation is considered as normal.¹⁸⁸ However, Cu intoxication may also be due to drinking contaminated water or consuming contaminated food, environmental exposure, multivitamin supplement intake, alcohol consumption, cigarette smoking, oral contraceptives intake,¹⁸⁹ etc.

Copper excess, as well as copper deficiency, can be manifested in several ways. Disturbance of nervous system can be an indicator of Cu excess. It can be linked to mental disorders as histapenia (schizophrenia-like disorder), schizophrenia,¹⁹⁰ Alzheimer disease.^{191–193} Also, it can be connected to adult insomnia and dementia dialytica. Also hepatic and renal disorders,¹⁹⁴ hypertension, diabetes,¹⁹⁵ and some types of cancer can be due to or related to Cu excess.^{196,197}

6.3 Diseases related to ATP-Transporter

As mentioned above, MD and WD are the most well recognized and understood disorders of copper homeostasis. They are linked to rare genetic disorders that affect the ATP-Transporter, causing severe Cu deficiency and severe Cu toxicity, respectively.

MD is a genetic disease X-linked and is caused by the mutation of the ATP7A gen. It was described for the first time by Menkes and co-workers in 1962.¹⁹⁸ Its incidence depends on the area. For example, the incidence calculated in Europa is 1 out of 300000,¹⁹⁹ in Japan is 1 in 360000²⁰⁰ and in Australia is 1 of 50000-100000.²⁰¹ The gen affected codifies the ATP7A protein (also known as ATPase 1) that is a copper membrane-transporter,¹⁸² and is presented in all the tissues except in the liver. This mutation is lethal. Symptoms usually appear during the first three months of life and the patients often die before the 4th or 5th year of life. MD principally affects the nervous system producing hypothermia, neuronal degeneration, mental retardation, epileptic seizures, among others, and connective tissue as bone fractures, aortic aneurysm, which tend to worsen. Moreover, the hair is abnormal (scalp hair that is called kinky or steel wool).^{202,203}

There is a mildest variant of MD, known as occipital horn syndrome (OHS). It is usually diagnosed around 5-10 years of age. The principal signs are related to connective tissue (skeletal abnormalities) that include occipital horns, short and broad clavicles, osteoporosis

and laxity of the skin. Moreover, there are symptoms similar to MD, such as hypothermia, hypotonia, jaundice, diarrhea, feed problems, urinary infections, delay in motor development, etc. However, OHS patients can live until adulthood.^{201,203}

On the other hand, WD is a genetic disease that is supposed to affect 1 out of 30,000 persons, estimated in a general mode, although the incidence depends on the geographical area.²⁰⁴ It was described for the first time by Wilson in 1912²⁰⁵. However, until 1993 the disease was not related to the ATP7B gene that is in the chromosome 13.^{206–208} This gene encodes the ATP7B protein (also known as ATPase 2), which is a trans-membrane copper-transporting ATPase, as it was shown before. Nowadays, it is known that there are more than 500 mutations described that cause WD.^{209–211} This protein is the central regulator of the hepatic Cu metabolism. This mutation induces the synthesis of a dysfunctional ATP7B protein, which assists the transfer of Cu ions to the main plasma Cu protein (ceruloplasmin). Moreover, it is involved in the process of Cu excretion into the bile. When this function is altered, free Cu levels start building up in the liver causing causes hepatocellular necrosis, portal and periportal inflammation, and fibrosis Hepatocellular necrosis may result in fulminant hepatitis that may cause hemolysis and, then, the release of free Cu into the bloodstream, which eventually results in Cu accumulation and irreversible damage to other organs of the body, such as the brain, the eyes (Kayser–Fleischer rings), the kidneys, etc.²¹² with the fatal consequences that this entail.

Clinical presentations are variable due to the heterogeneity of organs where Cu is accumulated. The presentations range from asymptomatic to chronic liver disease, acute liver failure or neurological disorders. Generally, the patients are asymptomatic during the early life period. After that, between an age of 8 and 18 years, hepatic problems appear. And finally, around the third decade of life, neurologic and psychiatric disorders arrive. However, the sequence does not always follow the same trends. For example, the youngest patients with cirrhosis diagnosed with WD was only 3 years old,²¹³ while others patients were diagnosed in the fifth, sixth decades of life or even later, either with hepatic or neurologic disease.^{214,215} The oldest patients diagnosed were around 70 or even 80 years old.^{216,217}

Some patients develop physical signs of WD. The most common is the Kayser-Fleischer ring in the eyes. It is due to the Cu deposition on Descemet's membrane of the cornea. This sign is not exclusive of the WD, and neither all the WD patients suffer this manifestation. It is usually present in patients with neurologic symptoms, while in patients with hepatic symptoms

it appears only in 50% of the patients. The hepatic and neurologic signs are variable. The most common neurological signs are dystonia, tremor, and ataxia. While the hepatic signs are not defined because any type of liver disease may be encountered, from asymptomatic (only with biochemical abnormalities) to a cirrhosis. Also, WD can be linked to acute hepatic failure associated with Coombs-negative hemolytic anemia and acute renal failure. In general, the symptoms are acute, progress very fast, and if WD is untreated, it can be lethal.

6.4 Wilson's disease treatment

The aim of the treatment is to restore Cu homeostasis to normal. Nowadays, the treatment is quite easy and depends on the clinical picture of the patient. However, the survival and the quality of life for the patients depends on the stage of liver and neurological disease at the moment of diagnose, and pharmacological treatment follow-up. Liver transplantation can also be needed in patients with acute liver failure or cirrhosis.²¹⁸

Currently, there are two kinds of treatment: the use of chelators for increasing Cu excretion, for instance D-penicillamine and trientine, and the use of Zn salts (Zn) as Cu absorption blockers.²¹⁹

D-penicillamine was introduced in 1956 as the first oral treatment for WD. This agent acts increasing Cu excretion through the urine. This drug, generally, is used in symptomatic patients to remove the Cu accumulated. It is effective in improving the symptoms and signs of hepatic and neurologic disorders. Generally, patients respond quickly to treatment. However, some side effects may appear, such as acute neuronal deterioration hypersensitivity reactions, bone marrow suppression, and the development of autoimmune disease. That may be due to Cu mobilization, which produces changes in copper distribution in the nervous system, as well as in other organs.

Trientine is an alternative to D-penicillamine with a similar effectiveness. It was introduced in 1969. This agent also produces an increasing Cu excretion by the kidneys. However, side effects seem to be lower, although it can also produce some side effects such as neurological worsening, but it is less common than with D-penicillamine. Cases of hemorrhagic gastritis, loss of taste, and rashes, among others, have been reported. Normally, it is used with symptomatic patients, and with patients who are intolerant to D-penicillamine.

Zn salts were introduced in the early 1960s. The mechanism of action is different from that of D-penicillamine and trientine. They act blocking the Cu absorption. Then, Cu is excreted in the feces. Neurological deterioration may be a side effect although it is unusual using Zn. However, gastric irritation and pancreatitis have been reported as side effects. Zn salts are recommended for asymptomatic patients and for maintenance therapy. In any case, Zn treatment produces fewer side effects and is better tolerated by patients.

The importance of carrying out an early diagnosis and being able to treat the patient as soon as possible to prevent an excessive accumulation of Cu, with the consequences that this entails, cannot be stressed enough. In any case, the treatment is for life and continuous follow up of the patients to control the doses of the treatment and their healthy state is mandatory.

6.5 Ways to diagnose Wilson’s disease

WD diagnosis is not straightforward and is mostly carried out after the patient has developed some of the symptoms of the disease, with the negative consequences that this entails. Generally, to diagnose WD several test are needed, because there are many false positive or negative results, as it is possible to appreciate in **Table 2**. Moreover, genetic tests are costly and difficult, so they cannot be done on a routine basis to a wide population.

Table 2. Routine tests for diagnosis of Wilson’s disease. Reproduced from European Association For The Study Of The Liver.²²⁰

Test	Typical finding	False “negative”	False “positive”
Serum ceruloplasmin	Decreased by 50% of lower normal value	Normal levels in patients with marked hepatic inflammation Overestimation by immunologic assay Pregnancy, estrogen therapy	Low levels in: -malabsorption - aceruloplasminemia - heterozygotes
24-hour urinary copper	>1.6 $\mu\text{mol}/24\text{ h}$ >0.64 $\mu\text{mol}/24\text{ h}$ in children	Normal: -incorrect collection -children without liver disease	Increased: - hepatocellular necrosis - cholestasis - contamination
Serum “free” copper	>1.6 $\mu\text{mol}/\text{L}$	Normal if ceruloplasmin overestimated by immunologic assay	
Hepatic copper	>4 $\mu\text{mol}/\text{g}$ dry weight	Due to regional variation -in patients with active liver disease -in patients with regenerative nodules	Cholestatic syndromes
Kayser-Fleischer rings by slit lamp examination	Present	Absent -in up to 50% of patients with hepatic WD -in most asymptomatic siblings	Primary biliary cirrhosis

Hence the importance of continuing the research on new methods to diagnose WD at an early stage, before any symptoms appear. In this regard, investigations about Cu isotopic analysis^{221–223} or parameters related with the Cu bound to ceruloplasmin and/ or free Cu^{224–227} are currently on the rise. More information will be provided in Chapters 5 and 7.

7. References

- 1 World health organization, *Human biomonitoring: facts and figures*, Copenhagen: WHO Regional Office for Europe., 2015.
- 2 J. Angerer, U. Ewers and M. Wilhelm, *Int. J. Hyg. Environ. Health*, 2007, **210**, 201–228.
- 3 M. Esteban and A. Castaño, *Environ. Int.*, 2009, **35**, 438–449.
- 4 S. J. Genuis, D. Birkholz, I. Rodushkin and S. Beesoon, *Arch. Environ. Contam. Toxicol.*, 2011, **61**, 344–357.
- 5 L. Caporossi, A. Santoro and B. Papaleo, *Biomarkers*, 2010, **15**, 475–487.
- 6 Y. Harahap, R. Diptasaadya and D. J. Purwanto, *Drug Des. Devel. Ther.*, 2020, **Volume 14**, 5757–5771.
- 7 S. A. Ejazi, S. Ghosh and N. Ali, *Immunol. Cell Biol.*, 2021, **99**, 21–33.
- 8 J. Kopel, H. Goyal and A. Perisetti, *Bayl. Univ. Med. Cent. Proc.*, 2021, **34**, 63–72.
- 9 E. Albert, I. Torres, F. Bueno, D. Huntley, E. Molla, M. Á. Fernández-Fuentes, M. Martínez, S. Poujois, L. Forqué, A. Valdivia, C. Solano de la Asunción, J. Ferrer, J. Colomina and D. Navarro, *Clin. Microbiol. Infect.*, 2021, **27**, 472.e7-472.e10.
- 10 R. T. Daniel, T. Klara, A. D. Richard and S. W. George, *Pure Appl Chem*, 1999, **71**, 2333–2348.
- 11 D. R. Thévenot, K. Toth, R. A. Durst and G. S. Wilson, *Biosens. Bioelectron.*, 2001, **16**, 121–131.
- 12 K. Cammann, *Fresenius Z. Für Anal. Chem.*, 1977, **287**, 1–9.
- 13 M. A. Morales and J. M. Halpern, *Bioconjug. Chem.*, 2018, **29**, 3231–3239.
- 14 S. K. Metkar and K. Girigoswami, *Biocatal. Agric. Biotechnol.*, 2019, **17**, 271–283.
- 15 C. Leland C. and C. Lyons, *Autom. Semi-Automated Syst. Clin. Chem.*, 1962, **102**, 29–45.
- 16 V. Perumal and U. Hashim, *J. Appl. Biomed.*, 2014, **12**, 1–15.
- 17 N. S. Oliver, C. Toumazou, A. E. G. Cass and D. G. Johnston, *Diabet. Med.*, 2009, **26**, 197–210.

- 18 Niraj, M. . Gupta, H. M. Varshney, S. Pandey and S. Singh, *Int. J. Ther. Appl.*, 2021, **6**, 28–37.
- 19 G. Stergiou, T. Mengden, P. L. Padfield, G. Parati and E. O'Brien, 2004.
- 20 E. M. Goldberg and P. D. Levy, *Curr. Hypertens. Rep.*, , DOI:10.1007/s11906-016-0650-9.
- 21 G. Casalino, G. Castellano and G. Zaza, in *2020 IEEE Symposium on Computers and Communications (ISCC)*, IEEE, 2020, pp. 1–7.
- 22 E. B. Bahadır and M. K. Sezgintürk, *Anal. Biochem.*, 2015, **478**, 107–120.
- 23 S. Kanchi, M. I. Sabela, P. S. Mdluli, Inamuddin and K. Bisetty, *Biosens. Bioelectron.*, 2018, **102**, 136–149.
- 24 D. Zhang and Q. Liu, *Biosens. Bioelectron.*, 2016, **75**, 273–284.
- 25 R. Guthrie and A. Susi, *Pediatrics*, 1963, **32**, 338–343.
- 26 I. Bang, *Fresenius Z. F Anal Chem.*, 1913, **52**, 521–523.
- 27 J. J. Pitt, *Clin. Biochem. Rev.*, 2010, **31**, 57.
- 28 S. Lehmann, C. Delaby, J. Vialaret, J. Ducos and C. Hirtz, *Clin. Chem. Lab. Med.*, , DOI:10.1515/cclm-2013-0228.
- 29 P. M. Edelbroek, J. van der Heijden and L. M. Stolk, *Ther. Drug Monit.*, 2009, **31**, 327–336.
- 30 C. P. Stove, A.-S. M. E. Ingels, P. M. M. De Kesel and W. E. Lambert, *Crit. Rev. Toxicol.*, 2012, **42**, 230–243.
- 31 P. A. Demirev, *Anal. Chem.*, 2013, **85**, 779–789.
- 32 A. J. Wilhelm, J. C. G. den Burger and E. L. Swart, *Clin. Pharmacokinet.*, 2014, **53**, 961–973.
- 33 M. Resano, M. A. Belarra, E. Garcia-Ruiz, M. Aramendia and L. Rello, *Trends Anal. Chem.*, 2018, **99**, 75–87.
- 34 T.W. McDade, S. Williams and J.J. Snodgrass, *Demography*, 2007, **44**, 899–925.
- 35 E. M. Crimmins, Y. S. Zhang, J. K. Kim, S. Frochen, H. Kang, H. Shim, J. Ailshire, A. Potter, J. Cofferren and J. Faul, *Am. J. Hum. Biol.*, 2020, **32**, e23390.
- 36 B. W. Adam, E. M. Hall, M. Sternberg, T. H. Lim, S. R. Flores, S. O'Brien, D. Simms, L. X. Li, V. R. De Jesus and W. H. Hannon, *Clin. Biochem.*, 2011, **44**, 1445–1450.
- 37 M. S. Lee and W. Li, Eds., *Dried blood spots: applications and techniques*, John Wiley & Sons, Inc, Hoboken, New Jersey, 2014.
- 38 G. Liu, Q. C. Ji, M. Jemal, A. A. Tymiak and M. E. Arnold, *Anal. Chem.*, 2011, **83**, 9033–9038.

- 39 Trifonova, Maslov, Balashova and Lokhov, *Metabolites*, 2019, **9**, 277.
- 40 J. C. Rockett, G. M. Buck, C. D. Lynch and S. D. Perreault, *Environ. Health Perspect.*, 2004, **112**, 94–104.
- 41 D. Carpentieri, A. Colvard, J. Petersen, W. Marsh, V. David-Dirgo, M. Huentelman, P. Pirrotte and T. A. Sivakumaran, *Biopreservation Biobanking*, 2021, **19**, 136–142.
- 42 J. V. Mei, J. R. Alexander, B. W. Adam and W. H. Hannon, *J. Nutr.*, 2001, **131**, 1631S–1636S.
- 43 M. O'Mara, B. Hudson-Curtis, K. Olson, Y. Yueh, J. Dunn and N. Spooner, *Bioanalysis*, 2011, **3**, 2335–2347.
- 44 N. Youhnovski, A. Bergeron, M. Furtado and F. Garofolo, *Rapid Commun. Mass Spectrom.*, 2011, **25**, 2951–2958.
- 45 S. Velghe, L. Delahaye and C. P. Stove, *J. Pharm. Biomed. Anal.*, 2019, **163**, 188–196.
- 46 P. Denniff and N. Spooner, *Anal. Chem.*, 2014, **86**, 8489–8495.
- 47 S. Velghe and C. P. Stove, *Anal. Chem.*, 2018, **90**, 12893–12899.
- 48 G. Lenk, S. Sandkvist, A. Pohanka, G. Stemme, O. Beck and N. Roxhed, *Bioanalysis*, 2015, **7**, 2085–2094.
- 49 R. Neto, A. Gooley, M. C. Breadmore, E. F. Hilder and F. Lapierre, *Anal. Bioanal. Chem.*, 2018, **410**, 3315–3323.
- 50 L. A. Leuthold, O. Heudi, J. Déglon, M. Raccuglia, M. Augsburger, F. Picard, O. Kretz and A. Thomas, *Anal. Chem.*, 2015, **87**, 2068–2071.
- 51 L. Delahaye, H. Veenhof, B. C. Koch, J.-W. C. Alffenaar, R. Linden and C. Stove, *Ther. Drug Monit.*, 2021, **43**, 310–321.
- 52 T. M. Blicharz, P. Gong, B. M. Bunner, L. L. Chu, K. M. Leonard, J. A. Wakefield, R. E. Williams, M. Dadgar, C. A. Tagliabue, R. El Khaja, S. L. Marlin, R. Haghgooie, S. P. Davis, D. E. Chickering and H. Bernstein, *Nat. Biomed. Eng.*, 2018, **2**, 151–157.
- 53 H. Y. Tey and H. H. See, *J. Chromatogr. A*, 2021, **1635**, 461731.
- 54 J.-H. Kim, T. Woenker, J. Adamec and F. E. Regnier, *Anal. Chem.*, 2013, **85**, 11501–11508.
- 55 A. G. Verstraete, *Drug Monit.*, 2004, **26**, 200–205.
- 56 F. V. Nakadi, R. Garde, M. A. M. S. da Veiga, J. Cruces and M. Resano, *J. Anal. At. Spectrom.*, 2020, **35**, 136–144.
- 57 B. U. W. Lei and T. W. Prow, *Biomed. Microdevices*, 2019, **21**, 21–81.
- 58 J. Řužička and E. H. Hansen, *Anal. Chim. Acta*, 1975, **78**, 145–157.

- 59 E. H. Hansen and M. Miró, *TrAC Trends Anal. Chem.*, 2007, **26**, 18–26.
- 60 M. Trojanowicz and K. Kołacińska, *The Analyst*, 2016, **141**, 2085–2139.
- 61 S. Clavijo, J. Avivar, R. Suárez and V. Cerdà, *TrAC Trends Anal. Chem.*, 2015, **67**, 26–33.
- 62 J. Wang and E. H. Hansen, *TrAC Trends Anal. Chem.*, 2003, **22**, 225–231.
- 63 M. D. Luque de Castro, J. Ruiz-Jiménez and J. A. Pérez-Serradilla, *TrAC Trends Anal. Chem.*, 2008, **27**, 118–126.
- 64 J. Mora, S. Maestre, V. Hernandis and J. L. Todolí, *TrAC Trends Anal. Chem.*, 2003, **22**, 123–132.
- 65 J. A. Burgener and Y. Makonnen, in *Sample Introduction Systems in ICPMS and ICPOES*, Elsevier, 2020, pp. 57–142.
- 66 N. H. Bings, J. O. Orlandini von Niessen and J. N. Schaper, *Spectrochim. Acta Part B At. Spectrosc.*, 2014, **100**, 14–37.
- 67 J. L. Todolí and J. M. Mermet, *Spectrochim. Acta Part B At. Spectrosc.*, 2006, **61**, 239–283.
- 68 J.-L. Todolí, S. Maestre, J. Mora, A. Canals and V. Hernandis, *Fresenius J. Anal. Chem.*, 2000, **368**, 773–779.
- 69 J. L. Todolí and J. M. Mermet, *TrAC Trends Anal. Chem.*, 2005, **24**, 107–116.
- 70 J.-L. Todolí, V. Hernandis, A. Canals and J.-M. Mermet, *J. Anal. At. Spectrom.*, 1999, **14**, 1289–1295.
- 71 J.-L. Todolí and J.-M. Mermet, *J Anal Spectrom*, 2002, **17**, 345–351.
- 72 J.-L. Todolí and J.-M. Mermet, *J Anal Spectrom*, 2004, **19**, 1347–1353.
- 73 Á. Cañabate, E. García-Ruiz, M. Resano and J.-L. Todolí, *J. Anal. At. Spectrom.*, 2017, **32**, 78–87.
- 74 E. Paredes, M. Grotti, J. M. Mermet and J. L. Todolí, *J. Anal. At. Spectrom.*, 2009, **24**, 903.
- 75 M. Grotti, F. Ardini and J. L. Todolí, *Anal. Chim. Acta*, 2013, **767**, 14–20.
- 76 G. Holland, S. D. Tanner and Royal Society of Chemistry (Great Britain), Eds., *Plasma source mass spectrometry: the new millennium*, Royal Society of Chemistry, Cambridge, 2001.
- 77 Teledyne CETAC Technologies, https://www.teledynecetac.com/site-products/Brochures/Brochure_Aridus3.
- 78 C. Gregoire, M. Lamoureux, C. L. Chakrabart, S. Al-Maawali and J. P. Byrne, *J. Anal. At. Spectrom.*, 1992, **7**, 579–585.

- 79 L'vov, B. V., *Inzhener-FizzhurAkad Nauk Belorus SSR*, 1959, 44–52.
- 80 J.D. Kerber, *Absorpt Newsl*, 1971, **10**, 104.
- 81 D. E. Nixon, V. A. Fassel and R. N. Kniseley, *Anal. Chem.*, 1974, **46**, 210–213.
- 82 A. M. Gunn, D. L. Millard and G. F. Kirkbright, *Analyst*, 1978, **103**, 1066–1073.
- 83 A. L. Gray and A. R. Date, *Analyst*, 1983, **108**, 1033–1050.
- 84 M. Lackner, Ed., *Lasers in chemistry*, Wiley-VCH, Weinheim, 2008.
- 85 M. Thompson, J. E. Goulter and F. Sieper, *The Analyst*, 1981, **106**, 32.
- 86 A. L. Gray, *The Analyst*, 1985, **110**, 551.
- 87 S. M. Eggins, L. P. J. Kinsley and J. M. G. Shelley, *Appl. Surf. Sci.*, 1998, **127**, 278–286.
- 88 D. Günther and C. A. Heinrich, *J. Anal. At. Spectrom.*, 1999, **14**, 1369–1374.
- 89 R. E. Russo, X. Mao, H. Liu, J. Gonzalez and S. S. Mao, *Talanta*, 2002, **57**, 425–451.
- 90 C. Liu, X. L. Mao, S. S. Mao, X. Zeng, R. Greif and R. E. Russo, *Anal. Chem.*, 2004, **76**, 379–383.
- 91 V. Možná, J. Pisonero, M. Holá, V. Kanický and D. Günther, *J Anal Spectrom*, 2006, **21**, 1194–1201.
- 92 J. Koch, A. von Bohlen, R. Hergenröder and K. Niemax, *J Anal Spectrom*, 2004, **19**, 267–272.
- 93 R. E. Russo, X. L. Mao, O. V. Borisov and H. Liu, *J. Anal. At. Spectrom.*, 2000, **15**, 1115–1120.
- 94 M. Motelica-Heino, O. F. X. Donard and J. M. Mermet, *J. Anal. At. Spectrom.*, 1999, **14**, 675–682.
- 95 D. Günther and C. A. Heinrich, *J. Anal. At. Spectrom.*, 1999, **14**, 1363–1368.
- 96 B. Fernández, F. Claverie, C. Pécheyran, O. F. X. Donard and F. Claverie, *TrAC Trends Anal. Chem.*, 2007, **26**, 951–966.
- 97 M. Guillong, I. Horn and D. Günther, *J Anal Spectrom*, 2003, **18**, 1224–1230.
- 98 D. Günther and B. Hattendorf, *TrAC Trends Anal. Chem.*, 2005, **24**, 255–265.
- 99 J. González, C. Liu, X. Mao and R. E. Russo, *J. Anal. At. Spectrom.*, 2004, **19**, 1165–1168.
- 100 R. Hergenröder, O. Samek and V. Hommes, *Mass Spectrom. Rev.*, 2006, **25**, 551–572.
- 101 I. Horn and D. Günther, *Appl. Surf. Sci.*, 2003, **207**, 144–157.
- 102 J. Gonzalez, X. L. Mao, J. Roy, S. S. Mao and R. E. Russo, *J Anal Spectrom*, 2002, **17**, 1108–1113.

- 103 Y. Wang, H. Zhu and K. Kannan, *Toxics*, 2019, **7**, 21.
- 104 V. Yusa, M. Millet, C. Coscolla and M. Roca, *Anal. Chim. Acta*, 2015, **891**, 15–31.
- 105 D. Rodbard, *Diabetes Technol. Ther.*, 2016, **18**, S2-3-S2-13.
- 106 V. Narwal, R. Deswal, B. Batra, V. Kalra, R. Hooda, M. Sharma and J. S. Rana, *Steroids*, 2019, **143**, 6–17.
- 107 A. Agapiou, A. Amann, P. Mochalski, M. Statheropoulos and C. L. P. Thomas, *TrAC Trends Anal. Chem.*, 2015, **66**, 158–175.
- 108 W. Maret, *Int. J. Mol. Sci.*, 2016, **17**, 66.
- 109 M. A. Zoroddu, J. Aaseth, G. Crisponi, S. Medici, M. Peana and V. M. Nurchi, *J. Inorg. Biochem.*, 2019, **195**, 120–129.
- 110 J. B. Vincent, *J. Nutr.*, 2017, **147**, 2212–2219.
- 111 K. R. Di Bona, S. Love, N. R. Rhodes, D. McAdory, S. H. Sinha, N. Kern, J. Kent, J. Strickland, A. Wilson, J. Beaird, J. Ramage, J. F. Rasco and J. B. Vincent, *JBIC J. Biol. Inorg. Chem.*, 2011, **16**, 381–390.
- 112 M. Jaishankar, T. Tseten, N. Anbalagan, B. B. Mathew and K. N. Beeregowda, *Interdiscip. Toxicol.*, 2014, **7**, 60–72.
- 113 M. Kabamba and J. Tuakuila, *Toxicol. Lett.*, 2020, **332**, 20–26.
- 114 K. A. Francesconi, *The Analyst*, 2007, **132**, 17–20.
- 115 E. C. Moody, S. G. Coca and A. P. Sanders, *Curr. Environ. Health Rep.*, 2018, **5**, 453–463.
- 116 T. G. Kazi, H. I. Afridi, N. Kazi, M. K. Jamali, M. B. Arain, N. Jalbani and G. A. Kandhro, *Biol. Trace Elem. Res.*, 2008, **122**, 1–18.
- 117 B. Welz and M. Sperling, *Atomic absorption spectrometry*, John Wiley & Sons, 2008.
- 118 Kirchhoff, G. and Bunsen, R., *Ann Phys-Berl.*, 1860, **110**, 161–189.
- 119 A. Walsh, *Spectrochim. Acta*, 1955, **7**, 108–117.
- 120 A. Walsh, *Anal. Chem.*, 1974, **46**, 698A–708a.
- 121 G. I. Goodfellow, *Appl. Spectrosc.*, 1967, **21**, 39–42.
- 122 B. Welz, Becker-Ross, H., Florek, S. and Heitmann, U, Eds., *High-resolution continuum source AAS: the better way to do atomic absorption spectrometry*, Wiley-VCH, Weinheim, 2005.
- 123 M. Resano, M. R. Flórez and E. García-Ruiz, *Anal. Bioanal. Chem.*, 2014, **406**, 2239–2259.
- 124 F. Vanhaecke and P. Degryse, *Isotopic Analysis: Fundamentals and Applications Using ICP-MS*, Weinheim, Wiley-VCH Verlag GmbH & Co. KGaA., 2012.

- 125 J.-L. Todolí, in *Reference Module in Chemistry, Molecular Sciences and Chemical Engineering*, Elsevier, 2018.
- 126 S. Greenfield, I. L. Jones and C. T. Berry, *Analyst*, 1964, **89**, 713–720.
- 127 Wendt, R.H. and Fassel, V.A., *Anal Chem*, 1965, **37**, 920–922.
- 128 X. Hou and B. T. Jones, *Encycl. Anal. Chem.*, 2000, **11**, 9468–9485.
- 129 M. Thompson, *Handbook of inductively coupled plasma spectrometry*, Springer Science & Business Media, 2012.
- 130 D. A. Skoog, F. J. Holler and S. R. Crouch, *Principles of Instrumental Analysis*, CENGAGE Learning, Boston, USA, 7th edition., 2018.
- 131 R. S. Houk, V. A. Fassel, G. D. Flesch, H. J. Svec, A. L. Gray and C. E. Taylor, *Anal. Chem.*, 1980, **52**, 2283–2289.
- 132 D. Beauchemin, *Anal. Chem.*, 2010, **82**, 4786–4810.
- 133 E. Bolea-Fernandez, L. Balcaen, M. Resano and F. Vanhaecke, *J. Anal. At. Spectrom.*, 2017, **32**, 1660–1679.
- 134 L. Balcaen, E. Bolea-Fernandez, M. Resano and F. Vanhaecke, *Anal. Chim. Acta*, 2015, **894**, 7–19.
- 135 B. Meermann and V. Nischwitz, *J. Anal. At. Spectrom.*, 2018, **33**, 1432–1468.
- 136 D. A. Skoog, F. J. Holler and S. R. Crouch, *Principles of instrumental analysis*, Thomson Brooks/Cole, Belmont, CA, 6th ed., 2007.
- 137 E. H. Evans and J. J. Giglio, *J. Anal. At. Spectrom.*, 1993, **8**, 1.
- 138 T. W. May and R. H. Wiedmeyer, *At. Spectrosc.*, 1998, **19**, 151–155.
- 139 V. Baranov and S. Tanner, *J. Anal. At. Spectrom.*, 1999, **14**, 1133–1142.
- 140 D. Pick, M. Leiterer and J. W. Einax, *Microchem. J.*, 2010, **95**, 315–319.
- 141 M. Iglesias, N. Gilon, E. Poussel and J.-M. Mermet, *J. Anal. At. Spectrom.*, 2002, **17**, 1240–1247.
- 142 F. Xian, C. L. Hendrickson and A. G. Marshall, *Anal. Chem.*, 2012, **84**, 708–719.
- 143 T.-S. Lum and K. Sze-Yin Leung, *J. Anal. At. Spectrom.*, 2016, **31**, 1078–1088.
- 144 J. W. Olesik and M. P. Dziewatkoski, *J. Am. Soc. Mass Spectrom.*, 1996, **7**, 362–367.
- 145 N. Praphairaksit and R. S. Houk, *Anal. Chem.*, 2000, **72**, 2356–2361.
- 146 J. A. Olivares and R. S. Houk, *Anal. Chem.*, 1985, **57**, 2674–2679.
- 147 G. R. Gillson, D. J. Douglas, J. E. Fulford, K. W. Halligan and S. D. Tanner, *Anal. Chem.*, 1988, **60**, 1472–1474.
- 148 W. Lund, *Fresenius J. Anal. Chem.*, 1990, **337**, 557–564.
- 149 L. Gaetke, *Toxicology*, 2003, **189**, 147–163.

- 150 J. J. Pitt, *Clin. Biochem. Rev.*, 2009, **30**, 19.
- 151 F. Albarede, P. Télouk, V. Balter, V. P. Bondanese, E. Albalat, P. Oger, P. Bonaventura, P. Miossec and T. Fujii, *Metallomics*, 2016, **8**, 1056–1070.
- 152 M. Costas-Rodríguez, S. Van Campenhout, A. A. M. B. Hastuti, L. Devisscher, H. Van Vlierberghe and F. Vanhaecke, *Metallomics*, 2019, **11**, 1093–1103.
- 153 M. Costas-Rodríguez, J. Delanghe and F. Vanhaecke, *TrAC Trends Anal. Chem.*, 2016, **76**, 182–193.
- 154 F. Larner, L. N. Woodley, S. Shousha, A. Moyes, E. Humphreys-Williams, S. Strekopytov, A. N. Halliday, M. Rehkämper and R. C. Coombes, *Metallomics*, 2015, **7**, 112–117.
- 155 G. W. Gordon, J. Monge, M. B. Channon, Q. Wu, J. L. Skulan, A. D. Anbar and R. Fonseca, *Leukemia*, 2014, **28**, 2112–2115.
- 156 S. K. Aggarwal, *Anal. Methods*, 2016, **8**, 942–957.
- 157 C. Walther and K. Wendt, in *Handbook of Radioactivity Analysis*, Elsevier, 2020, pp. 861–898.
- 158 K. G. Heumann, S. Eisenhut, S. Gallus, E. H. Hebeda, R. Nusko, A. Vengosh and T. Walczyk, *Analyst*, 1995, **120**, 1291–1299.
- 159 W. M. White, Ed., *Encyclopedia of Geochemistry: A Comprehensive Reference Source on the Chemistry of the Earth*, Springer International Publishing, Cham, 2018.
- 160 A. J. Walder and P. A. Freedman, *J. Anal. At. Spectrom.*, 1992, **7**, 571–575.
- 161 L. Yang, *Mass Spectrom. Rev.*, 2009, **28**, 990–1011.
- 162 F. Albarède, P. Telouk, J. Blichert-Toft, M. Boyet, A. Agranier and B. Nelson, *Geochim. Cosmochim. Acta*, 2004, **68**, 2725–2744.
- 163 C. N. Maréchal, P. Télouk and F. Albarède, *Chem. Geol.*, 1999, **156**, 251–273.
- 164 C. G. Fraga, *Mol. Aspects Med.*, 2005, **26**, 235–244.
- 165 R. A. Festa and D. J. Thiele, *Curr. Biol.*, 2011, **21**, R877–R883.
- 166 M. Altarelli, N. Ben-Hamouda, A. Schneider and M. M. Berger, *Nutr. Clin. Pract.*, 2019, **34**, 504–513.
- 167 M. Wikström, *Biochim. Biophys. Acta BBA - Bioenerg.*, 2004, **1655**, 241–247.
- 168 H. M. Kagan and P. C. Trackman, *Am J Respir Cell Mol Biol*, 1991, **5**, 206–210.
- 169 S. Osaki, D. A. Johnson and E. Frieden, *J. Biol. Chem.*, 1966, **241**, 2746–2751.
- 170 M. C. Linder, *Mutat. Res. Mol. Mech. Mutagen.*, 2012, **733**, 83–91.
- 171 M. Bost, S. Houdart, M. Oberli, E. Kalonji, J.-F. Huneau and I. Margaritis, *J. Trace Elem. Med. Biol.*, 2016, **35**, 107–115.

- 172 K. E. Mason, *J. Nutr.*, 1979, **109**, 1979–2006.
- 173 J. R. Turnlund, W. R. Keyes, H. L. Anderson and L. L. Acord, *Am. J. Clin. Nutr.*, 1989, **49**, 870–878.
- 174 J. R. Turnlund, *Am. J. Clin. Nutr.*, 1998, **67**, 960S–964S.
- 175 C. Abou Zeid and S. G. Kaler, in *Wilson Disease*, Elsevier, 2019, pp. 17–22.
- 176 P. V. van den Berghe and L. W. Klomp, *Nutr. Rev.*, 2009, **67**, 658–672.
- 177 M. Moriya, Y.-H. Ho, A. Grana, L. Nguyen, A. Alvarez, R. Jamil, M. L. Ackland, A. Michalczyk, P. Hamer, D. Ramos, S. Kim, J. F. B. Mercer and M. C. Linder, *Am. J. Physiol.-Cell Physiol.*, 2008, **295**, C708–C721.
- 178 P. Z. Neumann and A. Sass-Kortsak, *J. Clin. Invest.*, 1967, **46**, 646–658.
- 179 H. Roelofsen, H. Wolters, M. J. A. Van Luyn, N. Miura, F. Kuipers and R. J. Vonk, *Gastroenterology*, 2000, **119**, 782–793.
- 180 B. Sampson, M. A. Constantinescu, I. Chandarana and P. D. Cussons, *Ann. Clin. Biochem.*, 1996, **33**, 462–464.
- 181 N. Ben-Hamouda, M. Charrière, P. Voirol and M. M. Berger, *Nutrition*, 2017, **34**, 71–75.
- 182 H. Pierson, S. Lutsenko and Z. Tümer, in *eLS*, ed. John Wiley & Sons Ltd, John Wiley & Sons, Ltd, Chichester, UK, 2015, pp. 1–15.
- 183 Z. W. Myint, T. H. Oo, K. Z. Thein, A. M. Tun and H. Saeed, *Ann. Hematol.*, 2018, **97**, 1527–1534.
- 184 T. R. Halfdanarson, N. Kumar, C.-Y. Li, R. L. Phyllyk and W. J. Hogan, *Eur. J. Haematol.*, 2008, **80**, 523–531.
- 185 S. L. Pineles, C. A. Wilson, L. J. Balcer, R. Slater and S. L. Galetta, *Surv. Ophthalmol.*, 2010, **55**, 386–392.
- 186 L. M. Klevay, *J. Nutr.*, 2000, **130**, 489S–492S.
- 187 C. Muñoz, E. Rios, J. Olivos, O. Brunser and M. Olivares, *Br. J. Nutr.*, 2007, **98**, S24–S28.
- 188 J. Vukelic, A. Kapamadzija, D. Petrovic, Z. Grujic, A. Novakov-Mikic, V. Kopitovic and A. Bjelica, *Srp. Arh. Celok. Lek.*, 2012, **140**, 42–46.
- 189 Ž. Babić, B. Tariba, J. Kovačić, A. Pizent, V. M. Varnai and J. Macan, *Contraception*, 2013, **87**, 790–800.
- 190 M. Yanik, A. Kocyigit, H. Tutkun, H. Vural and H. Herken, *Biol. Trace Elem. Res.*, 2004, **98**, 109–117.
- 191 A. Hordyjewska, Ł. Popiołek and J. Kocot, *BioMetals*, 2014, **27**, 611–621.

- 192 A. I. Bush, *Curr. Opin. Chem. Biol.*, 2000, **4**, 184–191.
- 193 A. Prakash, G. K. Dhaliwal, P. Kumar and A. B. A. Majeed, *Int. J. Neurosci.*, 2017, **127**, 99–108.
- 194 A. A. Iyanda, J. Anetor and F. A. A. Adeniyi, *Biol. Trace Elem. Res.*, 2011, **143**, 1264–1270.
- 195 Q. Qiu, F. Zhang, W. Zhu, J. Wu and M. Liang, *Biol. Trace Elem. Res.*, 2017, **177**, 53–63.
- 196 C. C. Pfeiffer and R. Mailloux, *J. Orthomol. Med.*, 1987, **2**, 171–182.
- 197 M. Latorre, R. Troncoso and R. Uauy, in *Clinical and Translational Perspectives on Wilson Disease*, Elsevier, 2019, pp. 25–31.
- 198 J. H. Menkes, M. Alter, G. K. Steigleder, D. R. Weakley and J. H. Sung, *Pediatrics*, 1962, **29**, 764–769.
- 199 T. Tønnesen, W. J. Kleijer and N. Horn, *Hum. Genet.*, 1991, **86**, 408–410.
- 200 Y. H. Gu, H. Kodama, K. Shiga, S. Nakata, Y. Yanagawa and H. Ozawa, *J. Inherit. Metab. Dis.*, 2005, **28**, 473–478.
- 201 Z. Tümer and L. B. Møller, *Eur. J. Hum. Genet.*, 2010, **18**, 511–518.
- 202 A. N. Prasad and R. Ojha, *J. Multidiscip. Healthc.*, 2016, **Volume 9**, 371–385.
- 203 H. Kodama, Y. Murata and M. Kobayashi, *Pediatr. Int.*, 1999, **41**, 423–429.
- 204 O. Bandmann, K. H. Weiss and S. G. Kaler, *Lancet Neurol.*, 2015, **14**, 103–113.
- 205 K. Wilson, *Orig. Artic. Clin. Cases*, 1912, **34**, 295–509.
- 206 P. C. Bull, G. R. Thomas, J. M. Rommens, J. R. Forbes and D. W. Cox, *Nat. Genet.*, 1993, **5**, 327–337.
- 207 R. E. Tanzani, K. Petrukhin, I. Chernov, J. L. Pellequer, W. Wasco, B. Ross, D. M. Romano, E. Parano, L. Pavone, L. M. Brzustowics, M. Devoto, J. Peppercorn, A. I. Bush, I. Sternlieb, M. Pirastu, J. F. Gusella, O. Evgrafov, G. K. Penchaszadeh, B. Honig, I. . Edelman, M. B. Soares, I. H. Scheinberg and T. . Gilliam, *Nat. Genet.*, 1993, 344–350.
- 208 Y. Yamaguchi, M. E. Heiny and J. Gitlin, *Biochem. Biophys. Res. Communucations*, 1993, **197**, 271–277.
- 209 M. Bost, G. Piguet-Lacroix, F. Parant and C. M. R. Wilson, *J. Trace Elem. Med. Biol.*, 2012, **26**, 97–101.
- 210 Kenny S. M and Cox D. W., 2007, **12**, 1171–1177.
- 211 I. J. Chang and S. H. Hahn, in *Handbook of Clinical Neurology*, Elsevier, 2017, vol. 142, pp. 19–34.
- 212 J. D. Gitlin, *Gastroenterology*, 2003, **125**, 1868–1877.

- 213 D. C. Wilson, M. J. Phillips, D. W. Cox and E. A. Roberts, *J. Pediatr.*, 2000, **137**, 719–722.
- 214 M. E. Ross, I. M. Jacobson, J. L. Dienstag and J. B. Martin, *Ann. Neurol. Off. J. Am. Neurol. Assoc. Child Neurol. Soc.*, 1985, **17**, 411–413.
- 215 P. Ferenci, A. Członkowska, U. Merle, S. Ferenc, G. Gromadzka, C. Yurdaydin, W. Vogel, R. Bruha, H. T. Schmidt and W. Stremmel, *Gastroenterology*, 2007, **132**, 1294–1298.
- 216 A. Ala, J. Borjigin, A. Rochwarger and M. Schilsky, *Hepatology*, 2005, **41**, 668–670.
- 217 A. Członkowska, M. Rodo and G. Gromadzka, *Mov. Disord.*, 2008, **23**, 896–898.
- 218 A. Khanna, A. Jain, B. Eghtesad and J. Rakela, *Surg. Clin. North Am.*, 1999, **79**, 153–162.
- 219 I. Mohr and K. H. Weiss, *Ann. Transl. Med.*, 2019, **7**, S69–S69.
- 220 European Association For The Study Of The Liver, *J. Hepatol.*, 2012, **56**, 671–685.
- 221 M. Aramendía, L. Rello, M. Resano and F. Vanhaecke, *J. Anal. At. Spectrom.*, 2013, **28**, 675–681.
- 222 M. Resano, M. Aramendía, L. Rello, M. L. Calvo, S. Bérail and C. Pécheyran, *J Anal Spectrom*, 2013, **28**, 98–106.
- 223 M. C. García-Poyo, S. Bérail, A. L. Ronzani, L. Rello, E. García-González, B. Lelièvre, P. Cales, F. V. Nakadi, M. Aramendía, M. Resano and C. Pécheyran, *J. Anal. At. Spectrom.*, 2021, **36**, 968–980.
- 224 F. Woimant, N. Djebrani-Oussedik and A. Poujois, *Ann. Transl. Med.*, 2019, **7**, S70–S70.
- 225 F. Schmitt, G. Podevin, J. Poupon, J. Roux, P. Legras, J.-M. Trocello, F. Woimant, O. Laprévote, T. H. NGuyen and S. E. Balkhi, *PLoS ONE*, 2013, **8**, e82323.
- 226 S. El Balkhi, J.-M. Trocello, J. Poupon, P. Chappuis, F. Massicot, N. Girardot-Tinant and F. Woimant, *Clin. Chim. Acta*, 2011, **412**, 2254–2260.
- 227 O. Guillaud, A.-S. Brunet, I. Mallet, J. Dumortier, M. Pelosse, S. Heissat, C. Rivet, A. Lachaux and M. Bost, *Liver Int.*, 2018, **38**, 350–357.

Chapter 2: Objectives

The main goal of this work is the development and evaluation of novel methodologies for total Cu and Cu isotopic determinations, with very low sample volume requirements. This could allow preconcentrating the sample in case that the initial concentration of the element of interest is very low. The aim is to apply these new methods to improve the diagnosis and follow-up of Wilson's disease (WD).

The following specific objectives will be addressed to achieve this purpose:

- * Development of a method for elemental analysis of Cu in DBSs *via* solid sampling HR CS GFAAS. Moreover, four different DBS devices will be evaluated, namely Mitra, HemaXis DB10, Capitainer qDBS, and HemaPEN. It will be assessed whether the results obtained *via* DBS analysis are comparable to those that can be achieved through venipuncture.
- * Development of a new correction model to eliminate spectral interferences using only the spectrum obtained from the sample monitoring, without using any reference spectrum, by HR CS GFAAS.
- * Development and evaluation of a method for Cu elemental determination by ICP-MS, using only 1 μ L of pre-treated sample.
- * Evaluation of the efficiency of two resins for Cu isolation (AG-MP1 and Triskem).
- * Development and evaluation of three methods for Cu isotopic analysis in serum, with very low pre-treated sample volume requirements. For reaching this goal, an IR femtosecond (fs) laser and an electrothermal vaporizer (ETV) device will be coupled to a MC-ICP-MS. Finally, the last method will be developed to carry out the analysis by direct μ -injection into the nebulizer tubing.

The methods proposed will be used to evaluate both Cu concentration and the isotopic composition in the samples of interest, such as WD patients, healthy people (controls), patients with liver diseases different from WD and newborns.

Chapter 3:

Determination of Cu in blood *via* direct analysis of dried blood spots using high-resolution continuum source graphite furnace atomic absorption spectrometry

Abstract

The performance of state-of-the-art high-resolution continuum source graphite furnace atomic absorption spectrometry (HR CS GFAAS) instrumentation and four novel devices to produce dried blood spots of perfectly defined volumes are evaluated with the aim of developing a simple, direct method for the determination of Cu in blood samples.

In all cases, it is feasible to obtain accurate quantitative information using any of the four devices tested (Mitra, HemaXis DB10, Capitainer qDBS and HemaPEN) *via* simple external calibration with aqueous standards. One of the main differences in the performance of such devices is related with the blanks obtained, such that HemaXis DB10 and HemaPEN are preferred when abnormally low Cu levels ($500 \mu\text{g L}^{-1}$ or lower), associated with some diseases, need to be determined. The results prove that accurate values with RSD values below 10% can be achieved for these devices even for such Cu levels, while for Capitainer qDBS and, to a higher extent, for Mitra, the blank variations will ultimately increase the uncertainty.

It is important to stress that analysis of four real samples using both venipuncture and all the DBS specimens showed a very good agreement. Thus, the approach proposed could be readily applied, such that patients with disorders requiring Cu control can prepare their own samples and submit them *via* postal mail to the lab for HR CS GFAAS direct and fast analysis.

1. Introduction

Copper (Cu) is a transition metal that is essential for biological processes. Cu participates in many enzymatic activities and is present in proteins involved in oxidative stress and metabolic homeostasis.¹ Problems in Cu homeostasis are linked to numerous diseases,²⁻⁴ as explained in Chapter 1. Thus, the importance of Cu blood level determination. Cu blood level can be used for the diagnosis of some of these disorders, often in conjunction with other tests, and it can also be used as a marker of the disease state.⁴ Finally, Cu determination can also be used in order to better understand the metabolism of the diseases that are related with this element.

Conventionally, blood analysis to determine Cu levels is carried out after venipuncture in a clinical setting, with the traditional inconveniences that such approach represents. In order to overcome these disadvantages, the development of alternative sampling methods for biological fluids in general, and for blood in particular, is continuously under investigation (more details in Chapter 1). In particular, DBSs have been employed in neonatal screening programs throughout the world, and the research associated with such approach has grown exponentially.⁵⁻⁷ This is due to their advantages,^{5,8,9} already discussed in Chapter 1.

Traditionally, DBSs are prepared after the deposition of a volume in the range of 50 - 100 μ L of blood onto a standardized clinical filter paper, which should absorb a constant amount of blood per cm^2 . Later, after drying, a portion of the DBS (circles of 3.2 mm of diameter is often

the standard) is punched out and taken for analysis. With this approach, obtaining fully quantitative results is challenging, unless the volume deposited onto the paper is measured (e.g., with some pipette or calibrated capillary). Even then, the volume deposited per area for real samples depends on some physicochemical factors, such as the viscosity, which is ultimately determined by the hematocrit level.^{10–14} It has been demonstrated that the hematocrit level is the parameter that has more influence in the spread of blood on DBS materials; in fact there is an inverse relation between blood hematocrit level and spot area.^{10,15} Moreover, the distribution of the analyte across the DBS is typically not constant, as chromatographic effects appear when depositing any liquid onto a hydrophilic surface (“coffee ring effect” or “volcano effect”),^{12,16,17} which poses an issue of representativity if only a portion of the DBS is subjected to analysis.¹¹

Different strategies have been proposed in order to solve the hematocrit¹³ and coffee ring effect problems,¹⁸ but they often required extra measurements or more procedural steps that could be difficult to implement in a routine analysis. Analysis of the whole DBS is always a good option, provided that its size is manageable.

In the last years, this situation has started to change with the development of new specimens to produce DBSs with a reproducible and known volume,¹⁹ regardless of the hematocrit level. Such specimens differ in nature but have several aspects in common, such as the fact that they rely on smaller volumes (typically, 10 – 30 μL range) than the DBSs traditionally used in hospitals, among other reasons because they are designed with the patient in mind. These are intended not only for newborns, but for other situations where adults need frequent controls (e.g., for monitoring the evolution of a chronic condition or for screening a large population from an area of interest) and the auto sampling of larger volumes from a single

finger puncture is not so easy or comfortable. The idea behind these devices is to carry out the analysis of each DBS produced as a whole, without further subsampling.

In this work, four different specimens that were considered as particularly promising have been selected and tested. The first one called Mitra was introduced in 2014.²⁰ This material is based on the absorption of a fixed volume of sample (10, 20 or 30 μL) onto a porous hydrophilic tip by wicking. The second device is a microfluidic-based volumetric sampling system denominated HemaXis DB10 that was introduced in 2015.²¹ The sample is taken through a capillary (10 μL) and afterwards, by closing the card, it is deposited onto a clinical filter paper. The third device is known as Capitainer qDBS, and is an updated version of the Capitainer B, the latter being released in 2018.²² This system makes use of microfluidics to produce volume defined DBSs on conventional DBS filter paper, as explained elsewhere by Lenk *et al.*²³ In particular, this device produces a DBS with 10 μL of blood. The last device tested is the HemaPEN (QCPEN), and its last iteration was reported in literature also in 2018.²⁴ It is based on the volumetric application of blood onto pre-cut filter paper discs. This device is equipped with four integrated 2.74 μL microcapillaries, which are filled when they are put into contact with a droplet of blood. By applying pressure, such blood is deposited onto the four pre-cut filter papers, thus producing the DBSs. A more detailed description of each one of these microsampling devices is presented in Sections 2.2 and 2.3.

Use of these devices clearly helps in solving a key analytical challenge, as the exact blood volume used to produce the DBS can be known. Another problem is that, by using DBSs, a liquid sample is transformed into a solid sample, and most of the analytical techniques typically used for Cu determination are originally designed to work with solutions, such as flame atomic absorption spectrometry (FAAS),²⁵ inductively coupled plasma optical emission spectrometry (ICP-OES),²⁶ and inductively coupled plasma mass spectrometry (ICP-MS).²⁷

This entails that the DBS would have to be digested or subjected to an extraction procedure to release Cu from the filter paper, with the subsequent dilution and/or contamination or recovery issues.²⁸

The use of direct solid analysis may be an alternative to solve these problems and increase sample throughput. In cases where a single element is to be monitored, high-resolution continuum source graphite furnace atomic absorption spectrometer (HR CS GFAAS) can offer a robust performance, providing low limits of detection, good signal stability and potential to detect and correct for spectral overlaps,^{29–33} ideally relying on external calibration with aqueous standard solutions only. Such technique has been seldom evaluated in the past for this type of samples (only for Pb,³⁴ and for Fe and Zn,³⁵ in addition to an earlier work that used line source GFAAS³⁶). Moreover, in those cases, “traditional” DBSs, where a larger amount of blood is deposited and later some areas are punched out, were deployed, which can translate into some of the problems discussed before (e.g., heterogeneous analyte distribution).

This work aims at the evaluation of four novel DBS specimens in the context of Cu determination in blood, in order to develop a simple and accurate methodology based on the direct analysis of Cu using solid sampling HR CS GFAAS, while also assessing whether the results obtained *via* DBS monitoring are comparable to those that can be achieved by means of venipuncture.

2. Experimental

2.1 Instrumentation

All the measurements for Cu determination were carried out with a HR CS GFAAS spectrometer, ContrAA 800G (Analytik Jena, Jena, Germany). This instrument is equipped

with a xenon short-arc lamp as a continuous radiation source, a high-resolution double monochromator, and a CCD array detector. This detector possesses 588 pixels, of which 200 are used for monitoring the spectral window. The system is equipped with a SSA 600 fully automated solid sampler with liquid dosing unit.^{32,37}

2.2 Reagents and materials

A Cu mono-elemental solution of 1 g L⁻¹ (Merck, Darmstadt, Germany) was used for the preparation of the standards, by dilution in 1% v v⁻¹ HNO₃. Pd, Rh, Pt, Ir and Ru solutions of 1 g L⁻¹ (Merck) were tested as chemical modifiers. Ultrapure water (resistivity ≥ 18 MΩ cm) was deionized by a Milli-Q purifying system (Millipore, Bedford, USA). HNO₃ 65% and HCl 30% Suprapur were purchased from Merck.

Seronorm™ Trace Elements Whole Blood reference material (RM) Level 1 (L-1, Lot: 1406263), Level 2 (L-2, Lot: 1406264) and Level 3 (L-3, Lot: 1509408) produced by SERO AS (Billingstad, Norway) were utilized as reference materials to evaluate the analytical method. For simplicity, these materials will be referred to as blood RM L-1, L-2 and L-3, respectively. These RMs were available in lyophilized form and were reconstituted in 3 mL of ultrapure water, following the manufacturer instructions.

Four different DBS devices were tested: (i) Mitra; (ii) HemaXis DB10; (iii) Capitainer qDBS; and (iv) HemaPEN (QCPEN).

Mitra devices (Lot: 70615A-P5L18-1951) were acquired from Neoteryx (Torrance, USA). The absorptive part of the Mitra device (see **Figure 1**) is a hydrophilic polymer with an absorption volume of 11 ± 0.35 μL for water and 10.5 μL (uncertainty not provided by the manufacturer) for blood. These are the values provided by the manufacturer, although similar values were obtained in an independent previous work.³⁸ A value of 11 μL was used for calculations

concerning the reference materials (closer to water in terms of viscosity) while 10.5 μL were used for calculations concerning the real blood samples and the LOD determinations. HemaXis DB10 devices (Lot: 2019/002/285161) were obtained from DBS System SA (Gland, Switzerland). They incorporate a microfluidic chip of $10.0 \pm 0.5 \mu\text{L}$ (see **Figure 2**). Capitainer qDBS specimens (Lot: 800207) were purchased from CAPITAINER AB (Stockholm, Sweden). This device (see **Figure 3**) possesses a capillary microchannel of 10 μL (with a reproducibility better than 0.5 μL as one standard deviation). QCPEN (Lot: 44U-317685A) were supplied by Trajan Scientific Europe Ltd (Milton Keynes, United Kingdom). This is actually a simplified version (inner part) of the HemaPEN specimen (see **Figure 4A**), which is produced for work in clinical labs (thus the label QC), while the complete HemaPEN version is designed with the patients in mind, and it is easier to use. However, the operating principle is the same. The QCPEN is shown in **Figure 4B**. It is composed of four microcapillaries of $2.74 \pm 0.14 \mu\text{L}$. This device will be referred as HemaPEN from now on, for simplicity. In addition to the QCPEN devices, both Perkin Elmer 226 and Whatman 903 filter paper discs were provided by the manufacturer for testing.

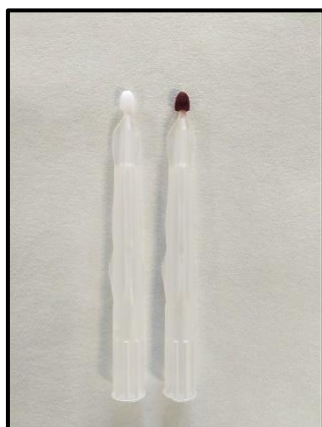


Figure 1. Mitra device without blood (left) and after collection of approximately 10 μL of blood (right).

3- Determination of Cu in blood via direct analysis of dried blood spots using high-resolution continuum source graphite furnace atomic absorption spectrometry

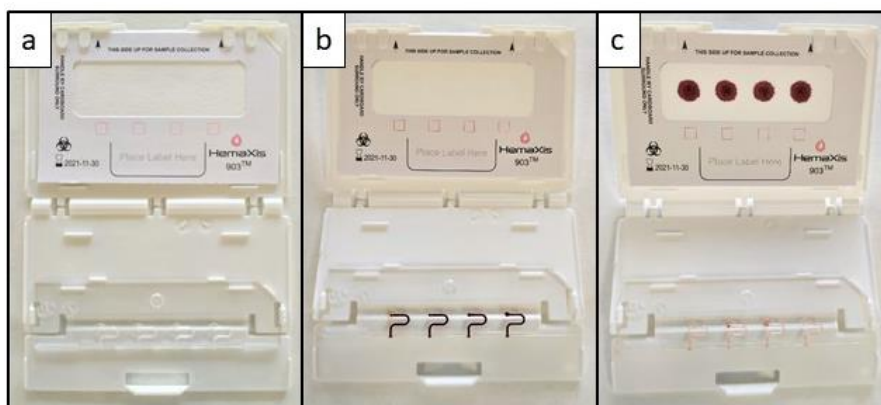


Figure 2. HemaXis DB10 device: (a) empty; (b) microfluidic chips filled with blood (approximately 10 μ L each); (c) after the device is closed and blood is deposited onto the filter paper for DBS production.

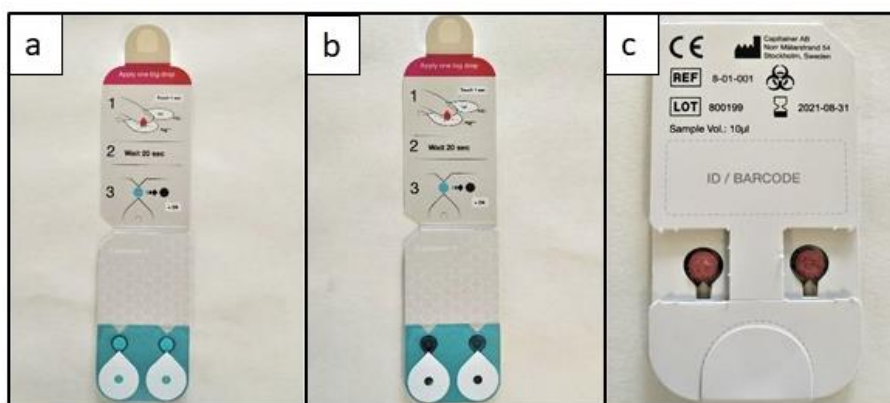


Figure 3. Capitainer qDBS device: (a) empty; (b) after blood deposition onto the indicated area; (c) DBSs produced after deposition of blood (approximately 10 μ L) onto the filter paper found in the back of the device.

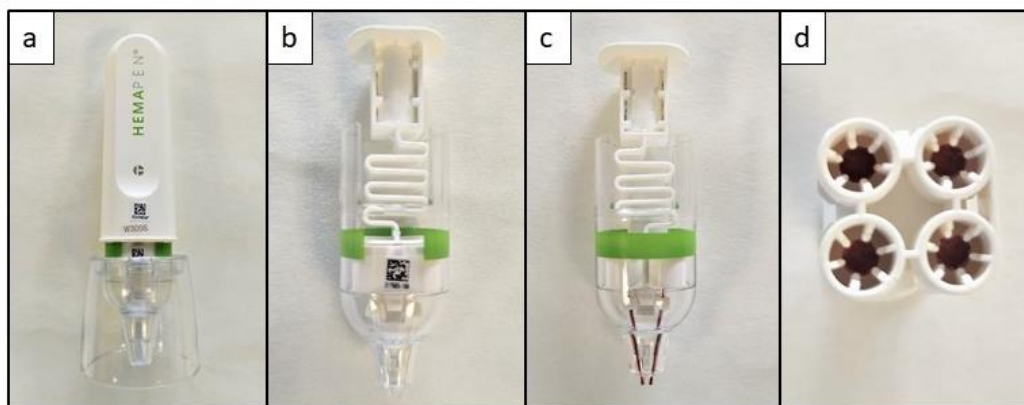


Figure 4. HemaPEN device: (a) fully commercial HemaPEN; (b) empty QCPEN (inner part of commercial HemaPEN); (c) QCPEN with microcapillaries filled with blood (approximately 2.74 μ L each); (d) after deposition of blood onto the filter paper for DBS production.

2.3 Samples and sample preparation

Blood samples from 4 volunteers (adults) were obtained from the Hospital Universitario Miguel Servet (Zaragoza, Spain). For comparison purposes, during the same session, the blood was extracted by both the conventional method (venipuncture) and by puncturing the finger with a small lancet to prepare the DBSs with the different devices. The principles outlined in the declaration of Helsinki regarding all the experimental research involving humans or animals were followed.

DBSs were prepared as recommended by the manufacturer with blood RMs and with the real blood samples, as detailed below. After the deposition of either blood RMs or real blood samples, all the devices were dried at room temperature during at least 4 hours, except for the HemaPEN, which was dried for at least 2 hours.

Mitra DBSs (see **Figure 1**) were prepared by introducing the absorptive part (the tip) into the reconstituted RMs for 5 seconds. For real blood samples, the tip of the device was put into contact with the blood droplet until it appeared to be full (visually).

HemaXis DB10 (see **Figure 2**) preparation with the reference material was carried out with the help of a micropipette with which a 12 μ L droplet (a volume higher than the volume of the microfluidic chip) was created and put into contact with the microfluidic chip inlet. For real blood samples, the microfluidic chip was put into contact with the blood droplet until it was full. In both cases, when the microfluidic chip was full, the HemaXis DB10 was closed, thus resulting in the blood being deposited onto the filter paper card (Whatman 903), producing

the blood spots of 10 μL . Once dried, each DBS was cut from the whole card with ceramic scissors before analysis.

Capitainer qDBS (see **Figure 3**) preparation with the RMs was carried out by depositing 15 μL of blood (a volume higher than the volume of the microchannel) of blood onto the inlet port with a micropipette. For real blood samples, a droplet of blood punctured directly from the finger was deposited onto the inlet port. In both cases, after deposition, a microchannel is filled with a constant volume of 10 μL . After that, a thin film at the inlet is dissolved by any excess of blood, and such excess of blood is absorbed by a paper matrix separating it from the microchannel. Finally, the blood filling the microchannel is transported by capillarity, dissolving another thin film and being deposited onto the pre-perforated filter discs (Ahlstrom grade 222) that are located on the other side of the device, forming DBSs of 10 μL .

For the HemaPEN (see **Figure 4**), DBSs were prepared by introducing the four capillaries of the QCPEN (HemaPEN) into the reconstituted RMs until it was observed that the capillaries were full. For real samples, the preparation was carried out taking the blood directly from the finger with the QCPEN. For that purpose, the four capillaries of the QCPEN were put into contact with the droplet of blood and filled directly. Next, in both cases, the capillaries were put into contact with the filter paper (Whatman 903) by pressing the system, as recommended by the manufacturer.

2.4 Measurement protocol

For the analysis, the sample has to be deposited onto the platform to be introduced into the graphite furnace. In all cases, the sample deposition and the addition of the chemical modifier was carried out manually. In the case of the liquid blood, 10 μL of blood were deposited onto the platform with a positive displacement micropipette and 10 μL of 1 g L^{-1} Pt was added as chemical modifier.

In the case of the Mitra device, only the absorptive part (the tip) was deposited onto the platform (see **Figure 5a**). Once inside the platform, 10 μL of 1 g L^{-1} Pt solution were added above the Mitra DBS trying to cover the device entirely. For the HemaXis DB10 device, the dried DBS was cut with ceramic scissors and was folded in order to be deposited onto the platform (see **Figure 5b**), where previously 10 μL of 1 g L^{-1} Pt had been placed. For Capitainer qDBS, after the drying process, the DBSs were detached from the support with a ceramic

knife and cut in half with ceramic scissors; the deposition onto the platform was carried out in four consecutive steps, the first one was the deposition of 5 μL of 1 g L^{-1} Pt followed by the deposition of half of the Capitainer qDBS. This sequence was repeated twice (see **Figure 5c**). In the case of the HemaPEN, the filter papers were removed from it with a metal free micropipette tip, in order to avoid contamination, and the filter paper was deposited onto the platform where previously 10 μL of 1 g L^{-1} Pt had been placed (see **Figure 5d**). In all cases, the introduction of the platform into the graphite furnace was carried out with the autosampler, controlled by the computer software. After sample atomization, a small amount of ash remains on the platform, which was withdrawn with a flow of compressed air after each replicate.

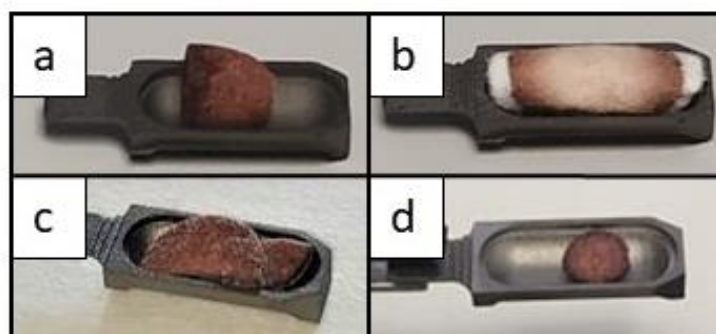


Figure 5. Deposition of DBSs onto the graphite platform before its introduction into the graphite furnace for subsequent HR CS GFAAS analysis. a) Mitra, b) HemaXis DB10, c) Capitainer qDBS and d) HemaPEN.

Two different wavelengths were used for analysis depending on the sensitivity required. For the liquid blood samples and for Mitra, HemaXis DB10 and Capitainer qDBS (approx. volume = 10 μL), the wavelength chosen was 249.21 nm (relative sensitivity of 1.1%, in comparison to the most sensitive line), while for the HemaPEN (approx. volume = 2.74 μL), the wavelength was 222.57 nm (relative sensitivity of 5% of the most sensitive line). The temperature program used is summarized in **Table 1**.

Table 1. Graphite furnace temperature program for Cu determination in DBS and liquid blood samples using HR CS GFAAS. Argon was used as purge gas.

Step	Temperature (°C)	Ramp (°C s ⁻¹)	Time (s)	Gas flow (L min ⁻¹)
Drying 1	120	3	30	2.0
Drying 2	150	5	30	2.0
Pyrolysis	1300	50	35	2.0
Gas adaption	1300	0	5	0
Atomization	2400 ^a /2300 ^b	3000	6	0
Cleaning	2500	500	4	2.0

a: Atomization temperature used for Mitra devices

b: Atomization temperature used for liquid RMs, liquid real blood samples and for HemaXis DB10, Capitainer qDBS and HemaPEN devices.

A continuous Ar flow of 2.0 L min⁻¹ was used in all the heating steps except during the atomization. The integration time was set to 6 s. Integrated absorbance (peak area) of the 3 central pixels was selected as measurement mode.

For quantitative analysis, external calibration with aqueous standards of adequate Cu levels was performed, introducing between 0.5 and 10 ng of Cu at 222.57 nm and between 5 and 40 ng of Cu at 249.21 nm.

For the evaluation of the accuracy, a liquid whole blood RM was analyzed (L-2) for which three replicates were carried out. Five replicates were measured in the analysis of the DBSs prepared with the different RMs. For DBS analysis, blank correction is mandatory. For this purpose, 10 blanks were measured for HemaXis DB10, Capitainer qDBS and HemaPEN devices, and 15 blanks for the Mitra device. The median of these blank values was subtracted from the signal obtained for every sample.

For analysis of real blood samples, 5 replicates were measured in the case of the liquid blood samples. For the DBSs prepared with such samples the number of replicates depends on the number of DBSs that each patient was able to produce. For blank correction, 5 blank

replicates were measured. The median of these blank values was subtracted from the signal obtained for every sample.

Concerning the sample throughput, it can be mentioned that the whole measurement of a replicate takes approximately 5 minutes. For every session, it is necessary to calibrate with aqueous standards (e.g., about 1 hour for a blank and 3 standards, if $n=3$), and measure the blank replicates of the target DBS (e.g., approx. 25 minutes, if $n=5$). Then, the DBS samples can be analyzed (approx. 25 minutes per sample, if $n=5$). No significant memory effects were observed after DBS analyses. In any case, running a measurement with an empty platform for cleaning after obtaining a high signal is always advisable in GFAAS.

3. Results and discussion

3.1 Method optimization

3.1.1 Wavelength selection

Cu offers several atomic lines, enabling to easily adapt the sensitivity to the demands of every particular application. In this case, the wavelength finally selected for the analyses depended on the amount of blood, and thus of Cu, introduced into the furnace. For the HemaPEN devices, containing only 2.74 μL of blood, the wavelength chosen was 222.570 nm, which shows a relative sensitivity of approx. 5% in comparison to the most sensitive line found at 324.754 nm. On the other hand, for the Mitra, HemaXis DB10 and Capitainer qDBS devices, all containing ca. 10 μL of blood, the atomic line found at 249.215 nm was chosen, which offers a relative sensitivity of roughly 1% compared to the most sensitive line. This fact clearly indicates that the technique is not lacking sensitivity when attempting this type of analysis, and in fact more sensitivity could be easily obtained, if required, by monitoring the main atomic lines for Cu.

3.1.2 Modifier selection

The study of the chemical modifiers was carried out with the Mitra device, a relatively large and thick matrix of unknown polymeric composition, which could be *a priori* more difficult to be efficiently removed than the others, which are all practically identical (except for the size) and based on cellulose. Mitra devices were prepared with blood RM L-2. For these tests, pyrolysis and atomization temperatures were fixed at 1300 and 2400 $^{\circ}\text{C}$, respectively.

Pd, Rh, Pt, Ir and Ru were tested as modifiers. The DBSs prepared with the Mitra device were deposited onto the platform together with 10 μL of 1 g L^{-1} solution of each modifier, separately. Moreover, in the case of Ir, this element was also tested as permanent modifier.

It was observed that, when Pd and Rh modifiers were used, the Mitra device did not decompose completely, obstructing the radiation from the source due to its size (see **Figure 6a**) and making analysis hardly feasible. However, with Pt, Ru and Ir, the Mitra-based DBSs decomposed better, leaving only a small amount of ash after each measurement. Such residue can be easily taken away with compressed air. **Figure 6b** shows a picture of the Mitra DBS after sample analysis using Pt as chemical modifier.

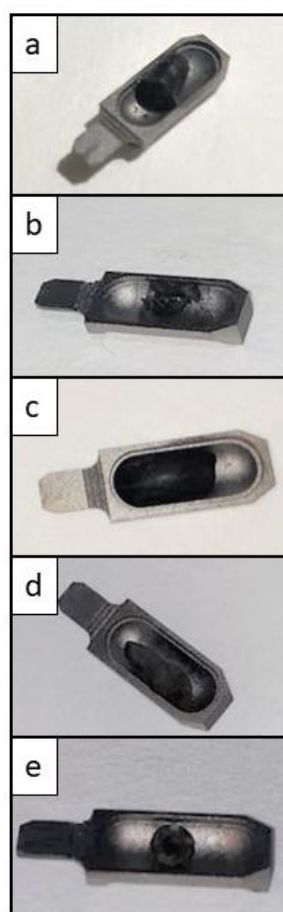


Figure 6. Devices after GFAAS temperature programme (See **Table 1**). a) Mitra using Pd; b) Mitra using Pt; c) HemaXis DB10 using Pt; d) Capitainer qDBS using Pt and e) HemaPEN using Pt.

However, it appears that the different behavior of these modifiers in terms of sample decomposition may have more to do with their matrix than with the nature of each element.

Pd standard solutions are prepared in 15% HNO₃ and Rh in 2-3% HNO₃, while Pt, Ru and Ir are prepared in 7% HCl. Further experiments were carried out adding just 15% HNO₃, which was not sufficient for efficient matrix removal, while using 7% HCl produced similar results as those reported for Pt solutions. It can also be mentioned that, if only concentrated HNO₃ (65%) is added, then the matrix is efficiently removed, probably because its oxidant effect is more pronounced than with a diluted solution. In fact, in the absence of any modifier, the device also decomposes, although the Cu signal is not so stable. Therefore, the presence of diluted HNO₃ seems to be detrimental for the decomposition of this polymeric material. Introduction of air during the pyrolysis (by adding an ashing step at 600 °C) was also tested without satisfactory results. Thus, addition of one of these modifiers (Pt, Ru and Ir) was further studied.

It was possible to observe that, when adding Pt, the areas and the peak profiles were rather constant, while that was not the case for Ru and even less for Ir. In fact, for Ir, a decreasing trend in terms of peak areas was observed. This may be explained as an amount of Ir can be deposited onto the platform, acting as permanent modifier. To corroborate this, the platform was prepared with Ir as permanent modifier. It was possible to observe that the Mitra was decomposed effectively under these conditions, but providing only half of the Cu signal than with Pt. Finally, the Pt solution was chosen as chemical modifier for the rest of the analyses carried out in this work, as it offers the best sensitivity and stability of all the modifiers tested.

Once this modifier solution was selected, it was also tested with the other DBS devices and with a whole blood RM L-2 analyzed directly. This approach offers sufficient matrix removal (see **Figure 6** for the minor residues observed for the DBS devices), good sensitivity and stable peak profiles in all cases.

3.1.3 Optimization of the temperature program

The optimization of the temperature program was carried out using two different materials. Mitra and HemaXis DB10 devices were selected: the first shows a different matrix (polymeric), while the second is similar to the rest of the other devices (cellulose), and their corresponding DBSs were produced after absorption of blood RM L-2. Also, Cu aqueous standards were investigated for comparison, as the ultimate goal was to carry out external calibration with them.

For Mitra, the atomization temperature was optimized between 2000 and 2500 °C, while keeping the pyrolysis temperature constant at 1300 °C. The results obtained are shown in **Figure 7**. Except for 2100 °C, peak areas and uncertainties are similar for all the temperatures tested. Finally, a value of 2400 °C was chosen to obtain a well-defined, almost gaussian peak profile (see **Figure 8a**). The pyrolysis temperature was then optimized from 1000 until 1500 °C. The results are also shown in **Figure 7**. Obviously, the use of temperatures below 1200 °C is unsuitable as it results in higher signal variation. When attempting direct solid sampling it can be expected that, below a certain pyrolysis temperature, proper matrix decomposition is not fully achieved. A value of 1300 °C was finally selected since, at this temperature, almost all the matrix was removed (except for minimal ash remains, as discussed in the previous section), without losing analyte. The final temperature program chosen for the Mitra device is shown in **Table 1**.

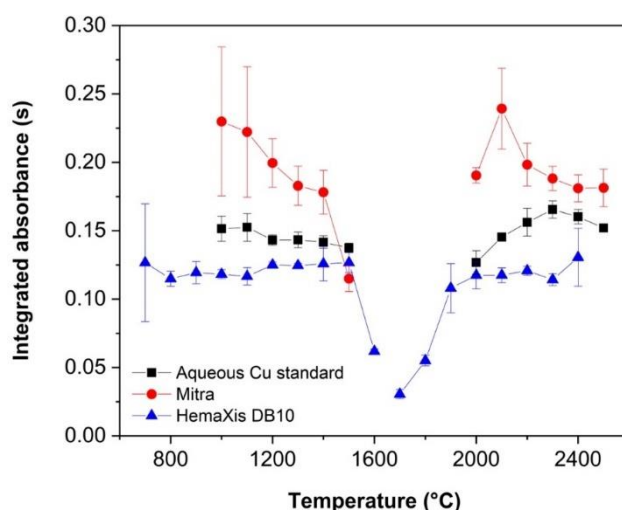


Figure 7. Atomization and pyrolysis temperature optimization. The error bars represent the standard deviation (n=5).

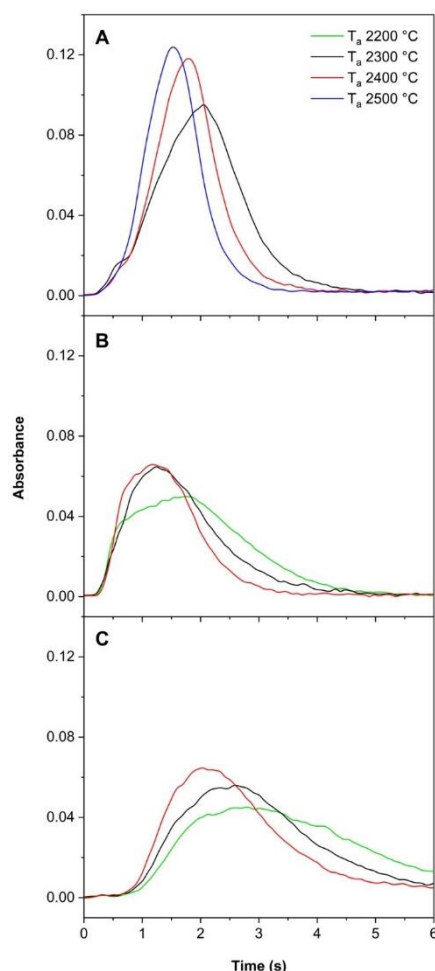


Figure 8. Time-resolved absorbance profile of the three central pixels, without blank correction, obtained from the optimization of the atomization temperature setting the pyrolysis temperature at 1300 °C for: a) Mitra, b) HemaXis DB10 and c) Cu standard solution.

For HemaXis DB10 devices, the atomization temperature was optimized by selecting a constant pyrolysis temperature at 1300 °C. The atomization temperature varied between 1700 and 2500 °C. The results obtained are shown in **Figure 7**. In view of the results, there are no significant differences for atomization temperatures between 2000 and 2300 °C. A final value of 2300 °C was chosen as atomization temperature as a profile better defined than that obtained at 2200 °C is observed (see **Figure 8b**). The signal appears a bit earlier than for the Mitra, which indicates that Cu is less stabilized by the modifier in this case.

It cannot be expected that all the devices provide exactly the same interaction between the analyte and the modifier. The way in which the modifier was added was designed to maximize such interaction, and that is discussed in detail in section 2.4. In the case of Mitra, the modifier is deposited on top of it and covers it well. In fact, a fraction may even be absorbed by the

device although this is not observed visually. Overall, it seems that a more intimate contact can be achieved for this device, resulting in delayed atomization. The HemaXis DB10 has to be rolled over to fit onto the platform (see **Figure 5b**). If the modifier is added on top, the material expands, and it is difficult to introduce it into the furnace. So, for this device, the modifier has to be deposited onto the platform, before placing the DBS.

In any case, a temperature of 2300 °C was chosen. Use of a temperature of 2400 °C seems also possible, thus unifying the conditions for both devices. However, in order to prolong the duration of the graphite parts, it is always beneficial to use a temperature as low as possible, so it was preferred to opt for 2300 °C.

The pyrolysis temperature was also optimized between 700 and 1600 °C and the results are shown in **Figure 7** (blue trace). Again, selection of a temperature of 1300 °C guarantees that most of the matrix is removed leaving only a small residual ash, with no loss of analyte and good precision.

Once the temperature program was optimized for the HemaXis DB10, the other devices (Capitainer qDBS and HemaPEN) were submitted to the same program to check its feasibility, and the peak profiles obtained are shown in **Figure 9**. The time-resolved spectra are similar to that obtained with the HemaXis DB10 device at 2300 °C (**Figure 8b**); although for HemaPEN a bit more tailing is observed. This could also indicate more interaction with Pt. Overall, Cu determination in these devices can be done applying the same conditions.

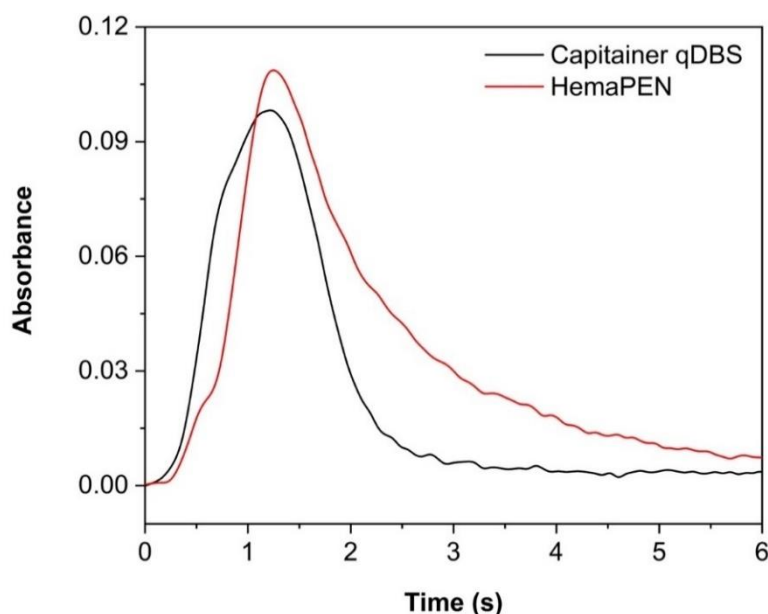


Figure 9. Time-resolved absorbance profile of the three central pixels, without blank correction, obtained using the temperature program shown in **Table 1** for DBSs produced via Capitainer qDBS ($\lambda=249.215$ nm) and for HemaPEN. ($\lambda=222.570$ nm).

Finally, the same optimization was performed using Cu standard solutions of similar concentration than that of the blood RM L-2 (1.34 ± 0.27 mg L⁻¹). The measurements were carried out by depositing 10 μ L of the liquid standard (1.45 mg L⁻¹) and 10 μ L of 1 g L⁻¹ Pt. The atomization temperature was first optimized between 2000 and 2500 °C, while the pyrolysis temperature was set at 1300 °C. The results obtained are shown in **Figure 7**.

As could be expected, the Cu absorption peak appears a bit delayed compared to the peaks obtained for the DBSs, since the interaction between Cu and Pt is potentially more effective if both are added as solutions. In any case, there are no significant differences between 2300 and 2400 °C in terms of peak definition and peak area (**Figure 8c**). Therefore, and in order to maintain the same conditions used with the DBS devices, a temperature of 2400 °C was chosen when measuring solutions for calibration when targeting Mitra-based DBSs, and of 2300 °C for the rest of them.

A pyrolysis temperature optimization was also carried out between 1000 and 1500 °C, with the atomization temperature set at 2400 °C. The results are also displayed in **Figure 7**. No differences in terms of signal intensities and uncertainties were observed in the range between 1200 and 1500 °C. A temperature of 1300 °C was chosen for pyrolysis in all cases.

Finally, and most important, the signals for aqueous standard solutions and for DBS samples showed similar sensitivities, confirming the possibility to carry out the direct determination of Cu in DBSs using external calibration with such aqueous standards.

3.2 Figures of merit

After method optimization, the main figures of merit were calculated, and the results are shown in **Table 2**. The instrumental limits of detection (LOD), in ng, were calculated as 3 times the standard deviation of 10 blanks divided by the sensitivity, respectively. In this case, 2.74 μL (for the HemaPEN method, $\lambda = 222.570 \text{ nm}$) or 10 μL (for the rest of the methods, $\lambda = 249.2 \text{ nm}$) of 1% v v⁻¹ HNO₃ plus 10 μL of 1 g L⁻¹ Pt solution were measured as blanks. For expressing the LOD values as concentrations, the limits were divided by the DBS volumes, achieving LOD values of 0.02 mg L⁻¹ of Cu in blood for all DBS.

Table 2. Figures of merit for the Cu determination using the current methods *via* HR CS GFAAS. For the method limits: 10 blank replicates were measured in each case, except for Mitra for which 15 measurements were carried out.

Wavelength (nm)	Device	Sensitivity (s ng ⁻¹)*	Characteristic mass (ng)*	Sample volume (μL)	Instrumental Limits	Method Limits
					LOD (ng / mg L ⁻¹)	LOD (mg L ⁻¹)
249.215	Mitra	0.009 ^a	0.48	10	0.20 / 0.02	0.78 ^a
	HemaXis DB10				0.22 / 0.02	0.06 ^b
	Capitainer qDBS					0.48 ^b
222.570	HemaPEN (Perkin Elmer 226)	0.050 ^b	0.10	2.74	0.07 / 0.02	0.08 ^b
	HemaPEN (Whatman 903)					0.23 ^b

* Calculated as the median of: a) Sensitivity values from 8 different days; b) Sensitivity values from 4 different days.

The method LODs were also calculated as 3 times the standard deviation of 10 blanks divided by the sensitivity, respectively. In this case, the blanks were the different materials used to produce the DBS but without blood, and also adding 10 μL of Pt 1 g L^{-1} . LODs were expressed as blood concentration considering the volumes absorbed by each device. The manufacturer of the Mitra device provides two slightly different absorption volumes for water solutions and for blood. For the calculation of these limits, the volume for real blood (10.5 μL) was used. In the case of the Mitra device, 15 blanks were monitored instead of 10, as such device shows a higher variation of the blank signals and obtaining a representative value is important for blank subtraction.

As it is possible to appreciate in **Table 2**, the method LODs are significantly higher than the instrumental limits. Overall, we believe that these method limits are overestimated. Most of these DBS specimens have been originally designed with other applications in mind and they are not always as clean as ideally required for trace element analysis. This fact agrees with previous reports.³⁹

Thus, the reason behind such high method LODs is probably related to the presence of Cu in the DBS devices, which distribution is furthermore not homogeneous. It has to be remembered that the definition of limit of detection is based on a blank that is “defined as the signal resulting from a sample which is identical, in principle, to the sample of interest, except that the substance sought is absent (or small compared to). The blank thus includes the effects of interfering species.”⁴⁰

We do not have such pure blanks in this case, so the traditional approach for LOD calculation may not apply herein. The problem here is not to be able to detect Cu (sensitivity is more than enough and baselines are stable), but to estimate properly and subtract the contribution of the blanks to the signal. If that is done, it is possible to carry out the determination of Cu in blood samples with good accuracy and sufficient precision at concentrations lower than those than can be inferred from the method LODs (e.g., calculating the limits of quantification as 3.33 times such LODs), as will be demonstrated in section 3.3.

In any case, this is a relevant aspect. **Table 3** shows the Cu concentration determined for the different materials tested in this work following the method described in section 2.4. and considering the volumes absorbed by each device for calculation of the concentrations. As can be seen, relatively high Cu concentration levels are observed in most devices, and

especially in the Mitra device. Moreover, confidence intervals are also large, reflecting the heterogeneous distribution of Cu in each individual device. High blank levels for some elements (including Cu) have already been reported for this device.^{41,42} It has to be indicated again that the Mitra is the only one prepared from a polymeric material.

Table 3. Cu concentrations obtained for the analysis of the blank devices tested using the method described in section 2.4. Results are expressed as $\bar{x} \pm U$, where $U = (t s)/\sqrt{n}$; for a 95% confidence interval. The concentration was calculated considering the volume absorbed by each type of DBS device.

	DBS Device				
	Mitra ^a	HemaXis DB10 (Whatman 903) ^b	Capitainer qDBS (Ahlstrom 222) ^b	HemaPEN (Perkin Elmer 226) ^b	HemaPEN (Whatman 903) ^b
Cu Concentration (mg L⁻¹)	0.40 ± 0.14	0.07 ± 0.01	0.33 ± 0.12	0.20 ± 0.02	0.19 ± 0.05
RSD (%)	65	25	52	13	39
Median of Cu Concentration (mg L⁻¹)	0.27	0.08	0.25	0.20	0.18

a) n=15; b) n=10.

Cleaning the absorptive materials before sample deposition is an option to further purify them.^{7,43,44} This option was explored for the Mitra devices by introducing them in EDTA solutions, rinsing with water and drying them subsequently. However, the decrease in Cu concentration was not significant, and it was observed that, after this procedure, the devices tended to absorb more liquid than the values provided by the manufacturers. This fact is problematic, as the absorbed volume should remain constant and has to be known in advance. As a result, such approach was not explored further. It is our understanding that some strategies to decrease these blanks are currently under investigation by the manufacturer of this device.

The rest of devices all use similar cotton-based fibers. The different clinical filter papers are listed in **Table 3** as well. Capitainer qDBS offers blanks that are higher than the others. It can be mentioned that the paper used for such device (Ahlstrom 222) is a bit thicker than the others. In the case of HemaPEN, the device may be equipped with two different filter paper types (Perkin Elmer 226 or Whatman 903), which actually offer similar blanks.

Finally, best blanks were obtained for the HemaXis DB10 device. Since the filter paper used in this device is the same as that used for one series of HemaPEN and actually the amount of filter paper is smaller in the case of HemaPEN, it is, *a priori*, a bit surprising to see this difference. However, the paper for HemaXis is probably manipulated to a lower extent, as it does not need to be precut, unlike the case for Capitainer qDBS and HemaPEN. Thus, the difference could be related with the way the paper is handled and protected, or it could be an artifact and the results for other lots may differ.

In any case, it is important to put these results in perspective. Blood Cu levels for persons with abnormally low levels (e.g., Wilson's patients), and, also, for newborns and infants, may be around 0.5 mg L^{-1} or even below, while for adults without any disorders it may be in the range $1.0\text{-}1.5 \text{ mg L}^{-1}$. Therefore, for detecting abnormal levels, all of them can perform, but for accurate and precise quantification of Cu in patients with some Cu-related disorders or in newborns, in principle, better blanks would be desirable for Mitra and Capitainer qDBS.

In any case, **Table 3** provides a clear reference regarding the Cu concentration that can be determined for the different DBS devices. Obviously, the closer the expected values are to these blanks, the higher imprecision that is going to be obtained, as will be demonstrated in the next section.

3.3 Determination of Cu in whole blood reference material using DBSs. Evaluation of the accuracy of the method.

Once the optimization procedure was carried out and the detection limits were calculated, the accuracy of the method was undertaken. For that purpose, three blood RMs (L-1, L-2, and L-3) were used to produce DBSs with every device and were subsequently analyzed. The blank contribution was subtracted from the signals of the samples. For this blank correction, 10 blanks were measured for all the devices except for Mitra, for which 15 blanks were measured. Furthermore, blood RM L-2 was also analyzed in liquid form.

In the case of the HemaPEN, as discussed before, it is possible to choose the paper found inside the device between Whatman 903 and Perkin Elmer 226 when ordering. Thus, these two different filter papers were first tested in a simple way: the DBSs were prepared by depositing the RMs directly with a positive displacement micropipette onto them. No significant differences were observed (see Supplementary Information **Table S1**). Finally, HemaPEN devices containing Whatman 903 were used in the next experiments.

The results obtained for these analyses can be found in **Table 4**, where a good agreement with the reference values is demonstrated, proving that the method performs well for Cu determination in DBSs. The uncertainty, in all cases, seems acceptable for clinical laboratories. There is, in any case, a clear correspondence between the uncertainty and the blank levels discussed in the previous sections, as could be anticipated (e.g., it is higher for Mitra and lower for HemaXis DB10 and HemaPEN, particularly at lower Cu concentration levels). Also, with less contaminated materials, the requirement to measure several blanks for the devices could be minimized.

Table 4. Direct Cu determination in whole blood reference materials *via* HR CS GFAAS using different DBS devices. Results are expressed as $\bar{x} \pm U$, where $U = (t s)/\sqrt{n}$ for a 95% confidence interval. The concentration was calculated taking into account the volume absorbed by each type of DBS device.

Sample	Reference value (Cu, mg L ⁻¹)	Direct (Cu, mg L ⁻¹) (n=3)	Mitra (Cu, mg L ⁻¹) (n=5)	HemaXis DB10 (Cu, mg L ⁻¹) (n=5)	Capitainer qDBS (Cu, mg L ⁻¹) (n=5)	HemaPEN (Cu, mg L ⁻¹) (n=5)
RM L-1	0.64 ± 0.13	-	0.73 ± 0.19 (RSD = 21%)	0.60 ± 0.05 (RSD = 7%)	0.64 ± 0.10 (RSD = 13%)	0.59 ± 0.08 (RSD=10%)
RM L-2	1.34 ± 0.27	1.30 ± 0.16	1.51 ± 0.27 (RSD = 14%)	1.42 ± 0.10 (RSD = 7%)	1.59 ± 0.18 (RSD = 9%)	1.40 ± 0.08 (RSD = 4%)
RM L-3	2.08 ± 0.42	-	2.42 ± 0.16 (RSD = 5%)	2.30 ± 0.08 (RSD = 3%)	2.48 ± 0.13 (RSD = 4%)	2.36 ± 0.15 (RSD = 5%)

When considering the origins of the definition of limit of quantification, “minimum working concentration as that for which the relative standard deviation was 10 %”,⁴⁰ it is clear that the levels are above such limit for HemaXis DB10 and HemaPEN. In the case of Capitainer

qDBS, RM L-1 is below this limit and, in the case of Mitra, both RM L-1 and RM L-2 are below such limit.

3.4 Cu determination in real blood samples. Venipuncture vs DBSs.

In order to further evaluate the potential of this procedure, real samples were also analyzed. Blood from four volunteers was obtained in the same session both by venipuncture and from finger puncture using a lancet, which was used for production of DBSs with the different devices tested. Samples were subsequently analyzed and results were compared to check whether there is any influence in the way in which blood is sampled.

For analysis of blood samples in liquid form, five replicates per sample were measured. For DBSs, the number of replicates depended on the number of specimens that the volunteers were able to produce per device tested. Five blanks were measured for each device for blank correction. **Table 5** shows the results with their respective uncertainty values, except for the volunteers 3 and 4 with the Mitra device, for which the uncertainty could not be estimated because only one sample was produced. It is noteworthy that in practice, the patient is not expected to be puncture several times to produce DBSs, but only one. Here it was done for research purposes.

Table 5. Results obtained for analysis of real blood samples both in liquid form and as DBS prepared with the different devices tested. Results are expressed as $\bar{x} \pm U$, where $U = (t s) / \sqrt{n}$ for a 95% confidence interval.

Volunteers	Liquid blood (Cu, mg L ⁻¹)	Mitra (Cu, mg L ⁻¹)	HemaXis DB10 (Cu, mg L ⁻¹)	Capitainer qDBS (mg L ⁻¹)	HemaPEN (Cu, mg L ⁻¹)
V1	0.85 ± 0.06 ^a	1.12 ± 0.26 ^b (RSD = 15%)	0.97 ± 0.24 ^c (RSD = 10%)	0.97 ± 0.16 ^c (RSD = 7%)	0.84 ± 0.15 ^c (RSD = 7%)
V2	0.83 ± 0.04 ^a	1.02 ± 0.44 ^b (RSD = 27%)	0.91 ± 0.05 ^c (RSD = 2%)	0.92 ± 0.09 ^a (RSD = 8%)	0.80 ± 0.09 ^a (RSD = 9%)
V3	0.98 ± 0.08 ^a	1.24 ^e	0.94 ± 0.12 ^c (RSD = 5%)	0.98 ± 0.46 ^d (RSD = 5%)	1.19 ± 0.14 ^c (RSD = 5%)
V4	0.99 ± 0.06 ^a	1.32 ^e	1.01 ± 0.16 ^c (RSD = 6%)	0.91 ± 0.29 ^d (RSD = 4%)	1.00 ± 0.51 ^d (RSD = 6%)

^a(n=5), ^b(n=4), ^c(n=3), ^d(n=2) and ^e(n=1).

As can be seen, the results obtained *via* direct analysis of DBS agree well with those obtained *via* a standard approach (venipuncture and analysis of the liquid samples). The uncertainties depend again on the type of device (higher for Mitra and Capitainer qDBS) but also the small number of replicates may play a role in some cases.

These results indicate that the way in which the sample is obtained does not show a significant influence in the determination of blood Cu levels. It is necessary to mention that while blood collection and the preparation of the DBSs were carried out almost simultaneously, sample analysis was not. Blood in liquid form was analyzed on the same day of blood collection, in order to avoid any stability issues, while the DBSs were stored at room temperature and were analyzed one month after blood collection. This reinforces the strategy discussed for DBSs before: the possibility to send the sample by ordinary post to be later analyzed when instrumental/personnel availability mandates.

Overall, these values can be considered as very encouraging for the use of DBS as a less invasive sampling methodology for Cu determination in blood. In particular, for those specimens less affected by blank contamination (HemaXis DB10 and HemaPEN) the results in terms of accuracy and precision are remarkable.

4. Conclusions

This work has evaluated the performance of different devices aiming at direct determination of Cu in blood *via* HR CS GFAAS analysis of DBS. Overall, all the devices enable such determination to be carried out in a simple way relying on external calibration with aqueous standards under optimized conditions and using 1 g L^{-1} Pt in 7% HCl as chemical modifier.

The different devices show, however, different strengths and issues. Mitra devices are easy to use and show suitable dimensions for direct analysis with the HR CS GFAAS technique, but Cu blanks are very high and variable, thus hampering determination of Cu for persons with abnormally low levels and requiring the monitoring of a considerable number of blanks for proper blank correction. Capitainer qDBS shows a similar but smaller problem in this regard. It is a device easy to use by the patient, but it is a bit large for the application intended herein, requiring cutting the DBSs before deposition onto the platform.

The best blanks are obtained for HemaXis DB10. It is a flexible specimen, as the filter paper card used for producing DBS can be easily replaced by the user for other types of materials.

Still, it is also a bit large for this application requiring further manipulation (cutting it and rolling it) before deposition onto the platform. It was considered also a bit more difficult for sampling by the volunteers.

Finally, the HemaPEN device offers an ideal size (filter papers of 3.2 mm diameter, which is one of the most common standards for this type of sample) for the graphite platform and the blanks seemed sufficiently low and stable. In its commercial version, it is probably also simpler to use by the patients, although the specimen tested in this work was a QCPEN device that is designed for method development. It produces DBSs with smaller volumes (2.74 μL instead of approx. 10 μL for the rest), but that is not a problem for this application. In fact, sensitivity is more than enough when trying direct analysis by HR CS GFAAS, such that less sensitive Cu lines need to be monitored. Another advantage of this device consists in obtaining 4 separate discs from only one puncture.

The values presented support the use of DBS as a minimally invasive approach that can provide blood Cu levels in good agreement with those achieved after venipuncture, and thus an appealing possibility for the control of chronic patients or patients subjected to some treatment related with Cu metabolism.

Acknowledgements

The authors are grateful to the European Regional Development Fund for financial support through the Interreg POCTEFA EFA 176/16/DBS, as well as to project PGC2018-093753-B-I00 (MCIU/AEI/FEDER,UE) and the Aragon Government (Construyendo Europa desde Aragón, Grupo E43_20R).

Conflicts of interest

There are no conflicts of interest to declare

5. References

- 1R. A. Festa and D. J. Thiele, *Curr. Biol.*, 2011, **21**, R877–R883.
- 2A. Hordyjewska, Ł. Popiółek and J. Kocot, *BioMetals*, 2014, **27**, 611–621.
- 3G. J. Brewer, in *Molecular, Genetic, and Nutritional Aspects of Major and Trace Minerals*, Elsevier, 2017, pp. 115–129.

- 4M. Latorre, R. Troncoso and R. Uauy, in *Clinical and Translational Perspectives on Wilson Disease*, Elsevier, 2019, pp. 25–31.
- 5M. Resano, M. A. Belarra, E. Garcia-Ruiz, M. Aramendia and L. Rello, *Trends Anal. Chem.*, 2018, **99**, 75–87.
- 6P. A. Demirev, *Anal. Chem.*, 2013, **85**, 779–789.
- 7P. J. Parsons, A. L. Galusha, Y. Cui, E. M. Faustman, J. C. Falman, J. D. Meeker and K. Kannan, *J. Anal. At. Spectrom.*, 2020, **35**, 2092–2112.
- 8T.W. McDade, S. Williams and J.J. Snodgrass, *Demography*, 2007, **44**, 899–925.
- 9P. Bhatti, D. Kampa, B. H. Alexander, C. McClure, D. Ringer, M. M. Doody and A. J. Sigurdson, *BMC Med. Res. Methodol.*, 2009, **9**.
- 10 R. de Vries, M. Barfield, N. van de Merbel, B. Schmid, C. Siethoff, J. Ortiz, E. Verheij, B. van Baar, Z. Cobb, S. White and P. Timmerman, *Bioanalysis*, 2013, **5**, 2147–2160.
- 11 M. O'Mara, B. Hudson-Curtis, K. Olson, Y. Yueh, J. Dunn and N. Spooner, *Bioanalysis*, 2011, **3**, 2335–2347.
- 12 G. Lenk, J. Hansson, O. Beck and N. Roxhed, *Bioanalysis*, 2015, **7**, 1977–1985.
- 13 P. M. De Kesel, S. Capiou, W. E. Lambert and C. P. Stove, *Bioanalysis*, 2014, **6**, 1871–1874.
- 14 P. M. De Kesel, N. Sadones, S. Capiou, W. E. Lambert and C. P. Stove, *Bioanalysis*, 2013, **5**, 2023–2041.
- 15 P. Denniff and N. Spooner, *Bioanalysis*, 2010, **2**, 1385–1395.
- 16 Deegan, R.D., Bakajin, O., Dupont, T.F., Huber, G., Nagel, S.R. and Witten, T.A., *NATURE*, 1997, **389**, 827–829.
- 17 M. Bonta, B. Hegedus and A. Limbeck, *Anal. Chim. Acta*, 2016, **908**, 54–62.
- 18 Y. Ooi, I. Hanasaki, D. Mizumura and Y. Matsuda, *Sci. Technol. Adv. Mater.*, 2017, **18**, 316–324.
- 19 S. Velghe, L. Delahaye and C. P. Stove, *J. Pharm. Biomed. Anal.*, 2019, **163**, 188–196.
- 20 P. Denniff and N. Spooner, *Anal. Chem.*, 2014, **86**, 8489–8495.
- 21 L. A. Leuthold, O. Heudi, J. Déglon, M. Raccuglia, M. Augsburger, F. Picard, O. Kretz and A. Thomas, *Anal. Chem.*, 2015, **87**, 2068–2071.
- 22 S. Velghe and C. P. Stove, *Anal. Chem.*, 2018, **90**, 12893–12899.
- 23 G. Lenk, S. Sandkvist, A. Pohanka, G. Stemme, O. Beck and N. Roxhed, *Bioanalysis*, 2015, **7**, 2085–2094.

- 24 R. Neto, A. Gooley, M. C. Breadmore, E. F. Hilder and F. Lapierre, *Anal. Bioanal. Chem.*, 2018, **410**, 3315–3323.
- 25 T. G. Kazi, H. I. Afridi, N. Kazi, M. K. Jamali, M. B. Arain, N. Jalbani and G. A. Kandhro, *Biol. Trace Elem. Res.*, 2008, **122**, 1–18.
- 26 A. Massadeh, A. Gharibeh, K. Omari, I. Al-Momani, A. Alomari, H. Tumah and W. Hayajneh, *Biol. Trace Elem. Res.*, 2010, **133**, 1–11.
- 27 J. A. Nunes, B. L. Batista, J. L. Rodrigues, N. M. Caldas, J. A. G. Neto and F. Barbosa, *J. Toxicol. Environ. Health A*, 2010, **73**, 878–887.
- 28 P. Abu-Rabie, *Bioanalysis*, 2011, **3**, 1675–1678.
- 29 B. Welz, Becker-Ross, H., Florek, S. and Heitmann, U, Eds., *High-resolution continuum source AAS: the better way to do atomic absorption spectrometry*, Wiley-VCH, Weinheim, 2005.
- 30 M. Resano, M. Aramendía and M. A. Belarra, *J Anal Spectrom*, 2014, **29**, 2229–2250.
- 31 M. Resano, E. García-Ruiz, M. Aramendía and M. A. Belarra, *J. Anal. At. Spectrom.*, 2019, **34**, 59–80.
- 32 B. Welz, S. Morés, E. Carasek, M. G. R. Vale, M. Okruss and H. Becker-Ross, *Appl. Spectrosc. Rev.*, 2010, **45**, 327–354.
- 33 B. Welz, M. G. R. Vale, É. R. Pereira, I. N. B. Castilho and M. B. Dessuy, *J. Braz. Chem. Soc.*, 2014, **25**, 799–821.
- 34 L. Rello, M. Aramendía, M. A. Belarra and M. Resano, *Bioanalysis*, 2015, **7**, 2057–2070.
- 35 A. L. Vieira, E. C. Ferreira, S. R. Oliveira, F. Barbosa and J. A. G. Neto, *Microchem. J.*, 2021, **160**, 105637.
- 36 M. Resano, L. Rello, E. García-Ruiz and M. A. Belarra, *J. Anal. At. Spectrom.*, 2007, **22**, 1250.
- 37 M. Resano, M. R. Flórez and E. García-Ruiz, *Anal. Bioanal. Chem.*, 2014, **406**, 2239–2259.
- 38 F. V. Nakadi, R. Garde, M. A. M. S. da Veiga, J. Cruces and M. Resano, *J. Anal. At. Spectrom.*, 2020, **35**, 136–144.
- 39 S. N. Chaudhuri, S. J. M. Butala, R. W. Ball and C. T. Braniff, *J Expo Sci Env. Epidemiol*, 2009, **19**, 298–316.
- 40 L. A. Currie, *Anal. Chem.*, 1968, **40**, 586–593.
- 41 Á. Cañabate, E. García-Ruiz, M. Resano and J.-L. Todolí, *J. Anal. At. Spectrom.*, 2017, **32**, 78–87.

- 42 E. Bolea-Fernandez, K. Phan, L. Balcaen, M. Resano and F. Vanhaecke, *Anal. Chim. Acta*, 2016, **941**, 1–9.
- 43 L. Pedersen, K. Andersen-Ranberg, M. Hollergaard and M. Nybo, *Clin. Biochem.*, 2017, **50**, 703–709.
- 44 W. E. Funk, J. D. Pleil, D. J. Sauter, T. W. McDade and J. L. Holl, *J. Environ. Anal. Toxicol.*

6. Supplementary information

Perkin Elmer 226 and Whatman 903 filter papers test

For testing the two filter paper (Perkin Elmer 226 and Whatman 903) supplied by the HemaPEN manufacturer, DBSs were prepared by taking 2.74 μL of the 3 RMs with a positive displacement micropipette and depositing that volume onto the filter paper. The analysis was carried out as was explained in section 2.4.

Table S1. Direct Cu determination in whole blood reference materials *via* HR CS GFAAS using different DBS filter papers. Results are expressed as $\bar{x} \pm U$, where $U = (t s)/\sqrt{n}$ for a 95% confidence interval. The concentration was calculated taking into account the volume absorbed by the DBS device.

Sample	Reference value (Cu, mg L ⁻¹)	HemaPEN (Perkin Elmer 226)b (mg L ⁻¹) (n=5)	HemaPEN (Whatman 903) b (mg L ⁻¹) (n=5)
RM L-1	0.64 \pm 0.13	0.66 \pm 0.07 (RSD = 8%)	0.65 \pm 0.05 (RSD = 6%)
RM L-2	1.34 \pm 0.27	1.30 \pm 0.07 (RSD = 4%)	1.35 \pm 0.10 (RSD = 6%)
RM L-3	2.08 \pm 0.42	2.26 \pm 0.14 (RSD = 5%)	2.48 \pm 0.15 (RSD = 5%)

Chapter 4:

Time-absorbance profile ratio background correction: introducing TAP to correct for spectral overlap in high- resolution continuum source graphite furnace atomic absorption spectrometry

Abstract

Technological developments have brought significant upgrades to classic analytical techniques, such as the evolution of atomic absorption spectrometry (AAS) to high-resolution continuum source (HR CS) AAS. The possibility to obtain more information about the vicinity of the analytical line, thus effectively transforming a 2-dimension technique (time *versus* absorbance) into a 3-dimension one (by adding wavelength information), represents a key advantage when dealing with potential spectral overlaps. Indeed, the occurrence of diatomic molecule absorption often resulted in high background values in classical AAS, affecting many analyses. The high spectral resolution provided by HR CS AAS in this third dimension enables the use of new tools, first to detect and later to solve this problem.

Currently, the software of commercially available HR CS AAS spectrometers is equipped with an algorithm for interference correction, the so-called least-squares background correction (LSBC). Using a spectrum from the interfering species as a correction model, LSBC can correct for the spectral interference by subtracting it. Nevertheless, this approach still poses some problems (*e.g.*, the need to identify the overlapping species). Moreover, there is still a lot of information contained in every measurement that is essentially unused and can help in correcting for spectral overlaps.

The time-absorbance profile (TAP) of a species, measured under the same instrumental HR CS AAS conditions using a graphite furnace (GF) as the atomizer, should be the same at every wavelength measured. Therefore, using a TAP normalized spectrum of the interfering species should be sufficient to subtract it from the normalized absorbance of the atomic line, leaving only the analytical signal of the analyte.

This work proposes the use of such an approach for the first time and discusses in detail how the TAP method can be deployed, without the need to perform any additional measurements or know in advance the nature of the overlapping species, demonstrating its usefulness for circumventing spectral overlaps (e.g., for the direct determination of Cu in dried plasma spots from whole blood Seronorm™ –they did not differ significantly from the certified concentration), as well as highlighting its current limitations.

1. Introduction

The progression experienced by atomic spectrometry techniques over the last decades is undeniable, particularly in terms of sensitivity. However, potential interferences are always present, and the way to deal with them vary depending on the technique used. There are two large groups of interferences: spectral and non-spectral. The non-spectral ones are produced by the physicochemical interaction of the species present in the matrix with the analyte, which may lead to analyte loss prior to its detection or variations in the sample introduction efficiency. There are several strategies to circumvent this type of interference, during sample preparation and/or instrumental steps (e.g., using a pyrolysis temperature step in graphite furnace atomic absorption spectrometry, GFAAS).¹

Spectral interferences occur when there is an overlap with the analyte analytical signal from another species. Trying to overcome this phenomenon is not always straightforward. In conventional GFAAS, besides the use of separation techniques, the traditional strategy consists in optimizing the pyrolysis temperature, in an attempt to temporally resolve the analyte signal from the interfering signal, or the use of chemical modifiers which can eliminate the interfering species or change the chemical environment over the graphite platform in order to ease the analyte atomization free from interference.¹

HR CS AAS offers a different way to circumvent spectral interferences. The possibility of evaluating the spectral vicinity of the analytical signal helps to elucidate such interferences, and mathematical tools can be then used to overcome them. For instance, **Figure 1A** represents a classical interference in AAS: the PO molecular (structured band) absorption affecting the Pb line at 217 nm. In this case, the interference is known (PO molecule), and it is possible to generate a reference spectrum of such species using the same temperature conditions and a suitable reagent, in this case ammonium dihydrogen phosphate (see **Figure 1B**).

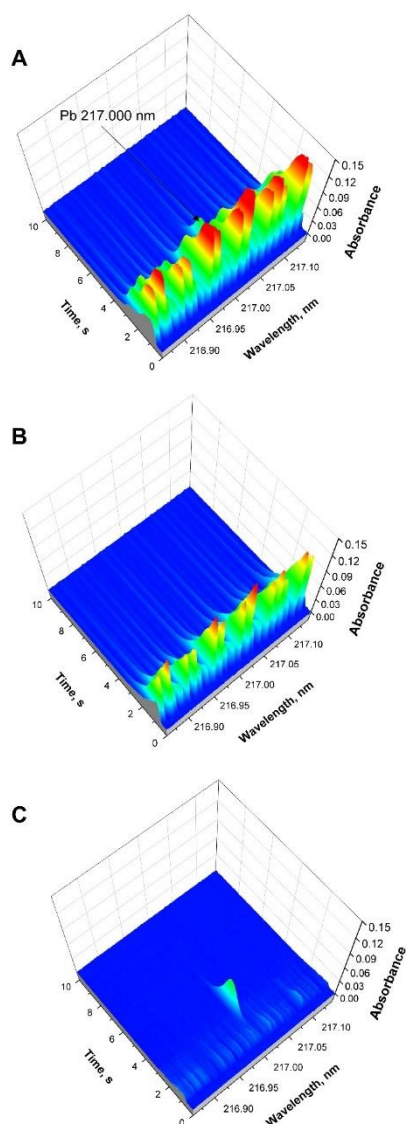


Figure 1. Wavelength- and time-resolved spectra recorded in the vicinity of 217.000 nm (spectral window = 0.28 nm) for: (A) 0.1 ng Pb and 10 μg P; (B) 10 μg P; and (C) Figure 1A corrected spectrum using LSBC. All the measurements were carried out using 5 μg Pd + 0.5 μg Mg as chemical modifiers. $T_{\text{pyrolysis}} = 800\text{ }^{\circ}\text{C}$, $T_{\text{atomization}} = 1600\text{ }^{\circ}\text{C}$.

The least square background correction (LSBC) algorithm uses “independent linear functions in a least-squares fitting algorithm and fitted each absorbance spectrum. The individual absorbance spectra corrected for fine-structured background are calculated”.² In short, a reference spectrum for every detector pixel and every time monitored is first obtained. This reference spectrum is then increased or decreased by multiplication with a magnification factor. The differences between the reference spectrum and the sample spectrum, as well as their squares, are calculated pixel by pixel, and the sum of the square values over all pixels is added up. After that, the mentioned magnification factor is varied in order to minimize the

sum of the squares or – in other words, to find the 'least squares'. Once the final reference spectrum that offers the best fit is calculated, it can be subtracted from the spectrum measured for the actual sample. Using this procedure, only that part of the structured background that corresponds to the fine structure of the reference spectrum should be eliminated.³

This kind of background correction corrects for any structured background 'under' the line measured simultaneously, although the correction is carried out 'off-line', after the measurement.⁴ Therefore, using the PO spectrum as reference (see **Figure 1B**) for LSBC, this spectral correction can be performed, and the result is a spectrum that is practically clear from /interferences (see **Figure 1C**).

This tool is very useful to correct for spectral interferences and it has been studied in many HR CS AAS works,^{5–25} (also some situation where its use is not recommended has been reported),²⁶ since its introduction by Becker-Ross *et al.*³ It is also possible to apply various correction reference spectra to correct for various overlapping species, although these have to be applied sequentially for each interfering species.¹⁴ The LSBC feature is integrated in the AspectCS software of the commercially available HR CS AAS, so it can be easily applied.

However, there are some drawbacks associated with this approach that should be mentioned. *A priori* knowledge is required, as the analyst needs to know the interfering species before correcting for it. The AspectCS software database usually shows the more recurrent molecules and/or atoms which can absorb in the spectral window, and one can always try to find more information in the literature. Despite all the information available, there are many cases where further studies needed to be carried out to discover the nature of the interference, with the corresponding investment in terms of time. Sometimes, the exact molecule is not uncovered, but a matrix-matching solution can be prepared to generate the interference and then perform LSBC, if sufficient information from the sample is available.¹⁸ This strategy is, however, hardly feasible when direct solid sampling is intended.

Moreover, there are two other effects that hamper a proper correction using LSBC. First, the concentration of the reference spectrum (interference) should be similar to the one found in the sample, the Voigt profile due to the convolution of Doppler and Lorenz broadening.¹ If the reference solution is much more concentrated than the sample, the peaks will be wider

(in terms of wavelength) and LSBC will probably overcorrect the baseline. If, on the other hand, the concentration is too low, maybe the interfering molecule cannot be generated and/or detected. The influence of the concentration will be further evidenced in section 3.1.

Another issue is the atomization/vaporization mechanism: there are cases in which the interfering species is generated at a very different time than in the sample, and then LSBC may not properly correct for the overlap. Finally, many species present in the matrix may alter the atomization/vaporization mechanism, such that it may not be simple to replicate it with any aqueous standard solution.

In short, as stated by Borges *et al.* "it is important not only to find the molecule responsible for the interferences, but it is also necessary to consider how the other components of the sample can affect the thermal behavior of this molecule and consequently, its absorption profile."¹⁸ Overall, the use of LSBC opened new possibilities for correcting overlaps, but it does not solve all the problems that can be encountered in HR CS GFAAS.

Therefore, in this work we propose a new correction model to eliminate spectral interferences without needing the use of any reference spectrum, but instead by using only the spectrum obtained from the sample. No information about the interfering species is needed, which can save significant time and effort during analysis. The theoretical and experimental fundamentals of this method is described in section 3.1.

2. Experimental

2.1. Instrumentation

All the AAS measurements were carried out using a high-resolution continuum source graphite furnace atomic/molecular absorption spectrometer contrAA 800G (Analytik Jena, Jena, Germany). More details about this type of instrument can be found elsewhere.^{2,27,28} All the samples (liquid and solid) were inserted in the graphite furnace using a solid autosampler SSA600 (Analytik Jena), and thus solid sampling graphite tubes (no orifice on the top) and platforms were used throughout the study.

For the validation of Cu values, a Perkin Elmer (Waltham, USA) NexION 300x inductively coupled plasma mass spectrometer (ICP-MS) was used.

2.2. Reagents, standards, and samples

All reagents were of analytical grade or higher. The solutions were prepared using HNO₃ 14 mol L⁻¹ Suprapur (Merck, Darmstadt, Germany) diluted to 0.14 mol L⁻¹ with deionized water purified by a Milli-Q system (Millipore, Bedford, USA).

For the determination of Pb, a Pd/Mg chemical modifier was prepared using stock solutions of 10 g L⁻¹ Pd (Merck) and 1 g L⁻¹ Mg (Merck). This modifier solution showed final Pd and Mg concentrations of 1 g L⁻¹ and 0.1 g L⁻¹, respectively. 5 µL of such solution were injected for all measurements. For Cu monitoring, a 1000 mg L⁻¹ Pt (Merck) solution was used directly as modifier. 10 µL of this solution were injected. Aqueous solutions of Pb and Cu were prepared from 1000 mg L⁻¹ standard solutions (Merck).

Ammonium dihydrogen phosphate (Merck) was dissolved in deionized water to obtain a final concentration of 10 g L⁻¹ of P, which was used as the interference source of PO in the case of Pb determination in aqueous solutions.

Three Seronorm™ whole blood (WB) reference materials (RMs), L-1 (Lot: 1406263), L-2 (Lot: 1406264) and L-3 (Lot: 1509408), produced by SERO AS (Billingstad, Norway) were prepared as dried plasma spots (DPSs) using a NoviPlex™ Remote Plasma Collection Device, named Noviplex UNO (Novilytic, West Lafayette, USA). DPSs were prepared for the analysis by adding a droplet of whole blood RM (approx. 10 µL) onto the device. A membrane filters this blood and leaves only a constant amount of plasma (2.5 µL) to be deposited onto the filter paper found below the membrane. DPSs were left to dry at room temperature for at least 4 hours before analysis. The DPSs were further analyzed as a solid sample for Cu determination.

2.3. Procedures for the development of the correction model and for analyses of the samples

For the development of the TAP model and the monitoring of Pb in aqueous solutions (see Section 3.1.), the analytical line of Pb at 217.000 nm was measured. After that, Cu determination in solid samples was carried out at 222.570 nm. In all cases, three detector pixels were used to measure the absorbance (center pixel and the two adjacent ones). All the temperature programs used in the different experiments of this study can be found in **Table 1**.

Table 1. Temperature program for the different analyses carried out by means of HR CS GFAAS. The wavelength range (spectral window) of each analyte is in parenthesis after the wavelength.

Pb 217.000 nm (0.28 nm)				
Step	Temperature °C	Ramp °C s ⁻¹	Hold s	Ar flow L min ⁻¹
Drying	90	3	20	2.0
Drying	110	5	10	2.0
Pyrolysis	800	300	20	2.0
Gas adaption	800	0	5	0
Atomization	1600	1500	10	0
Cleaning	2450	500	4	2.0
Cu 222.570 nm (0.15 nm)				
Step	Temperature, °C	Ramp, °C s ⁻¹	Hold, s	Ar flow, L min ⁻¹
Drying	120	3	30	2.0
Drying	150	5	30	2.0
Pyrolysis	1300	50	35	2.0
Gas adaption	1300	0	5	0
Atomization	2300	3000	6	0
Cleaning	2500	500	4	2.0

For ICP-MS analysis of DPSs, four DPSs samples were digested in 1 mL of HNO₃ 14 mol L⁻¹ in closed PTFE vessel during 4 h at 120 °C. After dilution to 10 mL, Cu was then determined by monitoring both ⁶³Cu and ⁶⁵Cu isotopes, using Rh 10 µg L⁻¹ as internal standard, and the collision cell filled with 2.5 mL min⁻¹ He to minimize overlaps from ²³Na⁴⁰Ar⁺ over ⁶³Cu⁺. The same procedure was performed with blank DPSs to subtract the Cu content.

3. Results and discussion

3.1. Time-absorbance profile

As described in the Introduction, one of the possible issues that hampers the successful application of LSBC is the difference in the time-profile for the reference when compared to that actually obtained for the sample. **Figure 2** describes a simple case in which this problem appears. **Figure 2A** shows a PO molecule absorbance profile in the vicinity of 217 nm (without Pb atomic absorption line), as an example of potential interference. In order to correct for it, PO molecules were generated (see **Figure 2B**) using a 10 times lower P mass, approximately, than the one used in **Figure 2A**, thus obtaining a reference spectrum. Thus, by applying LSBC, one would expect as a result a “baseline” spectrum, *i.e.*, no visual analytical signal displayed, only instrumental noise. This behavior did not occur, as shown in **Figure 2C**. There are some transitions that could not be corrected properly, even though the same temperature conditions were used. Obviously, this example illustrates a clear limitation of LSBC, because in a real situation the exact amount of the interference is probably unknown.

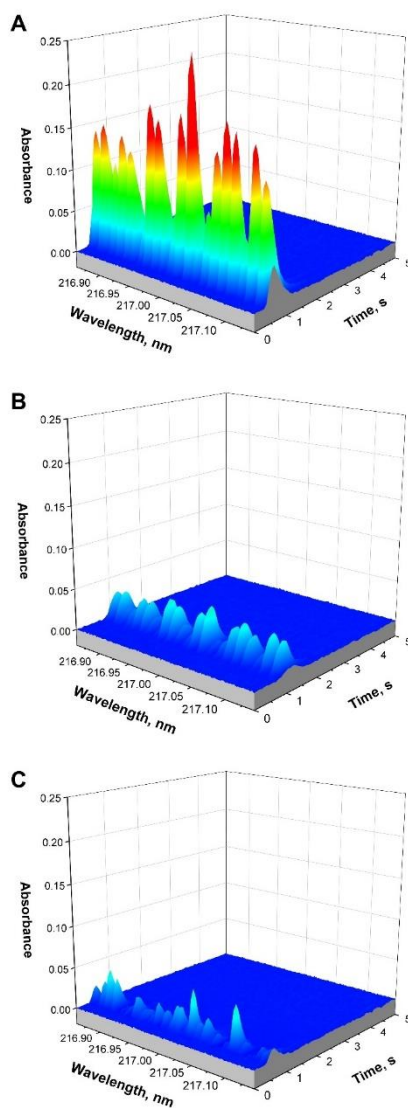


Figure 2. PO molecule absorption spectra recorded in the vicinity of 217.000 nm (spectral window = 0.28 nm) for: (A) 10 μg P; (B) 1.0 μg P; and (C) **Figure 2A** corrected spectrum using **Figure 2B** as reference for LSBC. All the measurements were carried out using 5 μg Pd + 0.5 μg Mg as chemical modifiers. $T_{\text{pyrolysis}} = 800\text{ }^{\circ}\text{C}$, $T_{\text{atomization}} = 1600\text{ }^{\circ}\text{C}$.

Figure 1 shows an example where LSBC works better, as the reference spectrum was obtained using the same P amount than that found in the sample. As a result, the Pb analytical line at 217 nm could be monitored interference free. Many other examples of LSBC application have been reported.^{3,5–25} However, there is an important drawback: one “must” know the interference in order to correct for it. When the molecule is not known, proper correction proves to be difficult, as discussed in the Introduction section.

However, the 3D spectrum obtained by a high-resolution spectrometer contains additional information that has not been exploited yet: the temporal behavior of the signal originating from diatomic molecules. Using **Figure 1A** as an example, there are more than 20 peaks within the spectral window from the PO molecule vibronic transition $X^2\Pi \rightarrow D^2\Pi(2,0)$ with a band head found at 216.99 nm.²⁹

If the spectrum in **Figure 1A** is rotated in order to show just two dimensions, absorbance *versus* time, and the maximum peaks (by pixel number) of the PO molecule are displayed, the resulting spectrum is shown in **Figure 3**. In this example, we only selected the PO peaks with maximum absorbance height over 0.05, *i.e.*, the better resolved peaks. This threshold can be adapted to the sensitivity of the transitions evaluated in every situation. It is noteworthy the threshold select the TAP which is within the selection, regardless the wavelength width profile of the interference. The analyte signal should not be included in this correction model, to prevent overcorrection, and thus the central pixel ± 6 (13 detector pixels in total) were also excluded when choosing the PO transitions. A total of 12 peaks were thus selected.

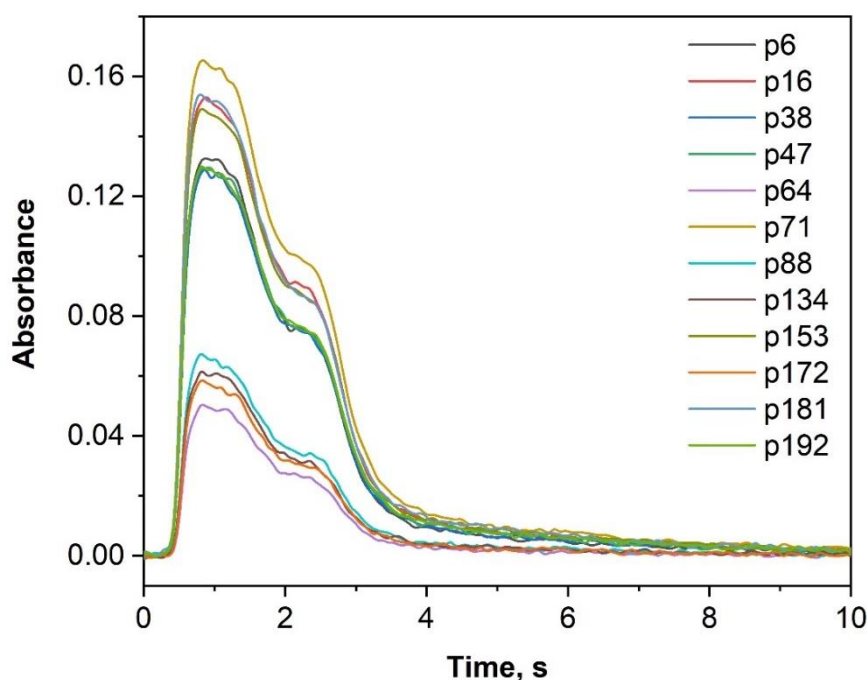


Figure 3. Time-resolved spectra of the PO molecule from **Figure 1A** (vicinity of 217.000 nm, spectral window 0.28 nm) for 12 different detection pixels (labelled “p” plus pixel number).

The PO transitions, each one with its respective sensitivity, provide a temporal profile that is consequence of several aspects and interactions: species containing PO in the solid phase before its vaporization, pyrolysis and vaporization temperature, heating ramp, etc. The

sum of all these phenomena will finally produce such temporal profile for every species found in the graphite furnace, whether they are atoms or molecules, and if the conditions do not change, this absorption peak profile should be identical for all measurements, *i.e.*, a time-absorbance profile (TAP). This concept is the basis of our new correction method. **Figure 3** shows that the PO molecules inside the GF undergo the same vaporization process through time, therefore their peak profiles possess the same shape. Obviously, there are slight differences due to, for instance, the signal-to-noise ratio for each transition, which is related to its sensitivity.

3.2. Ratio normalization in TAP

By evaluating the most sensitive transition of PO in this spectral window (pixel 71, $\lambda = 216.958$ nm) in detail, it is clearer how the instrument obtains the data for plotting the spectrum. It collects the absorbance for a period of time (~ 0.07 s) at each detection pixel and registers this information until the end of the integration time set (see **Figure 4**). The spectrum was zoomed between 0 and 5 seconds (see the entire integration time in the small spectrum inside **Figure 4**) for better visualization.

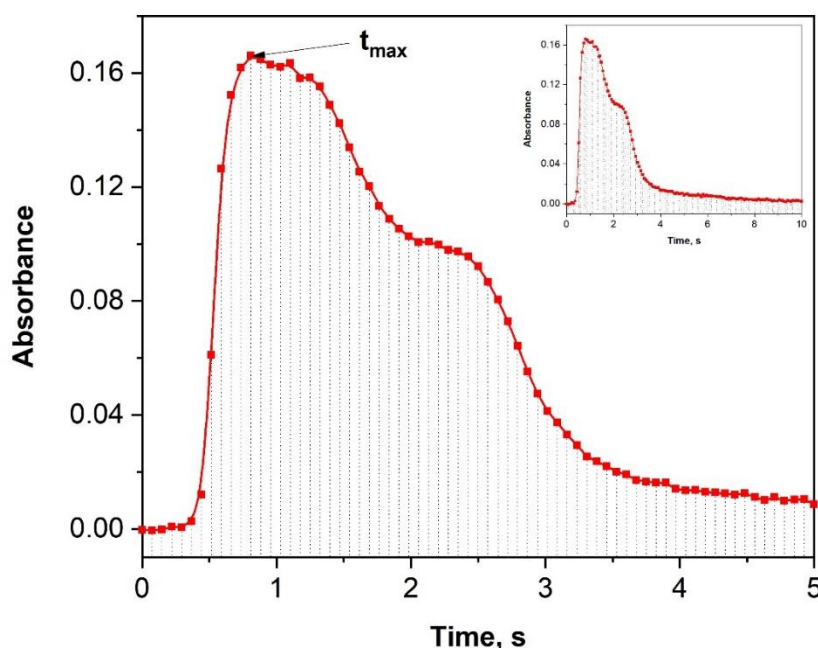


Figure 4. Time-resolved spectrum of pixel 71 ($\lambda = 216.958$ nm) from **Figure 1A**, showing every absorbance value obtained from the CCD detector each ~ 0.07 s (red squares).

Through the vaporization process, there is a specific moment (t_{\max} , see **Figure 4**) in which most of the molecules are in the gaseous phase absorbing the radiation from the light source, and, thus, the analytical signal reaches its maximum height. Therefore, if every transition is normalized to its maximum value, all the normalized spectra should show practically the same profile. **Figure 5** shows the normalized spectra of the peaks displayed in **Figure 3**.

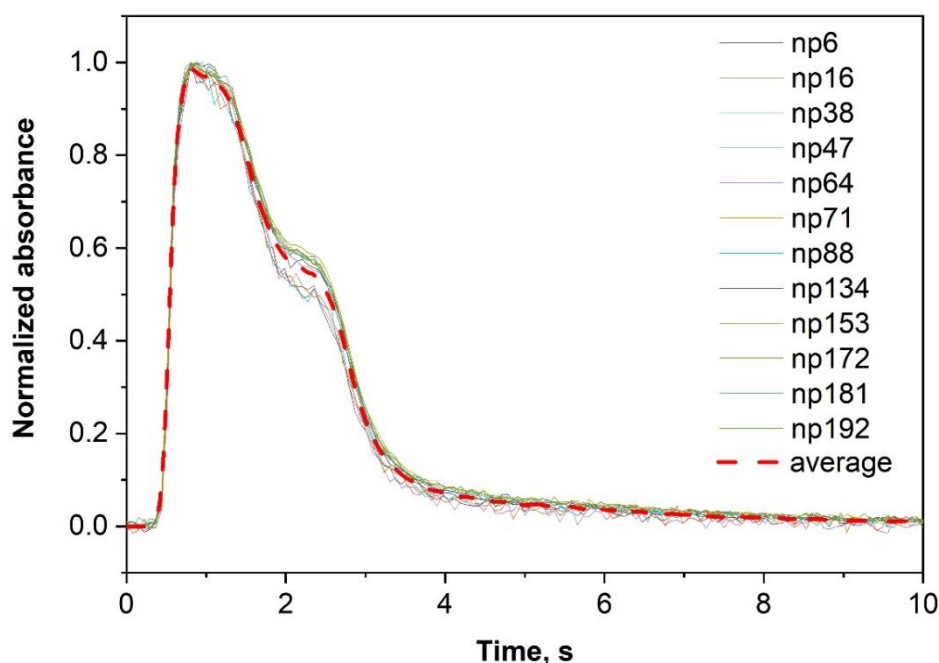


Figure 5. Time-resolved spectra of the PO molecule shown in **Figure 3** (vicinity of 217.000 nm, spectral window 0.28 nm) for 12 different detection pixels normalized to each t_{\max} (labelled “np” plus pixel number), and the average normalized absorbance (red-dashed line).

Figure 5 demonstrates that such assumption, normalized transitions producing the same temporal profile, is valid. As expected, small differences between transitions were observed, but these should not affect drastically the analyte signal. In this example, the larger difference (0.1047 in absolute normalized absorbance) was observed at 2.28 s between pixels 71 and 88. Although it seems a considerable variation (10.5%), it should be noticed that this bias would occur for one single measurement among all the 137 spectra data acquired through time. Moreover, if the analyst is not comfortable with this normalized difference, a threshold could be used (e.g., maximum 5%), in order to reject such transition from the correction model. In this study, all the normalized spectra were used.

3.3. Application of TAP correction

After acquiring the normalized spectra of the interference, an average normalized spectrum is calculated using all the selected PO molecule transitions (see **Figure 5**, red-dashed line). Finally, this correction model will be compared with the analytical signal at pixel 101 ($\lambda = 217.000$ nm), where both the atomic absorption line of Pb and the PO molecule interference (see **Figure 6A**) overlap. Obviously, the absorbance signal profile at this pixel is different from the one obtained in **Figure 5**. The difference when treating this data is that one cannot normalize to its maximum (in this case) because the analyte absorbance is higher than that originating from the interference. Thus, such maximum is mainly influenced by the Pb absorption. Therefore, it is very important to normalize this pixel to the signal corresponding to the t_{\max} of the PO molecule, in this case appearing at 0.84 s. After normalizing the spectrum of **Figure 6A** using the previous consideration, the result is shown as the black normalized spectrum in **Figure 6B**. As expected, this normalized spectrum shows values higher than 1 because the maximum for the PO molecule is much smaller than the overall peak maximum.

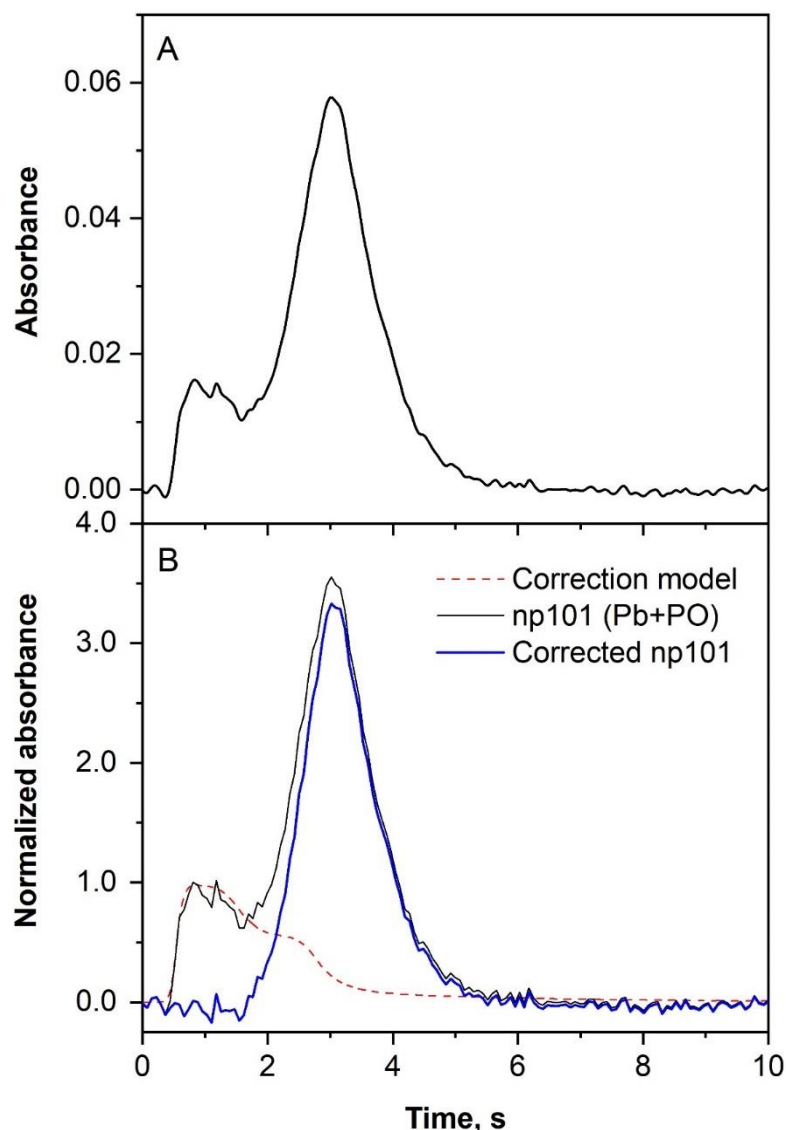


Figure 6. (A) Time-resolved spectrum for the pixel 101 from **Figure 1A** (vicinity of 217.000 nm, spectral window 0.28 nm) showing the overlap of the PO molecule and the Pb absorbance profiles; and (B) the normalized **Figure 6A** spectrum (np 101, black line), the TAP correction model (red-dashed line, see **Figure 5**), and the corrected normalized spectrum (blue line) obtained by subtracting the TAP model from np101.

Finally, subtracting the correction model obtained in **Figure 5** (red-dashed normalized spectrum in **Figure 6B**) from the normalized values at pixel 101, the result is a normalized absorbance Pb spectrum (blue normalized spectrum in **Figure 6B**) that should be free from the PO interference. All the spectra are normalized to (*i.e.*, divided by) its PO maximum height at 0.84 s, therefore if the normalized spectrum is multiplied by this value, the original spectrum is obtained, except for the interference. For analytical purposes, this correction can be done only at the pixels of interest for quantification. However, in order to see a complete 200-pixel

application, **Figure 7** shows the effect of this correction in data displayed in the **Figure 1A**. This was the first data obtained by a ContrAA instrument after correction by this novel strategy.

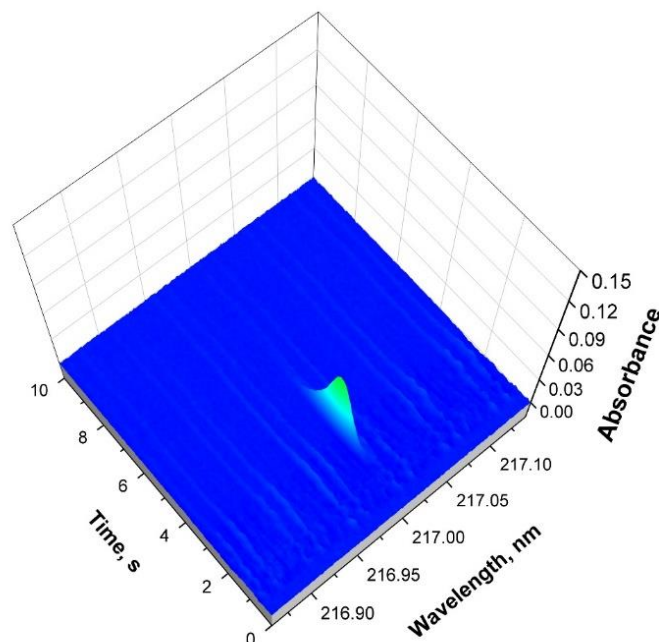


Figure 7. Time- and wavelength-resolved spectrum from **Figure 1A** (vicinity of 217.000 nm, spectral window 0.28 nm) corrected using TAP correction model.

Three replicates were measured with the temperature conditions described in **Table 1**, with 0.2 ng Pb, 5 μg Pd + 0.5 μg Mg as chemical modifiers, and 5 μg P to generate PO as interference (see **Table 2**). Obviously (see **Figure 6A**), if there is no correction, the analytical signal is overestimated. Using LSBC as a reference, TAP correction differs by 10-12%. **Figure 8** shows the difference between the corrected spectrum of the three center pixels using both LSBC and TAP for the third replicate of **Table 2**.

Table 2. Integrated absorbance data obtained after three measurements of Pb at 217.00 nm (3 detection pixels, CP±1) using 0.2 ng Pb (analyte), 5 µg Pd + 0.5 µg Mg (chemical modifiers) and 5 µg P (interference) by HR CS GFAAS.

Replicate	Integrated absorbance, s		
	No correction	LSBC	TAP
1	0.24642	0.18801	0.16687
2	0.30341	0.24144	0.21712
3	0.31094	0.22841	0.20015

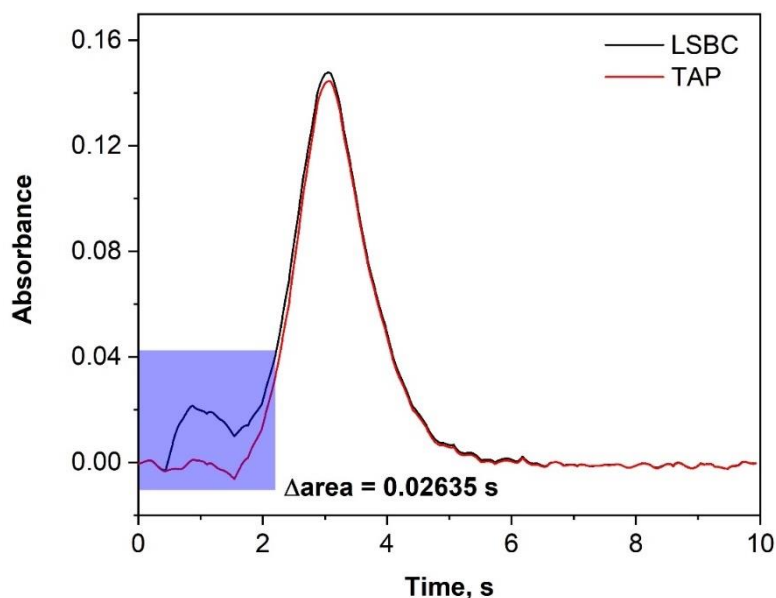


Figure 8. Time-resolved spectra of the sum of the three central pixels (100,101 and 102) of **Figure 1A** (vicinity of 217.000 nm, spectral window 0.28 nm) after correction with LSBC (black line) and TAP (red line).

The blue area highlights the area where obviously the interference has not been completely corrected after applying LSBC. The difference in integrated absorbance when comparing with TAP correction is 0.02635 s. The overall difference between both correction approaches is 0.02826 s, which corroborates their practical equivalence. The fact that TAP corrects better in this case than LSBC could already be appreciated by comparing the spectra from **Figure 1C** (LSBC) and **Figure 7** (TAP), the latter being obviously cleaner. It is noteworthy that LSBC is a powerful tool and, although in this example it could not correct the

PO molecule completely, it might be possible to further improve this correction by optimizing the analytical method, with the subsequent additional effort. In order to check other concentrations, the same temperature program and chemical modifier were used over 0.1 ng Pb, and 10, 50 and 100 μg of P. The integrated absorbance values of Pb after TAP correction do not differ between the different P mass (0.03818 ± 0.00295 , 0.03806 ± 0.00768 and 0.04123 ± 0.00491 s, respectively). **Figure S1** (see Electronic Supplementary Information) shows the three spectra of these experiments.

TAP correction offers significant advantages. First, the measurement itself provides the information for its correction within its spectral window. There is no need for a reference spectrum. Second, if the analyst has the expertise to recognize a molecule band-structured profile as interference, there is no need-to-know which molecule that would be. The correction works regardless. Even though the AspectCS provides a database of probable atoms and molecules that absorb in the analytical line vicinity, which can be used to prepare a solution containing the interference, working with direct solid analysis of inorganic complex matrices, *e.g.*, minerals, is not straightforward. The composition of these materials usually comprises a great number of elements found at high levels. Therefore, there is a larger probability of forming unusual diatomic molecules, thus requiring extensive literature searching for their identification, and even then, they may remain unknown. TAP correction can overcome this time-consuming procedure, providing a faster way for correcting for overlap.

Naturally, TAP also shows some limitations. As discussed in Section 3.2., it is important to define the maximum of the species interfering the analysis and, also, part of its time-absorption profile. If the analyte signal completely overlaps with that for the interference and it is not possible to visualize a “double peak” or even a “peak shoulder”, this model will correct the center pixel completely, leaving no analyte signal for evaluation. This issue, however, may be solved by modifying a bit the temperature program, as it is extremely unlikely to find an overlap that is complete under all working conditions for species that are, after all, different. Moreover, the TAP model as currently proposed works for a single interference, *i.e.*, if there are two interfering molecules at the same time, it cannot find a pattern suitable for the correction. Further investigation is needed to expand this concept to circumvent this handicap. For the moment, the authors suggest the sequential use of LSBC if possible (*e.g.*, the overlapping species are identified, and their spectrum can be reproduced) when more than one molecular spectrum overlaps with the signal of the analyte.

Finally, it is noteworthy that this study focuses on diatomic molecular interferences, because that is the most common overlap when using HR CS AAS. However, in those rare cases in which there is an overlap caused by an atomic species, this correction can be used as well, providing there are other atomic lines of the same interfering element within the spectral window to produce the correction model.

3.4. TAP correction for direct analysis of reference materials

The previous study investigated the effect of a known interference, although, for analytical purposes, the temperature could have been further optimized to try to temporally resolve the signal of both lead and phosphorus monoxide.

Generally speaking, the interference of diatomic molecules in HR CS GFAAS might not be as severe for samples that undergo some pretreatment (decomposition/extraction), as the matrix can be eliminated to some extent during such procedure. However, when direct analysis of solids or complex liquid samples is attempted, the situation is the opposite. Such approaches would benefit more from the TAP correction, as all the matrix is introduced into the GF system. Direct analysis of three reference materials were evaluated by determination of Cu ($\lambda = 222.57$ nm) in DPSs prepared with 3 different whole blood RMs with different Cu levels in each one (L-1, L-2, and L-3). More details of these materials are provided in section 2.2.

The Cu determination highlights another overlap that we found over the course of our research on the development of minimally invasive approaches for clinical analysis. The reader might not be familiar with DPSs and with dried matrix spots in general, so a short comment seems appropriate. Matrix dried spots such as dried blood spots (DBSs) are specimens of increasing clinical importance where a small amount of blood is deposited onto a clinical filter paper, left to dried and sent to the lab for analysis. This approach offers significant advantages to patients, as well as to develop biobanks. The importance of analysis of dried matrix spots and of determining Cu in particular, are discussed elsewhere,³⁰⁻³² and will not be covered herein for the sake of simplicity. DPSs represent an evolution of DBSs, where the spot contains plasma instead of whole blood, as sometimes the target of analysis is not blood but such plasma. This is a complex but very relevant sample for our research, and it was practically impossible to analyze it directly without the concurrence of the TAP

approach. To the best of the authors knowledge, this is the first time that direct elemental analysis of a dried plasma spot is performed.

DPSs were prepared for the analysis by adding a droplet of whole blood RM (approx. 10 μL , until a control spot is filled with the sample) onto the device, which contains a membrane that filters it and, in theory, leaves only 2.5 μL (value indicated by the manufacturer) of plasma to be collected by the clinical filter paper found below. More information about this DPS device can be found elsewhere.^{30,33}

The time- and wavelength-resolved spectra of the DPSs produced with whole blood L-1 (low Cu content) are displayed in **Figure 9**. As can be seen, the presence of the Cu atomic line at 222.570 nm is not apparent as it is hidden among the molecular absorption profile. Moreover, the authors could not identify which molecule causes such spectrum, hampering any successful recreation with standards to apply LSBC. It is noteworthy that, under several temperature conditions, the Cu atomic peak and the molecule absorption profile could not be resolved, and the overlap was observed for the DPS produced with the three whole blood RM samples.

Such molecule was found when the DPS filter paper was measured alone (see **Figure 9A**), which in principle opens the possibility to use LSBC with such blank to produce the reference spectrum. Unfortunately, there is also Cu contamination in the DPS filter paper, which is detrimental for this purpose, as will be discussed below. A previous work from our research group on direct determination of Cu in DBS already discussed the problem of contamination in the paper and the need to properly correct for the blanks.³² However, no such structures were found when measuring conventional cellulose-based clinical filter paper (Whatman 903 and Perkin Elmer 226) at this Cu wavelength (222.570 nm). The material used for the filter paper present in Noviplex DPS cards is not described in the information available from the manufacturer, so it could show a different composition, or it could contain some remains of the membrane located above. In any case, the occurrence of the overlap poses a challenge that needs proper correction.

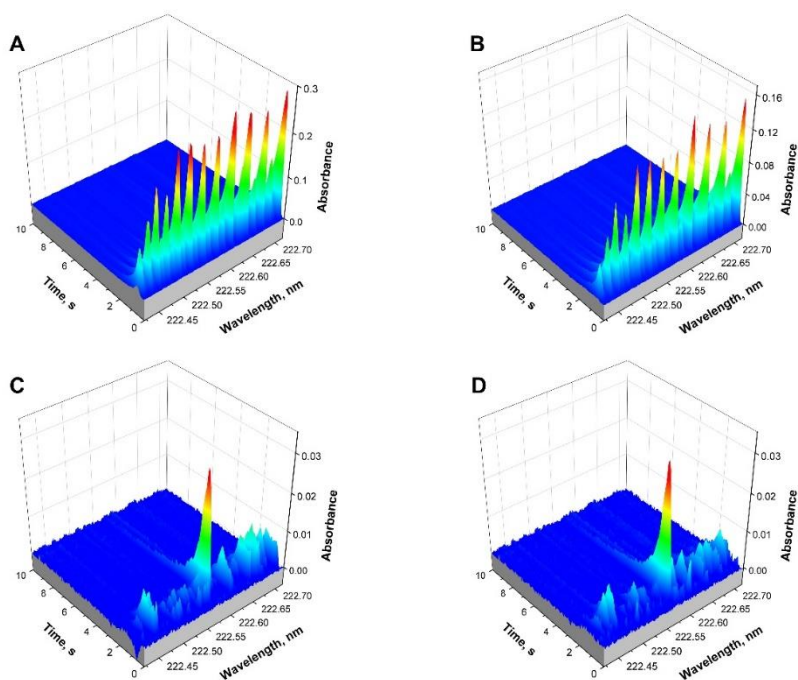


Figure 9. Time- and wavelength-resolved spectra recorded in the vicinity of Cu analytical line 222.570 nm (spectral window 0.15 nm) for: (A) DPS blank (without blood); (B) DPS of whole blood L-1; (C) spectrum of **Figure 9B** corrected using LSBC with DPS blank (**Figure 9A**) as reference; and (D) spectrum of **Figure 9B** corrected using TAP correction. The temperature program is displayed in **Table 1**.

Using the DPS blank (filter paper without blood, spectrum in **Figure 9A**) as a reference for LSBC, this correction was applied to all data of Cu determination in DPSs. An example of the raw spectrum for a DPS produced with whole blood L-1 is shown in **Figure 9B**. The results are displayed in **Table 3**. The molecular interference was not fully corrected (see **Figure 9C**). This is not surprising because the presence of Cu in the filter makes it impossible to obtain a proper reference spectrum containing only the overlapping molecule. However, as a result of this fact, overcorrection would have been expected and the results after LSBC are actually higher than expected. Thus, there must be another reason for this.

Table 3. Determination of the Cu concentration at 222.570 nm in whole blood RMs as DPSs using ICP-MS (with Rh as internal standard) and HR CS GFAAS (either applying none or else two different correction models). Experimental uncertainties are expressed as 95% confidence intervals (n=5).

Sample	Reference	Cu concentration, mg L ⁻¹			
		ICP-MS	No correction*	LSBC	TAP
WB L-1	0.64 ± 0.13	-	0.196 ± 0.130	0.98 ± 0.05	0.529 ± 0.101
WB L-2	1.34 ± 0.27	-	1.12 ± 0.15	1.94 ± 0.13	1.15 ± 0.21
WB L-3	2.08 ± 0.42	2.23 ± 0.70	2.32 ± 0.56	3.02 ± 0.33	2.05 ± 0.35
		(⁶³ Cu)			
		2.11 ± 0.71			
		(⁶⁵ Cu)			

* Indicating that neither LSBC nor TAP were applied, but blank subtraction was performed for all approaches.

On the other hand, despite the pronounced overlap between the unknown molecule and the Cu atomic line, it is still possible to appreciate some small differences. There is a peak shoulder appearing between 0.25 and 0.75 s that can be mainly attributed to the unknown molecule because at such time the overlapping molecule appears at other wavelengths. This exemplifies why simultaneous monitoring of a portion of the spectrum provides useful information to correct for overlaps and opens the possibility to apply TAP correction.

By applying the TAP model, this molecular profile (**Figure 10**, red-dashed line) can be calculated, and subtracted from the Cu+molecule raw absorbance profile (**Figure 10**, black line). The corrected spectrum (**Figure 10**, blue line) is thus obtained after this deconvolution. Although there is also a small overcorrection around 0.5 s (negative absorbance signal), this was not significant in comparison to the total analytical signal (total integrated absorbance = 0.09900 s, overcorrection = - 0.00113 s).

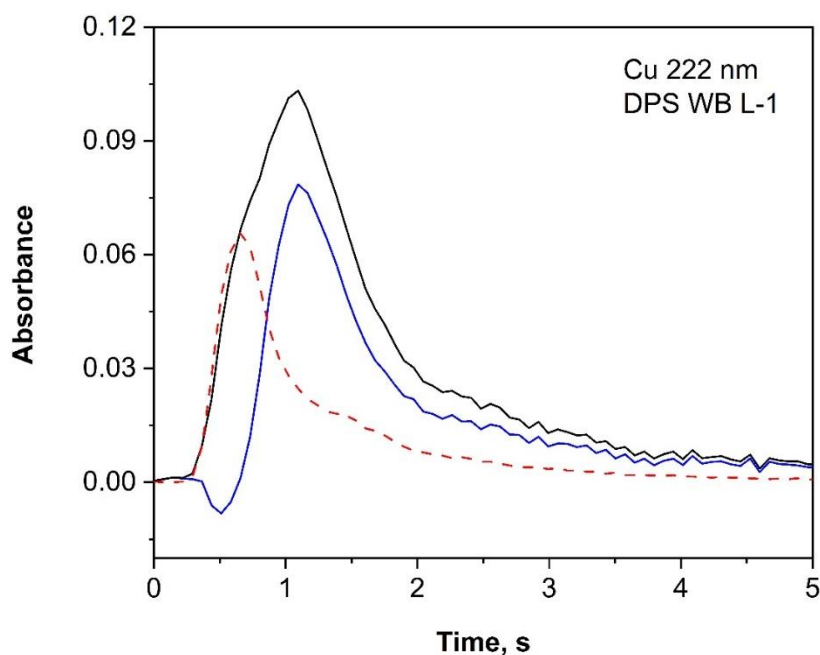


Figure 10. Time-resolved spectra of the Cu atomic line recorded at 222.570 nm (spectral window 0.15 nm) for DPS of whole blood L-1. The sum of the 3 central pixels is represented. The black line represents the raw spectrum, the red-dashed line is the TAP model, and the blue line shows the final, corrected spectra.

The resulting time- and wavelength-resolved spectra after TAP correction can be seen in **Figure 9D**. It is noticeable that there is still one molecular spectrum remaining. There is no evidence of this molecule overlapping with the Cu atomic absorption profile, so no further correction seems required. This finding explains why LSBC did not work properly because, as stated before, this correction model can be applied sequentially using one or more reference spectra, but not simultaneously.¹⁴ In the case of TAP, this molecule shows a low absorption that was below the threshold set to select transitions for the model, so it did not affect its application. Further work is in any case needed to explore the potential to correct from several spectral overlaps *via* TAP.

Therefore, using TAP correction for the three whole blood RMs, as DPSs, the results are in accordance with their reference values (considering the blood values as such), as can be seen in **Table 3**.

The results showed as “without correction” indicate the situation where no BC model was applied. It is interesting to note, however, that blank subtraction was carried out. Such blank (empty DPSs) includes already the Cu contamination and the molecular structures, so

its subtraction is a form of correction. Such form of crude correction works relatively well when the Cu level is much higher, but it does not work so well for lower levels. It is important to point out that even for proper blank correction the use of TAP is beneficial in this case, as it is the only way to get a reliable Cu-only signal from the blank.

Finally, it needs to be mentioned that this is a very complex sample in several ways. One is that the reference value corresponds to blood and not exactly to the plasma generated. In principle, literature points out to similar reference values for both whole blood and plasma Cu in humans.³⁴ It also needs to be considered that reconstituted blood RMs does not perfectly mimic real blood and the performance of the DPS device (with a simple membrane) may not be exactly the same as that of a centrifuge in a clinical lab, such that the term plasma may not be completely accurate. In fact, the color of the DPS generated is a bit reddish, which seems to indicate that some blood is present, and the resulting sample is thus even more similar to blood.

Again, a discussion of the clinical significance of the results is beyond the scope of the current work. However, for further analytical validation, acid digestion of DPSs produced with whole blood L-3 was performed, followed by ICP-MS analysis of the digests. The results for both Cu isotopes are shown in **Table 3**.

These values confirmed a good agreement between the blood reference value and the actual DPS result. A relatively high confidence interval is obtained, but this simply reflects the variations expected when submitting small (2.5 μ L) samples to the whole analytical procedure and proves that use of direct solid sampling actually can offer better precision by simplifying such procedure.

We believe this is a perfect example of how TAP can help to attain more accurate values in the case of a very complex, direct determination *via* HR CS GFAAS, neutralizing the overlap from an unknown molecule and making it feasible to properly correct for blank contamination.

4. Conclusions

While the benefits deriving from the use of LSBC for correcting spectral overlap in HR CS GFAAS are well-established, this approach is also hampered by some limitations. In principle, for such approach, one needs to know in advance the nature of the interfering

species. When the interference is unknown, the work required to try to find out the molecule giving rise to the overlap or to try to simulate the matrix is time-consuming, and there is no guarantee of a positive outcome. Therefore, a TAP model is proposed that offers an easier way to circumvent this problem. Using only the information within the measurement, a feasible strategy to correct for spectral interferences has been developed in this work.

There are currently some limitations to this approach. A complete overlap between the analyte signal and the interference cannot be corrected for (although the results for Cu prove that a very intense overlap can be corrected for efficiently), and the current model does not work for more than one interfering molecule (but the occurrence of a less intense and non-overlapping secondary molecular spectrum did not prevent the application of TAP for Cu determination in DPSs). Although the work is focused on “molecular interferences”, nothing precludes the use of the TAP approach to correct for the much rarer atomic interferences, providing there are more atomic lines of the interfering element within the same spectral window.

Overall, TAP is a new correction model for HR CS GFAAS (and it should work for other time-resolved techniques, such as electrothermal vaporization-ICP-OES, providing the spectra is acquired with sufficiently high-resolution) that can overcome spectral overlaps with no knowledge about the true nature of the interference, avoiding the use of further optimizations and enabling direct analysis of complex samples.

It can be mentioned that both approaches may be complementary: in a particular case both LSBC and TAP can be applied, and the spectra finally obtained evaluated to see which method offers a “cleaner” signal for the analyte.

Conflicts of interest

There are no conflicts of interest to declare.

Acknowledgements

The authors are grateful to the European Regional Development Fund for financial support through the Interreg POCTEFA EFA 176/16/DBS, as well as to project PGC2018-093753-B-I00 (MCIU/AEI//FEDER,UE) and the Aragon Government (Construyendo Europa desde Aragón, Grupo E43_20R).

5. References

- 1B. Welz and M. Sperling, *Atomic Absorption Spectrometry*, Wiley-VCH, Weinheim, 3rd edn., 1999.
- 2B. Welz, H. Becker-Ross, S. Florek and U. Heitmann, *High-Resolution Continuum Source AAS: The Better Way to Do Atomic Absorption Spectrometry*, Wiley-VCH, Weinheim, 2005.
- 3H. Becker-Ross, S. Florek and U. Heitmann, *J. Anal. At. Spectrom.*, 2000, **15**, 137–141.
- 4B. Welz, H. Becker-Ross, S. Florek, U. Heitmann and M. G. R. Vale, *J. Braz. Chem. Soc.*, 2003, **14**, 220–229.
- 5S. S. Fick, F. V. Nakadi, F. Fujiwara, P. Smichowski, M. G. R. Vale, B. Welz and J. B. de Andrade, *J. Anal. At. Spectrom.*, 2018, **33**, 593–602.
- 6Z. Kowalewska, *J. Anal. At. Spectrom.*, 2018, **33**, 260–273.
- 7Z. Kowalewska, J. Pilarczyk and Ł. Gościński, *Spectrochim. Acta Part B*, 2016, **120**, 45–56.
- 8J. L. Raposo, S. R. Oliveira, J. A. Gomes Neto, J. A. Nóbrega and B. T. Jones, *Anal. Lett.*, 2011, **44**, 2150–2161.
- 9J. L. Raposo, S. R. Oliveira, J. A. Nóbrega and J. A. Gomes Neto, *Spectrochim. Acta Part B*, 2008, **63**, 992–995.
- 10 O. Zvěřina, J. Kuta, P. Coufalík, P. Kosečková and J. Komárek, *Food Chem.*, 2019, **298**, 125084.
- 11 L. Husáková, I. Urbanová, M. Šafránková and T. Šídová, *Talanta*, 2017, **175**, 93–100.
- 12 M. Pozzatti, F. V. Nakadi, M. G. R. Vale and B. Welz, *Microchem. J.*, 2017, **133**, 162–167.
- 13 I. M. Dittert, D. L. G. Borges, B. Welz, A. J. Curtius and H. Becker-Ross, *Microchim. Acta*, 2009, **167**, 21–26.

- 14 R. G. O. Araujo, B. Welz, F. Vignola and H. Becker-Ross, *Talanta*, 2009, **80**, 846–852.
- 15 M. Fechetia, A. L. Tognon and M. A. M. S. da Veiga, *Spectrochim. Acta Part B*, 2012, **71–72**, 98–101.
- 16 B. Gómez-Nieto, M. J. Gissera, M. T. Sevilla and J. R. Procopio, *Talanta*, 2013, **116**, 860–865.
- 17 I. N. B. Castilho, É. R. Pereira, B. Welz, A. A. Shaltout, E. Carasek and I. B. Gonzaga Martens, *Anal. Methods*, 2014, **6**, 2870–2875.
- 18 A. R. Borges, E. M. Becker, L. L. François, A. de Jesus, M. G. R. Vale, B. Welz, M. B. Dessuy and J. B. de Andrade, *Spectrochim. Acta Part B*, 2014, **101**, 213–219.
- 19 R. M. de Andrade, J. S. de Gois, I. M. Toaldo, D. B. Batista, A. S. Luna and D. L. G. Borges, *Food Anal. Methods*, 2017, **10**, 1209–1215.
- 20 D. Bohrer, U. Heitmann, M. Huang, H. Becker-Ross, S. Florek, B. Welz and D. Bertagnolli, *Spectrochim. Acta Part B*, 2007, **62**, 1012–1018.
- 21 D. L. G. Borges, A. F. da Silva, B. Welz, A. J. Curtius and U. Heitmann, *J. Anal. At. Spectrom.*, 2006, **21**, 763.
- 22 B. Welz, M. G. R. Vale, M. M. Silva, H. Becker-Ross, M. Huang, S. Florek and U. Heitmann, *Spectrochim. Acta Part B*, 2002, **57**, 1043–1055.
- 23 M. B. Dessuy, M. G. R. Vale, F. G. Lepri, D. L. G. Borges, B. Welz, M. M. Silva and U. Heitmann, *Spectrochim. Acta Part B*, 2008, **63**, 337–348.
- 24 M. Resano, E. Mozas, C. Crespo, J. Briceño, J. del Campo Menoyo and M. A. Belarra, *J. Anal. At. Spectrom.*, 2010, **25**, 1864.
- 25 M. Resano, M. R. Flórez and E. García-Ruiz, *Anal. Bioanal. Chem.*, 2014, **406**, 2239–2259.
- 26 Z. Kowalewska, H. Laskowska and M. Gzylewski, *Spectrochim. Acta Part B*, 2017, **132**, 26–36.

- 27 M. Resano, E. García-Ruiz, M. Aramendía and M. A. Belarra, *J. Anal. At. Spectrom.*, 2019, **34**, 59–80.
- 28 M. Resano, M. Aramendía and M. A. Belarra, *J. Anal. At. Spectrom.*, 2014, **29**, 2229–2250.
- 29 R. W. B. Pearse and A. G. Gaydon, *The Identification of Molecular Spectra*, Chapman & Hall, London, 4th edn., 1976.
- 30 Noviplex, novilytic.com/noviplex, (accessed June 8, 2021).
- 31 P. J. Parsons, A. L. Galusha, Y. Cui, E. M. Faustman, J. C. Falman, J. D. Meeker and K. Kannan, *J. Anal. At. Spectrom.*, 2020, **35**, 2092–2112.
- 32 M. C. García Poyo, C. Pecheyran, L. Rello, E. Garcia Gonzalez, S. Alonso Rodríguez, F. V. Nakadi, M. Aramendía and M. Resano, *J. Anal. At. Spectrom.*, 2021, **36**, 1666–1677.
- 33 K. Koehler, E. Marks-Nelson, C. P. Braga, S. Beckford and J. Adamec, *Eur. J. Haematol.*, 2020, **104**, 554–561.
- 34 M. Krachler and K. J. Irgolic, *J. Trace Elem. Med. Biol.*, 1999, **13**, 157–169.

6. Supplementary information

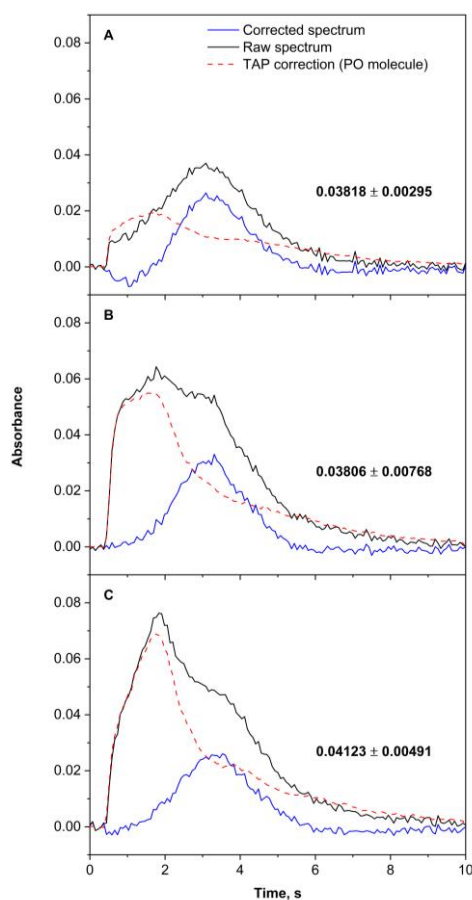


Figure S1. Time-resolved raw and corrected spectrum of 0.1 ng Pb at 217.000 nm (5 μ g Pd+0.5 μ g Mg) using TAP correction with P mass (as PO molecular interference) of (A) 10 μ g, (B) 50 μ g, and (C) 100 μ g. The value is the mean integrated absorbance of three measurements, and the uncertainty is the standard deviation.

Chapter 5

Laser ablation of microdroplets for copper isotopic analysis via MC-ICP-MS. Analysis of serum microsamples for the diagnosis and follow-up treatment of Wilson's disease.

Abstract

Cu isotopic analysis can provide valuable hindsight when investigating Wilson's disease (WD), but one of the problems related with this type of study is that usually low sample volumes are available and/or low Cu concentrations are found in these samples. This work presents a new approach for Cu isotope ratio determination that requires only 1 μL of pre-treated serum sample per replicate (after Cu separation and preconcentration to a Cu concentration range between 0.3 and 4 mg L^{-1}).

Cu determination was carried out by direct μ -injection of 1 μL of pretreated serum samples into an ICP-MS, offering a LOD of 3 $\mu\text{g L}^{-1}$. For Cu isotopic analysis, the method presented is based on micro-volume deposition on a pure silicon wafer and subsequent ablation analysis by fs-LA-MC-ICP-MS. Cu isotopic analysis of NIST 3114 at 1 mg L^{-1} Cu concentration with the self-bracketing method provided average $\delta^{65}\text{Cu}$ values of $-0.01 \pm 0.19\text{‰}$ (2SD) and for internal precision values of 517 ppm at 2SD.

This method was deployed for analysis of serum samples from WD patients under different treatments, as well as healthy newborns and patients with other liver disorders. The results seem to link decreased $\delta^{65}\text{Cu}$ values to Cu release from the liver, further demonstrating the interest of this type of analysis in the biomedical context.

1. Introduction

Copper (Cu) is an essential element for the body.¹⁻³ Cu is introduced in the human body through the diet. Most of Cu absorption occurs in the duodenum, the stomach and the proximal small intestine. Absorbed Cu is then secreted into the bloodstream and transported

to the liver together with albumin and the amino acid histidine. When Cu arrives to the liver, it is rapidly taken by the hepatocytes and bound to ceruloplasmin. This complex represents about 75-90% of total Cu content in blood. Of the total Cu absorbed by the body, only about 0.9 mg per day is needed while the rest is excreted, mostly through the bile.^{4,5}

Disorders in Cu metabolism may produce deficits or excesses of Cu in the body, which lead in turn to different health disorders (See Chapter 1).^{6,7} The examples of Cu related disorders due to low Cu levels in the body are Menkes disease (MD) or Occipital horn syndrome (a milder version of the same disease), while due to the accumulation of Cu in some tissues is Wilson's disease (WD).⁸ While Menkes disease does not have any treatment and is fatal, WD can be treated, hence it is important to continue research for improving both diagnosis and treatment follow up of this condition.

WD is a recessive genetic disease that is caused by mutations of the ATP7B gene that codifies the ATP7B protein. This mutation affects the transfer of Cu ions to the main plasma Cu protein (ceruloplasmin) and its release into the bloodstream, as well as the removal of excess Cu by secreting it into bile, and it results in a defective regulation of copper balance (positive balance).⁹ Treatment of WD is usually well tolerated and, if started early, can prevent the development of symptoms and irreversible consequences, especially hepatic and neurological, that can affect WD patients.^{10,11} As discussed in the Introduction, currently, there are two kinds of treatment: the use of chelators for increasing Cu excretion, for instance D-penicillamine (DPA) and Trientine (TETA), and the use of Zn salts (Zn) as Cu absorption blockers.¹² However, the main problem is to achieve early diagnosis of the disease before the onset of symptoms, in order to avoid irreversible damages and to reach better efficiencies for the therapeutic treatments.

WD diagnosis is not straightforward and is mostly carried out after the patient has developed symptoms of the disease, with the negative consequences that this entails. Besides the liver biopsy and detection of clear physical changes (e.g., Kayser-Fleischer rings) that usually lead to a WD diagnosis when symptoms are already severe, there are other less invasive methodologies that can be used for this purpose. While genetic analyses are possible, they are costly and difficult, because there are more than 500 mutations described for WD.¹³⁻¹⁵ As a consequence, WD diagnosis is normally based on blood analysis (for ceruloplasmin levels, total Cu concentration, transaminases, etc.) or urine analysis (for total Cu

concentration). Generally speaking, WD patients show decreased levels of serum total copper ($<1000 \mu\text{g L}^{-1}$) and ceruloplasmin ($<200 \text{mg L}^{-1}$) while at the same time increased levels of urinary copper ($>100 \mu\text{g}$ per 24 h).⁹ However, these determinations are often insufficient to diagnose or exclude WD due to false negative and positive tests.¹⁰ For example, overlapping intervals in total Cu concentration in serum have been observed between controls and WD patients, especially in newborns and infants due to the immaturity of their liver. Hence, it is important to research new non-invasive methods for the early diagnosis of WD, particularly in the field of pediatrics.^{16,17}

Currently, investigation of the isotopic analysis in biological samples is on the rise,^{18–22} and this parameter could add more information when monitoring Cu metabolism in WD patients, leading to the early diagnosis of this condition. As in all chemical reactions, isotopic fractionation may occur in bio-chemical processes, so one would expect that the protein ATP7B would not interact with the two existing Cu isotopes (^{63}Cu and ^{65}Cu) in exactly the same way. This would lead to different Cu isotopic ratios in biological fluids of healthy persons and WD patients, even if the differences are expected to be small. This kind of research could be useful for early diagnosis of WD, but also for following the evolution of a given treatment. In fact, studying isotopic differences in the biological fluids of patients undergoing different treatments (chelating agents or Zn) could shed light on their mechanism of action.

In this context, multicollector inductively coupled plasma mass spectrometry (MC-ICP-MS) is the preferred technique for investigating such isotopic variations.²³ In the case of WD, preliminary investigations have shown differences in the Cu isotopic composition in serum and urine between controls and WD patients.^{24,25} One of these studies developed a method for direct Cu isotopic analysis in urine samples deposited onto clinical filter papers using a femtosecond laser coupled to MC-ICP-MS.²⁵ The authors found that urine of untreated WD patients was depleted in ^{65}Cu compared to urine of control individuals. In another study,²⁴ the use of Cu isotopic analysis was investigated for the diagnosis of WD. A set of serum samples from patients with low Cu concentration (WD patients, patients who had a bariatric surgery and infants) were analyzed and compared with healthy patients (controls). This work found that the Cu isotopic pattern is fractionated toward the lighter isotope for WD patients and, to a lesser extent, for patients who had a bariatric surgery if compared to controls and infants. Results of these papers are only preliminary, as few cases are analyzed and differences in isotopic compositions do not seem to be sufficient to differentiate between WD and controls.

However, they show how the combination of isotopic composition with other parameters (such as total Cu concentration) could be useful for obtaining interesting information on the diagnosis and/or evolution of the disease, meriting further studies on the topic.

One of the problems associated with this type of studies is the small amount of sample available in some instances, such as studies with newborns or model rats, among other situations where just some μL can be obtained. Hence the importance of developing new sample introduction strategies capable of reaching accurate isotopic results when working with microsamples.

The aim of this work is the development and evaluation of a novel methodology for Cu isotopic determination in serum, with very low sample volume requirements. In particular, the method developed enables measurements to be carried out with a volume of only 1 μL of the pre-treated samples, with the final goal of addressing situations where only few μL of sample is available (1 μL was chosen because with standard laboratory pipettes, 0.5 – 1 μL is the minimum volume that can be taken accurately). For reaching this goal, an IR femtosecond (fs) laser was coupled to a MC-ICP-MS. This strategy combines the high precision of the MC-ICP-MS and the high sensitivity provided by the highly efficient fs-laser ablation (LA) device as sample introduction system to analyze microdroplets deposited onto a silicon wafer. The method proposed was used to evaluate the Cu isotopic composition of serum samples from WD patients without any treatment, WD patients treated with different drugs, newborns and patients with liver diseases different to WD.

2. Experimental

2.1 Instrumentation

Determination of Cu, Na and Mg levels was carried out with an ELAN DRC II quadrupole ICP-MS (Perkin Elmer, Waltham, USA). For the analyses requiring continuous sample introduction into the ICP-MS (in particular the resin efficiency tests), the conventional configuration using an autosampler and a peristaltic pump to deliver the sample to the nebulizer was used as the introduction system. For micro-analysis on the other hand, time resolved analysis (TRA) was used. In this case, 1 μL of pre-treated serum sample was manually introduced into the tube of the peristaltic pump, ID 0.25 mm x OD 2.07 mm (orange-blue), using an electronic-micropipette (Brand, Wertheim, Germany) (*cf.* section 2.4.1 for

details). In both cases, a PFA-ST MicroFlow Nebulizer (Elemental Scientific, Nebraska, USA) coupled to a twister cyclonic spray chamber (Glass expansion, Port Melbourne, Australia) was used.

A NexION 300X ICP-MS spectrometer (Perkin-Elmer, Waltham, USA) was also used for additional experiments.

Cu isotopic analyses were carried out using a Nu Plasma HR MC-ICP-MS instrument (from Nu instruments, Wrexham, UK). Sample introduction was carried out with a femtosecond laser ablation system ALFAMET (Nexeya, France). This laser is fitted with a diode-pumped KGW-Yb crystal laser source delivering 360 femtosecond pulses at 1030 nm. The laser source operates at high repetition rates with energy per pulse ranging from 0.85 mJ/pulse @ 1 kHz to 0.028 mJ/pulse @ 100 kHz. In order to enable the fast movement (up to 280 mm s⁻¹) and the high precision positioning ($\pm 1 \mu\text{m}$) of the laser beam, the laser is fitted with a galvanometric scanning module. Moreover, it is possible to synchronize the movement of the laser beam with the movement of the sample due to the monitoring of the XY stage of the ablation cell, such that complex trajectories can be carried out.^{26,27} The fs-LA unit was coupled to the MC-ICP-MS using a 2 m PFA tube (1.6 mm internal diameter) directly inserted into the torch injector. The torch used was a two-inlet torch (Nu instruments, Wrexham, UK), the first inlet for the laser and the second for the make-up gas (Ar). Helium was used as carrier gas to provide smaller particles for the ablated material and minimize particle redeposition onto the ablated surface.²⁸

The routine trinocular microscope ZEISS Primo Star 1000X (Zeiss, Zurich, Switzerland) was used to produce the pictures after ablation of the Si wafers. For sample digestion, an ULTRAWAVE microwave system (Milestone Inc., Shelton, USA) was used. An EVAPOCLEAN® unit (Analab, Bischheim, France) was deployed to evaporate samples by sub-boiling in a close environment.

2.2 Standards and reagents

For quantitative analyses, a multielemental solution of appropriate concentration was prepared from 1 g L⁻¹ Cu, Na and Mg single-element standards (SCP SCIENCE, Villebon-sur-Yvette, France) by dilution with 2% v v⁻¹ HNO₃. For this purpose, Instra grade HNO₃ 70% v v⁻¹ was purchased from JT Baker (New Jersey, USA) and further purified by sub-boiling in

a PFA system (DST 1000, Savilex), while ultrapure water (18.2 MΩ cm) was obtained from a Direct-Q3 system (Millipore, Molsheim, France).

For Cu isotopic analysis with the fs-LA-MC-ICP-MS configuration, the NIST 610 reference material was selected for system optimization. Si wafers (Type 3") used for standard and sample deposition were acquired from Eloïse Electron Optics Instruments Service (Tremblay, France). They were cut in a rectangle shape with a diamond pencil in order to fit it in the ablation cell. For mass bias correction, NIST SRM 3114 was chosen as a reference in the bracketing sequence (NIST, Gaithersburg, MD, USA). This standard has a similar composition to the NIST 976, which is currently out of stock.²⁹

Clincheck® (Lot: 1497) serum level I and II (Recipe Chemical, Munich, Germany) were used to validate the whole analytical procedure (digestion, Cu isolation and dilution). These reference materials were reconstituted with 3 mL of ultrapure water, according to the manufacturer's instructions.

For Cu isolation, Cu specific resin (Triskem, Bruz, France) was used.

2.3 Samples and sample preparation

Serum samples from 31 volunteers were obtained from the Hospital Universitario Miguel Servet (Zaragoza, Spain) and from the Centre Hospitalier Universitaire D'Angers (France). Twelve of these samples originated from Angers. Seven of these samples were obtained from patients affected by WD and following a chelating treatment (DPA or TETA), while the remaining five samples were obtained from patients with hepatic disorders other than WD. The rest of the samples (19) originated from Zaragoza. Eight of them belonged to WD patients: six treated with an inhibiting absorption treatment (Zn), one treated with a chelating treatment (TETA) plus an inhibiting absorption treatment (Zn), and one collected at the moment of diagnosis (without any treatment). The remaining eleven samples were obtained from healthy newborns (0 days until 3 months). The principles outlined in the declaration of Helsinki regarding all the experimental research involving humans or animals were followed.

For controlling sample contamination, all the sample preparation steps (digestion, isolation and dilution procedures) were done in an ISO 5 laminar bench flow fitted in an ISO 7 clean lab. Sample preparation started by sample digestion in a microwave oven. First, 0.2 - 0.5 mL of sample (depending on the total amount of sample available or the concentration, in the

case of the reference materials) were mixed with 3 mL of 14 M HNO₃ in quartz vials and were subjected to the program recommended by the manufacturer (for blood). The digest was subsequently transferred to Teflon Savillex® beakers and was evaporated to almost dryness at 95 °C using the EVAPOCLEAN® system. It has to be clarified at this point that this volume of sample was processed to be able to carry out the experiments presented in this work as well as other experiments intended for different publications. However, this does not mean that such a volume is needed for analysis. In fact, and as discussed in the results section, results shown in this work could be obtained with a minimum amount of sample ranging from 2 to 15 µL, depending on the total Cu concentration.

After sample digestion and evaporation, Cu isolation was carried out using a Triskem Cu specific resin as proposed by K. A. Miller et al.³⁰⁻³² In order to assess the Cu isolation effectiveness and to study the possibilities for sample preconcentration, the protocol was tested with two serum reference materials (Clincheck serum L-1 and L-2). For this purpose, the reference materials were redissolved in 500 µL of concentrated HCl and heated at 120 °C in a closed Teflon Savillex® vial for 24 h, to ensure that Cu is in its chloride form. The digest was then evaporated to almost dryness in the EVAPOCLEAN® system and redissolved in 4 mL of 5 mM HCl. This process was repeated twice before injection into the chromatographic column. Bio-Rad Poly-Prep columns were filled with 0.5 mL of Triskem Cu specific resin and a piece of cotton was used as a stopper on top of the resin bed. As recommended by the manufacturer, the resin was soaked in 20% v v⁻¹ EtOH/water overnight before introducing it into the columns. The isolation protocol is summarized in **Table 1**. The Cu fraction finally obtained was evaporated to almost dryness at 95 °C in an EVAPOCLEAN® system. For determination of the resin efficiency the evaporated Cu fraction was redissolved in 10 mL of 2% v v⁻¹ HNO₃. For the study on sample preconcentration, on the other hand, the Cu fraction was redissolved in 100, 50 and 25 µL of 2% v v⁻¹ HNO₃ and spiked with Ni at a final concentration of 50 µg L⁻¹.

Table 1. Protocol for the Cu isolation with the anion exchange chromatography Cu specific resin (Triskem)

Step	Volume (mL)	Medium
Resin loading	0.5	Cu-specific
Cleaning	10	6 M HCl
Conditioning	10	5 mM HCl
Sample load	4	5 mM HCl
Matrix elution	40	5 mM HCl
Cu elution	10	6 M HCl

Cu isolation in real samples was carried out in the same manner as for the reference materials. The only difference was that the Cu fraction was redissolved in 50 μL of 2% v v⁻¹ HNO₃ and spiked with Ni at a final concentration of 50 $\mu\text{g L}^{-1}$, in order to reach a pre-concentration factor ranging between 3 - 10 depending on the sample volume available. This fraction was used for total Cu analysis and for Cu isotopic analysis.

Before isotopic analysis, samples were divided into 4 groups, depending on the total Cu concentration. For the samples in each of these groups, and in order to avoid an additional source of mass bias, the Cu concentration was adjusted with 2% HNO₃ v v⁻¹ to 0.3, 0.5, 1 and 4 mg L⁻¹, respectively, matching those of the standards used for bracketing. It could also be noted that all samples and standards were spiked with 5 mg L⁻¹ Ni, in an attempt to use its signal for internal standardization. However, Ni signals were too low and internal standardization did not improve the results, and therefore such approach was discarded.

For fs-LA-MC-ICP-MS analysis, 1 μL of the pretreated sample was deposited onto Si wafers. These wafers were pre-ablated with the laser to create a circular mini-well of 1.8 mm diameter, following the same trajectories later used for sample ablation. After that, the Si wafer was warmed at 80 °C to prevent any movement of the deposited droplet along the wafer. The deposition of 1 μL of sample was carried out in two steps. First, 0.5 μL of sample were deposited and, once dry, the remaining 0.5 μL were deposited and dry. The double

deposition allows for having a higher Cu concentration, improving the homogeneity of the distribution as well. More details on this protocol are provided in section 3.3.1.

2.4 Measurement protocol

2.4.1. Determination of total Cu

For validating the protocol used for Cu isolation, Cu determination was carried out in continuous mode with the ELAN DRC II ICP-MS. Quantitative results were obtained after measuring a Cu + Na + Mg calibration curve between 10 and 150 $\mu\text{g L}^{-1}$ for each element.

For total Cu determination in real serum samples, time resolved analysis (TRA) after direct injection of 1 μL of sample into the ICP-MS introduction system was deployed. For allowing introduction of microvolumes (down to 1 μL) in the ELAN DRC II instrument, the following protocol was used (a visual schematics is shown in **Figure S1** included in supplementary information). First, a PFA-ST MicroFlow Nebulizer with a capillary sampling tube of 0.25 mm internal diameter (ID) was selected for analysis. This capillary was connected to a peristaltic pump tubing (orange-blue tube, ID 0.25 mm x OD 2.07 mm), connected to an additional capillary tube of 0.25 mm ID in the other extreme (external capillary). A flow rate of 0.1 mL min^{-1} was selected for the work. During the analysis, the external capillary tube was introduced into a 2% v v⁻¹ HNO_3 solution (blank solution), which was continuously aspirated. At the moment of sample introduction, the external capillary tube was disconnected from the peristaltic pump tubing, thus stopping the aspiration of HNO_3 solution for a few seconds. Afterwards, 1 μL of sample was directly introduced into the peristaltic pump tubing with an electronic micropipette. It was necessary to wait for a few seconds before re-connecting the tubes again and re-establishing the aspiration of the HNO_3 solution in order to have a well-defined peak, as a second peak appeared due to rinsing of the tubing, as shown in **Figure 1**. As seen from this figure, small variations on the peak shape and magnitude were obtained with this manual introduction system. To compensate for this effect, the use of an adequate internal standard (IS) seems compulsory. In this case, Ni was used as IS at a concentration of 50 $\mu\text{g L}^{-1}$. For quantitative results to be obtained, a Cu calibration curve between 0.1 and 20 mg L^{-1} was measured, and 50 $\mu\text{g L}^{-1}$ of Ni was used as IS. Peak area was considered for data treatment and five replicates per sample were carried out.

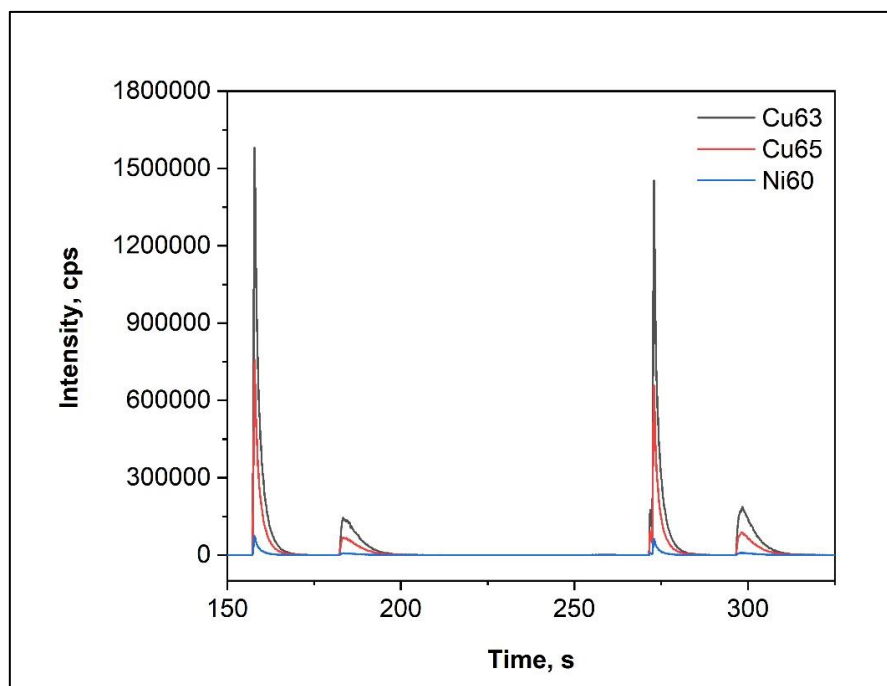


Figure 1. Example of two transient signals obtained with two consecutive injections of 1 μL of a solution containing 1 mg L^{-1} Cu and 50 $\mu\text{g L}^{-1}$ Ni at a flow rate of 100 $\mu\text{L min}^{-1}$. Conditions shown in **Table 2** for TRA analysis were used. The first peak corresponds to the 1 μL droplet introduction in the ICP-MS. The second peak corresponds to the rinsing of the tubing after the 2% v/v HNO_3 solution is reconnected to the peristaltic tube.

The instrument and data acquisition parameters finally used are gathered in **Table 2**. Use of the IS visibly improves both the precision and the linearity of the calibration curves for Cu, as shown in **Figure S2** (supplementary information). Under these conditions, the LOD and the LOQ were calculated as 3 and 10 times the SD of 10 blanks (IS corrected) and divided by the slope (calculated using the peak heights). With this method, the LOD and the LOQ were calculated to be 3 and 10 $\mu\text{g L}^{-1}$, respectively.

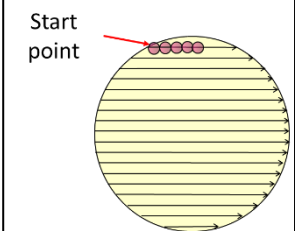
Table 2. ICP-MS Spectrometer setting and data acquisition parameters for the determination of total Cu in blood samples.

	Continuous Analysis	Time Resolved Analysis with 1 μL sample
Sample uptake rate ($\mu\text{L min}^{-1}$)	850	100
Nebulizer gas, Ar (L min^{-1})	0.82	0.95
Plasma gas, Ar (L min^{-1})	17	17
Auxiliary gas, Ar (L min^{-1})	1	1
RF power (W)	1000	1000
Dwell time (ms)	50	10
Signal acquisition	Continuous	TRA
Isotopes monitored	$^{23}\text{Na}, ^{24}\text{Mg},$ $^{60}\text{Ni}, ^{63}\text{Cu}, ^{65}\text{Cu}, ^{66}\text{Zn},$	$^{60}\text{Ni}, ^{63}\text{Cu}, ^{65}\text{Cu}$

2.4.2 Determination of Cu isotope ratios

Optimization of the fs-LA-MC-ICP-MS acquisition parameters was carried out aiming at maximum sensitivity and stability for the Cu signal while ablating the NIST 610 reference material. Considering that Cu was isolated from the samples before analysis, the mass spectrometer was operated at low resolution in order to maximize sensitivity. The fs-LA parameters used for sample ablation were optimized in order to be as close as possible to the ablation threshold, although making sure that the sample was completely ablated. More details on these optimizations are provided on section 3.3.2. The instrument settings and data acquisition parameters finally used are shown in **Table 3**.

Table 3. Instrumental conditions for Cu isotopic analysis of serum using fs-LA-MC-ICP-MS.

Laser ablation conditions															
Laser ablation system								ALFAMET							
Wavelength (nm)								1030							
Pulse duration (fs)								360							
Repetition rate (Hz)								6000							
Spot diameter (μm)								9							
Energy ($\mu\text{J}/\text{pulse}$) /Fluence (J/cm^2)								0.45/ 0.7							
Scan speed (mm s^{-1})								30							
Ablation strategy								<p style="text-align: center;">Scan Disk</p>  <p style="text-align: center;">(D=1.8mm, space between lines $5\mu\text{m}$)</p>							
Transport gas / Flow rate (mL min^{-1})								He / 493							
Nu MC-ICP-MS															
RF Power (W)								1300							
Instrument resolution								Low							
Integration time (s)								0.5							
Nebuliser Pressure (Psi)								0							
Mix gas (Make up) (L min^{-1})*								1.02							
Auxiliary gas (L min^{-1})								0.80							
Coolant gas (L min^{-1})								13							
Faraday cup configuration															
Collector	H7	H6	H5	H4	H3	H2	H1	Ax	L1	L2	IC0	L3	IC1	IC2	L4
m/z	65					63			62			61			

Ablation of the samples was carried out after deposition on Si wafers, as explained in section 2.3. The ablation strategy deployed (so-called Scan disk) consisted on covering the area of a 1.8 mm diameter circle with individual laser spots separated by $5\mu\text{m}$ both horizontally and vertically. To get this separation the trajectory of the laser over the samples followed

horizontal lines, working at a repetition rate of 6 kHz and moving at a speed of 30 mm s⁻¹. The space between lines, on the other hand, was fixed at 5 µm and the fluence was fixed at 0.7 J cm⁻². This ablation strategy was completed in approximately 20 seconds. Five replicate measurements were carried out per sample following the standard-sample-standard bracketing sequence using the NIST 3114 as standard. Isotope ratio calculations were done using the point by point method (PBP) on the stable part of the signal, as explained in detail in section 3.3.3. This method is based on the calculation of the isotope ratio for every measurement by averaging the ratios calculated for each acquired point over a given time interval (typically 10-40 points).³³

In addition, a method for correcting time lags between detectors was used (Time Drift Correction, TDC). The method applied (described by F. Claverie et al.³⁴) uses VBA data processing and is based on the synchronization of the two isotope signals. The coefficient of determination of the linear fit between the two isotopes (ideally R²=1) was selected as the best criterion to obtain accurate detector time lag.

Finally, the results were expressed as delta values (δ),³⁵ i.e., as a relative difference (in per mil) versus a reference (NIST 3114) following equation (1):

$$\delta^{65}\text{Cu} (\text{‰}) = \frac{R_{\text{sample}} - R_{\text{STD}}}{R_{\text{STD}}} \times 1000 \quad (1)$$

Where R_{sample} is the ⁶⁵Cu/⁶³Cu isotope ratio determined for a given sample and R_{STD} is the average ⁶⁵Cu/⁶³Cu isotope ratio determined for the standards measured before and after that particular sample.

3. Results and discussion

3.1 Sample preparation

3.1.1. Cu isolation

Careful sample preparation prior to Cu isotopic analysis is almost mandatory in order to completely isolate Cu from other concomitant ions, thus minimizing both the mass bias³⁵ due to the space charge effect,³⁶ and spectral interferences. In this regard, both Cu isotopes suffer from potential spectral overlap in the ICP-MS. The most serious problem is due to the presence of high levels of Na in serum samples (around 3000 mg L⁻¹) leading to substantial

$^{40}\text{Ar}^{23}\text{Na}^+$ formation in the plasma that interferes with $^{63}\text{Cu}^+$. Likewise, but less important, the presence of Mg (around 20 mg L^{-1} in serum) can give rise to $^{40}\text{Ar}^{25}\text{Mg}^+$ overlapping with $^{65}\text{Cu}^+$.

For achieving Cu isolation, ion-exchange resins are usually deployed, being the AG-MP1 the most commonly used resin. However, in this work, a different resin was tested: a Cu specific resin from Triskem. A comparison on the performance of these two resins for Cu isolation in blood samples (for which reference values on all analytes of interest were available) was conducted, and results are included in the electronic supplementary information. In fact, it was observed that with the Cu-specific resin only one separation step seems to be required to lower the amount of Na remaining in the eluate below 99.9% of the original concentration, in blood while with the AG-MP1 resin, two consecutive separation steps are needed for this purpose.^{37,38} As a result, the Cu-specific resin from Triskem was used for further analysis.

The method used with the Cu specific resin was validated with a serum reference material (Clincheck® (Lot: 1497) serum level I) for total Cu recovery (thus ensuring the absence of isotope fractionation) and for the percentage of Na and Mg removal. Five 0.5 mL aliquots of the reference material were subjected to the digestion and separation protocol described in Section 2.3. The percentage of Cu recovered obtained was $100 \pm 3\%$, which excludes the possibility of on-column Cu fractionation. With this protocol, on the other hand, an average procedure blank of 0.43 ng Cu was obtained.

The percentage of Na removal obtained was typically 99.99% or higher, which is acceptable in our case. As demonstrated in K.A Miller's PhD thesis, Cu isotopic ratios measured by MC-ICP-MS in low resolution mode are slightly affected when the Na/Cu concentration ratio is higher than 1, while they are significantly affected when the Na/Cu concentration ratio is 10 or greater.³⁰ Typical Na concentration in serum samples shows maximum values of about 3000 mg L^{-1} . As a result, and considering the percentage of Na removal determined for the isolation protocol based on the Triskem resin, the maximum amount of Na left in the Cu fraction would be lower than $300\text{ }\mu\text{g L}^{-1}$ (referred to the original sample volume). Cu levels in serum samples, on the other hand, contain around $1000\text{ }\mu\text{g L}^{-1}$ for healthy adult individuals, while for WD patients and newborns these values are usually around $300\text{ }\mu\text{g L}^{-1}$. As a result, the Na/Cu concentration ratio on the samples finally analyzed are always lower than or around 1, well within the zone where the ratio is practically unaffected by Na interferences.

As for Mg, the percentage removal obtained was typically 99.9%, which is also acceptable in our case. Detailed analytical results are provided in **Table S1** (supplementary information).

3.1.2 Preconcentration and volume of sample needed for analysis.

One of the problems with the isotopic analysis of Cu in serum samples from newborns and WD patients is the low concentration of Cu present in these samples. In fact, the Cu concentration usually found in samples for these individuals is below $700 \mu\text{g L}^{-1}$,²⁴ and much lower in many cases, as shown in section 3.2. for the samples analyzed in this work. The problem is aggravated when only some microliters of sample are available, which might occur in some instances (e.g., newborns). As a result, sample preconcentration and the possibility to perform the analytical measurements with low volumes are valuable tools for reaching a sufficiently high Cu concentration in the fractions ultimately measured, thus ensuring the best precision for isotopic analysis by MC-ICP-MS.

In this part of the work, the maximum preconcentration factor admissible for the analysis of the serum samples was studied. First, different aliquots of 0.5 mL of the reference material Clincheck Serum L-2 were subjected to the Cu isolation protocol described in section 2.3 (Triskem resin). Cu fractions thus obtained were evaporated and redissolved at room temperature in different solvent volumes and were finally tested for total Cu recovery. As shown in **Table 4**, all redissolution volumes tested yielded Cu values within the reference concentration range ($1.15 - 1.56 \text{ mg L}^{-1}$). However, redissolution volumes greater than or equal to $50 \mu\text{L}$ systematically result in values that are in better agreement with the average concentration of the reference value. This apparent recovery improvement is likely related to the leaching efficiency of a small volume of acid solution in the bottom of the Savillex tube. For the sake of simplicity and considering that the methods developed require only $1 \mu\text{L}$ per measurement, all samples were redissolved in $50 \mu\text{L}$. With this redissolution volume preconcentration factors between 3 and 10 were obtained (depending on the existing total sample volume), while sufficient volume was available for performing several replicates for both the total Cu and the Cu isotopic analysis. In any case, if sample availability and/or sample Cu concentration makes it advisable, smaller volumes could be considered by improving the solution leaching conditions (temperature, movement of the leaching solution in the bottom of the Savillex tube, etc). More details on minimum Cu concentration needed for obtaining adequate measurement precision will be discussed in section 3.4.

Table 4. Cu concentration obtained after Cu separation step in serum using Cu-specific resin (Triskem) and redissolution in 3 different volumes.

Redissolution volume (μL)	Concentration (g L^{-1}) Mean. ($\bar{x} \pm U$) n=3	Reference Concentration (g L^{-1}) ($\bar{x} \pm U$)
100	1.36 ± 0.05	1.36 ± 0.20
50	1.37 ± 0.01	
25	1.21 ± 0.08	

Where $U = (t_s) / \sqrt{n}$; for a 95% confidence interval.

3.2 Results for Cu concentration in the serum samples

Cu concentration levels found for WD patients, regardless of the treatment they follow, fall between 45 and $211 \mu\text{g L}^{-1}$, with the exception of one patient who showed a Cu concentration of 999 and $932 \mu\text{g L}^{-1}$ (sampling the serum at two different moments). These results will be further explained in section 3.5. For the newborns and infants, the Cu concentration was found to be between 43 and $1021 \mu\text{g L}^{-1}$. Patients with liver disorders (excluding WD) are in the range between 734 and $1578 \mu\text{g L}^{-1}$. According with the results obtained, there is overlapping between WD patients and healthy newborns, in agreement with reported observation elsewhere.²⁴ This further confirms that determination of total Cu does not suffice to properly diagnose WD.

3.3 Analysis with fs-LA-MC-ICP-MS

It has been demonstrated that the variation of concentration in samples and standards used for the bracketing correction in isotopic analysis can result in additional instrumental mass bias impacting the measured isotope ratios.³⁹ For the preconcentrated samples analyzed in this study, there is a wide range of Cu concentration values (between 0.3 and 15mg L^{-1}). Thus, to compensate for this fact, the samples were divided into four groups before isotopic analysis and their concentrations were adjusted to four different values (0.3 , 0.5 , 1 and 4mg L^{-1} , respectively) in order to match concentrations of the standards used for bracketing correction in each group.

3.3.1 Optimization of sample preparation for LA analysis

The approach for LA analysis was based on the deposition 1 μL of the pretreated samples onto an adequate support for ablation. The material chosen for the deposition was an ultrapure silicon wafer generally used for the fabrication of micro-chips.

The optimization of sample deposition was carried out in order to achieve a signal with good sensitivity and stability. Details of the different problems during the drying of the droplet are provided as Supplementary Information. Finally, before sample deposition, circular mini-wells of 1.8 mm diameter were engraved on the Si wafers, following the same ablation strategy used for the samples (cf. section 3.3.2).

The first question considered was optimization of the separation between laser spots (9 μm diameter) on the wafer with the final goal of having the laser spots as close as possible to each other but without much overlapping in order to obtain uniform ablated area, avoid excessive drilling and minimize the time of machining. This separation depends on the laser repetition rate, separation between lines of spots and translation speed of the laser beam. As a starting point, 20 kHz were chosen as repetition rate and two translation speeds, 200 and 100 mm s^{-1} , were tested. The speed of 200 mm s^{-1} combined with 20 kHz repetition rate provided a 10 μm separation between spots within one horizontal line, so that an ablation space between lines of 10 μm was also programmed thus providing a 10 μm separation between spots both lengthwise and crosswise. For 100 mm s^{-1} combined with 20 kHz repetition rate, on the other hand, 5 μm horizontal separation between the spots was obtained, and 5 μm separation between lines was consequently selected for matching horizontal and vertical separation. In **Figure 2**, optic microscope images of the ablated circles obtained with these two sets of conditions are shown. As seen from **Figure 2**, ablation of the sample is more homogeneous with 5 μm separation between spots and these were the conditions selected for further tests. The wafers were subsequently pre-heated at 80°C before deposition of the droplets.

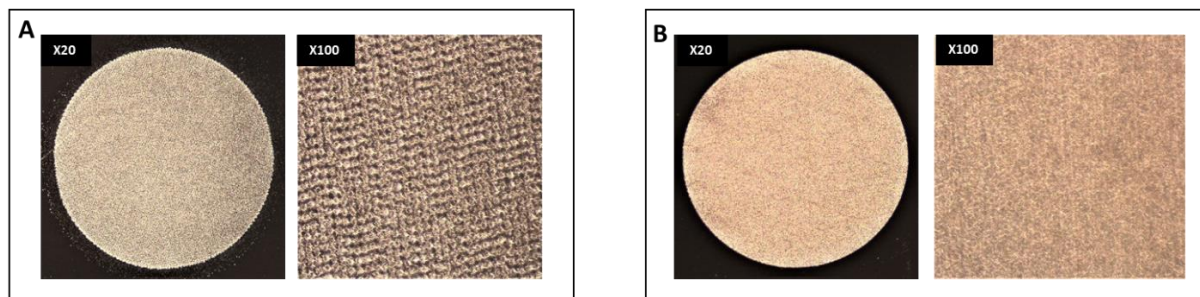


Figure 2. Optic microscope images of the Si wafers after ablation. A) Ablation with a space between spots of 10 μm (20 kHz, 200 mm s^{-1}) and B) ablation with a space between spots of 5 μm (20 kHz, 100 mm s^{-1}).

With this surface micro-structuration (spots spaced by 5 μm in X and Y directions), any movement of the droplet along the wafer was prevented. The size of these wells is appropriate for a droplet size of 0.5 μL , so that deposition of 1 μL of sample was carried out in two sequential steps to keep the samples within the limits of the pre-ablated wells. First, 0.5 μL of sample were deposited on the support and, once dry, the remaining 0.5 μL were deposited and let dry. This strategy improved deposit homogeneity and sensitivity since the 1 μL sample was spread over an area of 2.5 mm^2 compared to 7 mm^2 for a 3 mm circular drop. It also provided signals of adequate duration, and greatly facilitated the process of sample location and focusing for ablation, so that it was finally selected for sample analysis.

To assess the Cu (isotopic) distribution after drying of the droplet, images for both isotopes were obtained using fs-LA-MC-ICP-MS. For achieving good sensitivity for the images, a 100 mg L^{-1} Cu solution (NIST 3114) was deposited following the protocol described above. The fs-LA parameters used for acquiring the images were: 10 Hz repetition rate, 24 $\mu\text{m s}^{-1}$ translation speed, 7 μJ laser energy, while 0.5 s were selected as integration time in the MC-ICP-MS. The images are shown in **Figure 3**. As seen from **Figures 3B** and **3C**, an increased concentration of Cu is found in the perimeter of the dried droplet. This effect is typical for liquid droplets evaporating in solid surfaces, and it has been called “coffee ring effect” or “volcano effect”^{40–44} Using the image J software, the surface calculation of this coffee ring shows that 90% of the copper is concentrated in this zone. Although isotopic composition seems to be homogeneous along the droplet as shown in **Figure 3A**, it is important to design sampling strategies for achieving ablation of the whole sample, thus minimizing the possibility for fractionation.

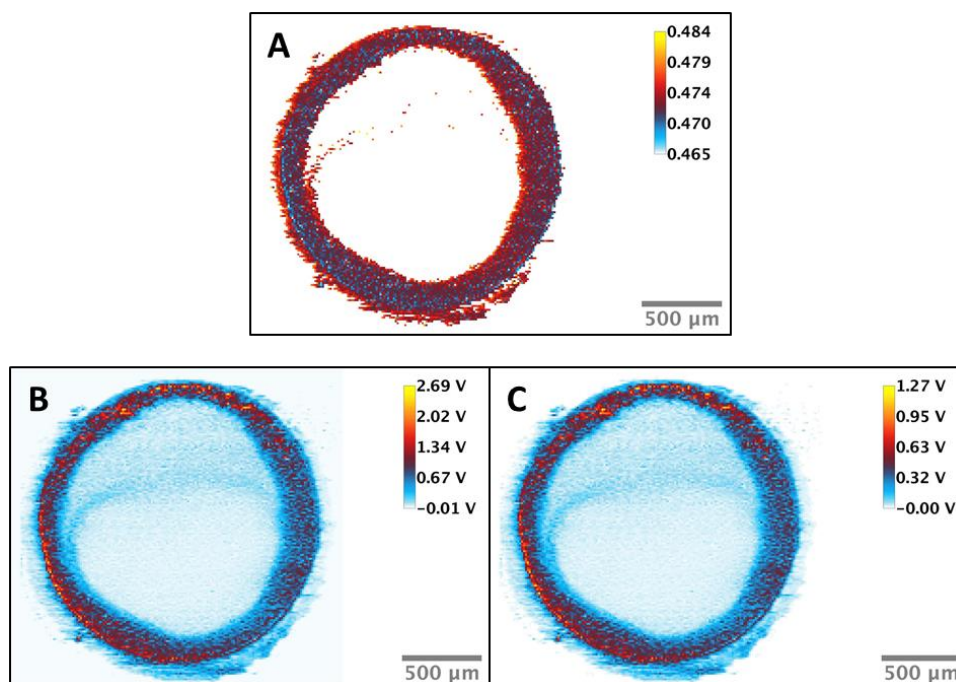


Figure 3. fs-LA-MC-ICP-MS image of 100 ng of Cu (double deposition of 0.5 μL of 100 mg L^{-1} onto pre ablated Si wafer heated at 80°C. A) Image of the uncorrected isotopic composition ($^{65}\text{Cu}/^{63}\text{Cu}$) B) Image of ^{63}Cu signal intensity and C) Image of ^{65}Cu signal intensity.

3.3.2 Optimization of LA-MC-ICP-MS instrumental parameters

The benefits of fs over ns lasers are already well-established,⁴⁵ typically providing improved precision and accuracy for isotopic analysis.⁴⁶ The system used here departs from conventional fs lasers as it can be operated at very high repetition rates and the laser beam can move at high speed due to a 2D scanner, allowing for great flexibility to ablate any area of any shape in a short time. In this case, an ablation pattern based on parallel lines of spots following the circular shape of the dried sample droplets was designed. As explained in detail in section 3.3.1, each laser spot was 9 μm diameter, spots were spaced by 5 μm in X and Y directions, while covering a total surface of 2.5 mm^2 .

The selection of the laser parameters to obtain signals of adequate intensity and duration was considered next. Regarding laser energy, and in order to limit matrix co-ablation, thus preventing the introduction of large amounts of silicon into the plasma, the laser was operated at a very low energy, 0.45 $\mu\text{J}/\text{pulse}$, trying to be as close to the ablation threshold as possible,

while still making sure that all the Cu is removed quantitatively from the silicon wafer. This energy corresponded to a fluence of 0.7 J cm^{-2} .

As for laser repetition rate and translation speed, it was observed that working at 20 kHz and 100 mm s^{-1} provided intense but too short sample signals (around 6 s) as to obtain stable isotope ratios. Thus, the parameters were readjusted, keeping the same fluence, in order to have longer signals and more stable ratios, even at the cost of losing some sensitivity. To keep the separation between spots at $5 \mu\text{m}$, the optimized repetition rate and the translation speed were decreased by the same factor, and best results were obtained when a repetition rate of 6 kHz and a speed of 30 mm s^{-1} were used. **Figure 4** shows a typical signal obtained under these conditions. As seen from this figure, the duration of the transient signal was around 20 s and the isotope ratios seemed stable, particularly in the central part of the signal. Considering signal intensity, acceptable values were obtained for the samples of lower concentration (0.3 mg L^{-1}), while Faraday cups of the MC-ICP-MS instrument were not saturated for samples of higher concentration (4 mg L^{-1}). Although signal intensity and shape depend on the particular sample ablated (shape of the droplet and sample concentration), typically higher intensities are obtained at the beginning and at the end of the transient signals. This is due to the type of ablation strategy deployed (scan disk, see **Table 3**) combined to the increased Cu concentration in the droplet perimeter (coffee-ring effect) explained in section 3.3.1.⁴⁰ In fact, when using the scan disk ablation strategy the first and last lines ablated correspond mostly to the droplet perimeter where Cu is concentrated, while the intermediate lines cover mostly the central part of the droplet.

Due to the particular MC-ICP-MS configuration used for analysis, only the Faraday cups (and not the ion multipliers) could be used for the simultaneous monitoring of m/z 63 and 65, which limited the sensitivity available. For this reason, and even if the MC-ICP-MS instrument can operate in pseudo-high resolution mode, all analysis were carried out in low resolution mode, in order to avoid any further sensitivity reduction. Besides, and as explained in detail in section 3.1.1, spectral overlaps were already minimized by sample purification. The integration time was chosen to be 0.5 s, as it was the minimum time necessary to obtain a good precision (below 0.2 - 0.1‰ (2SD) working with liquid sample introduction in continuous nebulization mode).

3.3.3 Calculating the isotope ratio

For calculation of isotope ratios, two different approaches were tested. First, the Linear Regression Slope (LRS) (originally proposed by Fietzke,^{47,48} and adapted for gas chromatography by Epov et al.⁴⁹) approach was investigated. However, precision for the isotope ratios obtained with this method was poor, maybe due to the kind of non-Gaussian signals obtained with the LA system shown in **Figure 4**, which are not well suited for LRS methodology. Consequently, data were finally processed using the traditional point-by-point method (PBP)³³ on the central part of the signal. This method calculates the $^{65}\text{Cu}/^{63}\text{Cu}$ ratios using the analyte signals (blank corrected) for each measured point to calculate the ratio per point (1 point every 0.5 s), and the $^{65}\text{Cu}/^{63}\text{Cu}$ ratio is estimated as the average of the ratios obtained for the complete signal. This method works better for signals with a steady part where integration limits are set, and hence entails some uncertainty derived from the fact that these limits are set arbitrarily. Integration limits were set manually, by visually selecting the stable part of the signal, which obviously entailed some additional source of uncertainty.

Data were also corrected for the effect of the different detector time responses (TDC) using VBA data processing as proposed by Claverie et al.³⁴. This method is based on the synchronization of the two isotope signals. The coefficient of determination of the linear fit between the two isotopes (ideally $R^2=1$) was selected as the best criterion to obtain accurate detector time lag.

An example of the results before and after TDC correction is shown in **Figures 4A** and **4B**, respectively. As can be observed in **Figure 4A** the ratios tend to go up along the peak. In **Figure 4B**, after the TDC correction, this effect is mostly eliminated. As a result, the internal precision after TDC is improved significantly. For the example shown in **Figure 4**, the internal precision improves by a factor 2 after TDC, although this improvement depends on the peak. Improvements ranging between 2 and 4 times were obtained for the samples analyzed in this work.

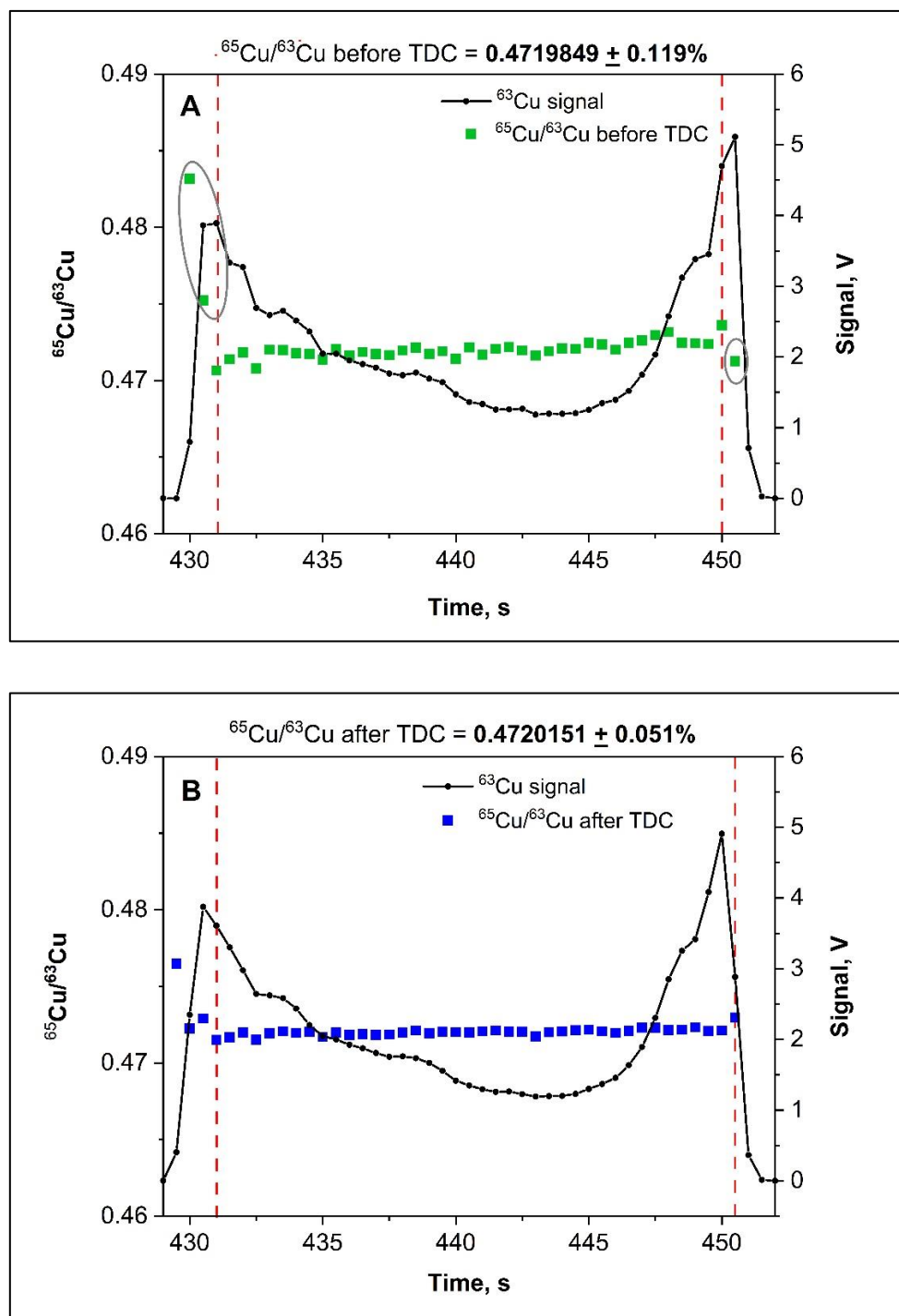


Figure 4. Example of transient signal obtained for ablation of 1 μL of a Cu standard solution of 4 mg L^{-1} (4 ng of Cu) deposited onto a silicon wafer and using the conditions described in section 3.3.2. A) before time drift correction and B) after time drift correction. The signal profile is represented by the black points, while the red bars represent the integration limits. Green points (A) and navy-blue points (B) represent the individual ratios calculated point by point (1 point every 0.5 s) before and after time drift correction, respectively.

3.4 Validation of Cu isotopic monitoring via fs-LA-MC-ICPMS

To check the MC-ICP-MS performance and subsequently validate the results obtained with the ablation of 1 μL of sample, the NIST 3114 was analyzed in continuous mode at a Cu concentration of 200 $\mu\text{g L}^{-1}$, typical for conventional MC-IP-MS analysis (for the analysis at least 1 mL of sample is needed which translates into a total amount of 200 ng of Cu) To calculate the delta values, the self-bracketing method was used, thus expecting a delta value of 0. With this method, each measured standard is treated both as sample and as standard for applying equation (1) (*cf.* section 2.4.2) (except for the first and the last ones that are only treated as standards). The average $^{65}\delta$ value found was -0.04 ± 0.09 (n=32).

To validate the Cu isotope determination with fs-LA, Cu isotopic analysis of NIST 3114 after deposition on Si wafers was performed at different concentration levels. 10 replicates were measured, and the results were expressed as delta values, using again the self-bracketing method. Results for the analysis are gathered in **Table 5**. External precision for the delta values is expressed as 2SD in ‰. Internal precision for the measured ratios is expressed as 2SD in ppm, which was calculated as the SD of the ratios calculated point by point.

Table 5. Results obtained with the fs-LA-MC-ICP-MS method through the analysis of the NIST 3114 at different concentrations using the PBP method for the isotopic calculation

Volume (μL)	[Cu] (ppb)	Mass (as Cu in ng)	^{63}Cu Signal* (V.s)	$^{65}\text{Cu}/^{63}\text{Cu}$ internal precision as 2SD (ppm)	$\delta^{65}\text{Cu}$ "self bracketing", \pm 2SD (‰), (n=10)
1	4000	4	30.8	590	0.02 \pm 0.19
1	1000	1	11.3	517	-0.01 \pm 0.19
1	500	0.5	4.8	937	-0.03 \pm 0.25
1	300	0.3	1.3	3355	-0.01 \pm 0.33

* Average signal for each concentration level was calculated as the area below the signal considering the integration limits established for calculation of the isotopic ratios.

As shown in **Table 5**, the method shows a good degree of accuracy, providing delta values close to zero, as expected. External precision improves with Cu concentration. However, such differences were not found to be statistically significant at the 95% confidence level. For internal precision, the same trend is observed, although in this case differences were found to be statistically significant at the 95% confidence level for every concentration tested. Self-evidently, worse precision values are obtained if compared to the continuous sample introduction system discussed above. In any case, precision values can be considered as satisfactory particularly taking into account that they are obtained using Cu amounts between 0.3 and 4 ng per sample only.^{50,51} As derived from **Table 5**, analysis with lower Cu amounts in the μL aliquots should be possible although at the cost of precision. Overall, the combination of the preconcentration, the amount of sample needed for an analysis (5 μL for 5 replicates) and for the limit of precision achievable with $300 \mu\text{g L}^{-1}$ shown in **Table 5** makes it possible to provide isotopic information from serum sample volumes as low as 1.5 μL for healthy individuals (Cu serum concentration around $1000 \mu\text{g L}^{-1}$) and 15 μL for WD patients (Cu serum concentration around $100 \mu\text{g L}^{-1}$).

3.5 Analysis of real samples

Next, real samples were analyzed. Five replicates per sample were measured, following a standard-sample-standard bracketing sequence. Isotope ratios were finally expressed as delta values, calculated following equation (1) and using the NIST 3114 as standard for bracketing correction. **Figure 5** shows $\delta^{65}\text{Cu}$ (‰) versus Cu total concentration values obtained for the samples under investigation.

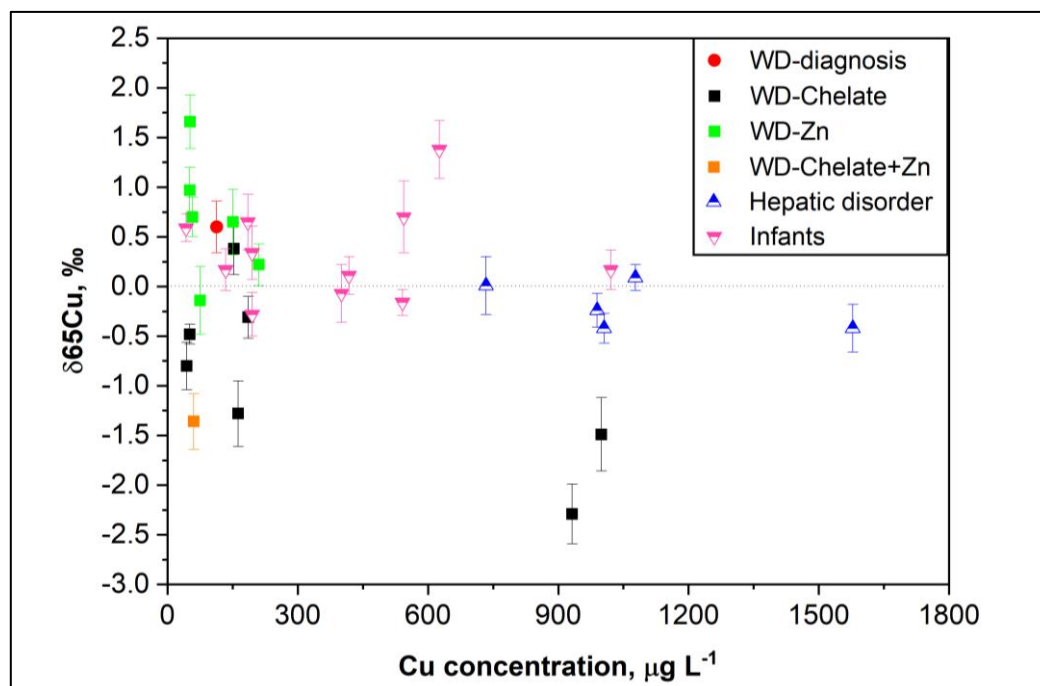


Figure 5. Concentration vs. isotopic information plot for the serum samples of the 5 different groups considered in the investigation. Isotope ratios presented were obtained with the fs-LA-MC-ICP-MS method. Uncertainties on the delta values are expressed as 2SD on the average value obtained for the five different replicates ($n = 5$) carried out for every sample.

The samples were divided into 5 groups: WD patients treated with a chelator, either trientine or DPCA (WD-C); WD patients treated with Zn (WD-Zn); patients with hepatic disorders other than WD (Hepatic disorders); healthy infants and newborns (Infants); and a sample from a WD patient at the moment of diagnosis, before any treatment was carried out (WD-diagnosis).

Results obtained for WD patients under a chelating treatment show negative $\delta^{65}\text{Cu}$ with a median value of -1.11‰ (range from -0.31 to -2.29‰) except for one sample (0.38‰). On the contrary, the samples from WD patients treated with Zn show positive $\delta^{65}\text{Cu}$ with a median value of 0.68‰ (range from -0.14 to 0.97‰) except for one patient that shows a $\delta^{65}\text{Cu}$ of -1.36‰ . This particular patient was treated with both Zn salts and trientine (chelator). The WD patient without any treatment shows a positive delta value (0.60‰). Results obtained for the infants show $\delta^{65}\text{Cu}$ around 0 or positive with a median value of 0.33‰ (range from -0.28 to 1.38‰) and the patients with hepatic disorders are around 0 or slightly negative with a median value of -0.20‰ (range from 0.09 to -0.42‰).

As seen from **Figure 5**, although combination of serum total copper and $\delta^{65}\text{Cu}$ values cannot fully discriminate among groups, some interesting trends are observed.

All groups of individuals show $\delta^{65}\text{Cu}$ values around zero or positive, except for WD patients under a chelating treatment. For these patients, negative $\delta^{65}\text{Cu}$ values are mostly obtained. This is consistent with ^{63}Cu being preferentially accumulated in the organs, as the chelator helps releasing the Cu built up in the liver or in other organs into the bloodstream. For these patients, the Cu total concentration depends on the time they have been under treatment and/or the degree of compliance with the treatment. As seen from **Figure 5**, most patients belonging to the WD-Chelate group show a low Cu total concentration, except for two points that show a high Cu concentration (999 and 932 $\mu\text{g L}^{-1}$). These two points correspond to the same patient sampled at different moments. This patient in particular was suspected of not complying with the chelating treatment continuously, which could explain the results. After a certain period of time without the chelating treatment, Cu accumulates in the organs. When the patient resumes the treatment (at the moment of sampling) a high amount of accumulated Cu enters the bloodstream, resulting in higher serum Cu levels and also in lower $\delta^{65}\text{Cu}$ values, the lowest for all the samples analyzed (-1.49 and -2.29‰). The same situation is expected for patients starting with a chelating treatment: high total Cu levels would be observed at the beginning of the treatment combined with very negative delta values. Total Cu levels would decrease along the treatment and delta values would become less negative, until very low total Cu levels combined to positive delta values, similar to those observed for patients without treatment or healthy people, would be obtained.

The situation for WD patients under treatment with Zn salts is different. The treatment with Zn acts by blocking the absorption of dietary Cu due to competition. Thus, it reduces the amount of Cu present in the bloodstream. However, Zn does not help releasing the Cu already accumulated in the body. Low Cu serum values and $\delta^{65}\text{Cu}$ values similar to those observed for patients without treatment are then expected for patients under treatment with Zn salts. This was in fact the trend observed, except for one case: that of a patient that was treated with both Zn and trientine (chelator), with a very negative delta value, which is consistent with the observed trend for patients under chelating agents. On the other hand, the WD patient without treatment, for which the sample was taken at the moment of diagnosis when no liver disorders were present, shows a positive delta value.

In conclusion, it seems that the negative delta values are due to Cu released from the organs where it is accumulated. In the case of WD patients, the observed deltas would depend on the treatment followed, as explained above, but also could serve as an indicator of the stage of the condition and, particularly, the state of the liver, where most Cu excess is accumulated. They could be positive if liver disorders are absent but could turn negative when liver disorders at an advanced stage are present, as the Cu would be ultimately released from the liver to the bloodstream as cells are destroyed. This hypothesis is consistent with results reported by Costa-Rodriguez et al.⁵² for people with cirrhosis, showing decreasing serum delta values as a function of the stage of the disease. It is important to add at this point that the delta values obtained in this work cannot be directly compared with those reported in other works²⁴, as a different references may have been used.

As ⁶⁵Cu is heavier than ⁶³Cu, the binding between ⁶⁵Cu and ceruloplasmin is more stable than that with ⁶³Cu. On the other hand, Cu exits the liver bond to the protein, so the reported results are consistent with the hypothesis that the isotope fractionation occurring in the body is driven by a thermodynamic effect.²³

Although further studies with a larger population would be needed to corroborate these findings, it seems clear that Cu isotopic analysis provides valuable information. Not only it is more specific than total Cu to differentiate infants and newborns from WD patients, but it also provides indications related to the evolution of the disease with the treatment and could also help to detect patients that are not complying with the treatment continuously.

4. Conclusion

This work examines the potential of micro analysis methods in serum samples, both for total Cu determination (direct μ -injection method) and for isotopic Cu analysis (fs-LA-MC-ICP-MS). In both cases, the measurements can be carried out with only 1 μ L of sample (after sample preparation). This fact combined with the possibility to preconcentrate samples up to a factor of 10 would permit to obtain accurate and precise results from very low sample volumes (down to 1.5 – 15 μ L of serum depending on the Cu concentration). This fact is important because in many cases (newborns, WD patients, studies with model rodents, etc.) low sample volumes and/or low Cu concentration values are found in the samples.

The fs-LA-MC-ICP-MS method developed shows a good degree of accuracy and acceptable precision. It requires the use of a high repetition rate fs-LA system, but it offers flexibility as to adapt signal intensity-sensitivity to the specific requirements of the sample analyzed. Although not studied in detail in this work, sample deposition (performing several consecutive depositions is always possible) and LA ablation parameters (namely repetition rate and scan speed) could be modified to increase or decrease sensitivity as needed.

Application of the method developed to real serum samples from WD patients under different treatments offers interesting conclusions. Results show decreased delta values linked to Cu release from the liver, either by the use of a chelating treatment (in the case of WD patients) or as a result of an advanced stage of liver damage (cirrhosis due to WD or other diseases). As a consequence, isotopic information opens the possibility to follow up the evolution of the treatment with chelators (i.e., the degree of Cu deposits removal), to detect possible cases of non-compliance with the treatments or to be used as a marker of liver damage.

Acknowledgements

The authors are grateful to the European Regional Development Fund for financial support through the Interreg POCTEFA EFA 176/16/DBS, as well as to project PGC2018-093753-B-I00 (MCIU/AEI//FEDER,UE) and the Aragon Government (Construyendo desde Aragón).

5. References

- 1 E. B. Hart, H. Steenbock, J. Waddell and C. A. Elvehjem, *J. Biol. Chem.*, 1928, **77**, 797–833.
- 2 M. A. Zoroddu, J. Aaseth, G. Crisponi, S. Medici, M. Peana and V. M. Nurchi, *J. Inorg. Biochem.*, 2019, **195**, 120–129.
- 3 C. G. Fraga, *Mol. Aspects Med.*, 2005, **26**, 235–244.
- 4 C. Wijmenga and L. W. J. Klomp, *Proc. Nutr. Soc.*, 2004, **63**, 31–39.
- 5 C. Abou Zeid and S. G. Kaler, in *Wilson Disease*, Elsevier, 2019, pp. 17–22.
- 6 L. M. Klevay, *J. Nutr.*, 2000, **130**, 489S–492S.

- 7 M. Altarelli, N. Ben-Hamouda, A. Schneider and M. M. Berger, *Nutr. Clin. Pract.*, 2019, **34**, 504–513.
- 8 A. Hordyjewska, Ł. Popiołek and J. Kocot, *BioMetals*, 2014, **27**, 611–621.
- 9 J. D. Gitlin, *Gastroenterology*, 2003, **125**, 1868–1877.
- 10 European Association For The Study Of The Liver, *J. Hepatol.*, 2012, **56**, 671–685.
- 11 H. Kodama, C. Fujisawa and W. Bhadhprasit, *Brain Dev.*, 2011, **33**, 243–251.
- 12 I. Mohr and K. H. Weiss, *Ann. Transl. Med.*, 2019, **7**, S69–S69.
- 13 M. Bost, G. Piguet-Lacroix, F. Parant and C. M. R. Wilson, *J. Trace Elem. Med. Biol.*, 2012, **26**, 97–101.
- 14 Cox DW, Bugbee D, Davies L and Kenny S, WD mutation database, <http://www.wilsondisease.med.ualberta.ca/database.asp>. (Last accessed October 2020)
- 15 I. J. Chang and S. H. Hahn, in *Handbook of Clinical Neurology*, Elsevier, 2017, **142**, 19–34.
- 16 W. A. Gahl, *Clin. Chem.*, 2008, **54**, 1941–1942.
- 17 E. A. Roberts and P. Socha, in *Handbook of Clinical Neurology*, Elsevier, 2017, **142**, 141–156.
- 18 F. Albarede, P. Télouk, V. Balter, V. P. Bondanese, E. Albalat, P. Oger, P. Bonaventura, P. Miossec and T. Fujii, *Metallomics*, 2016, **8**, 1056–1070.
- 19 M. Costas-Rodríguez, S. Van Campenhout, A. A. M. B. Hastuti, L. Devisscher, H. Van Vlierberghe and F. Vanhaecke, *Metallomics*, 2019, **11**, 1093–1103.
- 20 M. Costas-Rodríguez, J. Delanghe and F. Vanhaecke, *TrAC Trends Anal. Chem.*, 2016, **76**, 182–193.
- 21 F. Larner, L. N. Woodley, S. Shousha, A. Moyes, E. Humphreys-Williams, S. Strekopytov, A. N. Halliday, M. Rehkämper and R. C. Coombes, *Metallomics*, 2015, **7**, 112–117.

- 22 G. W. Gordon, J. Monge, M. B. Channon, Q. Wu, J. L. Skulan, A. D. Anbar and R. Fonseca, *Leukemia*, 2014, **28**, 2112–2115.
- 23 F. Vanhaecke and Degryse, Patrick, Eds., *Isotopic analysis: fundamentals and applications using ICP-MS*, Wiley-VCH-Verlag GmbH & Co. KGaA, Weinheim, 2012.
- 24 M. Aramendía, L. Rello, M. Resano and F. Vanhaecke, *J. Anal. At. Spectrom.*, 2013, **28**, 675–681.
- 25 M. Resano, M. Aramendía, L. Rello, M. L. Calvo, S. Bérail and C. Pécheyrán, *J. Anal. At. Spectrom.*, 2013, **28**, 98–106.
- 26 C. Pécheyrán, S. Cany, P. Chabassier, E. Mottay and O. F. X. Donard, *J. Phys. Conf. Ser.*, 2007, **59**, 112–117.
- 27 B. Fernandez, F. Claverie, C. Pecheyran, J. Alexis and O.F.X. Donard, *Anal. Chem.*, 2008, **80**, 6981–6994.
- 28 S. M. Eiggins, L. P. J. Kinsley and J. M. G. Shelley, *Appl. Surf. Sci.*, 1998, **127**, 278–286.
- 29 Q. Hou, L. Zhou, S. Gao, T. Zhang, L. Feng and L. Yang, *J. Anal. At. Spectrom.*, 2016, **31**, 280–287.
- 30 K. A. Miller, PhD Thesis, University of Calgary, 2018.
- 31 K. A. Miller, C. M. Keenan, G. R. Martin, F. R. Jirik, K. A. Sharkey and M. E. Wieser, *J. Anal. At. Spectrom.*, 2016, **31**, 2015–2022.
- 32 C. Dirks, B. Scholten, S. Happel, A. Zulauf, A. Bombard and H. Jungclas, *J. Radioanal. Nucl. Chem.*, 2010, **286**, 671–674.
- 33 V. N. Epov, P. Rodriguez-Gonzalez, J. E. Sonke, E. Tessier, D. Amouroux, L. M. Bourgoïn and O. F. X. Donard, *Anal. Chem.*, 2008, **80**, 3530–3538.
- 34 F. Claverie, A. Hubert, S. Bérail, A. Donard, F. Pointurier and C. Pécheyrán, *Anal. Chem.*, 2016, **88**, 4375–4382.

- 35 L. Yang, *Mass Spectrom. Rev.*, 2009, **28**, 990–1011.
- 36 S. D. Tanner, *Spectrochim. Acta Part B At. Spectrosc.*, 1992, **47**, 809–823.
- 37 S. Lauwens, M. Costas-Rodríguez, J. Delanghe, H. Van Vlierberghe and F. Vanhaecke, *Talanta*, 2018, **189**, 332–338.
- 38 S. Lauwens, M. Costas-Rodríguez and F. Vanhaecke, *Anal. Chim. Acta*, 2018, **1025**, 69–79.
- 39 A. J. Pietruszka, R. J. Walker and P. A. Candela, *Chem. Geol.*, 2006, **225**, 121–136.
- 40 G. Lenk, J. Hansson, O. Beck and N. Roxhed, *Bioanalysis*, 2015, **7**, 1977–1985.
- 41 W. Nischkauer, F. Vanhaecke, S. Bernacchi, C. Herwig and A. Limbeck, *Spectrochim. Acta Part B At. Spectrosc.*, 2014, **101**, 123–129.
- 42 Y. Ooi, I. Hanasaki, D. Mizumura and Y. Matsuda, *Sci. Technol. Adv. Mater.*, 2017, **18**, 316–324.
- 43 Deegan, R.D., Bakajin, O., Dupont, T.F., Huber, G., Nagel, S.R. and Witten, T.A., *NATURE*, 1997, **389**, 827–829.
- 44 M. Bonta, B. Hegedus and A. Limbeck, *Anal. Chim. Acta*, 2016, **908**, 54–62.
- 45 F. Claverie, B. Fernández, C. Pécheyran, J. Alexis and O.F.X Donard, *J. Anal. At. Spectrom.*, 2009, **24**, 891–902.
- 46 K. Ikehata, K. Notsu and T. Hirata, *J. Anal. At. Spectrom.*, 2008, **23**, 1003.
- 47 J. Fietzke, V. Liebetrau, D. Günther, K. Gürs, K. Hametner, K. Zumholz, T. H. Hansteen and A. Eisenhauer, *J. Anal. At. Spectrom.*, 2008, **23**, 955.
- 48 J. Fietzke, M. Frische, T. H. Hansteen and A. Eisenhauer, *J. Anal. At. Spectrom.*, 2008, **23**, 769.
- 49 V. N. Epov, S. Berail, M. Jimenez-Moreno, V. Perrot, C. Pecheyran, D. Amouroux and O. F. X. Donard, *Anal. Chem.*, 2010, **82**, 5652–5662.

- 50 F. Vanhaecke, L. Balcaen and D. Malinovsky, *J. Anal. At. Spectrom.*, 2009, **24**, 863.
- 51 K.-Y. Chen, H.-L. Yuan, P. Liang, Z.-A. Bao and L. Chen, *Int. J. Mass Spectrom.*, 2017, **421**, 196–203.
- 52 M. Costas-Rodríguez, Y. Anoshkina, S. Lauwens, H. Van Vlierberghe, J. Delanghe and F. Vanhaecke, *Metallomics*, 2015, **7**, 491–498.

6. Supplementary information

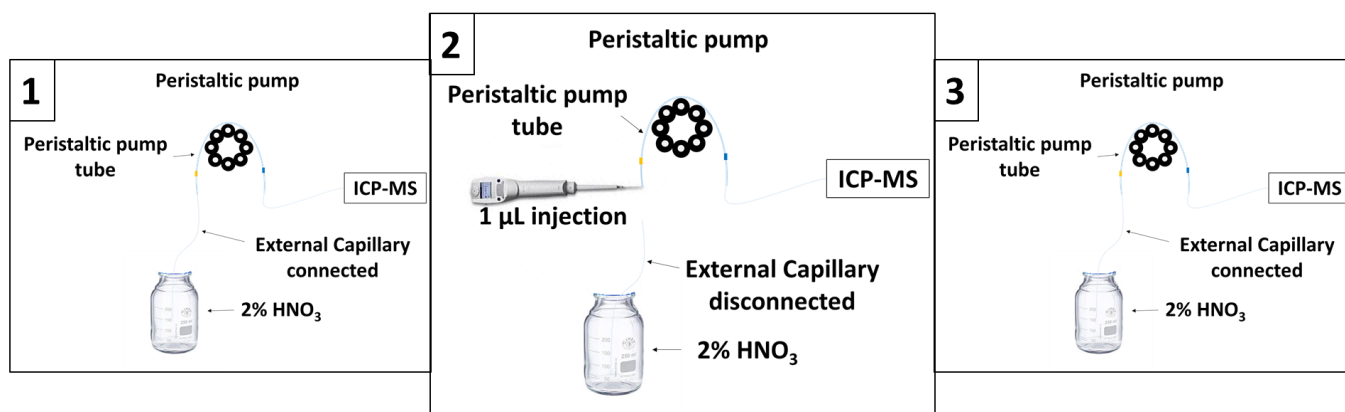


Figure S1: Schematic of the 1 µl injection process.

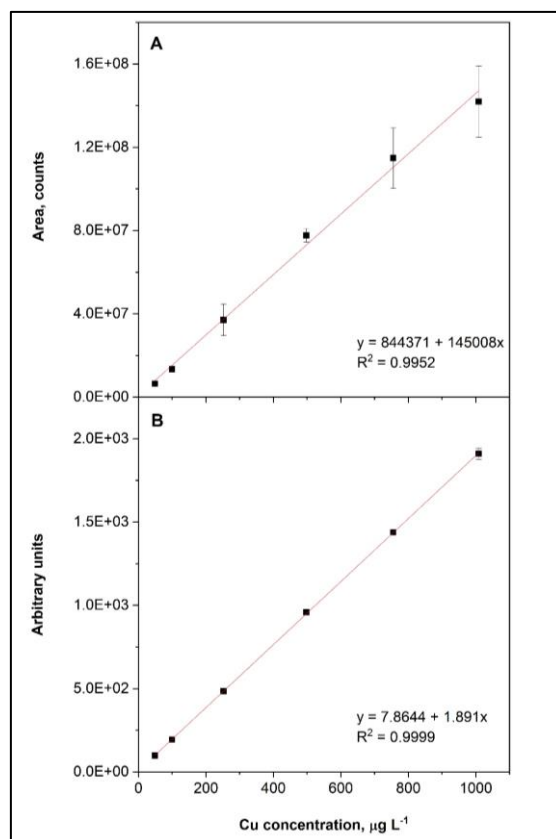


Figure S2. Cu calibration curves using the analytical protocol described in S1 A) without IS correction and B) with correction of Ni as IS.

S - 3.1.1. Cu isolation

In order to compare the efficiency of the two resins tested for Cu isolation (AG-MP1 and Triskem), elution profiles were determined for the Clincheck whole blood L-3 reference material and are shown in **Figure S3** (supplementary information). Elements included in the elution profiles comprised the analyte (Cu), matrix elements originating potential interferences (Mg and Na) and elements usually deployed as internal standard for Cu isotopic analysis with MC-ICP-MS (Ni and Zn)^{53,54}. The elution profiles show a much broader elution peak for Cu when using AG-MP1 resin (7 mL) compared to the Triskem (1 mL). In both cases Ni, Na and Mg are eluted in the early matrix elution step (first 4 ml), although with higher efficiency for the Triskem resin. In fact, one of the clear advantages of the Cu-specific resin approach is that only one separation step seems to be required to minimize the amount of Na remaining in the eluate, while with the AG-MP1 resin, two consecutive separation steps are needed for this purpose.^{37,38} On the other hand, while Zn is also eluted in the matrix elution step with the Triskem resin, it is continuously eluted with the AG-MP1.

5- Laser ablation of microdroplets for copper isotopic analysis via MC-ICP-MS. Analysis of serum microsamples for the diagnosis and follow-up treatment of Wilson's disease.

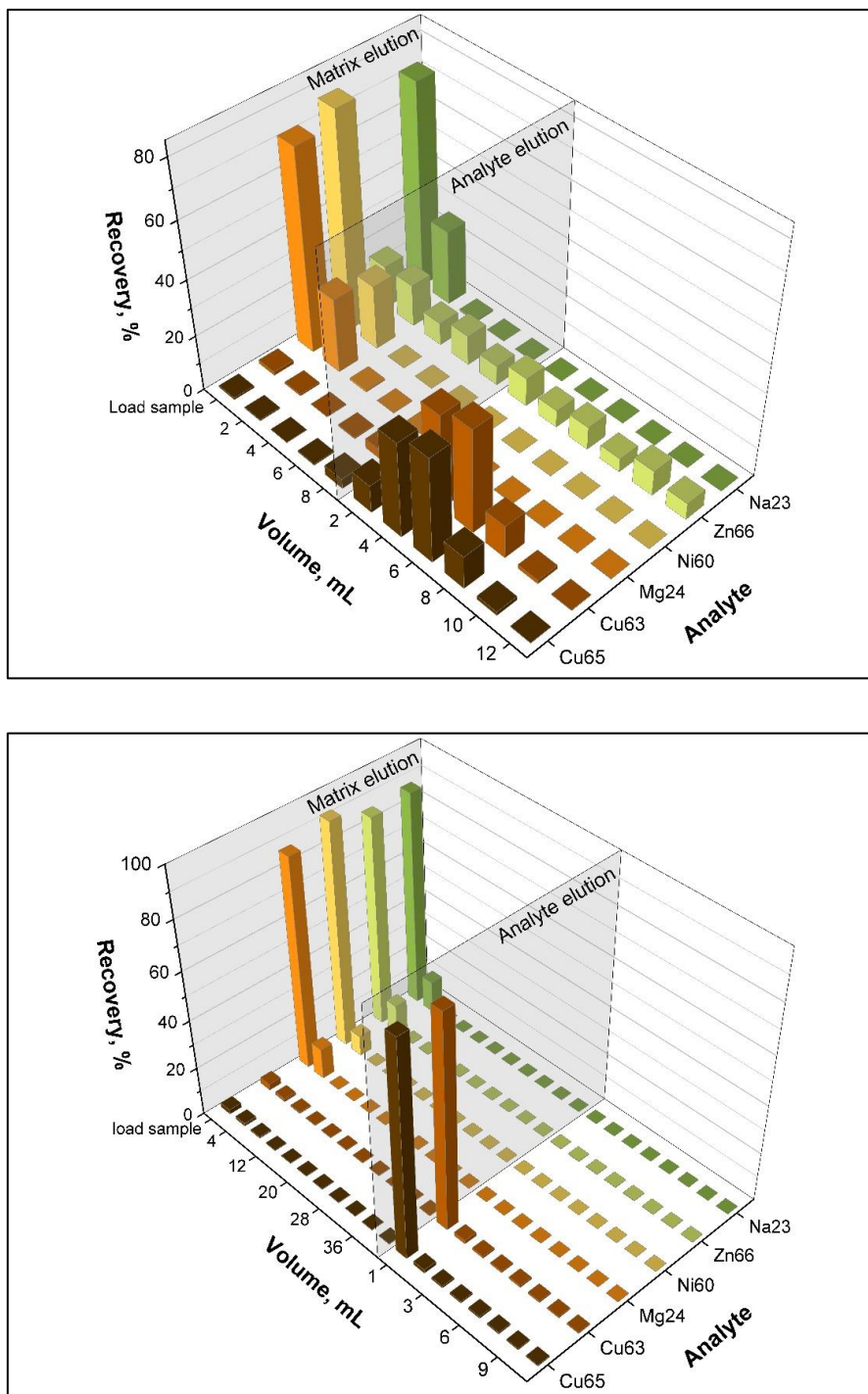


Figure S3. A) Elution profile for selected elements using AG-MP1 resin (Bio-Rad). B) Elution profile for selected elements using Cu-specific resin (Triskem). The Clincheck whole blood reference material L-3 (as described in section 2.3) was measured.

Cu isolation efficiency was then studied, with special attention to Na removal, and for three different reference materials: whole blood (Clinchek whole blood L-1), trace elements in tomato leaves (NIST 1573a) and trace elements in spinach leaves (NIST 1570a). Results on Cu recovery and Na elimination are shown in **Figure S4**. As seen from **Figure S4A** the percentage of Cu recovery is always higher with the Cu specific resin (for which only one separation procedure was performed) than with the AG-MP-1 resin using two consecutive separation procedures, reaching values close to 100%. Regarding the percentage of Na removal shown in **FigureS4B**, both protocols show a very good percentage of Na removal, always higher than 99.9 %. However, values obtained for the Cu specific resin are consistently better than those obtained with the AG-MP1 resin and with only one separation step needed, which is indeed a significant improvement.

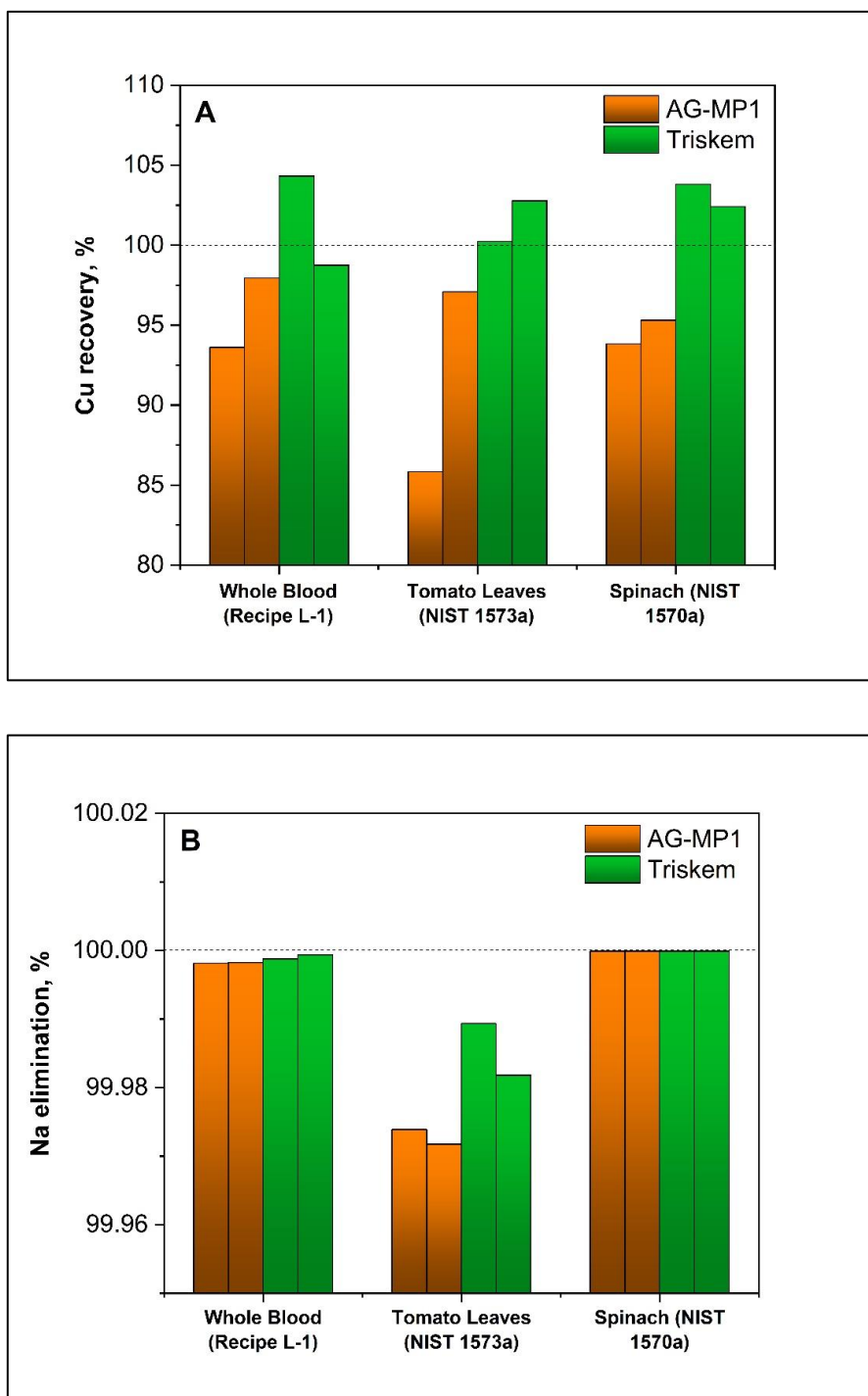


Figure S4. A) Cu recovery in 3 different reference materials after 2 consecutive separations using AG-MP1 (orange bars) and only one separation step employing the Cu-specific resin (Triskem) (green bars). B) Na removal in 3 different reference materials after 2 consecutive separations using AG-MP1 (orange bars) and only one separation step employing the Cu-specific resin (Triskem) (green bars). Two replicates were carried out per sample.

Table S1. Concentration of Cu, Na and Mg and percentage of Cu recovery and percentage of Na and Mg removal obtained after Cu separation step using Cu-specific resin (Triskem). Results are expressed as $\bar{x} \pm U$, where $U = (t s)/\sqrt{n}$; for a 95% confidence interval (n=5).

	CONCENTRATION AFTER SEPARATION ($\mu\text{G L}^{-1}$)	CERTIFIED/ REFERENCE CONCENTRATION ($\mu\text{G L}^{-1}$)			
⁶⁵ Cu	738 ± 19	738 ± 110	%RECOVERY	⁶⁵ Cu	100 ± 3
⁶³ Cu	736 ± 25	738 ± 110		⁶³ Cu	100 ± 3
²³ Na	14 ± 15	2438000*	%REMOVAL	²³ Na	99.999 ± 0.001
²⁴ Mg	14 ± 14	15900 ± 1600		²⁴ Mg	99.91 ± 0.09

*THE NA CONCENTRATION DETERMINATION WAS CARRIED OUT WITH A DXC700 AU BECKMAN COULTER USING THE SELECTIVE ELECTRODE TECHNIQUE (NA-AG/AGCL) IN THE HOSPITAL MIGUEL SERVET.

S - 3.3.1 Optimization of sample preparation for LA analysis

First, deposition of 1 μL of sample onto the Si wafer and drying at room temperature was tested. The diameter of the droplet at the moment of the deposition was around 3 mm, but it decreased down to approx. 0.3 mm until it was completely dry. The shape of the dried droplets was also highly variable. Ablation of these droplets would provide intense but very short transient signals with which it would not be possible to calculate the isotopic ratio in a stable and precise manner.

To avoid excessive droplet shrinking during drying, preheating of the Si wafer at 80 °C before deposition of the 1 μL droplet was tested next. With this strategy, the drying process was very fast, so that the diameter of the droplet (about 3 mm) did not vary significantly until it was completely dry. With this larger droplet area, longer signals could be obtained, although surface Cu concentration was not high enough to have good sensitivity with the samples of low concentration. Moreover, droplets often moved along the Si wafer surface before drying, so that mixing with other droplets. Due to this effect, it was also difficult to locate the position of the dried droplet with the laser camera.

For these reasons, before sample deposition, circular mini-wells of 1.8 mm diameter were engraved on the Si wafers, following the same ablation strategy used for the samples.

S - 3.5 Analysis of real samples

	Cu concentration ($\mu\text{g L}^{-1}$)	$\delta^{65}\text{Cu}$ Raw (‰) sample	2SD	
ANGERS	163	-1.28	0.33	WD-C
	153	0.38	0.26	WD-C
	45	-0.8	0.24	WD-C
	999	-1.49	0.37	WD-C
	932	-2.29	0.3	WD-C
	186	-0.31	0.21	WD-C
	51	-0.48	0.1	WD-C
	1578	-0.42	0.24	HP
	1077	0.09	0.13	HP
	734	0.01	0.29	HP
	989	-0.24	0.17	HP
	1005	-0.42	0.15	HP
MIGUEL SERVET	113	0.6	0.26	WD
	151	0.65	0.33	WD-Zn
	211	0.22	0.21	WD-Zn
	52	1.66	0.27	WD-Zn
	60	-1.36	0.28	WD-C + Zn
	58	0.7	0.2	WD-Zn
	51	0.97	0.23	WD-Zn
	75	-0.14	0.34	WD-Zn
	541	-0.16	0.13	NB
	544	0.7	0.36	NB
	43	0.59	0.14	NB
	626	1.38	0.29	NB
	134	0.17	0.21	NB
	418	0.11	0.19	NB
	195	0.34	0.27	NB
	401	-0.07	0.29	NB
	185	0.65	0.28	NB
	1021	0.17	0.2	NB
195	-0.28	0.22	NB	

Chapter 6:

Evaluation of electrothermal vaporization for sample introduction aiming at Cu isotopic analysis via multicollector-inductively coupled plasma mass spectrometry

Abstract

A new method for Cu isotopic analysis was developed using a commercially available electrothermal vaporization (ETV) device coupled to multicollector-inductively coupled plasma mass spectrometry (MC-ICP-MS).

The method demonstrated potential for the isotopic analysis of microsamples (e.g., 5 μ L) in a biological context. For example, Cu isotopic analysis of NIST 3114 (diluted to 1 mg L⁻¹ Cu) using self-bracketing provided average $\delta^{65}\text{Cu}$ values of $0.00 \pm 0.17\text{‰}$ (2SD, n=10) and internal precision values of 712 ppm. In order to achieve this level of accuracy and precision, it is critical to properly deal with the short transient signals generated by the ETV-MC-ICP-MS, which implies using point by point calculations and time lag detector correction (TDC), as well as a criterion to reject potential outliers.

The results of this technique were compared with the results obtained *via* femtosecond-laser ablation-MC-ICP-MS using the same pre-treated serum samples. No significant differences were observed among the results obtained in both cases, while external precision was 0.26‰ for ETV-MC-ICP-MS and 0.24‰ for fs-LA-MC-ICP-MS, expressed as median value of 2SD (n=27), further proving the usefulness of the approach proposed in this context, as the use of ETV results in a more straightforward approach.

1.Introduction

Electrothermal vaporization (ETV) is a technique that can be used for sample introduction and treatment prior to measurement *via* different approaches. Depending on the design, the

sample (liquid or solid) can be deposited onto a platform, which is subsequently introduced into the electrothermal device (such as a graphite furnace), or it can be directly introduced through a sample dosing port. Inside this electrothermal device, heating causes the sample release into the gas phase, which finally arrives to the system of detection. ETV was coupled to inductively coupled plasma optical emission spectrometry (ICP-OES) in 1974.^{1,2} In 1983, the first work on ETV coupled to inductively coupled plasma mass spectrometry (ICP-MS) was published by Gray and Date.³ This coupling showed promising potential advantages, such as a high sample transport efficiency and thus low requirements in terms of sample volume/mass, the possibility to analyze solid and complex liquid matrixes directly, and even the possibility to separate the analyte from the matrix in some occasions, leading to a reduction of interferences (spectral and non-spectral).⁴⁻⁹ Due to these interesting features, ETV-ICP-MS became popular for many decades resulting in more than 416 publications up to the present date¹⁰. However, the lack of commercial support, the success of other sampling techniques (*e.g.*, laser ablation) and the level of experience required to achieve the full potential of the technique (which required both expertise in graphite furnace and in ICP-MS) have made this technique to be seldom used in the literature during the last decade (88 publications out of 416).^{11,12}

Generally, ETV-ICP-MS can be used for monoelemental or multielemental analysis in different areas such as industrial, environmental, clinical and biological, food and beverages, among others.^{9,13} Also, it has been occasionally used for speciation studies.¹⁴⁻¹⁶ Finally, isotopic ratio monitoring has been explored, but to a much lesser extent.

One of the reasons for this could be that the typical precision for elemental analysis obtained with an ETV-ICP-MS is around 3-5% RSD, and that is for liquid samples, while 1-2% values for isotopic dilution (ID) has been reported.¹⁷ It has to be remembered that the ETV system provides very short transient signals from small sample volumes, which are not considered as ideal for precise isotopic ratio analysis, especially when coupled to sequential mass analyzers. Still, this level of precision could be enough for isotopic dilution calibration^{17,18} and, in some particular occasions, for clinical or archaeological applications,¹⁹⁻²¹ as long as the expected differences between the ratios are high enough.

Naturally, in order to deal with transient signals and improve the precision for isotopic ratios, ETV could be coupled to instrumentation with more potential for simultaneous monitoring,

such as TOF-MS²² or, for best precision in isotope analysis, multicollector (MC)-ICP-MS. However, the latter coupling has only been reported twice in the literature.

The first article was published in 2007 by Rowland *et al.*²³ In that work, ETV-MC-ICP-MS is used for separating the signals originating from ⁸⁷Sr and ⁸⁷Rb in time, thus making it possible to measure Sr isotopic ratios directly without any sample preparation (e.g., chromatographic separation). This approach was used for Rb-Sr dating; the potassium feldspar reference material NIST SRM 607 was used for method validation. The precision reported was around 0.3% RSD on ⁸⁷Sr/⁸⁶Sr ratio, which is much better than the typical precision obtained with ETV-ICP-MS with a quadrupole analyzer, as stated before. However, this precision is still too high for the majority of geo-applications. It has to be mentioned that today, direct analysis of Sr ratios can be performed by means of laser ablation with a precision between 0.02 – 0.05% RSD in wet plasma and ICP-MS/MS.^{24,25}

The second work was published in 2014 by Okabayashi *et al.*²⁶ in which a micro-ETV (based on the use of a Re filament) coupled to MC-ICP-MS was evaluated for W isotopic analysis, introducing only a few nanograms of sample. The ¹⁸²W/¹⁸³W ratio was determined in 3 different iron meteorite samples, which had been previously analyzed by a desolvating nebulizer system.²⁷ The precision reported was around 0.005% expressed as 2RSD.

Nowadays, the interest in microvolume and/or microsample analysis is growing because, in many cases, the amount of sample available is limited and/or the sample is very valuable. These problems are very common in the field of clinical analysis where sometimes it is only possible to obtain a minimal amount of sample, such as studies with newborns or model rats, among other situations where just some microliters of sample can be obtained. To deal with these situations, ETV can still be useful as a sample introduction device, and a deeper insight into the possibilities of this technique for isotope ratio determination would be valuable.

In this regard, both aforementioned works were performed with home-made ETV devices. While developing simple ETV devices is certainly interesting, it makes it more difficult to replicate the methods developed in other labs. In this work, a method for Cu isotopic analysis in biological samples by ETV-MC-ICP-MS has been developed using a commercially available ETV vaporizer, with the aim to explore the potential of this technique to facilitate analysis of microvolumes under conditions easily replicable for laboratories. This application was chosen as Cu isotopic analysis has been reported to be of interest to help in the

diagnosis and follow-up of some disorders (e.g., Wilson's disease²⁸⁻³⁰), where analysis of microvolumes is very interesting. Overall, isotopic analysis *via* MC-ICP-MS in a biomedical context has become a new topic of relevance during the last decade, in a field previously dominated by geo-applications.³¹⁻³⁵

To validate the method the NIST SRM 3114 reference material was used. Additionally, analysis of several serum samples was carried out and results were compared to those obtained in a previous work³⁰ for the same samples but using fs-LA-MC-ICP-MS, since this technique also enables analysis of microvolumes.

2. Experimental

2.1 Instrumentation

Cu total determination was carried out with an ELAN DRC II quadrupole ICP-MS (Perkin Elmer, Waltham, USA) using time resolved analysis (TRA), as described elsewhere³⁰.

Cu isotopic analysis in serum samples was carried out with a high-resolution multicollector inductively coupled plasma mass spectrometer Nu Plasma 1700 (Nu Instruments, Wrexham, UK) coupled to the electrothermal vaporization system (ETV), ETV - 4000c (Spectral Systems, Fürstfeldbruck, Germany). Pyrolytic graphite furnace and platforms were acquired from the latter company.

For sample digestion and sample evaporation, an ULTRAWAVE microwave system (Milestone Inc., Shelton, USA) and an EVAPOCLEAN® unit (Analab, Bischheim, France) were used, respectively.

2.2 Standards and reagents

For isotopic analysis, the NIST SRM 3114 (NIST, Gaithersburg, MD, USA) was deployed as a reference in the bracketing sequence. It shows a similar composition to the NIST SRM 976, which is out of stock.³⁶ It consists of an acidified aqueous solution (approximately 1.6 mol/L of HNO₃ in volume) prepared gravimetrically to contain a known mass fraction of copper.

A Pd monoelemental standard solution of 1000 mg L⁻¹ (SCP SCIENCE, Villebon-sur-Yvette, France) was used as chemical modifier.

Instra grade HNO₃ 70% was purchased from JT Baker (Phillipsburg, USA) and further purified by sub-boiling in a PFA system (DST 1000, Savillex, Eden Prairie, USA). HCl 35% ultratrace® was acquired from Scharlab (Barcelona, Spain). Ultrapure water (resistivity ≥ 18.2 MΩ cm) was obtained from a Direct-Q3 system (Millipore, Molsheim, France).

For Cu isolation, a Cu specific resin (Triskem, Bruz, France) was used.

2.3 Samples and sample preparation

To evaluate the Cu isotopic analysis using the ETV system, we analyzed the same samples that had been analyzed in our group by fs-LA-MC-ICP-MS.³⁰ The serum samples were obtained from the Hospital Universitario Miguel Servet (Zaragoza, Spain) and from the Centre Hospitalier Universitaire d'Angers (France). The principles outlined in the declaration of Helsinki regarding all the experimental research involving humans or animals were followed.

In short, such samples were subjected to sample digestion with concentrated HNO₃ in a microwave oven, evaporation to almost dryness, redissolution in concentrated HCl, and chromatographic separation with Triskem Cu specific resins. The Cu fraction was finally evaporated and redissolved in 50 μL of 2% v v⁻¹ HNO₃ in order to achieve the maximum preconcentration factor available working under these conditions, because in some cases only a small amount of sample was available and/or the Cu concentration was low. All the details on this procedure and also on the subsequent analysis of the samples for total Cu using ICP-MS and for isotopic analysis using fs-LA-MC-ICP-MS are provided elsewhere³⁰. Briefly, for total Cu determination, 1 μL of the pretreated samples was directly injected into the peristaltic pump tubing of the ICP-MS using a micropipette.

For Cu isotopic analysis, and in order to avoid mass bias due to the variation of concentration between samples and standards (bracketing correction), Cu concentration was adjusted in the fractions used for analysis to 0.3, 0.5, 1 and 4 mg L⁻¹ using 2% HNO₃ v v⁻¹ for that purpose. Dilution factors depended on the original sample Cu concentration (ranging between 0.043 and 1.578 mg L⁻¹) which after preconcentration, varied between 0.3 and 9.7 mg L⁻¹.

2.4 Measurement protocol

Isotopic analysis was carried out with an ETV-MC-ICP-MS coupling. The optimization of the system was performed in liquid mode with pneumatic nebulization using a 200 μg L⁻¹ Cu and

Ni solution. For that purpose, the nebulizer and the cyclonic chamber were coupled to one of the entrances of a 2-inlet torch connected to the MC-ICP-MS, while the ETV was coupled to the other via a 10 cm long PTFE tube (6 od x 4 id mm). The ETV gas (Ar) was maintained at 0.55 L min^{-1} during the whole procedure (optimization and measurements). Considering that samples were pretreated for Cu isolation, the mass spectrometer was operated in low resolution, in order to maximize sensitivity. Although this instrument houses 5 electron multipliers in addition to 16 Faraday cups, the signal was recorded on Faraday cups only in order to favor signal stability and isotopic measurement precision. The MC-ICP-MS was then optimized to achieve maximum signal intensity and stability. Conditions used for the isotopic analysis are shown in **Table 1**. For analysis of the samples $5 \mu\text{L}$ of sample plus $10 \mu\text{L}$ of 1000 mg L^{-1} Pd were deposited onto the platform, which was subsequently manually introduced into the graphite furnace with tongs. The ETV temperature program is also included in **Table 1**. Under these conditions, the signal peak duration was around 15 seconds with a pseudo gaussian profile. Five measurements were carried out per sample following the standard-sample-standard bracketing sequence using the NIST SRM 3114 as standard. Isotope ratio calculations were performed using the point by point method (PBP).³⁷ This method is based on the calculation of the isotope ratio as the average of the ratios calculated for each point acquired (every 0.5 s, which was a parameter used in a previous work devoted to fs-LA introduction of the samples, also producing transient signals, and eventually enabling a fair comparison of results³⁰) during a certain time interval.

Table 1. ETV temperature program and instrumental conditions for Cu isotopic analysis of serum using ETV-MC-ICP-MS.

ETV temperature program																					
Temperature program		Temperature (°C)					Ramp (°C s ⁻¹)					Hold time (s)									
Drying step 1		80					2.7					30									
Drying step 2		110					1					30									
Pyrolysis step		350					24					30									
Vaporization step		600					12.5					20									
Cleaning step		2600					2000					4									
Nu MC-ICP-MS 1700																					
RF Power (W)										1300											
Instrument resolution										Low											
Acquisition Mode										Time Resolved Acquisition (TRA)											
Integration time (s)										0.5											
Nebulizer Pressure (Psi)										8.20 - 9.8 ^a											
Auxiliary gas (L min ⁻¹)										1.10											
Plasma gas (L min ⁻¹)										13.00											
Faraday cup configuration																					
Collecto	H9	H8	H7	H6	H5	H4	H3	H2	H1	Ax	L1	L2	L3	IC	IC	IC	L4	IC	L5	IC	L6
r														0	1	2		3		4	
m/z		67		66			65			64			63						61		60

a: Optimized daily

Please notice that the measurements were carried out in continuous mode. Therefore, the time axis does not start at time zero. Regardless, every peak was processed individually considering the stable part of the isotope ratio.

When recording transient signal, isotope ratios measured by MC-ICP-MS generally shows a drift during signal acquisition attributed to the different time response of the Faraday pre-amplifiers.³⁸ As short transient signal were recorded in this study, a systematic correction of time lags between Faraday cups (TDC) was performed following the method described by Claverie *et al.*³⁹, which is based on the synchronization of the two isotope signals obtained for ⁶⁵Cu and ⁶³Cu following the criterion that the coefficient of determination of the linear regression for the two isotopes would be as close as possible to 1. Finally, the results were

expressed as delta values (δ) using the NIST SRM 3114 as standard, following the equation (1):

$$\delta(\text{‰}) = \frac{R_{\text{sample}} - R_{\text{STD}}}{R_{\text{STD}}} \times 1000 \quad (1)$$

where R_{sample} is the $^{65}\text{Cu}/^{63}\text{Cu}$ isotope ratio obtained for the sample and R_{STD} is the average $^{65}\text{Cu}/^{63}\text{Cu}$ isotope ratio determined for the NIST 3114 measured before and after that particular sample.

The TDC correction is described in detail elsewhere.³⁹ In short, the determination of the time lag was performed iteratively using a VBA macro. The isotopes signals were first interpolated ($N=1000$) and then shifted one over the other by one increment until the optimal value for the criterion was obtained. Once the optimal time lag was obtained, averages of data points were calculated, in order to obtain the exact same numbers of data points per second than before the interpolation.

3. Results

3.1 Optimization of the temperature program

The optimized temperature program used for analysis is included in **Table 1**. Optimization of this program does not follow exactly the same premises as for quantitative analysis with ETV-ICP-MS. In this case, three main factors were considered: (i) to avoid pre-vaporization of Cu during drying and pyrolysis steps that could cause Cu isotopic fractionation, (ii) to achieve a signal profile providing the best stability for the isotopic ratios ($^{65}\text{Cu}/^{63}\text{Cu}$) and (iii) to minimize blanks and memory effects between analyses.

In our case, the pyrolysis step is not very critical in terms of matrix removal, as the samples were pre-treated for Cu isolation. Therefore, the pyrolysis temperature was selected in order to avoid a sudden change of temperature in the plasma, which might affect signal stability and the final precision for the ratios. The temperature chosen was 350 °C, a temperature roughly in between the drying and the vaporization temperatures.

For vaporization, different temperatures were tested. Use of high temperatures (such as 2500 °C) was discarded because at this temperature blanks were high while below 900°C the blanks were almost zero. This is probably due to recondensation of particles on colder parts

of the system and revaporization when heating back at high temperatures, an issue that seems to be typical of this ETV device according to the authors' experience. Moreover, it was observed that Cu starts to vaporize around 500 °C, however, the signals were not reproducible at these low temperatures. In order to find the best vaporization temperature providing reproducible signals, different modifiers (Pd and Pt) and different vaporization temperatures between 400 °C and 900 °C were tested. Pd was chosen as modifier as it provided higher intensity and better reproducibility. As for the temperature, it was observed that between 600 °C and 700 °C the signals were more reproducible, and the peaks obtained showed a unimodal profile (see **Figure 1**). Since the profiles of both Cu isotopes followed the same behavior, in the next figures only ^{63}Cu signal and the ratio will be shown for the sake of simplicity. The vaporization temperature finally chosen was 600 °C, as it generally offered a higher stability for the isotope ratios, as shown in **Figure 1**. It can be observed in **Figure 1A** that, at a vaporization temperature of 600 °C, the ratios obtained during the duration of the signal (corresponding to 5 μL of aqueous standard) are rather stable. There is a small increase in the ratios along the transient signal but this is mostly due to the Faraday detector time lag ^{38–40}, as will be discussed in the next section. At 700 °C, on the other hand, **Figure 1B**, the ratios varied much more, and the profile is not constant among replicates. This behavior cannot be attributed to time lags, and it may obey to variations in the vaporization process.

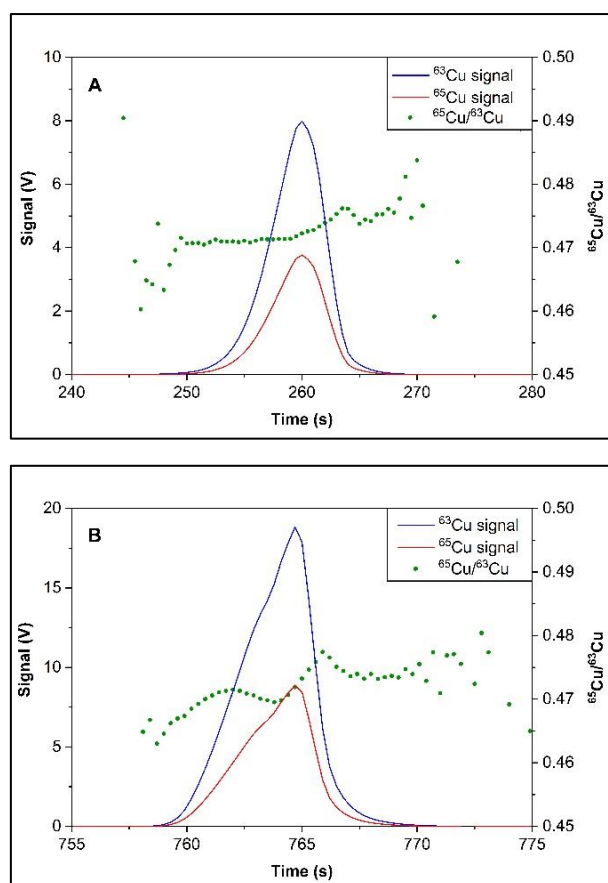


Figure 1. Example of transient signals of both ^{65}Cu (red) and ^{63}Cu (blue) isotopes obtained using 5 μL of a Cu standard of 1 mg L^{-1} (5 ng of Cu) and 10 μL of a Pd standard of 1 g L^{-1} carried out with a temperature program with $T_{\text{pyrolysis}} = 350\text{ }^{\circ}\text{C}$ and A) $T_{\text{vaporization}} = 600\text{ }^{\circ}\text{C}$ and B) $T_{\text{vaporization}} = 700\text{ }^{\circ}\text{C}$. No TDC has been applied at this stage.

3.2 Data treatment

ETV sample introduction system provides transient signals that, if working conditions are well optimized, show a unimodal profile. This kind of signal is, in principle, optimal for applying the Linear Regression Slope (LRS) method for the isotope ratio calculation. The LRS method was proposed by Fietzke *et al.*^{41,42}, and it is based on the representation of the signal achieved for one isotope (^{65}Cu) versus the signal for the other (^{63}Cu), adjusting the data to a linear regression, where the slope corresponds to the ratio. This method takes into account the whole signal but, as in any linear regression model, the points with higher signal intensity ultimately show a higher influence in the calculated slope than those with lower signal intensities. During the experiments, it was possible to observe that sometimes, not very often, the ratio profile discussed in section 3.1 at 600 $^{\circ}\text{C}$ (**Figure 1A**), was altered and resembled

the profile obtained at 700 °C (**Figure 1B**). This may reflect problems in the device used to always keep the desired temperature, which would not be surprising, among other reasons including the deterioration of consumables, namely the graphite parts. This effect is shown in **Figure 2**, where it can be seen that the deviation from the typical ratio profile (**Figure 2A**) was not always the same, in some cases the drop was slight (**Figure 2B**) while for others it was far more pronounced (**Figure 2C**).

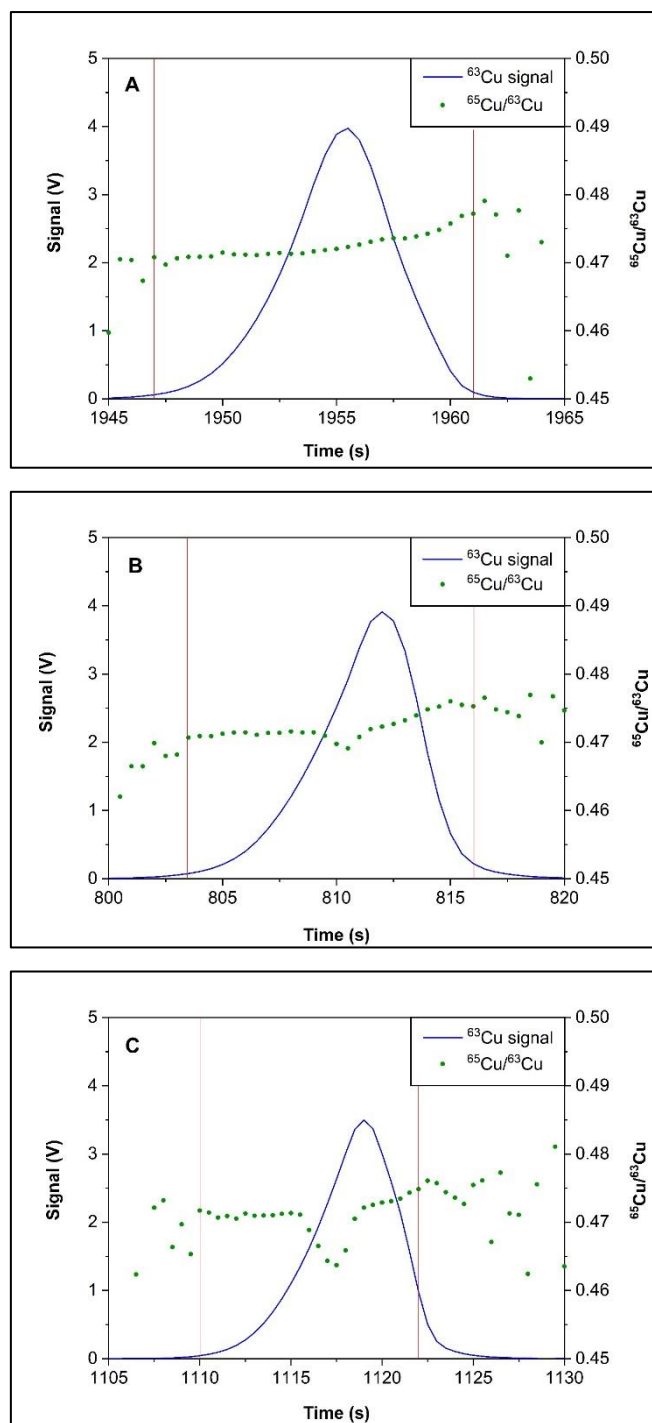


Figure 2. Examples of transient signals with their respective representations of the individual ratios calculated for each point (1 point every 0.5s) for 5 μL of a solution of 0.5 mg L^{-1} of Cu prepared with the NIST SRM 3114 + 10 μL of 1 g L^{-1} of Pd. In all cases, the conditions used were the same ($T_{\text{pyrolysis}} = 350\text{ }^{\circ}\text{C}$ and $T_{\text{vaporization}} = 600\text{ }^{\circ}\text{C}$). No TDC has been applied at this stage. (A) Typical ratio profile; (B) ratio profile altered but with a slight drop; and (C) ratio profile altered with a more pronounced drop. The portion of the signal using for calculation is represented between the red bars.

When performing the calculation with the LRS method, the precision obtained for the isotope ratios was poor. With this method, the drop in the ratio profile significantly affected the results even when it is very slight, because such deviation is produced in the area close to the maximum of the peak, and as discussed before, the points with higher intensities eventually influence more the slope value.

Thus, the point by point method (PBP)³⁷ was tested instead. For this method, setting of the data processing limits is an important parameter to optimize. As seen from **Figure 2**, the data processing limits (between red bars) was set considering only the most stable part of the signal, which includes most of the peak, excluding only the initial and final parts, where ratios are not reliable.

Results for the analyses showed that the influence of the variations in the isotope ratio are lower working with the PBP method than with the LRS method. However, if the drop is very pronounced, then the influence becomes significant. Thus, it is necessary to set a value for rejection. A practical criterion was developed for this purpose. This criterion was applied for rejection based on the difference in the isotope ratio between the negative peak apex (x_2) and the last point before the drop (*i.e.*, the left limit of the negative peak, x_1), as shown in **Figure 3**. Experimentally (using NIST SRM 3114), it was observed that if the difference between x_1 and x_2 (see **Figure 3**) was higher than 0.003, the ratio obtained was significantly lower than the typically expected ratio. Therefore, if the difference in the $^{65}\text{Cu}/^{63}\text{Cu}$ isotope ratio was lower than 0.003 the measurement was considered for further calculations with the PBP approach and time lag detector correction (TDC), but if the difference was higher than 0.003 (isotopic ratio drops substantially), then the whole measurement was rejected. It must be stated that this is a criterion developed for this particular application and set-up, and it should not be directly applied to other situations without further studies. The overall percentage of signals rejected was between 5 and 10% depending on the day.

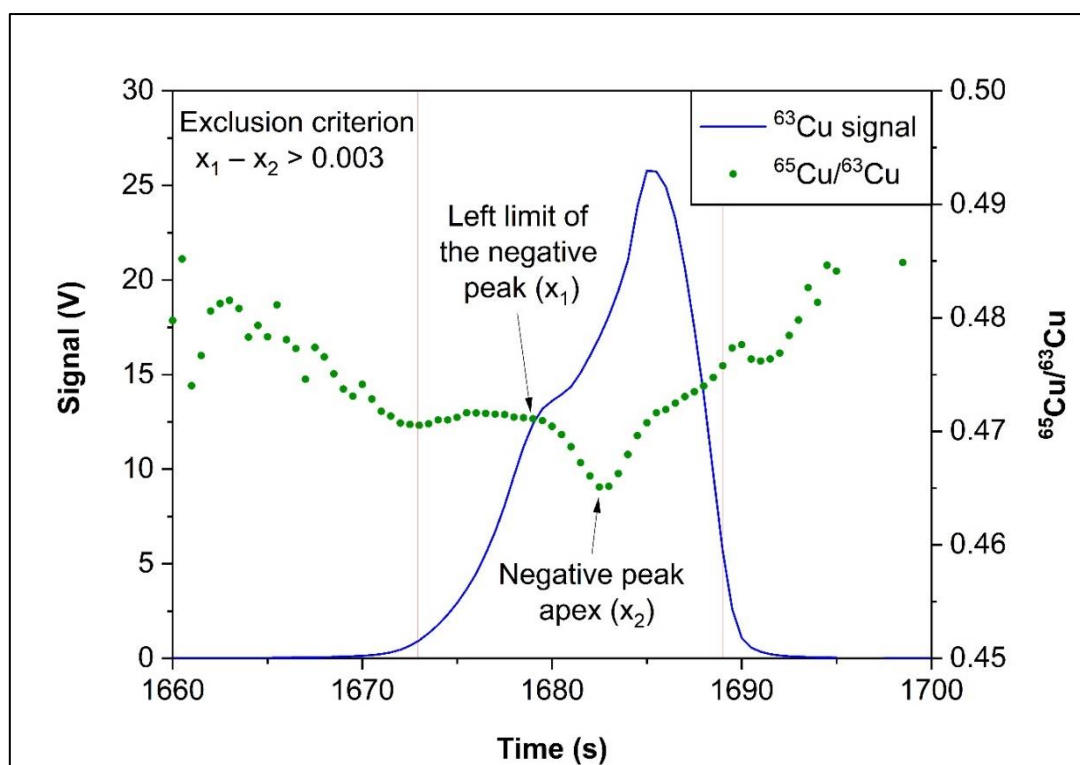


Figure 3. Example of application of the exclusion criterion. No TDC has been applied at this stage. (

A quick look at **Figure 4A** and previous figures shows that the ratios trend up during the measurement. One explanation for that could be thermal fractionation during the vaporization process. This is a topic that, to the best of the authors' knowledge, has not been investigated before. However, this trend may also be an artifact due to time lag between detectors, which is a problem that has been detected before.^{38–40} To verify the actual cause of this trend, TDC was systematically applied prior PBP isotope ratio calculation. **Figure 4** shows an example of the results before and after TDC correction. As can be observed in **Figure 4A**, before the TDC the ratios are going up along the peak, while after TDC this effect is practically eliminated (see **Figure 4B**). In this case in particular, the internal precision improves by a factor of 6 after TDC. That clearly indicates that this trend upwards in the ratio was produced by the time lag and not by any possible fractionation occurring during the vaporization of the analyte because, if this trend were due to the thermal fractionation, the TDC correction would not be able to correct it. This improvement in internal precision is not constant but varies for each peak: the precision improves by a factor between 1.5 and 7.0.

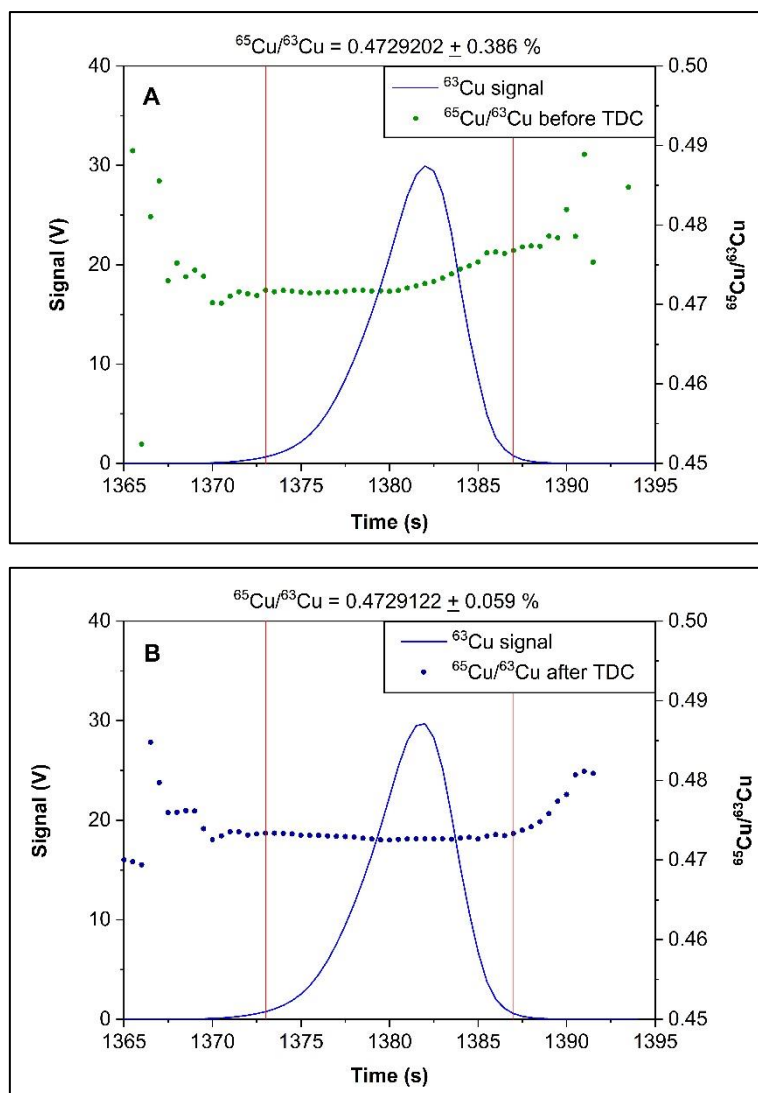


Figure 4. Example of transient signal obtained for the introduction with an ETV of 5 μL of a 4 mg L^{-1} (20 ng of Cu) Cu standard solution A) before time drift correction and B) after time drift correction. The signal profile is represented by the blue points, while the red bars represent the data processing limits. Green points (A) and navy-blue points (B) represent the individual ratios calculated point by point (1 point every 0.5 s) before and after time drift correction, (TDC) respectively

3.3 Precision and accuracy of the method

For precision and accuracy study of the method developed, Cu isotopic analysis of NIST SRM 3114 was carried out at different Cu concentration levels.

For analysis of NIST SRM 3114, 10 replicates of each concentration were measured, and the results were expressed as delta values applying equation (1) (*cf.*, section 2.3.) and using self-bracketing, which means that NIST SRM 3114 was treated as standard and as sample,

except for the first and the last measurements that were only used as standards. Since the NIST 3114 is both the sample and the standard, the delta value expected would be 0. **Table 2** shows the results obtained. External precision for the delta values is expressed as two times the standard deviation (2SD) in ‰. Internal precision was calculated as the SD of the ratios obtained point by point (one ratio each 0.5 s), and it is expressed as 2SD in ppm.

Table 2. Results of the analysis of the NIST SRM 3114 at different concentrations.

Volume (μL)	[Cu] (μg L ⁻¹)	Mass (as Cu in ng)	⁶³ Cu Signal* (V.s)	⁶⁵ Cu/ ⁶³ Cu	δ ⁶⁵ Cu
				internal precision as 2SD (ppm)	"self bracketing", ± 2SD (‰), (n=10)
5	300	1.5	11	808	0.03 ± 0.24
5	500	2.5	16	860	-0.05 ± 0.20
5	1000	5	47	712	0.00 ± 0.17
5	4000	20	156	685	-0.02 ± 0.14

*The average signal for each concentration level was calculated as the area below the signal considering between the data processing limits set for the calculation of the isotopic ratio.

As it is possible to appreciate in the **Table 2**, the results obtained show internal precision values within 685 ppm and 860 ppm and good accuracy, with δ⁶⁵Cu values very close to zero. These internal precision values are rather high, but this is not unusual for highly transient signals. It should be reminded that external precision values are the ones that provide a representative estimation of the uncertainty among replicates. These values ranged between 0.14 and 0.24‰. Also note that both external and internal precision seem to slightly improve with the Cu concentration likely as a results of better counting statics. However, statistically significant differences were not found at the 95% confidence level (*via* F-tests).

Next, real samples were analyzed with the ETV-MC-ICP-MS. Five replicates per sample were measured following the sequence standard-sample-standard bracketing and the results were expressed as delta value using the equation (1). These results were compared with the results obtained *via* fs-LA-MC-ICP-MS, which are published in ref. ³⁰. That is an alternative method in which 1 μL samples are deposited and dried in silicon wafers, in which micro-wells

were previously produced. Results obtained for both analyses are graphed in **Figure 5**. The correlation equation was obtained using the software Origin Pro2019b and it is $y = (0.89194 \pm 0.21196) x + (0.09455 \pm 0.11821)$, which indicates that significant difference between both methods cannot be established at the 95% confidence level. The conclusions obtained with ETV-MC-ICP-MS in terms of the interpretation of the results would be analogous to those reported in ref.³⁰, so they will not be duplicated here. It will just be mentioned that the ratios obtained depend on the medical condition (Wilson's disease or other disorders vs controls) and on the treatment. In short, delta values biased low can be attributed to the release of Cu release previously accumulated in the liver, which can be the result of medical treatment with a chelating agent after the diagnosis of WD disease, or else the result of an advanced stage of liver damage (cirrhosis due to WD or other diseases).

In terms of external precision, the median value for real samples *via* fs-LA-MC-ICP-MS would be 0.24‰ (range between 0.10 and 0.36‰), and 0.26‰ (range between 0.09 and 0.66‰) *via* ETV- MC-ICP-MS.

Overall, ETV seems like a viable alternative for analysis in which only sample microvolumes are finally available, which is not unusual in biomedical contexts.

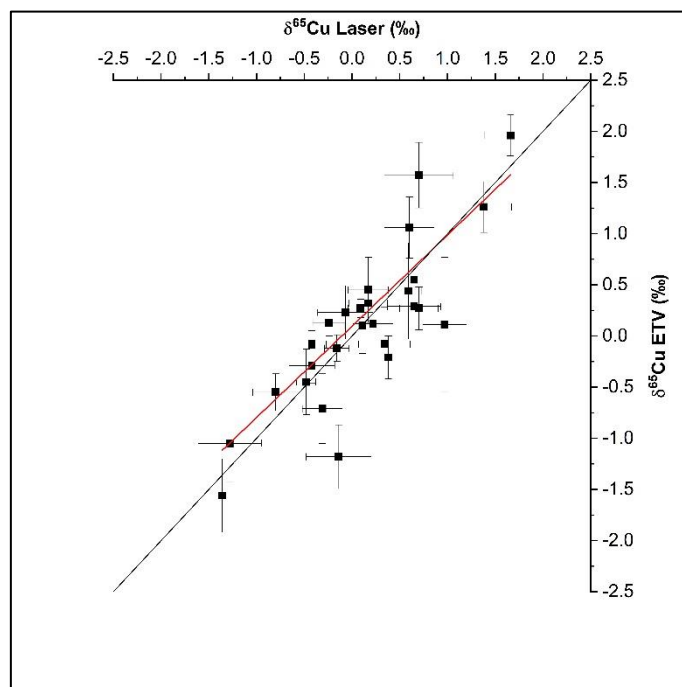


Figure 5. Correlation analysis for the $\delta^{65}\text{Cu}$ (‰) values obtained for the same samples analyzed by the ETV-MC-ICP-MS and *via* fs-laser-MC-ICP-MS. Error bars represent external

precision as 2SD (n=5). The black line represents a perfect agreement (slope=1), while the red line represents the actual regression

4. Conclusions

This work examines the coupling of a commercially available ETV device to a MC-ICP-MS to monitor Cu isotope ratios for the first time. The results obtained demonstrate that this sample introduction strategy can provide information of similar quality in comparison with other more complex MC-ICP-MS approaches also relying on micro-analysis, which is furthermore of sufficient precision and accuracy to be of biomedical significance.

One of the advantages of this approach is the possibility to deploy commercially available ETV instrumentation, but also to develop cheap and simple home-made devices (as shown in reference ²⁶), thus providing new ways to obtain isotopic information from microsamples.

Acknowledgements

The authors are grateful to the European Regional Development Fund for financial support through the Interreg POCTEFA EFA 176/16/DBS as well as to project PGC2018-093753-B-I00 (MCIU/AEI//FEDER, UE) and the Aragon Government (Construyendo desde Aragón).

Declarations of interest

The authors declare no conflict of interest.

5. References

- 1 D. E. Nixon, V. A. Fassel and R. N. Kniseley, *Anal. Chem.*, 1974, **46**, 210–213.
- 2 A. M. Gunn, D. L. Millard and G. F. Kirkbright, *Analyst*, 1978, **103**, 1066–1073.
- 3 A. L. Gray and A. R. Date, *Analyst*, 1983, **108**, 1033–1050.
- 4 E. Björn, W. Frech, E. Hoffmann and C. Lüdke, *Spectrochim. Acta Part B At. Spectrosc.*, 1998, **53**, 1765–1776.
- 5 R.E. Sturgeon and J.W. Lam, *J. Anal. At. Spectrom.*, 1999, **14**, 785–791.
- 6 J. M. Carey, E. H. Evans, J. A. Caruso and W.-L. Shen, *Spectrochim. Acta Part B At. Spectrosc.*, 1991, **46**, 1711–1721.
- 7 F. Vanhaecke, S. Boonen, L. Moens and R. Dams, *J. Anal. At. Spectrom.*, 1995, **10**, 81–87.

- 8 K. Grünke, H.-J. Stärk, R. Wennrich, H. M. Ortner and J. A. C. Broekaert, *Fresenius J. Anal. Chem.*, 1997, **359**, 465–468.
- 9 M. Resano, F. Vanhaecke and M. T. C. de Loos-Vollebregt, *J. Anal. At. Spectrom.*, 2008, **23**, 1450–1475.
- 10 Web of Science, <https://apps.webofknowledge.com>. (Last accessed April 2021)
- (11 J. S. Silva, A. S. Henn, V. L. Dressler, P. A. Mello and E. M. M. Flores, *Anal. Chem.*, 2018, **90**, 7064–7071.
- 12 J. Patočka, T. Černohorský, A. Krejčová and S. Slang, *Talanta*, 2019, **204**, 555–560.
- 13 M. Aramendía, M. Resano and F. Vanhaecke, *Anal. Chim. Acta*, 2009, **648**, 23–44.
- 14 I. Gelaude, R. Dams, M. Resano, F. Vanhaecke and L. Moens, *Anal. Chem.*, 2002, **74**, 3833–3842.
- 15 H. Kataoka, Y. Okamoto, S. Tsukahara, T. Fujiwara and K. Ito, *Anal. Chim. Acta*, 2008, **610**, 179–185.
- 16 L. Xia, B. Hu, Z. Jiang, Y. Wu, R. Chen and L. Li, *J. Anal. At. Spectrom.*, 2006, **21**, 362–365.
- 17 M. Resano, M. Aramendía and F. Vanhaecke, *J. Anal. At. Spectrom.*, 2006, **21**, 1036–1044.
- 18 L. F. Dias, G. R. Miranda, T. D. Saint’Pierre, S. M. Maia, V. L. A. Frescura and A. J. Curtius, *Spectrochim. Acta Part B At. Spectrosc.*, 2005, **60**, 117–124.
- 19 D. C. Grégoire and J. Lee, *J. Anal. At. Spectrom.*, 1994, **9**, 393–397.
- 20 D. C. Gregoire, *Anal. Chem.*, 1990, **62**, 141–146.
- 21 C. G. Lee, K. Iguchi, K. Esaka, M. Magara, F. Esaka, S. Sakurai, K. Watanabe and S. Usuda, *Anal. Chim. Acta*, 2004, **517**, 215–220.
- 22 P. P. Mahoney, S. J. Ray, G. Li and G. M. Hieftje, *Anal. Chem.*, 1999, **71**, 1378–1383.
- 23 A. Rowland, T. B. Housh and J. A. Holcombe, *J. Anal. At. Spectrom.*, 2008, **23**, 167–172.
- 24 E. Bolea-Fernandez, S. J. M. Van Malderen, L. Balcaen, M. Resano and F. Vanhaecke, *J. Anal. At. Spectrom.*, 2016, **31**, 464–472.
- 25 D. Bevan, C. D. Coath, J. Lewis, J. Schwieters, N. Lloyd, G. Craig, H. Wehrs and T. Elliott, *J. Anal. At. Spectrom.*, 2021, **36**, 917–931.
- 26 S. Okabayashi, S. Sakata and T. Hirata, *Anal. Chim. Acta*, 2015, **853**, 469–476.
- 27 A. Markowski, G. Quitte, A. Halliday and T. Kleine, *Earth Planet. Sci. Lett.*, 2006, **242**, 1–15.

- 28 M. Aramendía, L. Rello, M. Resano and F. Vanhaecke, *J. Anal. At. Spectrom.*, 2013, **28**, 675–681.
- 29 M. Resano, M. Aramendía, L. Rello, M. L. Calvo, S. Bérail and C. Pécheyran, *J. Anal. At. Spectrom.*, 2013, **28**, 98–106.
- 30 M. C. García-Poyo, S. Bérail, A. L. Ronzani, L. Rello, E. García-González, B. Lelièvre, P. Cales, F. V. Nakadi, M. Aramendía, M. Resano and C. Pécheyran, *J. Anal. At. Spectrom.*, 2021, **36**, 968–980.
- 31 M. Costas-Rodríguez, J. Delanghe and F. Vanhaecke, *TrAC Trends Anal. Chem.*, 2016, **76**, 182–193.
- 32 F. Vanhaecke and P. Degryse, *Isotopic Analysis: Fundamentals and Applications Using ICP-MS*, Weinheim, Wiley-VCH Verlag GmbH & Co. KGaA., 2012.
- 33 T. Walczyk and F. von Blanckenburg, *Science*, 2002, **295**, 2065–2066.
- 34 F. Larner, M. Rehkämper, B. J. Coles, K. Kreissig, D. J. Weiss, B. Sampson, C. Unsworth and S. Strekopytov, *J. Anal. At. Spectrom.*, 2011, **26**, 1627.
- 35 F. Albarede, P. Télouk, V. Balter, V. P. Bondanese, E. Albalat, P. Oger, P. Bonaventura, P. Miossec and T. Fujii, *Metallomics*, 2016, **8**, 1056–1070.
- 36 Q. Hou, L. Zhou, S. Gao, T. Zhang, L. Feng and L. Yang, *J Anal Spectrom*, 2016, **31**, 280–287.
- 37 V. N. Epov, P. Rodriguez-Gonzalez, J. E. Sonke, E. Tessier, D. Amouroux, L. M. Bourgoin and O. F. X. Donard, *Anal. Chem.*, 2008, **80**, 3530–3538.
- 38 A. Gourgiotis, S. Bérail, P. Louvat, H. Isnard, J. Moureau, A. Nonell, G. Manhès, J.-L. Birck, J. Gaillardet, C. Pécheyran, F. Chartier and O. F. X. Donard, *J. Anal. At. Spectrom.*, 2014, **29**, 1607–1617.
- 39 F. Claverie, A. Hubert, S. Berail, A. Donard, F. Pointurier and C. Pécheyran, *Anal. Chem.*, 2016, **88**, 4375–4382.
- 40 T. Hirata, Y. Hayano and T. Ohno, *J. Anal. At. Spectrom.*, 2003, **18**, 1283–1288.
- 41 J. Fietzke, V. Liebetrau, D. Günther, K. Gürs, K. Hametner, K. Zumholz, T. H. Hansteen and A. Eisenhauer, *J. Anal. At. Spectrom.*, 2008, **23**, 955–961.
- 42 J. Fietzke, M. Frische, T. H. Hansteen and A. Eisenhauer, *J. Anal. At. Spectrom.*, 2008, **23**, 769–772.

Chapter 7:

Comparison of different biomarkers for diagnosis and follow up of Wilson's disease

Abstract

Information about Cu speciation and Cu isotopic composition can be useful when investigating Wilson's disease (WD). It can provide a better understanding of the metabolism of Cu in general and, especially, for WD patients. It may also provide a way to diagnose and follow up WD patients. In this work, Cu determination and Cu isotopic analysis were carried out both in bulk serum and in exchangeable copper (Cu Exch) fraction. Cu Exch is the labile fraction of Cu that is not bound to the ceruloplasmin. In this fraction, Cu is loosely bound to proteins such as albumin, alpha-2 macroglobulin (α -2M), and some amino acids. The Cu Exch protocol was evaluated, before real samples analysis, in terms of Cu recovery and, also, in terms of mass fractionation. The whole analytical procedure (Cu Exch and Cu isolation) was investigated in this regard. In both cases, the results were satisfactory: good recovery and no significant mass fractionation. After that, the analyses were carried out for controls (healthy persons), new-borns (NB), patients with hepatic disorders, and WD patients. It was observed that the only parameter that could discern between WD patients and the rest of the patients tested (No WD) in this work was the relative exchangeable copper (REC). All the WD patients showed a REC higher than 17%, while the rest showed lower REC values. Based on the isotopic analysis, the most conclusive results were obtained by performing the isotopic analysis from the bulk serum. They showed that $\delta^{65}\text{Cu}$ were lower for WD under chelating treatment and for patients with hepatic problems than for WD under Zn treatments, controls, and newborns (NB). They were even lower than the $\delta^{65}\text{Cu}$ value obtained for a WD patient at the moment of the diagnosis. It should be noted that this patient was asymptomatic. Hence, these low $\delta^{65}\text{Cu}$ values seem to be linked to Cu release from the liver. The rest of the

parameters tested were also useful both to understand better the Cu metabolism and to follow up the disease.

1. Introduction

Wilson's disease (WD), as described in Chapter 1, is a recessive genetic disease produced by a mutation in the ATP7B gene. This mutation prevent both excretion of Cu from the hepatocytes into the bile and incorporation of Cu into the ceruloplasmin¹⁻³ with the consequences that this entail.^{3,4} In general, the survival rate depends on the stage of liver and/or neurological disease, and also on treatment follow-up. At present, there are two kinds of treatments for WD: one based on the administration of chelators for increasing excretion of the Cu that is already accumulated in the organs, such as D-penicillamine (DPA) and Trientine (TETA), and another based on blocking the absorption of Cu with Zn salts (Zn).^{5,6} The treatment of choice depends on the clinical picture of the patient, but both are easy to follow (see Chapter 1).

The problem is to achieve the diagnosis before the onset of symptoms, to avoid the consequences that they entail. Nowadays, the most common way to carry out the diagnosis is based on the symptoms. Genetic tests could be useful to diagnose the disease. However, they cannot be undertaken as routine because they are costly and tedious, as there are more than 500 genetic mutations that cause WD.⁷⁻⁹ For this reason, the diagnosis mostly relies on clinical symptoms and biological tests, such as blood or urine analyses,¹⁰ as it was commented in Chapter 1 and in Chapter 5. However, these kinds of tests may provide unreliable and/or inconclusive results. As a consequence, it is often necessary to carry out several tests to confirm the disease and, even then, sometimes the diagnosis is not clear.^{3,12}

Hence the importance of continuing the research on new methods to diagnose WD in an easy way and at an early stage, before any symptoms appear. In this regard, investigations about Cu isotopic analysis¹³⁻¹⁵ or parameters related with the Cu bound to ceruloplasmin and/ or free Cu^{12,16-18} are currently on the rise.

In the context of isotopic analysis, investigations with biological samples are growing.¹⁹⁻²³ To carry out the isotopic analysis, multicollector inductively coupled plasma mass spectrometry (MC-ICP-MS) is the technique most commonly used.²⁴ In the case of WD, preliminary studies about isotopic analysis in WD patients showed that samples from WD patients present a lighter isotopic composition than that for controls, both in serum and in urine samples.^{13,14} This view has been qualified in a recent work where it was observed that

the lighter isotopic compositions seem to be linked to Cu release from the liver, regardless of whether this release is due to the medical treatment with a chelating agent or due to liver damage (cirrhosis).¹⁵ Although further studies with larger populations would be needed to fully understand Cu metabolism in relation to WD, Cu isotopic analysis seems to provide interesting information such as indications related to the evolution of the disease, the treatment and even the detection of patients that do not follow the treatment continuously.

On the other hand, studies about Cu bound to ceruloplasmin and/or free Cu (*i.e.*, Cu that is not bound to ceruloplasmin) are also increasing, as WD affects the binding of Cu to ceruloplasmin. In this context, concepts such as ultrafiltrable Cu (Cu UF), that is the Cu bound to low molar mass molecules (amino acids), and exchangeable Cu (Cu Exch), that corresponds to the Cu fraction that is not bound to ceruloplasmin and easily complexed with high-Cu-affinity chelating agents such as EDTA, have been described.^{25,26} Moreover, the relative exchangeable Cu (REC), which is calculated following the equation (1), has also been used in this context:

$$REC = \frac{Cu\ Exch}{Total\ Cu} \times 100 \dots\dots\dots(1)$$

El Balkhi *et al.* described a method to obtain Cu UF and Cu Exch and established reference values for healthy individuals²⁵. While Cu UF was found to be hardly relevant for WD diagnosis, Cu Exch and REC were proposed as new biological markers for WD diagnosis.¹⁷ Cu Exch seems to be related to liver failure¹⁶ and it is not specific to WD, but it could be useful also in this context. On the other hand, REC seems to be a sensitive and specific biomarker for WD diagnostics, providing values close to 100% in terms of sensitivity and specificity. However, different cutoffs are proposed by different authors.^{16-18,27,28} Hence, the necessity of following with the investigation.

This work aims to unify both types of studies, investigating the Cu concentration and the isotopic composition in both bulk serum (total Cu) and exchangeable Cu fractions (Cu Exch) from a series of healthy people (controls), patients with liver diseases different from WD, newborns, and WD patients under different treatments (chelators and/or Zn salts). The information obtained was also complemented with REC values to better understand WD and to diagnose this disease more efficiently.

2. Experimental

2.1 Instrumentation

Development and evaluation of the Cu Exch method was carried out with an ELAN DRC II quadrupole ICP-MS and a NexION 300X ICP-MS both from Perkin Elmer (Waltham, USA). The conventional configuration using a peristaltic pump to deliver the sample to the nebulizer was used as the sample introduction system. Conditions are shown in **Table 1**.

Table 1. ICP-MS spectrometer settings and data acquisition parameters for the determination of total Cu and Cu Exch in serum samples.

	NexION 300X ICP-MS	ELAN DRC II quadrupole ICP-MS	
	Continuous mode	Continuous mode	Time resolved analysis (TRA)
Sample uptake rate ($\mu\text{L min}^{-1}$)	300	100	100
Nebulizer gas, Ar (L min^{-1})	1.00	0.90	0.92
Plasma gas, Ar (L min^{-1})	15.00	17.00	17.00
Auxiliary gas, Ar (L min^{-1})	1.20	1.00	1.00
RF power (W)	1600	1000	1000
Dwell time (ms)	50	50	10
Gas / Flow reaction cell gas (mL min^{-1})	He / 1.5	NH_3 / 0.7	-
RPa	0	0	0
RPq	0.25	0.8	0.25
Signal acquisition	Continuous	Continuous	TRA
Nuclides monitored	$^{63}\text{Cu}^+$, $^{65}\text{Cu}^+$	$^{63}\text{Cu}^+$, $^{65}\text{Cu}^+$	$^{60}\text{Ni}^+$, $^{63}\text{Cu}^+$, $^{65}\text{Cu}^+$

Determinations of total Cu and Cu Exch in the samples were carried out with an ELAN DRC II quadrupole ICP-MS (Perkin Elmer, Waltham, USA). A PFA-ST MicroFlow Nebulizer (Elemental Scientific, Nebraska, USA) coupled to a twister cyclonic spray chamber (Glass expansion, Port Melbourne, Australia) was used for this purpose.

Cu isotopic analyses were carried out using a Nu 1700 MC-ICP-MS instrument (Nu Instruments, Wrexham, UK) coupled to an Aridus3 (Cetac Teledyne, USA) as desolvating system, which include a MicroMist 100 $\mu\text{L min}^{-1}$ nebulizer.

For sample digestion, an ULTRAWAVE microwave system (Milestone Inc., Shelton, USA) was used. An EVAPOCLEAN® unit (Analab, Bischheim, France) was deployed to evaporate samples by sub-boiling in Teflon vessels in a close environment. A Centrifuge 5810R (Eppendorf, Hamburg, Germany) was used for Cu Exch separation.

2.2 Materials and reagents

For Cu Exch separation, Amicon® Ultra-4 centrifugal filter devices with 30-kDa cut-off Ultracel® regenerated cellulose membrane from Merck Millipore (Cork, Ireland) were used. Ethylenediaminetetraacetic acid (EDTA) purchased from Sigma-Aldrich (St. Louis, USA) and potassium chloride (KCl) from Merck (Darmstadt, Germany) were also used for this purpose.

Poly-prep polypropylene chromatography columns (Bio-Rad, Temse, Belgium) and Cu-specific resin (Triskem, Bruz, France) were used for Cu isolation prior to isotopic analyses. For the preparation of the different eluting solutions, HCl 35% ultratrace ® (Scharlau, Barcelona, Spain) was used.

For quantitative analysis, single-element standard solutions of Cu and Ni (1 g L^{-1}), acquired from SCP SCIENCE (Villebon-Sur-Yvette, France) were used. For Cu isotopic analysis, NIST SRM 3114 (NIST, Gaithersburg, MD, USA) was chosen as a reference in the bracketing sequence. This standard shows a similar composition to the NIST 976, which is currently out of stock.²⁹ NIST SRM 986 (Ni) was used as internal standard for mass bias correction.

To evaluate the Cu Exch protocol, Seronom Trace Elements Serum level 1 (Lot: 1309438) and 2 (Lot: 1309416) (RM, Sero, Billingstad, Norway) were used. These reference materials were reconstituted with 3 mL of ultrapure water, according to the manufacturer's instructions.

Intra grade HNO₃ 70% (m m⁻¹) was purchased from JT Baker (New Jersey, USA) and further purified by sub-boiling in a PFA system (DST 1000, Savilex, Eden Prairie, USA). Ultrapure water (18.2 MΩ cm) was obtained from a Direct-Q3 system (Millipore, Molsheim, France).

2.3 Samples and sample preparation

Before analysis of the real samples, the protocol for obtaining the Cu Exch fraction was evaluated with serum reference materials, and the developed method was then applied to real samples (see explanation hereinafter). In this process, it was also necessary to carry out the total Cu determination to corroborate that the analyses were done under optimal conditions and, also, to calculate the REC. For that purpose, the serum reference materials (L-1 and L-2) were diluted 30 times with 2% v v⁻¹ HNO₃.

Serum samples from 55 volunteers were obtained from the Hospital Miguel Servet (Zaragoza, Spain). Thirteen of these samples were controls, fourteen originated from patients with hepatic disorders (different from WD), eight came from newborns/infants and twenty samples originated from WD patients. The principles outlined in the declaration of Helsinki regarding all the experimental research involving humans or animals were followed.

To avoid sample contamination, the sample preparation was done in an ISO 5 laminar bench flow fitted in an ISO 7 clean lab.

Each serum sample was split into two fractions, one for total Cu and the other for Cu Exch determination. For each fraction both Cu determination and isotopic analysis was carried out.

The first step was to obtain the Cu Exch fraction. The procedure proposed by El Balkhi *et al*²⁵ was followed but, instead of using NaCl, KCl was selected to avoid the introduction of additional sources of Na, thus preventing spectral overlaps (⁴⁰Ar²³Na⁺) for ⁶³Cu⁺ in the ICP-MS. Then, in order to obtain the Cu Exch fraction, 200 μL of serum were mixed in an Eppendorf tube with 200 μL of 3 g L⁻¹ EDTA in 0.9% (m m⁻¹) KCl. The tube was then vortexed for 20 s. After that, the mixture was incubated for at least 1 hour to ensure that the equilibrium of Cu Exch between proteins and EDTA had been achieved. The mixture (400 μL) was then transferred to the Amicon® Ultra-4 centrifugal filter with a 30-kDa cut-off membrane to be centrifuged for 45 min at 2000 g at 4 °C. For Cu Exch determination, 100 μL of the filtration were transferred to another centrifuge tube and diluted with 2% v v⁻¹ HNO₃ up to 1 mL. The rest of the filtrate was kept for isotopic analysis.

To save sample (as a limited amount was available), total Cu determination was carried out after sample preparation (Cu isolation) for isotopic analysis, as mentioned below.

For isotopic analysis, both the total Cu fraction (bulk serum) and the Cu Exch fraction (after ultrafiltration step) were treated in the same way. The first step for Cu isolation was sample digestion. For that purpose, 0.15 - 0.5 mL of bulk serum and the remaining amount of the Cu Exch fraction, around 0.15 mL (note that the exact sample volumes depend on the total sample amount available), were mixed in quartz vials with 3 mL of 14 M HNO₃ and were digested in a microwave system following the program recommended by the manufacturer for blood. The digest was then transferred to Teflon Savillex® vials to be evaporated until almost dryness at 95 °C using an EVAPOCLEAN system.

Once the digestion and the evaporation were concluded, Cu isolation was carried out using a Triskem Cu specific resin following the method proposed by Miller *et al.*³⁰⁻³² which was further validated for serum samples in our research group.¹⁵ The evaporated fraction was redissolved in 500 µL of 12 M HCl and heated at 120 °C in a closed Teflon Savillex® vial for 24 h, to ensure that Cu is found in its chloride form at the highest oxidation state. Then, the sample was evaporated until almost dryness in the EVAPOCLEAN system and redissolved in 4 mL of 5 mM HCl. This process was repeated twice to ensure that excess HCl was eliminated. The chromatographic columns were prepared adding 0.5 mL of Triskem Cu specific resin into the Bio-Rad Poly-Prep columns. A piece of cotton was used as stopper on the top of the resin. The resin was soaked in 20% v v⁻¹ EtOH aqueous solution overnight before its use, as recommended by the manufacturer. The chromatographic separation was carried out as described elsewhere for serum samples¹⁵ and the protocol is summarized in **Table 2.**

Table 2. Protocol for Cu isolation with the anion exchange Cu specific resin (Triskem)

Step	Volume (mL)	Medium
Resin loading	0.5	Cu-specific
Cleaning	10	6 M HCl
Conditioning	10	5 mM HCl
Sample load	4	5 mM HCl
Matrix elution	40	5 mM HCl
Cu elution	10	6 M HCl

The Cu fraction obtained was then evaporated until almost dryness at 95 °C in an EVAPOCLEAN system and redissolved in 50 µL of 2% v v⁻¹ HNO₃

For total Cu determination using the ICP-MS, the fraction of total Cu was spiked with Ni at a final concentration of 50 µg L⁻¹, as this element was chosen as internal standard.

For isotopic analysis, both fractions (total Cu and Cu Exch) for each sample were divided into 6 groups, depending on the total Cu concentration. The Cu concentration was adjusted with 2% v v⁻¹ HNO₃ to 50, 100, 150, 200, 350, and 1000 µg L⁻¹, matching with the standard used for the bracketing correction method to avoid additional mass bias. Moreover, the samples were spiked with Ni (NIST 986) at a final concentration of 2 mg L⁻¹, to have enough sensitivity, as this element was selected as internal standard for mass bias correction.

2.4 Measurement protocol

2.4.1 Determination of both exchangeable Cu and total Cu.

The ICP-MS was optimized daily for maximum stability and sensitivity.

The evaluation of the Cu Exch protocol was carried out in two different laboratories as commented previously (in Zaragoza using the Perkin Elmer Nexion 300X and in Pau using the Perkin Elmer DRC II). The measurement for both total Cu and Cu Exch were carried out in continuous mode under the conditions shown in **Table 1**. Quantitative results were obtained using a calibration curve between 5 and 100 µg L⁻¹. In all cases, three replicates per sample were measured.

Exchangeable Cu determination in real samples was carried out in continuous mode with the ELAN DRC II ICP-MS using the reaction cell with NH_3 gas, to minimize spectral overlap. The instrument and data acquisition parameters used during these analyses are gathered in **Table 1**. For quantification, a calibration curve between 1 and 10 $\mu\text{g L}^{-1}$ Cu was used.

As the sample volume was limited and in order to keep the maximum of this volume for MC-ICP-MS analysis, total Cu determination in real samples was performed using time-resolved analysis (TRA) *via* the direct μ -injection method developed and evaluated by our research group.¹⁵ In this case, the sample introduction system consisted of a PFA-ST MicroFlow Nebulizer with a capillary sampling tube of 0.25 mm internal diameter mounted in a peristaltic pump. This capillary was connected to a PVC tubing (orange-blue tube, ID 0.25 mm x OD 2.07 mm from Glass Expansion), which in turn was connected to another additional capillary tube of 0.25 mm ID in the other end (external capillary) functioning as a sample probe. During the analysis, except for the time of sample introduction, a solution of 2% v v⁻¹ HNO_3 was continuously aspirated to rinse the system. For that purpose, the external capillary was introduced into the vial with the HNO_3 solution. For sample injection, the external capillary was disconnected from the peristaltic pump tube, for a few seconds and, after that, 1 μL of sample was introduced into the air space formed in the peristaltic pump tube with the help of an electronic micropipette. After the injection, it was necessary to wait for a few seconds before reconnecting the external capillary to the peristaltic pump tube to obtain a well-defined peak (See **Figure S1**, supplementary information). For quantitative results, a Cu calibration curve between 0.1 and 20 mg L^{-1} , spiked with Ni as IS (at a final concentration of 50 $\mu\text{g L}^{-1}$), was measured. The instrument and data acquisition parameters used for total Cu determination are gathered in **Table 1**. Peak area was used for quantification, and three replicates per sample were carried out.

2.4.2 Determination of Cu isotope ratios

The optimization of the MC-ICP-MS instrument coupled to a Teledyne CETAC Aridus3 Desolvating Nebulizer System was carried out in continuous mode with a solution at 50 $\mu\text{g L}^{-1}$ as both Cu and Ni, aiming at maximum sensitivity and stability. Note that the Aridus3 was not connected to an additional nitrogen flow, our experience having shown that this did not bring any improvement in sensitivity on our Nu1700 instrument. The low-resolution mode was used to maximize the sensitivity, considering that Cu had been isolated from the samples

before the analysis, thus minimizing the risk for spectral overlap. The instrumental parameters selected are summarized in **Table 3**.

Table 3. Instrumental conditions for Cu isotopic analysis of serum using direct injection to MC-ICP-MS.

Desolvating Nebulizer System ARIDUS3																					
N ₂ Gas (mL min ⁻¹)										0											
Ar Gas (L min ⁻¹)										8											
Chamber Temperature (°C)										140°C											
Membrane temperature (°C)										160°											
Nu MC-ICP-MS 1700																					
RF Power (W)										1300											
Instrument resolution										Low											
Integration time (s)										0.5											
Nebuliser Pressure (Psi)										35.10 – 35.30 ^a											
Auxiliary gas (L min ⁻¹)										0.8											
Coolant gas (L min ⁻¹)										13											
Faraday cup configuration																					
Collect or	H9	H8	H7	H6	H5	H4	H3	H2	H1	Ax	L1	L2	L3	IC0	IC1	IC2	L4	IC3	L5	IC4	L6
m/z	66, 6	6 6		6 5			6 4			63			6 2						6 0		

a: optimized daily

For isotopic analysis, sample introduction was carried out in a similar way as for the determination of total Cu (*cf.* section 2.4.1), but, in this case, 3 µL of pre-treated sample were injected instead of 1 µL, and the sample was introduced by self-aspiration (no peristaltic pump was used). For that purpose, the sample was directly injected into the nebulizer tubing (1.3

mm OD x 0.25 mm ID) with an electronic micropipette. Under these conditions, the signal duration was around 30 - 40 seconds (See **Figure 2S**, supplementary information), depending on the Cu concentration. Between injections, a 2% v v⁻¹ HNO₃ solution was aspirated for cleaning. Five measurements were carried out per sample following a standard-sample-standard bracketing sequence using NIST 3114 as standard. Cu isotopic ratio calculations were carried out with the Linear Regression Slope (LRS) method. With this method, values obtained for both Cu isotopes are confronted to obtain a linear regression. The Cu isotope ratio is calculated as the slope of this regression.³³ For mass bias correction, a combination of internal normalization according to the exponential model described by Maréchal *et al.*³⁴ using the ⁶²Ni/⁶⁰Ni ratio, following the equation (2) and (3) and the standard-sample-standard bracketing sequence with the NIST 3114 were used.

$$R_{Cu} = r_{Cu} \times \frac{1}{\left(\frac{65}{63}\right)^f} \quad (2)$$

Where R_{Cu} is the real ⁶⁵Cu/⁶³Cu isotope ratio, r_{Cu} is the measured isotope ratio and f is the exponential fractionation coefficient calculated following the equation (3)

$$f = \frac{\ln \frac{r_{Ni}}{R_{Ni}}}{\ln \frac{62}{60}} \quad (3)$$

Where R_{Ni} is the real of ⁶²Ni/⁶⁰Ni value and r_{Ni} is the measured value.

Finally, the results were expressed as delta values (δ),³⁵ *i.e.*, as a relative difference (in per mil) versus a reference (NIST 3114) following equation (4):

$$\delta^{65}Cu (\text{‰}) = \frac{R_{sample} - R_{STD}}{R_{STD}} \times 1000 \quad (4)$$

where R_{sample} is the $^{65}\text{Cu}/^{63}\text{Cu}$ isotope ratio determined for a given sample and R_{STD} is the average $^{65}\text{Cu}/^{63}\text{Cu}$ isotope ratio determined for the standards measured before and after that particular sample.

3. Results and discussion

3.1 Evaluation of the method for Cu Exch determination

To determine Cu Exch, careful sample preparation is mandatory. To evaluate the method and validate the results before real sample analyses were conducted, an interlaboratory study was performed. The same serum reference material (L-1 and L-2) were subjected to the Cu Exch separation procedure (as explained in section 2.3), and subsequent analyses in two different laboratories, one in Pau (France) and the other in Zaragoza (Spain), were carried out. In addition to Cu Exch, total Cu was also determined, and REC was calculated following equation (1). The results obtained are shown in **Table 4**. The total Cu concentration values observed in both laboratories slightly differ (higher levels were obtained in Zaragoza), but both concentrations are within the concentration range provided by the reference material. These differences may be due to small variations in the sample preparation facilities, because the reference material is freeze-dried and it is necessary to reconstitute it. Cu Exch values follow the same trend (a bit higher values are obtained in Zaragoza), but the REC values are rather similar in both cases, which points to differences in the reconstitution step, as was commented before. The results were overall considered as fit-for-purpose, and analysis of the real samples was undertaken next.

Table 4. Results obtained by the two laboratories for analysis of serum RM. Results are expressed as $\bar{x} \pm U$, where $U = (t.s)/\sqrt{n}$ for a 95% confidence interval.

	Pau			Zaragoza			Serum Reference material
	Total Cu (mg L ⁻¹)	Cu Exch (µg L ⁻¹)	REC (%)	Total Cu (mg L ⁻¹)	Cu Exch (µg L ⁻¹)	REC (%)	Total Cu (mg L ⁻¹)
CRM L-1	1141 ± 20	362 ± 35	32 ± 3	1258 ± 37	424 ± 10	33 ± 1	1066 ± 215
CRM L-2	1901 ± 61	1260 ± 51	66 ± 3	2009 ± 90	1419 ± 109	71 ± 3	1925 ± 387

Once the Cu Exch separation protocol was evaluated in terms of Cu recovery, mass fractionation during the whole analytical procedure was investigated. The whole analytical procedure includes the procedure for Cu Exch separation and the procedure for Cu isotopic isolation. Cu isotopic isolation is mandatory before isotopic analysis to minimize mass bias³⁵ due to both space charge effect³⁶ and spectral overlap. In the case of Cu, both Cu isotopes may suffer spectral overlap in ICP-MS. The principal problem is that serum samples contain high Na level (around 3000 mg L⁻¹) and ²³Na⁴⁰Ar shows the same nominal mass as ⁶³Cu. The same occurs with the presence of Mg (around 20 mg L⁻¹) because ²⁵Mg⁴⁰Ar overlaps with ⁶⁵Cu when the spectrometer is operated in the low-resolution. For Cu isolation, a Cu specific ion-exchange resin (Triskem) was used following the procedure proposed by K.A. Miller^{30,31} and validated in our group for serum samples.¹⁵ To verify that no mass fractionation occurs during these sample preparation steps, three aliquots of NIST 3114 were subjected to both procedures consecutively, as detailed in section 2.3. After the two consecutive protocols, each aliquot was adjusted to a different Cu concentration for analysis: 250, 500, and 1000 µg L⁻¹.

Before these measurements (in TRA mode), the MC-ICP-MS coupled to the desolvating nebulizer system was optimized and the performance was checked in continuous mode. For

this purpose, a mixture of NIST 3114 (Cu) and NIST SRM 986 (Ni) at a final concentration of 2 mg L⁻¹ for each element was used. The $^{65}\delta$ value was calculated using the self-bracketing method ($^{65}\delta$ value expected is 0). This method follows equation (2) but, in this case, the standard is considered as standard and as sample at the same time, except for the first and the last measured standards, which are only considered as standards. Moreover, Ni was used for mass bias correction. The average $^{65}\delta$ value obtained was $0.00 \pm 0.18 \text{ ‰}$ (n=10, 2SD).

Next, isotopic analyses in TRA mode were performed, using the direct μ -injection method. 10 replicates per sample were measured, and the results were expressed as $^{65}\delta$ value, with the standard-sample bracketing method, where the standard is the NIST 3114, and the sample is the NIST 3114 after suffering the two consecutive sample preparation procedures (Cu Exchange separation and Cu isolation). If no isotope fractionation is present, the recorded $^{65}\delta$ value should be 0. Results obtained are shown in **Table 5** and external precision is expressed as 2SD in ‰. As can be seen from this table $^{65}\delta$ values were around 0, meaning that under our conditions no detectable fractionation occurs during both procedures.

Table 5. Results obtained with the μ -injection method through the analysis of the 3 μ L of NIST3114 after the two consecutive procedures at different concentrations using the LRS method for the isotopic calculation

Cu concentration ($\mu\text{g L}^{-1}$)	Cu mass (ng)	$\delta^{65}\text{Cu}$ " bracketting", $\pm 2\text{SD (‰)}$, (n=10)
250	0.75	-0.18 ± 0.24
500	1.5	-0.05 ± 0.26
1000	3	0.11 ± 0.19

These results are in accordance with previous investigations. In fact, a similar procedure was also validated by Lawens *et al.*³⁷ In that case, a different procedure was carried out for Cu isolation using the AG-MP-1 resin, which had already been proved not to induce Cu fractionation in serum samples.¹³ Additionally, the Cu isolation procedure using the Cu-specific resin had also been validated for avoiding fractionation during the Cu isolation process.¹⁵

3.2 Analysis of the samples for total copper, exchangeable copper and REC

To interpret these analyses, the samples were divided into four different groups: controls (healthy patients, C), patients with hepatic disorders different from WD (HD), newborns/infants (NB) and WD patients (WD).

Total Cu determination was carried out after the procedure for Cu isolation with an ion-exchange resin (see section 2.3), to save sample for other tests because the amount of sample available was limited. The analysis was carried out as explained in section 2.4, and the results obtained are displayed in **Figure 1**.

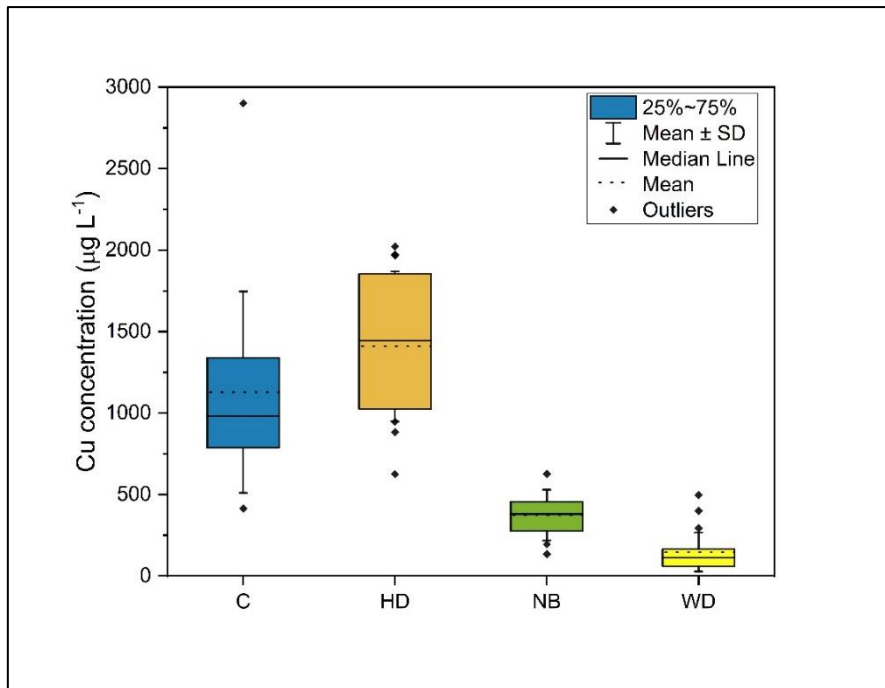


Figure 1. Results of total Cu determination of serum samples of the four different groups considered in this study after Cu isolation step with Cu specific resin (Triskem). C refers to control samples, HD to hepatic disease patients, NB to newborns and WD to Wilson's disease patients.

The Cu concentration obtained for WD patients, regardless of the treatment, ranged between 49 and 498 $\mu\text{g L}^{-1}$ (mean value = 147 $\mu\text{g L}^{-1}$). For newborns and infants, the concentration found varied between 134 and 626 $\mu\text{g L}^{-1}$ (mean value = 373 $\mu\text{g L}^{-1}$). For controls and patients with other liver disorders, values between 414 and 2901 $\mu\text{g L}^{-1}$ (mean value = 1128 $\mu\text{g L}^{-1}$), and between 625 and 2022 $\mu\text{g L}^{-1}$ (mean value = 1410 $\mu\text{g L}^{-1}$), respectively, were observed. According to these results, WD patients show lower Cu levels than the rest of the groups tested in this work. However, some overlapping between WD patients Cu levels and those of the rest can be observed, and particularly with newborns and infants, as reported elsewhere.^{13,15} This confirms that total Cu determination is useful, but it is not a selective biomarker for WD diagnosis.

Exchangeable copper (Cu Exch) has been defined as the fraction of Cu that is not bound to ceruloplasmin, which means that this Cu fraction is bound to albumin and to a lesser extent, to transcuprein (alpha-2-macroglobulin) (α -2M)), and to amino acids. Analysis was carried out as described in section 2.4.1. The results are plotted in **Figure 2**.

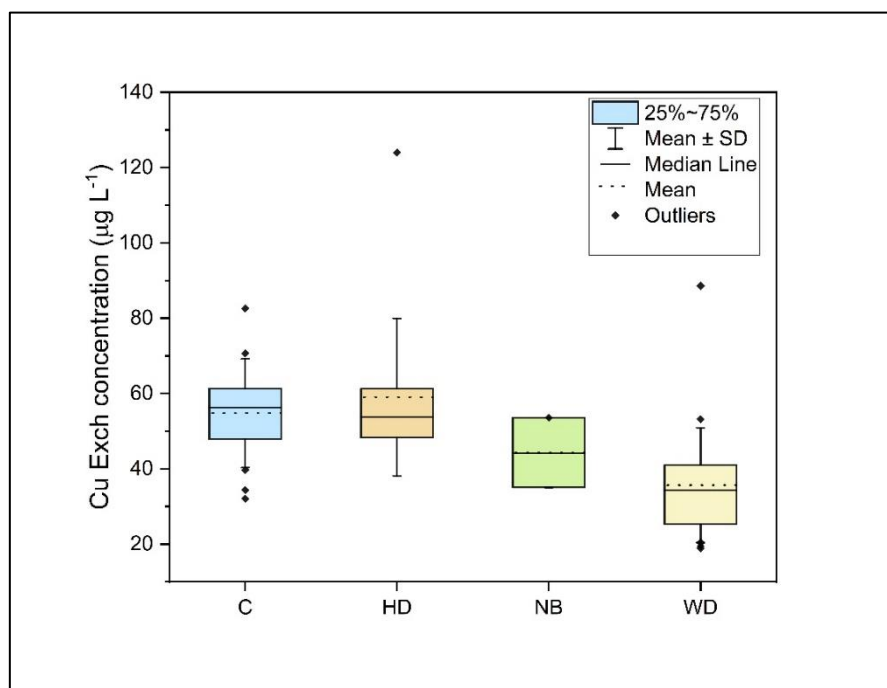


Figure 2. Results of Cu Exch levels of serum samples of the four different groups considered in this work. C refers to control samples, HD to hepatic disease patients, NB to newborns and WD to Wilson's disease patients.

No differences were found among the four groups regarding Cu Exch (see **Figure 2**). Cu Exch concentration found in WD patients ranged between 19.5 and 88.6 $\mu\text{g L}^{-1}$ (mean = 36 $\mu\text{g L}^{-1}$), overlapping with the Cu Exch found in the controls, patients with other liver disorders and newborns/infants, which showed ranges of 32.1 - 70.7 $\mu\text{g L}^{-1}$ (mean = 55 $\mu\text{g L}^{-1}$), 42.7 - 124.0 $\mu\text{g L}^{-1}$ (mean = 59 $\mu\text{g L}^{-1}$) and 13.9 - 47.6 $\mu\text{g L}^{-1}$ (mean = 37 $\mu\text{g L}^{-1}$), respectively. The results obtained in this study for the controls agree with the reference values established by El Balkhi *et al*²⁵ for Cu Exch and also for WD patients, although the number of patients

analyzed in the current study is small. In studies with animal models, Schmitt *et al.*¹⁶ observed that Cu Exch values were correlated with acute liver disease and with the dietary Cu intake. Guillaud *et al.*¹⁸ observed for humans that Cu Exch levels were higher for WD patients (symptomatic when diagnosed) and for patients that did not follow the treatment correctly with respect to those WD patients that followed the treatments properly or were asymptomatic; and also, Cu Exch values were high in patients with other liver disorders, depending on the stage of the disorder. Moreover, an overlapping was found for Cu Exch levels obtained for WD patients under treatment and for patients with other liver disorders, which agrees with our results. It is necessary to remark that all WD patients analyzed in this study were under treatment, except for one patient. Moreover, a patient who was not following the treatment correctly was also identified. Such patient presents the highest Cu Exch level ($88.6 \mu\text{L L}^{-1}$), which again agrees well with the report by Guillaud *et al.*¹⁸

On the other hand, the WD patient without treatment shows a Cu Exch level of $38.4 \mu\text{L L}^{-1}$, which seems to be low for a patient newly diagnosed and without any treatment. However, this patient was asymptomatic at the moment of blood collection, which agrees with a previous work.¹⁸ In view of the results, it is possible to state that Cu Exch determination by itself is not enough for reliable WD diagnosis. However, it could be used to follow up the evolution of the disease. In any case, further studies with a larger population are needed to verify these aspects, although it is always hard to carry out such studies when dealing with a rare disorder such as WD.

Relative exchangeable copper (REC) is a parameter of increasing interest. It is indeed promising as a sensitive and specific test for WD. It is calculated as indicated in Eq (1), dividing the Cu Exch by the total Cu expressed in %.

The results obtained show differences between REC values for WD patients and for the other group of persons subjected to study. WD patients show higher REC% than the other groups tested (see **Figure 3**). In particular, the REC obtained for WD patients fall in the range between 17.8 and 64.7%, while the rest of the groups show REC values between 2.3 and 14.9%. With the population under study, a cutoff of 17 %, REC would offer a selectivity and a specificity of 100% for detection of WD. The current work indicates that REC seems to be a useful parameter with the capacity to identify WD patients from other groups. It is even possible to differentiate WD patients from healthy newborns, which indicates that this biomarker could be used in neonatal screening programs.

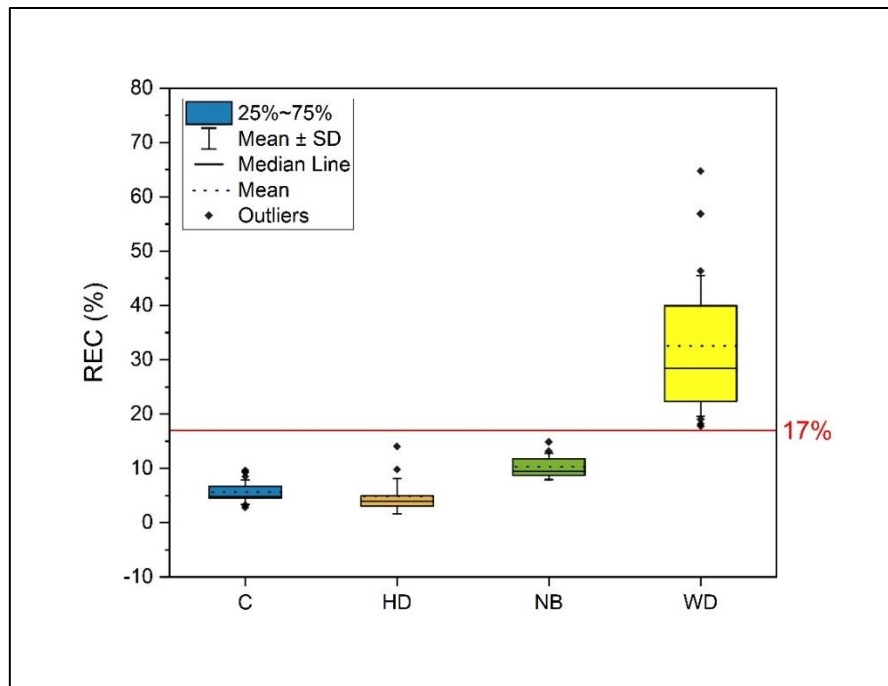


Figure 3. Results of REC of serum samples of the 4 different groups considered in the current work. C refers to control samples, HD to hepatic disease patients, NB to newborns and WD to Wilson's disease patients.

Similar conclusions have been drawn in the literature, although the cutoff value is not clearly defined in those works. In their first study with REC, El Bakhi *et al*¹⁷ found a cutoff of 18.5%

providing a 100% sensitivity and specificity for distinguishing WD patients from controls, wild-type homozygous and heterozygous. Guillaud *et al.*¹⁸, on the other hand, could also distinguish WD patients from controls (patients with hepatic disease different to WD) using the REC. A cutoff of 18.5 % was set taking into account only WD patients sampled at the moment of diagnosis or who failed to respond to treatment because of non-compliance. However, if WD patients on stable condition under medical treatment were also included, the cutoff decreased to 14 % and provided one false positive. Moreover, they found that the REC was not influenced by the presence of hepatic disorders being indistinguishable from healthy controls. Also, no differences in the REC values were observed between WD patients with/without cirrhosis. Trocello *et al.*²⁷ used the REC for family screening and showed that, setting a cutoff of 15%, it was possible to differentiate WD patients from the subjects without WD (ATP7B Heterozygous carrier and without mutation) with 100% of sensitivity and specificity. On the other hand, in studies with animals where it is possible to control almost all the external parameters, Schmitt *et al.*¹⁶ found that, with a cutoff of 19 %, it was possible to discriminate Long-Evans Cinnamon rats (LEC, with an ATP7B mutation causing WD) from Long-Evans rats (LE, without any mutation) with a sensitivity of 97.3% and specificity of 100%. They also showed that the REC is not influenced by the presence of liver damage or by the Cu intake. In another animal model, Heissat *et al.*²⁸ set a cutoff at 20% for achieving a sensitivity and specificity of 100% between WD rats and wild-type rats. In a recent study, subjects with alcoholic cirrhosis showed REC values \leq 19%, except for two patients showing REC values of 21 and 25%.³⁷ However, no genetic tests were carried out in that work to investigate the potential disease of such patients.

Overall, according to our results as well as those previously published, the REC value was found to be a sensitive and specific tool for diagnosing WD. However, further studies (with a

higher number of both WD and controls) are needed to be able to set a reliable and constant cutoff for the REC, and to know the limitations of this biomarker.

3.3. Isotopic analysis

To interpret these analyses, the samples were divided into six different groups: controls (healthy patients, C), patients with hepatic disorders different from WD (HD), healthy infants and newborns (NB), WD under treatment with a chelator (WD-C), WD under treatment with a Zn salt (WD-Zn) and one sample from a WD patient obtained at the moment of diagnosis, without any treatment (WD).

Next, these samples were analyzed for Cu isotopic composition in both bulk serum and the Cu Exch fraction. Five replicates per sample were carried out, following the bracketing sequence (standard-sample-standard), using the NIST 3114 as standard. After the measurements, the results were corrected for mass bias using Ni and expressed as delta value ($\delta^{65}\text{Cu}$), following the equation (4). **Figure 4** shows the results of $\delta^{65}\text{Cu}$ (‰) obtained in both bulk serum (dark colors) and Cu Exch fraction (light colors) for the samples under investigation.

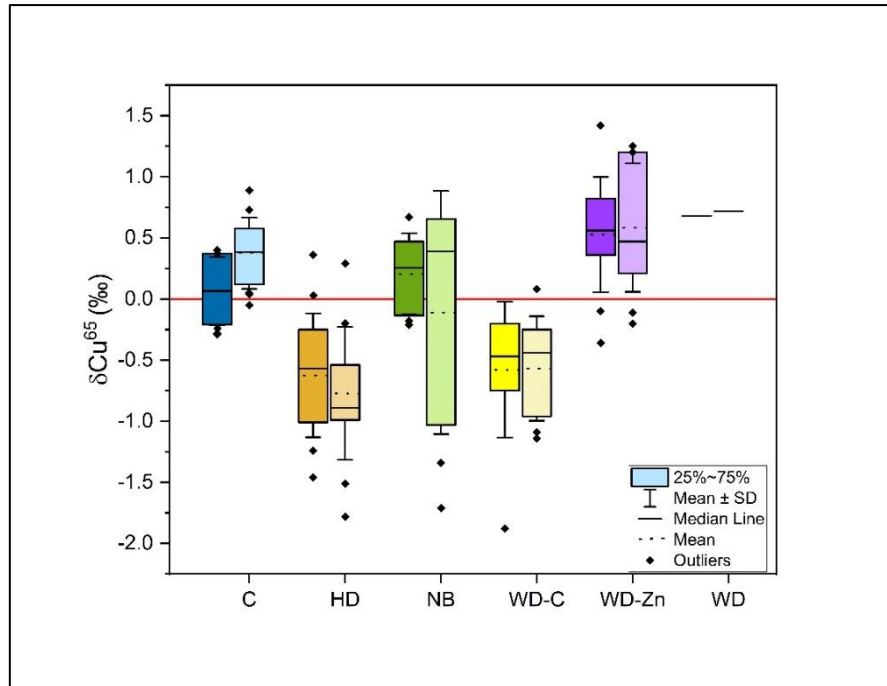


Figure 4. Boxplot obtained for Cu isotopic composition, expressed as $\delta^{65}\text{Cu}$ (‰) of both fractions of serum samples analyzed (Bulk serum, dark colors, and Cu Exch fraction, light colors) for the six different groups considered in this investigation. Where, C refers to control samples, HD to hepatic disease patients, NB to newborns and WD-C to Wilson's disease patients under chelator treatment, WD-Zn to Wilson's disease patients under zinc salts treatment and WD to Wilson's disease patients at the moment of diagnosis,

Isotopic composition in bulk serum for control subjects show $\delta^{65}\text{Cu}$ values around 0 with an average $\delta^{65}\text{Cu}$ value of $0.06 \pm 0.28\text{‰}$ (expressed as $\bar{x} \pm \text{SD}$). Patients with other hepatic disorders show an average $\delta^{65}\text{Cu}$ of $-0.62 \pm 0.51\text{‰}$. Results obtained for newborns show $\delta^{65}\text{Cu}$ values around 0 or positive, with an average value of $0.21 \pm 0.33\text{‰}$. For WD patients under treatment with a chelator (WD-C), a negative $\delta^{65}\text{Cu}$ value was found, with an average value of $-0.58 \pm 0.56\text{‰}$, while WD patients under treatment with Zn salts (WD-Zn) show positive delta values, with an average value of $0.53 \pm 0.47\text{‰}$. In the latter group, there is an exception that shows a negative $\delta^{65}\text{Cu}$ (-0.36‰). This sample corresponds to the same patient that showed a $\delta^{65}\text{Cu}$ of -1.88‰ , in the group of WD under chelator treatment (value

outside the boxplot for WD-C) in a previous sampling when the patient was under treatment with both a chelator and a Zn salt. That means that when the patient stopped the treatment with the chelator keeping only the Zn salt treatment, the $\delta^{65}\text{Cu}$ shifted to heavier values. However, it is still negative. The sample of the patient (asymptomatic) at the moment of the WD diagnosis shows a $\delta^{65}\text{Cu}$ of 0.68‰.

Results of $\delta^{65}\text{Cu}$ obtained in bulk serum for controls were statistically equal to the results reported in the literature.³⁷⁻³⁹ Results obtained for patients with other hepatic disorders seem to be lighter than the results obtained for the control patients and they agree with previously published results.^{37,39,40} For newborns, the results obtained are similar to the values obtained for the controls, and also they agree with previous reported data.¹⁵ In the same way, the results obtained for WD, regardless of treatment, are in agreement with the results reported in the literature.¹⁵ The $\delta^{65}\text{Cu}$ values for WD patients treated with a chelator are lighter than for WD patients treated with Zn salts, and they are comparable with the $\delta^{65}\text{Cu}$ obtained for patients with other hepatic problems. That is coherent with the hypothesis of ^{63}Cu being preferably accumulated in the liver, and the negative delta values being due to Cu released from the liver, either by the treatment with a chelator or by liver disorders, postulated in a previous publication.¹⁵

On the other hand, the isotopic composition in the Cu Exch fraction shows average $\delta^{65}\text{Cu}$ values of $0.38 \pm 0.29\text{‰}$ for control subjects. For patients with hepatic disorders (no WD) the average value is $-0.77 \pm 0.54\text{‰}$, while the newborns show a mean value of $-0.11 \pm 0.99\text{‰}$. For WD patients under chelating treatment, the mean value of $\delta^{65}\text{Cu}$ is $-0.57 \pm 0.43\text{‰}$, while for the patient under Zn salt treatments, this value is $0.58 \pm 0.53\text{‰}$. The WD patient without any treatment (at the moment of WD diagnosis) shows a positive delta value of 0.72‰ .

Results of $\delta^{65}\text{Cu}$ obtained in the Cu Exch fractions seem to follow the same trend as $\delta^{65}\text{Cu}$ obtained in bulk serum. That means lighter values were observed for patients with hepatic problems and WD patients under chelating treatment, while heavier values were found for controls, WD patients under Zn salt treatment, and for the only sample of WD without treatment and asymptomatic. In the case of newborns/infants, there is a very high variability in comparison with bulk serum.

To enable direct comparison of the results obtained in both fractions (bulk serum and Cu Exch) for the same sample, the $\Delta^{65}\text{Cu}$ values were calculated following the equation (5) and are plotted in **Figure 5**.

$$\Delta^{65}\text{Cu} = \delta^{65}\text{Cu}_{\text{Exch}} - \delta^{65}\text{Cu}_{\text{bulk serum}} \quad (5)$$

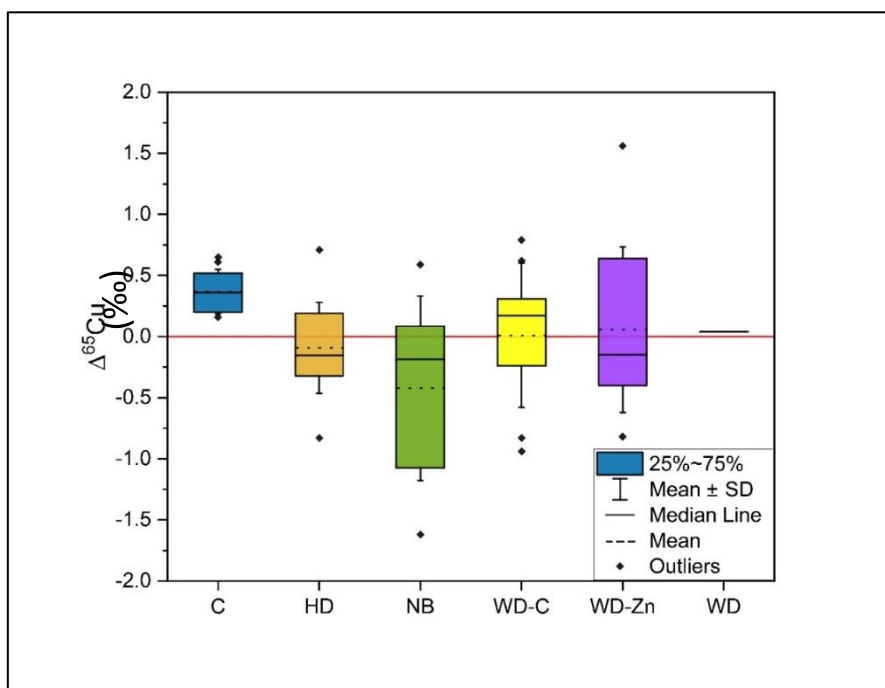


Figure 5. Boxplot obtained for $\Delta^{65}\text{Cu}$ (‰) for the six different groups considered in the current study. C refers to control samples, HD to hepatic disease patients, NB to newborns and WD-C to Wilson's disease patients under chelator treatment, WD-Zn to Wilson's disease patients under zinc salts treatment and WD to Wilson's disease patients at the moment of diagnosis,

It is possible to observe that the only group that follows a clear trend is the control group. In this group, it is possible to observe that, in all cases, the isotopic composition of Cu Exch fraction shifts to heavier values compared to the isotopic composition in bulk serum. Meanwhile, for the rest of the samples under investigation, a high variability between them prevents obtaining a clear conclusion.

The average $\Delta^{65}\text{Cu}$ value for control subjects was $0.37 \pm 0.18\text{‰}$. For patients with other hepatic disorders, the average $\Delta^{65}\text{Cu}$ was $-0.09 \pm 0.37\text{‰}$. Newborns and infants, show an average value of $\Delta^{65}\text{Cu}$ $-0.42 \pm 0.75\text{‰}$. WD patients, show average values of $0.01 \pm 0.59\text{‰}$ and $0.06 \pm 0.68\text{‰}$ for patients under chelator treatment or under treatment with Zn salts, respectively.

The mean value obtained for controls is in agreement with the result obtained by Lauwens *et al.*³⁷ ($0.41 \pm 0.15\text{‰}$). On the other hand, Tennant *et al.*⁴¹ via computational calculation obtained that $\delta^{65}\text{Cu}_{\text{albumin}}$ should be around 60% heavier than $\delta^{65}\text{Cu}_{\text{bulk serum}}$, assuming that serum consists of 10% albumin and 90% ceruloplasmin. In that study, healthy patients (controls) show an average $\delta^{65}\text{Cu}_{\text{albumin}}$ 37% heavier than in bulk serum. Our results show the same trend, but the differences between $\delta^{65}\text{Cu}_{\text{Exch}}$ and $\delta^{65}\text{Cu}_{\text{bulk serum}}$ are not so significant because not all Cu-Exch is bound to albumin. Cu may also be loosely bound to other proteins, α -2M and other low molar mass molecules, such as amino acids³⁷ which were not taken into account for the computational calculation. Moreover, the nature of these compounds might be highly variable among subjects belonging to the same group.

The mean value obtained for patients with hepatic disorders (not WD) is also in agreement with the value reported previously (give the values).³⁷ Despite this fact, it was not possible to find any clear trend, as both positive and negative $\Delta^{65}\text{Cu}$ were observed. The same occurs

for WD independently of the treatment, and for newborns and infants where the variability in the results is high.

To try to explain the variability in the $\Delta^{65}\text{Cu}$, it is important to keep in mind that the liver is the principal source of serum proteins. Liver disorders or liver immaturity (in the case of newborns) can affect hepatic metabolism, causing changes in the levels of some proteins (such as ceruloplasmin, $\alpha_2\text{M}$, amino acids, etc.) and in the coordination environment of Cu affecting to the isotopic composition. Moreover, it has to be taken into account that isotopic fractionation in general is influenced by the ligand coordination and by the oxidation state^{42,43}. Generally, heavy isotopes prefer bonding with ligands with stronger electronegativity ($\text{O} > \text{N} > \text{S}$). Specifically, if the metal is in its highest oxidation state. Therefore, it will be expected to have a lighter isotopic composition in Cu bound to cysteine or methionine (Cu-S) than Cu bound to histidine (Cu-N).

In control patients, it is possible to see a clear trend for $\Delta^{65}\text{Cu}$. Not all healthy bodies are equal, but they tend to work similarly. However, for the rest, since Cu can bond to different molecules depending on the disorder and on its state, it seems not feasible to appreciate a clear trend above the variability. Information about patients in terms of ceruloplasmin, albumin levels, $\alpha_2\text{M}$, etc. was not available for this study, which could enhance the understanding about this topic.

4. Conclusion

This work examines the potential of Cu speciation and Cu isotopic analysis in serum samples in both bulk serum and Cu Exch fraction for WD diagnosis and follow up.

The REC was observed to be the only parameter able to differentiate all WD patients from non-WD patients, regardless of their symptoms. The rest of parameters obtained can be used for following the disease and the treatment. The less useful parameter was the isotopic

analysis in the Cu Exch fraction, because high variability was found in all the patients tested, except for the controls. More information about levels of ceruloplasmin, albumin, transaminases; aminoacids, etc. might help to better interpret these results.

The fact that REC is the parameter that promises to be able to diagnose WD even in newborns, before symptoms appear, is very good news. To calculate the REC, only the total Cu concentration and the Cu Exch concentrations are necessary. This information can be obtained in an easy way, which permits to carry out this determination routinely in hospitals, using techniques such as AAS and ICP-MS that already are implements in their labs.

However, more studies about the REC are still needed in order to set a universal cut-off value and to establish the reliability of this test.

Acknowledgements

The authors are grateful to the European Regional Development Fund for financial support through the Interreg POCTEFA EFA 176/16/DBS, as well as to project PGC2018-093753-B-I00 (MCIU/AEI//FEDER,UE) and the Aragon Government (Construyendo desde Aragón).

5. References

- 1M. Schaefer and J. D. Gitlin, *Am. J. Physiol.-Gastrointest. Liver Physiol.*, 1999, **276**, G311–G314.
- 2S. Lutsenko and M. J. Petris, *J. Membr. Biol.*, 2003, **191**, 1–12.
- 3J. D. Gitlin, *Gastroenterology*, 2003, **125**, 1868–1877.
- 4A. Ala, A. P. Walker, K. Ashkan, J. S. Dooley and M. L. Schilsky, *The Lancet*, 2007, **369**, 397–408.
- 5I. Mohr and K. H. Weiss, *Ann. Transl. Med.*, 2019, **7**, S69–S69.
- 6E. Roberts, *Hepatology*, 2003, **37**, 1475–1492.
- 7M. Bost, G. Piguet-Lacroix, F. Parant and C. M. R. Wilson, *J. Trace Elem. Med. Biol.*, 2012, **26**, 97–101.
- 8Cox DW, Bugbee D, Davies L and Kenny S, WD mutation database, <http://www.wilsonsdisease.med.ualberta.ca/database.asp>.
- 9I. J. Chang and S. H. Hahn, in *Handbook of Clinical Neurology*, Elsevier, 2017, vol. 142, pp. 19–34.

- 10 E. A. Roberts and M. L. Schilsky, *Hepatology*, 2008, **47**, 2089–2111.
- 11 C. D. Romero, P. H. Sanchez, F. L. Blanco, E. R. Rodríguez and L. S. Majem, *J. Trace Elem. Med. Biol.*, 2002, **16**, 75–81.
- 12 F. Woimant, N. Djebrani-Oussedik and A. Poujois, *Ann. Transl. Med.*, 2019, **7**, S70–S70.
- 13 M. Aramendía, L. Rello, M. Resano and F. Vanhaecke, *J. Anal. At. Spectrom.*, 2013, **28**, 675–681.
- 14 M. Resano, M. Aramendía, L. Rello, M. L. Calvo, S. Bérail and C. Pécheyran, *J Anal Spectrom*, 2013, **28**, 98–106.
- 15 M. C. García-Poyo, S. Bérail, A. L. Ronzani, L. Rello, E. García-González, B. Lelièvre, P. Cales, F. V. Nakadi, M. Aramendía, M. Resano and C. Pécheyran, *J. Anal. At. Spectrom.*, 2021, **36**, 968–980.
- 16 F. Schmitt, G. Podevin, J. Poupon, J. Roux, P. Legras, J.-M. Trocello, F. Woimant, O. Laprèvote, T. H. NGuyen and S. E. Balkhi, *PLoS ONE*, 2013, **8**, e82323.
- 17 S. El Balkhi, J.-M. Trocello, J. Poupon, P. Chappuis, F. Massicot, N. Girardot-Tinant and F. Woimant, *Clin. Chim. Acta*, 2011, **412**, 2254–2260.
- 18 O. Guillaud, A.-S. Brunet, I. Mallet, J. Dumortier, M. Pelosse, S. Heissat, C. Rivet, A. Lachaux and M. Bost, *Liver Int.*, 2018, **38**, 350–357.
- 19 M. Costas-Rodríguez, J. Delanghe and F. Vanhaecke, *TrAC Trends Anal. Chem.*, 2016, **76**, 182–193.
- 20 F. Albarede, P. Télouk, V. Balter, V. P. Bondanese, E. Albalat, P. Oger, P. Bonaventura, P. Miossec and T. Fujii, *Metallomics*, 2016, **8**, 1056–1070.
- 21 T. Walczyk and F. von Blanckenburg, *SCIENCE*, 2002, **295**, 2065–2066.
- 22 G. W. Gordon, J. Monge, M. B. Channon, Q. Wu, J. L. Skulan, A. D. Anbar and R. Fonseca, *Leukemia*, 2014, **28**, 2112–2115.
- 23 F. Vanhaecke, L. Balcaen and D. Malinovsky, *J. Anal. At. Spectrom.*, 2009, **24**, 863.
- 24 Prof. Dr. Frank Vanhaecke and Prof. Dr. Patrick Degryse, *Isotopic Analysis: Fundamentals and Applications Using ICP-MS*, Weinheim, Wiley-VCH Verlag GmbH & Co. KGaA., 2012.
- 25 S. El Balkhi, J. Poupon, J.-M. Trocello, A. Leyendecker, F. Massicot, M. Galliot-Guilley and F. Woimant, *Anal. Bioanal. Chem.*, 2009, **394**, 1477–1484.
- 26 J. M. Walshe, in *Advances in Clinical Chemistry*, Elsevier, 2010, vol. 50, pp. 151–163.

- 27 J.-M. Trocello, S. El Balkhi, F. Woimant, N. Girardot-Tinant, P. Chappuis, C. Lloyd and J. Poupon, *Mov. Disord.*, 2014, **29**, 558–562.
- 28 S. Heissat, A. Harel, K. Um, A.-S. Brunet, V. Hervieu, O. Guillaud, J. Dumortier, A. Lachaux, E. Mintz and M. Bost, *J. Trace Elem. Med. Biol.*, 2018, **50**, 652–657.
- 29 Q. Hou, L. Zhou, S. Gao, T. Zhang, L. Feng and L. Yang, *J Anal Spectrom*, 2016, **31**, 280–287.
- 30 K. A. Miller, PhD Thesis, University of Calgary, 2018.
- 31 K. A. Miller, C. M. Keenan, G. R. Martin, F. R. Jirik, K. A. Sharkey and M. E. Wieser, *J. Anal. At. Spectrom.*, 2016, **31**, 2015–2022.
- 32 C. Dirks, B. Scholten, S. Happel, A. Zulauf, A. Bombard and H. Jungclas, *J. Radioanal. Nucl. Chem.*, 2010, **286**, 671–674.
- 33 J. Fietzke, V. Liebetrau, D. Günther, K. Gürs, K. Hametner, K. Zumholz, T. H. Hansteen and A. Eisenhauer, *J. Anal. At. Spectrom.*, 2008, **23**, 955–961.
- 34 C. N. Maréchal, P. Télouk and F. Albarède, *Chem. Geol.*, 1999, **156**, 251–273.
- 35 L. Yang, *Mass Spectrom. Rev.*, 2009, **28**, 990–1011.
- 36 S. D. Tanner, *Spectrochim. Acta Part B At. Spectrosc.*, 1992, **47**, 809–823.
- 37 S. Lauwens, M. Costas-Rodríguez, J. Delanghe, H. Van Vlierberghe and F. Vanhaecke, *Talanta*, 2018, **189**, 332–338.
- 38 F. Albarède, P. Telouk, A. Lamboux, K. Jaouen and V. Balter, *Metallomics*, 2011, **3**, 926–933.
- 39 M. Costas-Rodríguez, Y. Anoshkina, S. Lauwens, H. Van Vlierberghe, J. Delanghe and F. Vanhaecke, *Metallomics*, 2015, **7**, 491–498.
- 40 S. Lauwens, M. Costas-Rodríguez, H. Van Vlierberghe and F. Vanhaecke, *Sci. Rep.*, , DOI:10.1038/srep30683.
- 41 A. Tennant, A. Rauk and M. E. Wieser, *Metallomics*, 2017, **9**, 1809–1819.
- 42 T. Fujii, F. Moynier, M. Abe, K. Nemoto and F. Albarède, *Geochim. Cosmochim. Acta*, 2013, **110**, 29–44.
- 43 E. A. Schauble, *Rev. Mineral. Geochem.*, 2004, **55**, 65–111.

6. Supplementary information

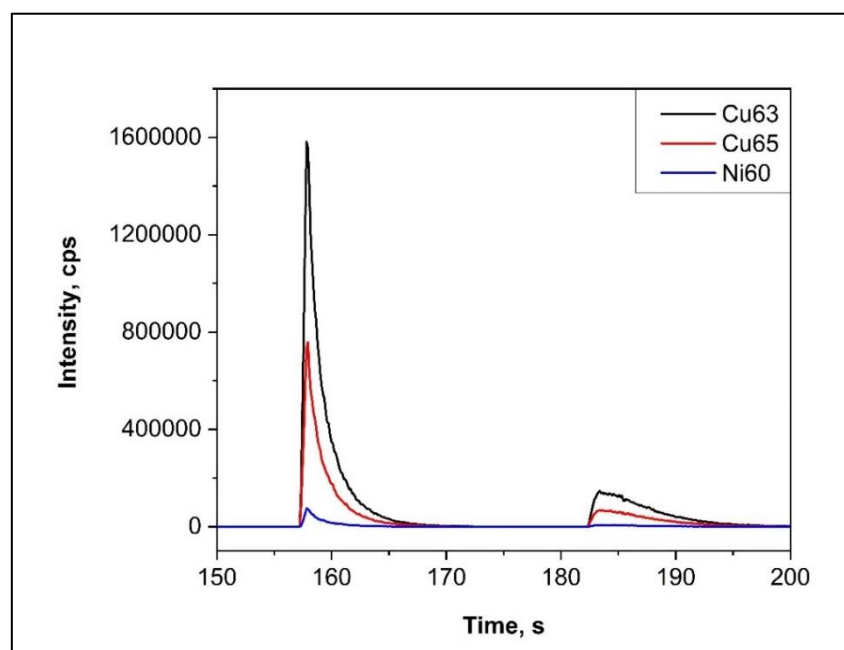


Figure S1. Example of transient signal obtained with injections of 1 μL of a solution containing 1 mg L^{-1} Cu and 50 $\mu\text{g L}^{-1}$ Ni at a flow rate of 100 $\mu\text{L min}^{-1}$. Conditions shown in **Table 1** for TRA analysis were used. The first peak corresponds to the 1 μL droplet introduction in the ICPMS. The second peak corresponds to the rinsing of the tubing after the 2% HNO_3 solution is reconnected to the peristaltic tube.

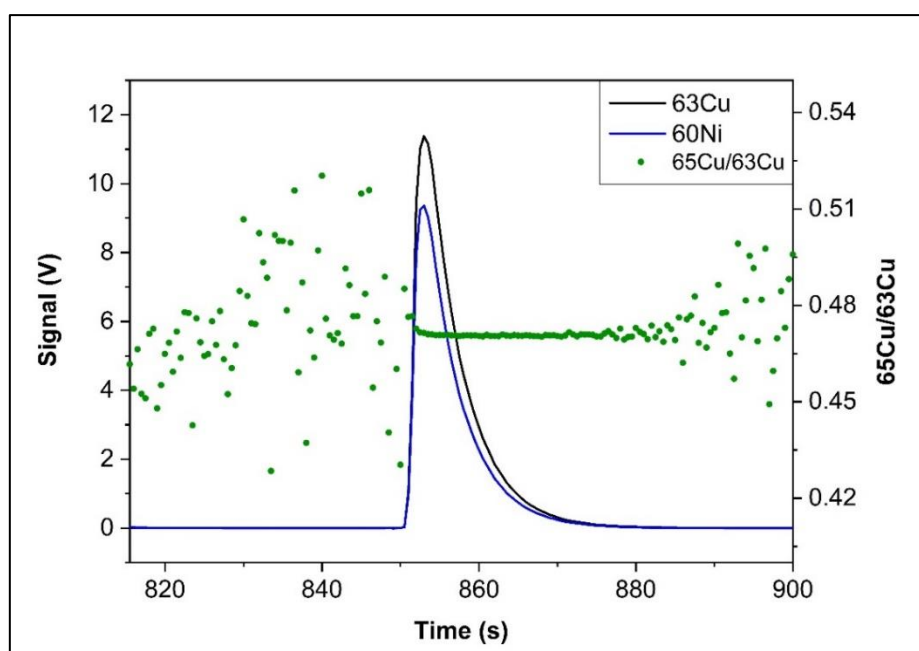


Figure S2. Example of transient signal obtained when 3 μL of 1 mg L^{-1} sample is injected (3 ng of Cu). Cu ratios showed are uncorrected by Ni.

Chapter 8: Conclusion

During this work, different new methodologies have been developed and examined both for elemental and isotopic Cu determination. These new methods were then applied to improve the way to diagnose and follow up Wilson disease.

For elemental analysis, two methods have been developed, one for direct solid analysis and the other for liquid sample analysis.

The direct solid analysis method has been developed for elemental Cu determination in blood via HR CS GFAAS with four different DBS devices (Mitra, HemaXis DB10, Capitainer qDBS, and HemaPen). All the devices enable carrying out Cu determination in a simple way, using external calibration with aqueous standards under optimized conditions. The results obtained for blood reference materials agree well with the reference value. Moreover, real samples were analyzed, and the results obtained *via* DBS are comparable to those that can be achieved through venipuncture.

The disadvantage of this method is that the blanks obtained for the empty devices were not very good. Hence, the necessity of Cu quantification in empty DBS to estimate properly and subtract the contribution of the blanks to the signal. Moreover, the precision obtained depends on such blanks and on the analyte levels, as values closer to the blanks were characterized by higher imprecision.

Also using HR CS AAS, a new correction model able to efficiently minimize spectral interferences by using only information available in the spectrum obtained from the own sample has been developed. This demonstrates that high resolution AAS coupled to charge

transfer device detection (CCD) for simultaneous detection of spectra around the atomic/ionic lines of interest offers a wide range of information that are still not fully exploited by the user.

This mathematical model is simple and could be implemented in the manufacturer software. It has been successfully applied for the determination of Cu in DPS devices, and would certainly require to be tested in several case studies beyond biomedical applications before being implemented in the manufacturer's software.

Using ICP-MS, a new method for liquid sample analysis has been developed aiming at Cu determination in serum samples using only 1 μL of a pre-treated sample. The analysis was carried out by direct injection of the sample into the peristaltic pump tubing using a micropipette. To obtain reproducible results, it is necessary to use an IS. With this method, the LOD and the LOQ were 3 and 10 $\mu\text{g L}^{-1}$, respectively.

Since before isotopic analysis *via* MC-ICP-MS it is mandatory to isolate the analyte to avoid interferences, two different resins (AG-MP1 and Triskem) were tested for this purpose. The Triskem resin provided better results in terms of Cu recovery and Na removal with only one separation process than the AG-MP-1 resin after two consecutive separation processes, which is remarkable.

For Cu isotopic analysis, three different methods have been developed.

The first method evaluated the coupling a femtosecond laser to a MC-ICP-MS. The measurements were carried out with only 1 μL of sample (after sample preparation) deposited onto a Si wafer. To evaluate the method, Cu isotopic analyses of NIST 3114 were carried out. $\delta^{65}\text{Cu}$ values of $-0.01 \pm 0.19\text{‰}$ (2SD, $n=10$) were obtained for 1 mg L^{-1} Cu (i.e. 1 ng of copper) with the self-bracketing method.

The second method investigated the coupling of an ETV to a MC-ICP-MS instrument. The analyses, in this case, were carried out using 5 μL of sample (i.e. 5 ng of Cu) after sample preparation, adding Pd as modifier. To evaluate this method, NIST 3114 (1 mg L⁻¹ Cu) was also analyzed, obtaining a $\delta^{65}\text{Cu}$ value of $0.00 \pm 0.17\text{‰}$ (2SD, n=10).

Finally, a direct μ -injection method was developed. For that purpose, 3 μL of pre-treated sample were directly injected into the nebulizer tubing with an electronic micropipette. In this case, a desolvator system was used to obtain higher sensitivity. To evaluate this method, NIST 3114 was analyzed as well, providing $\delta^{65}\text{Cu}$ values of $0.11 \pm 0.19\text{‰}$ (2SD, n=10).

The three methods presented for isotopic analysis offered similar analytical performances, although their applicability differs slightly. The fsLA-MC-ICP-MS method requires the use of a high repetition rate fs-LA system, but it offers more flexibility as to adapt the sensitivity to the specific requirements of the sample analyzed. In fact, sample deposition (performing several consecutive depositions is always possible) and LA ablation parameters (namely repetition rate and scan speed) can be modified to increase or reduce sensitivity as needed. The ETV-MC-ICP-MS method requires the use of an ETV instrument. However, it is possible to develop cheap and simple homemade devices, thus providing new ways to obtain isotopic information from microsamples. Finally, the direct μ -injection method is easy to implement as it does not require any special instrument for sample introduction except for a simple 3 μL micropipette. Moreover, in case the sensitivity of the method is not suitable for a given sample, a desolvator system can be used, as done in this work.

The possibility of carrying out the analysis with volumes between only 1 and 5 μL permits preconcentrating samples up to a factor of 10, which is crucial to obtain accurate and precise results from very low sample volumes. This fact is important because in many cases

(newborns, WD patients, studies with model rodents, etc.) low sample volumes and/or low Cu concentration values are found in the samples.

Finally, these methods were used for both elemental and isotopic Cu determination in samples of Wilson's disease patients (WD) under different treatment, healthy people (controls), patients with liver diseases different from WD and newborns.

Elemental analyses were carried out in both bulk serum (total Cu) and exchangeable Cu fractions (Cu Exch). Moreover, relative exchangeable Cu (REC) was calculated.

The Cu concentration obtained for WD patients in whole serum was lower than the rest of the groups tested. However, some overlapping between the Cu levels of WD patients and those of the rest can be observed, and particularly with newborns and infants. For Cu concentration in Exch fraction, no differences were found among the four groups. However, higher values of Exch Cu seem to be linked with WD patients (symptomatic when diagnosed) and with patients that did not follow the treatment correctly.

REC showed differences between WD patients and the rest of the groups tested. All the WD patients showed REC values higher than 17%, while the rest showed lower REC values.

Cu isotopic analysis in whole serum showed lower delta values ($\delta^{65}\text{Cu}$) for WD patients under chelator treatment and for patients with hepatic disorders (no WD). Higher delta values were found for WD patients under Zn treatment, while the values for controls and newborns were close to zero. This was coherent with the hypothesis of ^{63}Cu being preferably accumulated in the liver, and the negative delta values being due to Cu release from the liver, either by the treatment with a chelator or by liver disorders.

The results of $\delta^{65}\text{Cu}$ obtained in the Cu Exch fractions seem to follow the same trend as $\delta^{65}\text{Cu}$ obtained in whole serum.

Summarizing, estimating the REC leads to better WD diagnosis. The other parameters obtained can be used for following the disease and the treatment.

The advances in Cu determination (concentration and isotopes) in ultra-low volumes could be applicable for other scientific field or medical issues. In the last years, isotopic analysis has been seen as a new fantastic tool for diagnosis (for example, some cancer diagnosis). However, for diagnosis of WD, isotopic analysis is not the best suited because it depends on the liver damage causing Cu to leave the liver.

Conclusión

Durante este trabajo se han desarrollado y examinado diferentes metodologías nuevas tanto para la determinación elemental como isotópica del Cu. Además, estos nuevos métodos se han aplicado para mejorar tanto la forma de diagnosticar como el seguimiento de la enfermedad de Wilson.

Para el análisis elemental, se han desarrollado dos métodos, uno para el análisis sólido directo y otro para el análisis de muestras líquidas.

El método de análisis sólido directo se ha desarrollado para la determinación elemental de Cu en sangre mediante HR CS GFAAS en cuatro dispositivos DBS diferentes (Mitra, HemaXis DB10, Capitainer qDBS y HemaPen). Todos los dispositivos permiten llevar a cabo la determinación de Cu de forma sencilla, utilizando una calibración externa con estándares acuosos en condiciones optimizadas. Los resultados obtenidos para los materiales de referencia de sangre concuerdan con el valor de referencia. Además, se analizaron muestras reales, y los resultados obtenidos mediante DBS son comparables a los que se pueden conseguir mediante venopunción.

La desventaja de este método es que los blancos obtenidos para los dispositivos vacíos no fueron muy buenos. De ahí la necesidad de cuantificar el Cu en los DBS vacíos para estimar adecuadamente y restar la contribución de los blancos a la señal. Además, la precisión obtenida depende de dichos blancos y de los niveles de analito, ya que los valores más cercanos a los blancos se caracterizaron por una mayor imprecisión.

Utilizando HR CS AAS, también se ha desarrollado un nuevo modelo de corrección capaz de minimizar eficientemente las interferencias espectrales utilizando únicamente la

información disponible en el espectro obtenido de la propia muestra. Esto demuestra que el equipo de AAS de alta resolución acoplado a la detección por dispositivo de transferencia de carga (CCD) con un atomizador de horno de grafito ofrece una amplia gama de información que aún no es aprovechada completamente por el usuario para la detección simultánea de los espectros alrededor de las líneas atómicas/iónicas de interés. Este modelo matemático es sencillo y puede implementarse en el software del fabricante. Se ha aplicado con éxito para la determinación del Cu en dispositivos DPS, y ciertamente requeriría ser probado en varios casos de estudio más allá de las aplicaciones biomédicas antes de ser implementado en el software del fabricante.

Utilizando ICP-MS, se ha desarrollado un nuevo método para el análisis de muestras líquidas para la determinación de Cu en muestras de suero utilizando sólo 1 μL de muestra pretratada. El análisis se llevó a cabo mediante la inyección directa de la muestra en el tubo de la bomba peristáltica de forma manual. Para obtener resultados reproducibles, es necesario utilizar un IS. Con este método, el LOD y el LOQ fueron 3 y 10 $\mu\text{g L}^{-1}$, respectivamente.

Dado que antes del análisis isotópico mediante MC-ICP-MS es obligatorio aislar el analito para evitar interferencias, para ello, se probaron dos resinas diferentes (AG-MP1 y Triskem). La resina Triskem proporcionó mejores resultados en cuanto a la recuperación de Cu y la eliminación de Na con un solo proceso de separación que la resina AG-MP-1 después de dos procesos de separación consecutivos, lo cual es notable.

Para el análisis isotópico del Cu se han desarrollado tres métodos diferentes.

El primer método evaluó el acoplamiento de un laser femtosegundo a un MC-ICP-MS. Las mediciones se llevaron a cabo con sólo 1 μl de muestra (después de la preparación de la muestra) depositada en una oblea de Si. Para evaluar el método, se realizaron análisis

isotópicos de Cu del NIST 3114. Se obtuvieron valores de $\delta^{65}\text{Cu}$ de $-0,01 \pm 0,19\text{‰}$ (2SD, $n=10$) para 1 mg L^{-1} (i.e. 1 ng de cobre) de Cu con el método de “*self-bracketing*”.

El segundo método investigó el acoplamiento de un ETV a un instrumento MC-ICP-MS. Los análisis, en este caso, se llevaron a cabo utilizando $5 \mu\text{L}$ de muestra (i.e. 5 ng de Cu), después de la preparación de la muestra, añadiendo Pd como modificador. Para evaluar este método, se analizó también el NIST 3114 (1 mg L^{-1} Cu), obteniendo un valor de $\delta^{65}\text{Cu}$ de $0,00 \pm 0,17\text{‰}$ (2SD, $n=10$).

Finalmente, se desarrolló el método de microinyección directa. Para ello, se inyectaron directamente $3 \mu\text{L}$ de muestra pretratada en el tubo del nebulizador con una micropipeta electrónica. En este caso, se utilizó un sistema desolvador para obtener una mayor sensibilidad. Para evaluar este método, se analizó también el NIST 3114, proporcionando valores de $\delta^{65}\text{Cu}$ de $0,11 \pm 0,19\text{‰}$ (2SD, $n=10$).

Los tres métodos presentados para el análisis isotópico ofrecieron rendimientos analíticos similares, aunque su aplicabilidad difiere ligeramente. El método fs-LA-MC-ICP-MS requiere el uso de un sistema fs-LA de alta tasa de repetición, pero ofrece más flexibilidad en cuanto a la adaptación de la sensibilidad a los requisitos específicos de la muestra analizada. De hecho, la deposición de la muestra (siempre es posible realizar varias deposiciones consecutivas) y los parámetros de ablación del LA (concretamente la tasa de repetición y la velocidad de barrido) pueden modificarse para aumentar o disminuir la sensibilidad según sea necesario. El método ETV-MC-ICP-MS requiere el uso de un instrumento ETV. Sin embargo, es posible desarrollar dispositivos caseros baratos y sencillos, proporcionando así nuevas formas de obtener información isotópica a partir de micromuestras. Por último, el método de microinyección directa es fácil de aplicar, ya que no requiere ningún instrumento especial para la introducción de la muestra, salvo una micropipeta de $3 \mu\text{L}$. Además, si la

sensibilidad del método no es adecuada para una muestra, se puede utilizar un sistema de desolvatación, como se ha hecho en este trabajo.

La posibilidad de realizar el análisis con volúmenes entre 1 y 5 μL permite preconcentrar las muestras hasta un factor de 10, lo cual es crucial para obtener resultados exactos y precisos a partir de volúmenes de muestra muy bajos. Este hecho es importante porque en muchos casos (recién nacidos, pacientes con WD, estudios con roedores, etc.) los volúmenes de muestra disponible son bajos y/o la concentración de Cu es baja.

Por último, estos métodos se utilizaron para la determinación tanto elemental como isotópica del Cu en muestras de pacientes con la enfermedad de Wilson (WD) sometidos a diferentes tratamientos, de personas sanas (controles), de pacientes con enfermedades hepáticas distintas de la WD y de recién nacidos.

Los análisis elementales se llevaron a cabo tanto en el suero total (Cu total) como en las fracciones de Cu intercambiable (Cu Exch). Además, se calculó el Cu intercambiable relativo (REC).

La concentración de Cu obtenida para los pacientes con WD en el suero total fue inferior a la del resto de los grupos analizados. Sin embargo, se observa un cierto solapamiento entre los niveles de Cu de los pacientes con WD y los del resto, en particular con los recién nacidos y los lactantes. En cuanto a la concentración de Cu en la fracción intercambiable (Cu Exch), no se encontraron diferencias entre los cuatro grupos. Sin embargo, los valores más elevados de Cu Exch parecen estar relacionados con los pacientes con WD (sintomáticos en el momento del diagnóstico) y con los pacientes que no siguieron correctamente el tratamiento.

El REC mostró diferencias entre los pacientes con WD y el resto de los grupos analizados. Todos los pacientes con WD mostraron valores de REC superiores al 17%, mientras que el resto mostró valores de REC inferiores.

El análisis isotópico del Cu en suero completo mostró valores delta más bajos ($\delta^{65}\text{Cu}$) para los pacientes con WD bajo tratamiento quelante y para los pacientes con trastornos hepáticos (sin WD). Se encontraron valores delta más altos para los pacientes con WD bajo tratamiento con Zn, mientras que los valores para los controles y los recién nacidos eran cercanos a cero. Esto es coherente con la hipótesis de que el ^{63}Cu se acumula preferentemente en el hígado y los valores delta negativos se deben a la liberación de Cu del hígado, ya sea por el tratamiento con un quelante o por trastornos hepáticos.

Los resultados de $\delta^{65}\text{Cu}$ obtenidos en las fracciones de Cu Exch parecen seguir la misma tendencia que los de $\delta^{65}\text{Cu}$ obtenidos en suero entero.

Resumiendo, la estimación del REC conduce a un mejor diagnóstico de la WD. Los otros parámetros obtenidos pueden utilizarse para el seguimiento de la enfermedad y el tratamiento.

Los avances en la determinación del Cu (concentración e isótopos) en volúmenes ultrabajos podrían ser aplicables a otros campos científicos o temas médicos. En los últimos años, el análisis isotópico se ha visto como una nueva herramienta fantástica para el diagnóstico (por ejemplo, algunos diagnósticos de cáncer). Sin embargo, para el diagnóstico de la enfermedad de Wilson, el análisis isotópico no es el más adecuado porque depende del daño hepático que provoca la salida de Cu del hígado.

Conclusion

Au cours de ce travail, de nouvelles méthodologies ont été développées et évaluées pour la détermination du Cu élémentaire et isotopique. Elles ont ensuite été appliquées à l'amélioration du diagnostic et du suivi de la maladie de Wilson.

Pour l'analyse élémentaire, deux méthodes ont été développées, l'une pour l'analyse directe de solide et l'autre pour l'analyse d'échantillons liquides.

La méthode d'analyse directe de solide a été développée pour la détermination du Cu élémentaire dans le sang par HR CS GFAAS avec quatre dispositifs de prélèvement par DBS différents (Mitra, HemaXis DB10, Capitainer qDBS, et HemaPen). Tous ont permis de réaliser la détermination du Cu de manière simple, en utilisant une calibration externe avec des standards aqueux dans des conditions optimisées. Les résultats obtenus pour les matériaux de référence sanguins correspondent bien à la valeur de référence. De plus, des échantillons réels ont été analysés, et les résultats obtenus par DBS sont comparables à ceux qui peuvent être obtenus par ponction veineuse.

Bien que cette méthode soit rapide et offre un grand potentiel en termes de déploiement sur le terrain, nous en avons conclu qu'elle présente l'inconvénient que les blancs obtenus à partir de ces dispositifs de prélèvement n'étaient pas très bons. Il est alors nécessaire de quantifier soigneusement le Cu dans les DBS vierges afin d'estimer correctement et de soustraire la contribution des blancs au signal. Par ailleurs, la précision obtenue dépend de ces blancs et des niveaux de cuivre dans les échantillons, les valeurs les plus proches des blancs étant caractérisées par une plus grande imprécision.

En utilisant également le HR CS AAS, un nouveau modèle de correction capable de minimiser les interférences spectrales en utilisant uniquement les informations disponibles dans le spectre obtenu à partir du propre échantillon a été développé. Cela démontre que la spectroscopie d'absorption atomique à haute résolution couplée à une détection par dispositif à transfert de charge (CCD) pour la détection simultanée des spectres autour des raies atomiques/ioniques d'intérêt offre un large éventail d'informations qui ne sont pas encore pleinement exploitées par l'utilisateur. Ce modèle mathématique est simple et pourrait être mis en œuvre au niveau du logiciel du fabricant. Il a été appliqué avec succès pour la détermination du Cu dans les dispositifs DBS, et nécessiterait certainement d'être testé dans plusieurs cas d'études, au-delà des applications biomédicales, avant d'être implémenté dans le logiciel du fabricant.

En utilisant l'ICP-MS, une nouvelle méthode d'analyse d'échantillons liquides a été développée pour la détermination du Cu dans des échantillons de sérum en utilisant seulement 1 μL d'un échantillon prétraité. L'analyse a été réalisée par injection manuelle de l'échantillon dans le tube de la pompe péristaltique à l'aide d'une micropipette. Pour obtenir des résultats reproductibles, il est nécessaire d'utiliser un étalon interne. Avec cette méthode, les LOD et LOQ étaient respectivement de 3 et 10 $\mu\text{g L}^{-1}$.

L'analyse isotopique par MC-ICP-MS nécessitant obligatoirement d'isoler l'analyte de la matrice pour éviter les interférences, deux résines différentes (AG-MP1 et Triskem) ont été testées à cet effet. La résine Triskem a fourni d'excellent résultats en termes de récupération du Cu et d'élimination du Na. En effet avec un seul processus de séparation, cette résine donne de meilleurs résultats que la résine AG-MP-1 après deux processus de séparation consécutifs, ce qui est remarquable.

Pour l'analyse isotopique du Cu, trois méthodes différentes ont été développées.

La première méthode a évalué le couplage d'un laser femtoseconde à un MC-ICP-MS. Les mesures ont été effectuées avec seulement 1 μL d'échantillon (après préparation de l'échantillon) déposé sur un wafer de silicium. Pour évaluer la méthode, des analyses isotopiques du Cu du NIST 3114 ont été réalisées. Des valeurs de $\delta^{65}\text{Cu}$ de $-0,01 \pm 0,19\text{‰}$ (2SD, n=10) ont été obtenues pour 1 mg L^{-1} de Cu, soit une masse de 1 ng de Cu, avec la méthode dite de « self bracketing ».

La deuxième méthode a porté sur le couplage d'un ETV à un instrument MC-ICP-MS. Les analyses, dans ce cas, ont été effectuées en utilisant 5 μL d'échantillon (soit 5 ng), après préparation de l'échantillon, en ajoutant du Pd comme modificateur de matrice. Pour évaluer cette méthode, l'échantillon NIST 3114 (1 mg L^{-1} Cu) a également été analysé, obtenant une valeur $\delta^{65}\text{Cu}$ de $0,00 \pm 0,17\text{‰}$ (2SD, n=10).

Enfin, une méthode de micro-injection directe a été développée. Pour cela, 3 μL d'échantillon prétraité ont été directement injectés dans le cathéter du nébuliseur à l'aide d'une micropipette électronique. Dans ce cas, un désolvateur a été utilisé pour obtenir une plus grande sensibilité. Pour évaluer cette méthode, le NIST 3114 a également été analysé, fournissant des valeurs de $\delta^{65}\text{Cu}$ de $0,11 \pm 0,19\text{‰}$ (2SD, n=10).

Les trois méthodes présentées pour l'analyse isotopique ont offert des performances analytiques similaires, bien que leur applicabilité diffère légèrement. La méthode fsLA-MC-ICP-MS nécessite l'utilisation d'un laser femtoseconde à haute cadence de tir mais elle offre plus de flexibilité quant à l'adaptation de la sensibilité aux exigences spécifiques de l'échantillon analysé. En fait, le dépôt de l'échantillon (il est toujours possible d'effectuer plusieurs dépôts consécutifs) et les paramètres d'ablation laser (à savoir la fréquence de tir et la vitesse de balayage du scanner) peuvent être modifiés pour augmenter ou diminuer la sensibilité selon les besoins. La méthode ETV-MC-ICP-MS nécessite l'utilisation d'un

instrument ETV. Cependant, il est possible de développer des appareils maison simples et bon marché, offrant ainsi de nouveaux moyens d'obtenir des informations isotopiques à partir de micro-échantillons. Enfin, la méthode de micro-injection directe est facile à mettre en œuvre car elle ne nécessite aucun instrument spécial pour l'introduction des échantillons, à l'exception d'une micropipette de 3 μL . De plus, si la sensibilité de la méthode n'est pas adaptée à un échantillon, un désolvateur peut être utilisé, comme cela a été fait dans ce travail.

La possibilité de réaliser l'analyse avec des volumes compris entre 1 et 5 μL ne permet de préconcentrer les échantillons jusqu'à un facteur 10, ce qui est appréciable pour obtenir des résultats exacts et précis à partir de très faibles volumes d'échantillons. Ce fait est important car dans de nombreux cas (nouveau-nés, patients atteints de maladies chroniques, études sur des rongeurs modèles, etc.), de faibles volumes d'échantillons et/ou de faibles valeurs de concentration de Cu sont trouvés dans les échantillons.

Enfin, ces méthodes ont été utilisées pour la détermination du Cu élémentaire et isotopique dans des échantillons de patients atteints de la maladie de Wilson (WD) sous différents traitements, de personnes saines (témoins), de patients atteints de maladies hépatiques différentes de la maladie de Wilson et de nouveau-nés.

Les analyses élémentaires ont été réalisées à la fois dans le sérum brut (Cu total) et dans les fractions de Cu échangeable (Cu Exch). En outre, le Cu échangeable relatif (REC) a été calculé.

La concentration de Cu obtenue pour les patients atteints de WD dans le sérum total était inférieure à celle du reste des groupes testés. Cependant, on observe un certain chevauchement entre les niveaux de Cu des patients atteints de WD et ceux des autres groupes, en particulier chez les nouveau-nés et les nourrissons. Pour la concentration de Cu

dans la fraction Exch (Cu Exch), aucune différence n'a été trouvée entre les quatre groupes. Cependant, des valeurs plus élevées de Cu Exch semblent être liées aux patients atteints de WD (symptomatiques au moment du diagnostic) et aux patients qui n'ont pas suivi le traitement correctement.

Le REC a montré des différences entre les patients atteints de WD et les autres groupes testés. Tous les patients atteints de WD ont montré des valeurs de REC supérieures à 17%, tandis que les autres ont montré des valeurs de REC inférieures.

L'analyse isotopique du Cu dans le sérum entier a montré des valeurs delta plus faibles ($\delta^{65}\text{Cu}$) pour les patients atteints de WD sous traitement chélateur et pour les patients souffrant de troubles hépatiques (pas de WD). Des valeurs delta plus élevées ont été trouvées pour les patients atteints de WD sous traitement au Zn, tandis que les valeurs pour les témoins et les nouveau-nés étaient proches de zéro. Ceci est cohérent avec l'hypothèse selon laquelle le ^{63}Cu s'accumule de préférence dans le foie et les valeurs delta négatives sont dues à la libération du Cu du foie, soit par le traitement avec un chélateur, soit par des troubles hépatiques.

Les résultats du $\delta^{65}\text{Cu}$ obtenus dans les fractions Cu Exch semblent suivre la même tendance que le $\delta^{65}\text{Cu}$ obtenu dans le sérum total.

En résumé, l'estimation du REC permet de mieux diagnostiquer les maladies de Wilson. Les autres paramètres obtenus peuvent être utilisés pour le suivi de la maladie et du traitement.

Les progrès dans la détermination du Cu (concentration et isotopes) dans des volumes ultra-faibles pourraient être applicables à d'autres domaines scientifiques ou à des questions médicales. Ces dernières années, l'analyse isotopique a été considérée comme un nouvel outil fantastique pour le diagnostic (par exemple, pour le diagnostic de certains cancers).

Cependant, pour le diagnostic de la maladie de Wilson, l'analyse isotopique n'est pas la plus adaptée, car elle dépend des lésions hépatiques qui provoquent la sortie du Cu du foie.

Statement of the contribution of each author:

This thesis has already resulted in four publications.

Chapter 3: Determination of Cu in blood *via* direct analysis of dried blood spots using high-resolution continuum source graphite furnace atomic absorption spectrometry.

M. Carmen García-Poyo, Christophe Pécheyran, Luis Rello, Elena García-González, Sharay Alonso Rodríguez, Flávio V. Nakadi, Maite Aramendía, Martín Resano. **J. Anal. At. Spectrom.**, 2021,**36**, 1666-1677

M. Carmen García-Poyo: Data curation, Formal analysis, Investigation, Methodology, Validation, Writing – original draft, Writing – review & editing; **Christophe Pécheyran:** Conceptualization, Funding acquisition, Project administration, Supervision, Writing – review & editing; **Luis Rello:** Funding acquisition, Resources, Writing – review & editing; **Elena García-González:** Resources, Writing – review & editing; **Sharay Alonso Rodríguez:** Data curation, Writing – review & editing; **Flávio V. Nakadi:** Data curation, Methodology, Supervision, Writing – review & editing; **Maite Aramendía:** Writing – review & editing; **Martín Resano:** Conceptualization, Funding acquisition, Methodology, Resources, Project administration, Supervision, Writing – review & editing.

Chapter 4: Time-absorbance profile ratio background correction: introducing TAP to correct for spectral overlap in high-resolution continuum source graphite furnace atomic absorption spectrometry.

Flávio V. Nakadi, M. Carmen García-Poyo, Christophe Pécheyran, Martín Resano. **J. Anal. At. Spectrom.**, 2021,**36**, 2370-2382

Flávio V. Nakadi: Conceptualization, Data curation, Formal analysis, Investigation, Methodology, Software, Validation, Writing – original draft, Writing – review & editing; **M. Carmen García-Poyo:** Data curation, Formal analysis, Investigation, Validation, Writing – review & editing; **Christophe Pécheyran:** Funding acquisition, Project administration,

Supervision, Writing – review & editing; **Martín Resano**: Funding acquisition, Project administration, Methodology, Resources, Supervision, Writing – review & editing.

Chapter 5: Laser ablation of microdroplets for copper isotopic analysis via MC-ICP-MS. Analysis of serum microsamples for the diagnosis and follow-up treatment of Wilson's disease. M. Carmen García-Poyo, Sylvain Bérail, Anne Laure Ronzani, Luis Rello, Elena García-González, Bénédicte Lelièvre, Paul Cales, Flávio V. Nakadi, Maite Aramendía, Martín Resano and Christophe Pécheyran.

M. Carmen García-Poyo: Data curation, Formal analysis, Investigation, Methodology, Validation, Writing – original draft, Writing – review & editing; **Sylvain Bérail**: Methodology, Resources, Writing – review & editing; **Anne Laure Ronzani**: Methodology, Validation, Writing – review & editing; **Luis Rello**: Resources, Validation, Funding acquisition, Writing – review & editing; **Elena García-González**: Resources; **Bénédicte Lelièvre**: Resources, Writing – review & editing; **Paul Cales**: Validation, Writing – review & editing; **Flávio V. Nakadi**: Writing – review & editing; **Maite Aramendía**: Conceptualization, Methodology, Supervision, Writing – original draft, Writing – review & editing; **Martín Resano**: Conceptualization, Funding acquisition, Methodology, Project administration, Supervision, Writing – review & editing; **Christophe Pécheyran**: Conceptualization, Funding acquisition, Methodology, Project administration, Resources, Software, Supervision, Writing – review & editing.

Chapter 6: Evaluation of electrothermal vaporization for sample introduction aiming at Cu isotopic analysis via multicollector-inductively coupled plasma mass spectrometry.

M. Carmen García-Poyo, Anne Laure Ronzani, Jérôme Frayret, Sylvain Bérail, Luis Rello, Elena García-González, Bénédicte Lelièvre, Flávio V. Nakadi, Maite Aramendía, Martín Resano, Christophe Pécheyran.

M. Carmen García-Poyo: Data curation, Formal analysis, Investigation, Methodology, Validation, Writing – original draft, Writing – review & editing; **Anne Laure Ronzani**: Methodology, Validation, Writing – review & editing; **Jérôme Frayret**: Methodology, Writing – review & editing; **Sylvain Bérail**: Methodology, Resources, Writing – review & editing; **Luis**

Rello: Resources, Funding acquisition, Writing – review & editing; **Elena García-González:** Resources; **Bénédicte Lelièvre:** Resources, Writing – review & editing; **Flávio V. Nakadi:** Data curation, Investigation, Writing – review & editing; **Maite Aramendía:** Methodology, Supervision, Writing – review & editing; **Martín Resano:** Conceptualization, Funding acquisition, Methodology, Project administration, Supervision, Writing – review & editing; **Christophe Pécheyran:** Conceptualization, Funding acquisition, Methodology, Project administration, Resources, Software, Supervision, Writing – review & editing.